Spring 2020

Strengthening QC relaxations of optimal power flow problems by exploiting various coordinate changes

Mohammad Rasoul Narimani

Department: Electrical and Computer Engineering

STRENGTHENING QC RELAXATIONS OF OPTIMAL POWER FLOW PROBLEMS BY EXPLOITING VARIOUS COORDINATE CHANGES

by

MOHAMMAD RASOUL NARIMANI

A DISSERTATION

Presented to the Graduate Faculty of the

MISSOURI UNIVERSITY OF SCIENCE AND TECHNOLOGY

In Partial Fulfillment of the Requirements for the Degree

DOCTOR OF PHILOSOPHY

in

ELECTRICAL ENGINEERING

2020

Approved by

Mariesa L. Crow, Advisor
Daniel K. Molzahn
Pourya Shamsi
Mehdi Ferdowsi
Jonothan W. Kimball
Suzanna Long

PUBLICATION DISSERTATION OPTION

This dissertation consists of the following five articles which have been submitted for publication, or will be submitted for publication as follows:

Paper I: Empirical investigation of non-convexities in optimal power flow problems. Published in American Control Conference, pp. 27-54.

Paper II: Improving QC Relaxations of OPF Problems Via Voltage Magnitude Difference Constraints and Envelopes for Trilinear Monomials. Published in Power Systems Computation Conference, pp. 55-78.

Paper III: Comparison of Various Trilinear Monomial Envelopes for Convex Relaxations of Optimal Power Flow Problems, pp.79-94.

Paper IV: Tightening QC Relaxations of AC Optimal Power Flow Problems Via Complex Per Unit Normalization. Submitted to IEEE Transaction on Power System, pp. 95-131.

Paper V: Tightening QC Relaxations of OPF Problems by Independently Rotating the Trigonometric Terms. is intended to submit to IEEE Transaction on Power System, pp. 132-163.

ABSTRACT

Motivated by the potential for improvements in electric power system economics, this dissertation studies the AC optimal power flow (AC OPF) problem. An AC OPF problem optimizes a specified objective function subject to constraints imposed by both the non-linear power flow equations and engineering limits. The difficulty of an AC OPF problem is strongly connected to its feasible space's characteristics. This dissertation first investigates causes of nonconvexities in AC OPF problems. Understanding typical causes of nonconvexities is helpful for improving AC OPF solution methodologies.

This dissertation next focuses on solution methods for AC OPF problems that are based on *convex relaxations*. The quadratic convex (QC) relaxation is one promising approach that constructs convex envelopes around the trigonometric and product terms in the polar representation of the power flow equations. This dissertation proposes several improvements to strengthen QC relaxations of OPF problems. The first group of improvements provides tighter envelopes for the trigonometric functions and product terms in the power flow equations. Methods for obtaining tighter envelopes includes implementing Meyer and Floudas envelopes that yield the convex hull of trilinear monomials. Furthermore, by leveraging a representation of line admittances in polar form, this dissertation proposes tighter envelopes for the trigonometric terms. Another proposed improvement exploits the ability to rotate the base power used in the per unit normalization in order to facilitate the application of tighter trigonometric envelopes.

The second group of improvements propose additional constraints based on new variables that represent voltage magnitude differences between connected buses. Using "bound tightening" techniques, the bounds on the voltage magnitude *difference* variables can be significantly tighter than the bounds on the voltage magnitudes themselves, so constraints based on voltage magnitude differences can improve the QC relaxation.

ACKNOWLEDGMENTS

Firstly, I would like to express my sincere gratitude to my advisor Prof. Mariesa Crow for the continuous support of my Ph.D study and related research, for her patience, motivation, and immense knowledge. Her guidance helped me in all the time of research and writing of this dissertation. I would also like to express my deepest gratitude to my co-advisor, Dr. Daniel Molzahn. The depth and breadth of his knowledge showed me the importance of drawing on ideas from a variety of areas to solve practical and challenging problems. It has been a great experience to work under his guidance and I attribute the level of my PhD degree to his encouragement and effort. I will forever remain indebted for his tutelage. I am also very grateful for the assistance and advice provided by my doctoral committee. Dr. Mehdi Ferdowsi guidance in numerous situations and his support through GAAN fellowship have been invaluable. Dr. Pourya Shamsi inspired me to pursue a research career in electric power. I also greatly benefited from Dr. Kimball vast knowledge of power electronic and electric machines. Drawing on this knowledge would be essential to my career. I would also like to thank Dr. long for serving on my committee.

I would like to express my deepest gratitude for the support and love of my family. I can never thank my parents, enough for their encouragement and love. Finally, I greatly appreciate the companionship and patience of my wife, Fatemeh Narimani. Her support throughout my graduate studies was essential to my success. It would never have done without her support. I can never thank my wife enough for her encouragement and love. I will forever remain indebted for her support. I gratefully acknowledge the support of the research assistantships funded by grants from the Department of Energy, and the GAAN fellowship funded from the Department of Education.

TABLE OF CONTENTS

Page

LIST OF ILLUSTRATIONS

LIST OF TABLES

SECTION

1. INTRODUCTION

1.1. MOTIVATION

The AC Optimal Power Flow (ACOPF) is at the heart of many problems in power system area. Independent System Operators (ISO) solve the AC OPF problem for various time slots, every year for system planning, everyday for day-ahead markets, every hour, and every five minutes for system operation [1]. The OPF is a fundamental optimization problem in power system that seeks decision variables to yield an optimal operating point in terms of a specific objective and subject to network equality constraints and engineering limits. Various objectives have been considered for solving OPF problems ranging from electricity generation cost, emission, power losses, reliability, etc. Economic operation of electric power systems is a major concern of power system engineers. With the large size of the power system industry in the United States even a slight improvement in electricity generation cost can save million of dollars annually. As one measure of industry size, electric industry revenues in the United States were $369 billion in 2010 [2], so, improvements in power system economics have the potential for significant impacts. This dissertation discusses research into the "optimal power flow" problem of minimizing generation cost while satisfying physical network constraints and engineering limits. Physical network constraints represent power flow equations that relates voltage phasors and power flow in lines. Engineering limits present practical restrictions of power systems such as voltage magnitudes, active and reactive generation, and line flow limits.

A wide range of engineering limits are involved in a typical OPF problem ranging from active and reactive power generation, bus voltage magnitudes, transmission line and transformer flows, and possibly network stability constraints. Like many optimization problems in power systems, power flow equations play a crucial role in the OPF problem relating voltage at buses to active and reactive power injections to buses. Nonconvexity in typical OPF formulations enters largely through the nonlinear power flow equations representing physical constraints on the electric grid. Using the nonlinear AC power flow model to accurately represent the power flow physics results in the AC OPF problem, which is non-convex, may have multiple local optima [1], and is generally NP-Hard [2], [3]. A wide variety of algorithms have been applied in order to find locally optimal solutions [4], [5]. The power flow equations are typically solved using iterative numerical techniques for systems of non-linear equations, such as the Newton-Raphson and Gauss-Seidel methods [6].

Many recent research efforts have developed convex relaxations of OPF problems to obtain bounds on the optimal objective values, certify infeasibility, and, in some cases, achieve globally optimal solutions. Solutions from a relaxation are also useful for initializing certain local solution techniques [7]. Convex relaxations are under active development with ongoing efforts aiming to improve the relaxations' computational tractability and tightness. Recent work is surveyed in [7]. The quadratic convex (QC) relaxation [5] is one promising approach that uses convex envelopes around the trigonometric functions, squared terms, and bilinear products in the polar form of the power flow equations.

Using the QC relaxation of the optimal power flow problem, this dissertation details enhancements that enable economic operation of electric power systems. The power flow equations model the physical network constraints inherent to the optimal power flow problem, which is used to minimize system operating costs. This dissertation investigates a QC relaxation relaxation of the optimal power flow problem and provides modeling necessary for application to electric power systems. Before delving into these contributions, this in-

troduction first provides a background on the power flow equations. Next a literature review on different convex relaxations of power flow equations is presented. Then the optimal power flow problem, and QC relaxation of OPF problem is explained.

1.2. THE POWER FLOW EQUATIONS

The goal of a power-flow study is to obtain voltages angle and magnitude information for each bus in a power system for specified load and generator real power and voltage conditions. All active and reactive power flow on each branch as well as generator reactive power output can be analytically determined by voltage angle and magnitudes. The underlying voltage-to-current relationships of the network are linear, but the nature of equipment in a power system is such that injected/demanded complex power at a bus is typically specified, rather than current. The relation of interest is between the active and reactive power injected at each bus and the complex voltages at each bus, and hence the associated equations are non-linear. Due to the nonlinear nature of this power flow equations, numerical methods are employed to obtain a solution that is within an acceptable tolerance. Using polar representation for complex voltages and rectangular "active/reactive" representation of complex power, the power balance equations at bus i are given by

$$P_i = V_i \sum_{k=1}^{n} V_k \left(G_{ik} \cos(\delta_i - \delta_k) + B_{ik} \sin(\delta_i - \delta_k)\right) \tag{1.1a}$$

$$Q_i = V_i \sum_{k=1}^{n} V_k \left(G_{ik} \sin(\delta_i - \delta_k) - B_{ik} \cos(\delta_i - \delta_k)\right) \tag{1.1b}$$

where P_i and Q_i are the active and reactive power injections, respectively, at bus i, V_i and δ_i are the voltage magnitude and phase angle, respectively, at bus i, $Y = G + jB$ is the network admittance matrix [8], and n is the number of buses in the system.

The first step in solving the power flow problem is defining the known and unknown variables in the system. The known and unknown variables are dependent on the type of bus. A bus without any generators connected to it is called a Load Bus or PQ bus. PQ buses treat P_i and Q_i as specified quantities, and enforce the active power (1.1a) and reactive power (1.1b) equations at that bus. With one exception, a bus with at least one generator connected to it is called a generator bus or PV bus. The exception is one arbitrarily-selected bus that has a generator. This bus is referred to as the slack bus. PV buses, which typically correspond to generators, specify a known voltage magnitude V_i and active power injection P_i, and enforce only the active power equation (1.1a). The associated reactive power Q_i may be computed as an "output quantity," via (1.1b). Finally, a single slack bus, with specified V_i and δ_i (typically chosen to be 0°) is selected. The active power P_i and reactive power Q_i at the slack bus are determined from (1.1a) and (1.1b), respectively.

The line flows can be equivalently modeled using a polar representation of the line's mutual admittance, $Y_{ik}e^{j\delta_{ik}}$, where $Y_{ik} = \sqrt{G_{ik}^2 + B_{ik}^2}$ and $\delta_{ik} = \arctan\left(B_{ik}/G_{ik}\right)$ are the magnitude and angle of the mutual admittance for line $(i,k) \in \mathcal{L}$, respectively. Using polar admittance coordinates, the complex power flows into each terminal of the line $(i,k) \in \mathcal{L}$, are:

$$P_i = V_i \sum_{k=1}^{n} V_k \left(Y_{ik} \cos(\delta_i - \delta_k - \theta_{ik})\right) \tag{1.2a}$$

$$Q_i = V_i \sum_{k=1}^{n} V_k \left(Y_{ik} \sin(\delta_i - \delta_k - \theta_{ik})\right) \tag{1.2b}$$

The non-linear power flow equations require iterative numerical solution techniques, such as Gauss-Seidel or, most commonly, Newton-Raphson [8]. The Newton-Raphson method begins with initial guesses of all unknown variables. Next, a Taylor Series is written, with the higher order terms neglected, for each of the power balance equations (1.1a) and (1.1b).

The result is a linear system of equations that can be expressed as:

$$\begin{bmatrix} \Delta\theta \\ \Delta|V| \end{bmatrix} = -J^{-1} \begin{bmatrix} \Delta P \\ \Delta Q \end{bmatrix}. \tag{1.3}$$

ΔP and ΔQ are the mismatch equations that can be expresed as follow:

$$\Delta P_i = -P_i + V_i \sum_{k=1}^{n} V_k \left(G_{ik}\cos(\delta_i - \delta_k) + B_{ik}\sin(\delta_i - \delta_k)\right) \tag{1.4a}$$

$$\Delta Q_i = -Q_i + V_i \sum_{k=1}^{n} V_k \left(G_{ik}\sin(\delta_i - \delta_k) - B_{ik}\cos(\delta_i - \delta_k)\right) \tag{1.4b}$$

J is the Jacobian matrix which consists of different partial derivatives of injected active and reactive power to each bus with respect to voltage magnitude and angle. The Jacobian matrix can be expressed as follow:

$$J = \begin{bmatrix} \frac{\partial \Delta P}{\partial \Delta\theta} & \frac{\partial \Delta P}{\partial \Delta|V|} \\ \frac{\partial \Delta Q}{\partial \Delta\theta} & \frac{\partial \Delta Q}{\partial \Delta|V|} \end{bmatrix}. \tag{1.5}$$

The voltage magnitude and angles can be computed iteratively using the linearized system of equations in (1.3) and an initial guess of the solution voltage magnitudes and angles as follow:

$$\theta^{m+1} = \theta^m + \Delta\theta \tag{1.6}$$

$$|V|^{m+1} = |V|^m + \Delta|V| \tag{1.7}$$

The iterative solving process continues until a stopping condition is met. A common stopping condition is to terminate if the norm of the mismatch equations is below a specified tolerance.

Note that the Newton-Raphson's convergence performances strongly depends on the initial guess of the solution voltage magnitudes and angles. Newton methods are only locally convergent; there is no guarantee to converge to a particular solution from an arbitrary initial guess [6]. A initial guess consisting of a "flat start" voltage profile with uniform voltage magnitudes and zero phase angles can often be used to find a solution for "typical" parameters. However, it is important to recognize that as parameters move outside of routine operating ranges the behavior of the power flow equations can be highly complex, resulting in convergence failure for these solution techniques.

The properties of the Newton-Raphson iteration guarantee (under suitable differentiability assumptions) convergence to a solution for an initial condition selected in a sufficiently small neighborhood around that solution [9]. The existence of a power flow solution is necessary for power system stability analysis and plays a crucial role in power system reliability. However, selecting an arbitrary initial guess for power flow equation might give rise to divergence issues. The important point here is that the user cannot distinguish the "no feasible solution" property for power flow equations and "bad initial guess" when they encounter divergence issues.

Power flow equations may have a very large number of solutions; for example, the work of [10] establishes cases for which the number of solutions grows faster than polynomial with respect to network size. Note that power systems typically operate at a high-voltage, stable solution. Thus, other power flow solutions, particularly those exhibiting low-voltage magnitude, are important to power system stability assessment and bifurcation analysis [11]- [15].

Convergence of local solution methods such as Newton Raphson method strongly depends on the selected initialization. Thus, initializing a local algorithm with various power flow solutions corresponding to random operating points is one approach for computing multiple local optima.

1.3. LITERATURE REVIEW

This section overviews convex relaxations of the power flow equations. Different variations of relevant power flow relaxation including Semi-Definite Programming, Second-Order Cone Programming, and Linear relaxation of power flow equation are overviewed in this section.

1.3.1. Semidefinite Programming Relaxations of the Power Flow Equations.

Expressing voltage in rectangular coordinate turns the power flow equations into a quadratic polynomials in the voltage components V_d and V_q. Having power flow equations as a quadratic polynomials facilitates the application of polynomial optimization theory, including the Shore relaxation and hierarchies of moment/sum-of-squares relaxations which are explained in the following subsections.

1.3.1.1. The Shor relaxation. The shore relaxation is a SDP relaxation of non-convex quadratically constrained quadratic programs (QCQPs) which was first introduced in 1987 [16]. The first application of the Shor relaxation on power system problems was the relaxation of the optimal power flow (OPF) problem [17]. The SDP relaxation of OPF problems became an active avenue of research after showing that the SDP relaxation can solve the OPF problem globally for many IEEE test cases [18]. The first step in implementing Shor relaxation of power flow equations is expressing power flow equations such that all non-convexities contained within a rank constraint. The SDP relaxation of power flow equation is then developed by neglecting the rank constraint.

Let e_k be defined as the k^{th} column of the identity matrix. For each bus $i \in \mathcal{N}$, define the matrices $L_{P,k}$, $L_{Q,k}$, M_k, and N_k as follow:

$$L_{P,k} = \frac{1}{2}\begin{bmatrix} \mathrm{Re}(Y^T e_k e_k^T + e_k e_k^T Y) & \mathrm{Im}(Y^T e_k e_k^T - e_k e_k^T Y) \\ \mathrm{Im}(Y^T e_k e_k^T - e_k e_k^T Y) & \mathrm{Re}(Y^T e_k e_k^T + e_k e_k^T Y) \end{bmatrix}, \tag{1.8}$$

$$L_{Q,k} = -\frac{1}{2}\begin{bmatrix} \mathrm{Im}(Y^T e_k e_k^T + e_k e_k^T Y) & \mathrm{Re}(Y^T e_k e_k^T - e_k e_k^T Y) \\ \mathrm{Re}(Y^T e_k e_k^T - e_k e_k^T Y) & \mathrm{Im}(Y^T e_k e_k^T + e_k e_k^T Y) \end{bmatrix}, \tag{1.9}$$

$$M_k = \begin{bmatrix} e_k e_k^T & 0 \\ 0 & e_k e_k^T \end{bmatrix}, \tag{1.10}$$

$$N_k = \begin{bmatrix} 0 & 0 \\ 0 & e_k e_k^T \end{bmatrix}. \tag{1.11}$$

Using these matrices, the power flow equations can be expressed as:

$$P_i = \mathrm{tr}(L_{P,k} W), \tag{1.12}$$

$$Q_i = \mathrm{tr}(L_{Q,k} W), \tag{1.13}$$

$$V_i^2 = \mathrm{tr}(L_k W), \tag{1.14}$$

$$0 = \mathrm{tr}(N_1 W), \tag{1.15}$$

$$W = x x^T. \tag{1.16}$$

where $x = [V_{d1} \ldots V_{dn} V_{q1} \ldots V_{qn}]^T$. Note that equation (1.15) sets the angle at the slack bus to zero. Note that equation (1.16) contains all the non-convexities. To form the SDP relaxation equation (1.16) can be replaced with a less stringent positive semi-definite constraint as follow:

$$W \succeq 0. \tag{1.17}$$

After solving the SDP relaxation optimization problem if the solution W^* satisfies the rank condition,

$$\mathrm{rank}(W) = 1, \tag{1.18}$$

then the SDP relaxation is exact and globally optimal decision variables can be recovered. Let λ be the non-zero eigenvalue of the solution W^* with associated unit-length eigenvector v. Denote v_d and v_q as the vectors consisting of the entries of v from v_1 to v_n and v_{n+1} to v_{2n}, respectively. The globally optimal voltage phasors are

$$V^* = \sqrt{\lambda}(v_d + jv_q). \tag{1.19}$$

The Shor relaxation can also be implemented as a complex value relaxation. Interested readers are directed to [7] for more information. Despite being exact for many IEEE test systems, there are multiple test cases in which the Shor relaxation fails to be exact. Thus, exactness of the Shor relaxation for different optimization problems in power system including the OPF problem remains an active area of research.

1.3.1.2. Moment/sum-of-square relaxation hierarchies. Despite solving the OPF problem globally for many IEEE test cases, there are several test cases in which the Shor relaxation leaves a reasonable optimality gap behind. One approach to solve these test cases globally is the Lasserre hierarchy for polynomial optimization problem. Lasserre hierarchy for polynomial optimization problem is the generalization of SDP relaxation (i.e., Shor relaxation) that can solve every polynomial optimization globally under specific technical condition [19, 20]. Relaxation from the Lasserre hierarchy are formulated as SDPs with matrices of increasing size. In addition to the Lasserre hierarchy, several other closely related relaxations based on Lasserre hierarchy are proposed to solve optimization problems in power systems. Interested readers are directed to [7] for more information.

1.3.2. Second-Order Cone Programming Relaxation of the Power Flow Equations. SOCP relaxation of power system optimization problems was first introduced by Jabr's formulation of the OPF problem for radial networks [21]. Different power flow mod-

els, bus injection and branch flow models, give rise to various SOCP relaxations of power system optimization problems. This section overviews various SOCP relaxations for power system problems.

1.3.2.1. Bus injection model relaxations. The first group of SOCP relaxations, Jabr's relaxation [21] and the Quadratic Convex (QC) relaxation, are based on the bus injection model of the power flow equations which are discussed in following sections. Note that the *Strong SOCP* relaxation proposed in [22] strengthens Jabr's relaxation with a variety of linear constraints. More information about those linear constraints can be found in [7]. Moreover, the tightness of Jabr and strong SOCP relaxations are compared with other relaxations' tightness in Figure 1.2.

- Jabr's SOCP relaxation. Jabr's SOCP relaxation [21] convexify the power flow equations for radial network by defining lifted variables for the squared voltage magnitude at bus i, $c_{ii} = |V_i|^2 = V_{di}^2 + V_{qi}^2$, the real part of the product of the voltage phasors at buses i and k, $c_{ik} = |V_i||V_k|cos(\theta_i - \theta_k) = V_{di}V_{dk} + V_{qi}V_{qk}$, and negative imaginary part of the product of the voltage phasors at buses i and k, $s_{ik} = -|V_i||V_k|sin(\theta_i - \theta_k) = V_{di}V_{qk} - V_{qi}V_{dk}$. These lifted variables, which were first proposed in [23], results in the following representation of the power flow equations for a radial network:

$$P_i = G_{ii}c_{ii} + \sum_{\substack{k=1,\dots,n \\ k\neq i}} G_{ik}c_{ik} - B_{ik}s_{ik}, \qquad \forall i \in \mathcal{N}, \tag{1.20a}$$

$$Q_i = -B_{ii}c_{ii} + \sum_{\substack{k=1,\dots,n \\ k\neq i}} -B_{ik}c_{ik} - G_{ik}s_{ik}, \qquad \forall i \in \mathcal{N}, \tag{1.20b}$$

$$c_{ik} = c_{ki}, \qquad \forall (i,k) \in \mathcal{L} \tag{1.20c}$$

$$s_{ik} = -s_{ki}, \qquad \forall (i,k) \in \mathcal{L} \tag{1.20d}$$

$$c_{ik}^2 + s_{ik}^2 = c_{ii}c_{kk}, \qquad \forall (i,k) \in \mathcal{L}. \tag{1.20e}$$

Despite being exact for radial networks, the power flow formulation in (1.20) is a relaxation for mesh networks due to the fact that it does not ensure the ability to recover a set of voltage angles that sum to zero around each loop [7]. Let θ_i denotes the voltage angle associated with bus i. Augmenting (1.20) with the nonconvex constraint $\tan(\theta_k - \theta_i) = \frac{s_{ik}}{c_{ik}}, \forall (i,k) \in \mathcal{L}$ results in a formulation that is equivalent to the power flow equations for a mesh network [7].

Note that equality constraint (1.20e) makes the formulation (1.20) nonconvex. The formulation (1.20) convexifies by replacing (1.20e) with a less-stringent inequality constraint:

$$c_{ik}^2 + s_{ik}^2 \leqslant c_{ii} c_{kk} \qquad \forall (i,k) \in \mathcal{L}. \tag{1.21}$$

Note that equation (1.21) is a rotated SOCP constraint. Thus, standard SOCP solution techniques can be applied to the resulting problem. The formulation defined by (1.20a)-(1.20d), (1.21) is hereafter denoted as "Jabr's relaxation".

- QC Relaxation. The "Quadratic Convex" (QC) relaxation [24] extends Jabr's relaxation by adding new variables for the voltage angle, θ_i, and voltage magnitude, $|V_i|$, $\forall i \in \mathcal{N}$. These new variables enables QC relaxation to convexify trigonometric terms, in the polar representation of the power flow equations, using linear and SOCP constraints.

  The QC relaxation is particularly effective when applied to OPF problems with small admissible ranges for both voltage magnitude and angle differences between connected busses. Moreover, the QC relaxation's constraints implicitly account for the relaxation of the angle consistency condition around cycles. Thus, the QC relaxation inherently can be applicable to mesh networks. The QC relaxation of the power flow equations and optimal power flow problems are explained in detail in Section 1.6.

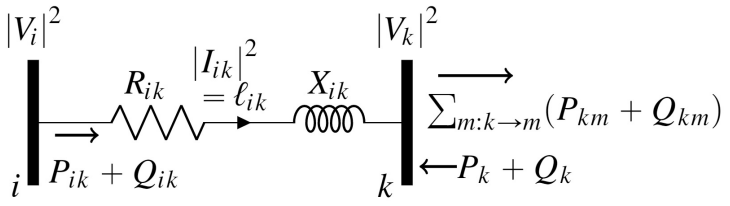

Figure 1.1. Explanation of the variables in the DistFlow equations for line $(i, k) \in \mathcal{L}$ [7].

1.3.2.2. Branch flow model relaxations. The branch flow formulation of power flow equations can be convexified as SOCP relaxations. This section overviews the branch flow relaxation derived from the DistFlow equations [7] and the SOCP relaxation in [25, 26].

- Relaxation of DistFlow Equations. DistFlow is a power flow representation for radial network that focuses on currents and powers on the branches. DistFlow has been used mainly for modeling distribution circuits which tend to be radial [27, 28].

  Let $\mathcal{L}$ denotes the set of branches, with $i \to k$ representing a branch connecting buses i and k where bus k is located "downsream" (further from the substation in a radial distribution system) from bus i. Let P_{ik}, Q_{ik} and ℓ_{ik} be the active power, reactive power, and the squared magnitude of current flowing out from buses i to bus k. With lines modeled as series impedances $R_{ik} + jX_{ik}$ (see Figure 1.1), the DistFlow equations are defined for each line $(i, k) \in \mathcal{L}$ as:

$$P_{ik} = R_{ik}\ell_{ik} - P_k + \sum_{m:k\to m} P_{km}, \tag{1.22a}$$

$$Q_{ik} = X_{ik}\ell_{ik} - Q_k + \sum_{m:k\to m} Q_{km}, \tag{1.22b}$$

$$|V_k|^2 = |V_i|^2 - 2(R_{ik}P_{ik} + X_{ik}Q_{ik}) + (R_{ik}^2 + X_{ik}^2)\ell_{ik}, \tag{1.22c}$$

$$\ell_{ik}|V_i|^2 = P_{ik}^2 + Q_{ik}^2. \tag{1.22d}$$

Similar to (1.20), the DistFlow equations neglect the voltage phase angles and are thus an exact representation for radial networks but a relaxation of mesh networks. It is important to note that the DistFlow equations are linear in the flows of squared current magnitude ℓ_{ik}, active power P_{ik} and reactive power Q_{ik} on line $(i,k) \in \mathcal{L}$ as well as the squared voltage magnitude $|V_i|^2$ at each bus $i \in \mathcal{N}$. The branch flow relaxation is formed by replacing the equality constraint $\ell_{ik}|V_i|^2 \geqslant P_{ik}^2 + Q_{ik}^2 \forall (i,k) \in \mathcal{L}$ with an inequality that takes the form of a rotated SOCP constraint:

$$\ell_{ik}|V_i|^2 \geqslant P_{ik}^2 + Q_{ik}^2, \qquad \forall (i,k) \in \mathcal{L}. \tag{1.23}$$

An exactness dominance comparison between DistFlow and other power flow relaxations is illustrated in Figure 1.2.

1.3.3. Linear Relaxation of the Power Flow Equations. Compared to SDP and SOCP relaxations, linear relaxation usually yields a weaker objective value bounds (i.e. they are not as tight as SDP and SOCP relaxations). However, linear relaxations usually have better computational advantages compared to SDP and SOCP relaxations. This section overviews the different linear relaxation of power flow equations.

Depending on the form of the objective function, linear relaxations can be formulated either as linear programs or quadratic programs.

1.3.3.1. The network flow relaxation. The power flow equation requires that the flows entering and leaving a node obey Ohm's and Kirchhoff's laws. In contrast, the *network flow* relaxation [29, 30] does not enforce Ohm's and Kirchhoff's laws on power flow entering and leaving a node. Instead the *network flow* relaxation requires active and reactive power losses on each line to be non-negative. Let $g_{sh,i} + jb_{sh,i}$ denote the shunt admittance at bus i. Denote the total shunt susceptance associated with the Π-circuit model of the line (i,k) as $b_{c,ik}$. The network flow relaxation is formulated in terms of the active power flows P_{ik} and reactive power flows Q_{ik} for each line $(i,k) \in \mathcal{L}$ and the squared voltage magnitudes

$|V_i|^2$ at each bus $i \in \mathcal{N}$:

$$P_i = g_{sh,i}|V_i|^2 + \sum_{(i,k)\in\mathcal{L}} P_{ik} + \sum_{(k,i)\in\mathcal{L}} P_{ki}, \qquad \forall i \in \mathcal{N}, \tag{1.24a}$$

$$Q_i = -b_{sh,i}|V_i|^2 + \sum_{(i,k)\in\mathcal{L}} Q_{ik} + \sum_{(k,i)\in\mathcal{L}} Q_{ki}, \qquad \forall i \in \mathcal{N}, \tag{1.24b}$$

$$P_{ik} + P_{ki} \geqslant 0, \qquad \forall (i,k) \in \mathcal{L}, \tag{1.24c}$$

$$Q_{ik} + Q_{ki} \geqslant -\frac{b_{c,ik}}{2}(|V_i|^2 + |V_k|^2), \qquad \forall (i,k) \in \mathcal{L}. \tag{1.24d}$$

Note that the network flow formulation in (1.24) is a valid relaxation for systems where all lines have series impedances with non-negative resistances and non-negative reactances [29, 30].

1.3.3.2. The copper plate relaxation. The "copper plate" relaxation does not enforce power flow equations in order to yield a simple power balance constraint relating all power injections in the network. Using the same definitions as in Section 1.3.3.1, the copper plate model is:

$$\sum_{i\in\mathcal{N}} P_i \geqslant \sum_{i\in\mathcal{N}} g_{sh,i}|V_i|^2, \tag{1.25a}$$

$$\sum_{i\in\mathcal{N}} Q_i \geqslant -\sum_{i\in\mathcal{N}} b_{sh,i}|V_i|^2 - \sum_{(i,k)\in\mathcal{L}} \frac{b_{c,ik}}{2}\left(|V_i|^2 + |V_k|^2\right). \tag{1.25b}$$

The copper plate model is a valid relaxation of power flow equations for systems where all lines have series impedances with non-negative resistances and non-negative reactances [29, 30].

1.3.3.3. The Taylor-Hoover relaxation. The linear power flow relaxation proposed by Taylor and Hoover in [31] uses lifted variable $|V_i|^2$ for the squared voltage magnitude at bus $i \in \mathcal{N}$. Furthermore, different variables including P_{ik}, P_{ki}, Q_{ik} and Q_{ki} are used to account for the active and reactive power flows into each terminal of line $(i,k) \in \mathcal{L}$. For a line modeled as a Π circuit with mutual admittance $g_{ik} + jb_{ik}$ and total shunt susceptance

$b_{c,ik}$, the Taylor-Hoover relaxation [31] enforces following equalities

$$g_{ik}\left(P_{ik}-P_{ki}\right)-b_{ik}\left(Q_{ik}-Q_{ki}\right)=\left(g_{ik}^{2}+b_{ik}^{2}+b_{ik}\frac{b_{c,ik}}{2}\right)\left(|V_{i}|^{2}-|V_{k}|^{2}\right), \tag{1.26a}$$

$$b_{ik}\left(P_{ik}+P_{ki}\right)+g_{ik}\left(Q_{ik}+Q_{ki}\right)=-g_{ik}\frac{b_{c,ik}}{2}\left(|V_{i}|^{2}+|V_{k}|^{2}\right). \tag{1.26b}$$

The equalities in (1.26) results from the relaxation of linear combinations of the nonlinear expressions for the active and reactive line flows. Note that non-physical negative line losses may result when using this relaxation [29].

1.3.3.4. McCormick relaxations. McCormick envelopes can be employed to construct linear relaxations of the following rectangular power flow equations if the bounds on variables are known [32]:

$$P_{i}=\sum_{k=1}^{n}V_{di}\left(G_{ik}V_{dk}-B_{ik}V_{qk}\right)+V_{qi}\left(B_{ik}V_{dk}+G_{ik}V_{qk}\right) \tag{1.27a}$$

$$Q_{i}=\sum_{k=1}^{n}V_{di}\left(-B_{ik}V_{dk}-G_{ik}V_{qk}\right)+V_{qi}\left(G_{ik}V_{dk}-B_{ik}V_{qk}\right), \tag{1.27b}$$

$$|V_{i}|^{2}=V_{di}^{2}+V_{qi}^{2}. \tag{1.27c}$$

where $Y=G+jB$ is the line admittance matrices and $V=V_{d}+jV_{q}$ is the voltage at the bus in rectangular coordinate, respectively. The McCormick relaxation of a bilinear product formulates as follows:

$$\langle xy\rangle^{M}=\left\{t:\begin{cases}t\geqslant x_{min}y+y^{min}x-x^{min}y^{min},\\ t\geqslant x^{max}y+y^{max}x-x^{max}y^{max},\\ t\leqslant x^{min}y+y^{max}x-x^{min}y^{max},\\ t\leqslant x^{max}y+y^{min}x-x_{max}y^{min}.\end{cases}\right. \tag{1.28a}$$

where x and y are generic variables with bounds x^{min}, x^{max}, and y^{min}, y^{max} and $\langle xy \rangle^M$ denotes the McCormick envelopes.

The "Rectangular McCormick" relaxation in [22] applies (1.28a) to the rectangular form of the power flow equations (1.27) using the bounds $V_{di}, V_{qi} \in [-V_i^{max}, V_i^{max}]$. The tightness of the McCormick relaxation depends on the size of the bounds on the voltage magnitude. Therefore, bound tightening techniques, which use convex relaxations to infer tighter bounds than those initially specified in the power flow problem data, can improve the McCormick relaxation's tightness.

A stronger linear relaxation is derived by applying McCormick envelopes to the formulation used in Jabr's relaxation (1.20) [22]. The bounds available for the variables c_{ik} and s_{ik} facilitate a tighter linear relaxation when combined with "lifted" variables C_{ik}, S_{ik}, and $D_{ik}, \forall (i,k) \in \mathcal{L}$:

$$-V_i^{max} V_k^{max} \leqslant c_{ik}, s_{ik} \leqslant V_i^{max} V_k^{max}, \tag{1.29a}$$

$$(v_i^{min})^2 \leqslant c_{ii} \leqslant (v_i^{max})^2, \tag{1.29b}$$

$$C_{ik} + Sik = D_{ik}, \tag{1.29c}$$

$$C_{ik} \geqslant 0, S_{ik} \geqslant 0, \tag{1.29d}$$

$$D_{ik} \in \langle c_{ii} c_{kk} \rangle^M, C_{ik} \in \langle c_{ik} c_{ik} \rangle^M, S_{ik} \in \langle s_{ik} s_{ik} \rangle^M, \tag{1.29e}$$

$$\text{Equations (1.20a)} - \text{(1.20d)}. \tag{1.29f}$$

The McCormick relaxation formulation in (1.29) is referred as alternative McCormick relaxation.

1.3.3.5. Bienstock-Munoz LP relaxations. The approach in [33] developes a family of LPs that approximate (to arbitrary accuracy) the solution of power system optimization problems that may include integer constraints. This approach is particularly useful for power system optimization problems that have small treewidth since the numbers of variables and constraints in the resulting LPs scale exponentially with the treewidth, linearly with the

size of the network, and logarithmically with the desired accuracy. The "treewidth" of a graph is defined as one less than the size of the largest maximum clique among all possible chordal extensions of the graph. The approach in [33] has strong theoretical properties but its effectiveness remain to be demonstrated for practical test cases.

1.3.3.6. Mixed-integer linear programming relaxations. Several relaxations employ discrete variables to model the power flow non-linearities. A relaxation proposed in [25] uses a technique from [34] to discretize the voltage component variables using binary variables. Specifically the discretization in [25] effectively represents each variable as a number in a binary format to a specified precision (i.e., a generic non-negative continuous variable u is written as $u = \sum_{k=1}^{T} 2^{-k} y_k + \delta$, where the precision is given by the integer parameters $T > 1$, $y \in 0, 1^T$, and $0 \geqslant \delta \geqslant 2^{-T}$). With this discretization for each variable, the bilinear products in the power flow equations can be written as the sum of the products of the continuous and binary variables. Since each term in these summations can be exactly linearized, the power flow equations can be represented to a specified precision as a MILP. Thus, the precision of the formulation can be precisely controlled.

A similar discretization approach is proposed in [35] for problems with radial network topologies. Formulated in the context of graphical models, this approach exploits radial network structures through a use of a dynamic programming algorithm. This algorithm has a running time that is linear in the network size and polynomial in the discretization precision. Future work proposed in [35] includes several directions for extension of this approach to more general network topologies.

The discretization approach proposed in [36] uses eigenvector calculation to reformulate the power flow equations as a symmetric paraboloids. Delaunay triangulation and binary variables are then used to develop piecewise-line interpolation of the paraboloid functions. A further contribution of [36] is a disjunctive convex optimization approach that constructs outer approximations of the paraboloids to obtain a relaxation.

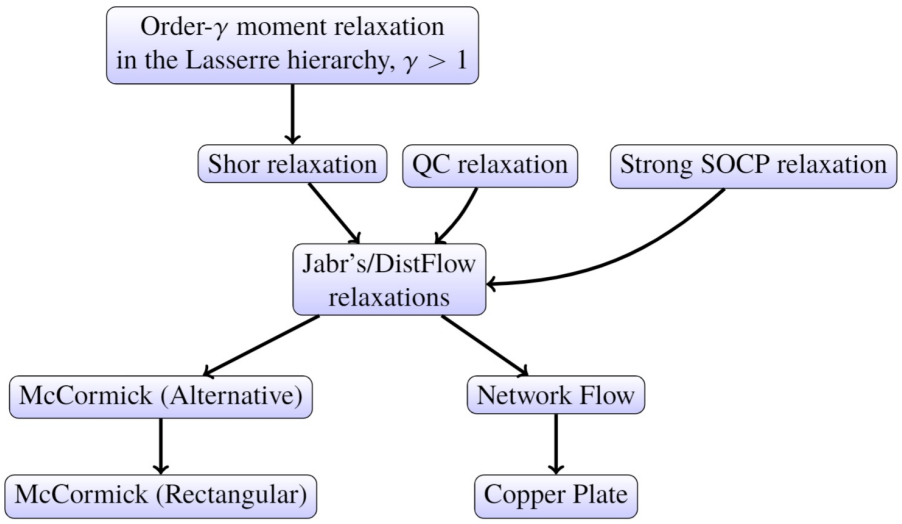

Figure 1.2. Proven dominance relationships among relaxations. The arrows point from the tighter relaxation to the dominated relaxation. Both the QC relaxation and the Strong SOCP relaxation neither dominate nor are dominated by the Shor relaxation [5]. Note that combining relaxations which do not have a dominance relationship yields a generally tighter relaxation (e.g., the combination of the Shor and QC relaxations studied in [38] is generally tighter than Shor and QC relaxations individually).

1.4. THE OPTIMAL POWER FLOW PROBLEM

The optimal power flow (OPF) problem seeks an operating point that optimizes a specified objective subject to constraints from the network physics and engineering limits. Using the nonlinear AC power flow model to accurately represent the power flow physics results in the AC OPF problem, which is non-convex, may have multiple local optima [37], and is generally NP-Hard [3, 4].

This section provides a mathematical description of the OPF problem as it is classically formulated. Consider an n-bus system, where $\mathcal{N} = \{1, \ldots, n\}$, $\mathcal{G}$, and $\mathcal{L}$ are the sets of buses, generators, and lines. Let $P_i^d + jQ_i^d$ and $P_i^g + jQ_i^g$ represent the active and reactive load demand and generation, respectively, at bus $i \in \mathcal{N}$, where $j = \sqrt{-1}$. Let $g_{sh,i} + jb_{sh,i}$ denote the shunt admittance at bus i. Let V_i and θ_i represent the voltage magnitude and angle at bus $i \in \mathcal{N}$. For each generator $i \in \mathcal{G}$, define a quadratic generation cost function

with coefficients $c_{2,i} \geqslant 0$, $c_{1,i}$, and $c_{0,i}$. Denote $\theta_{lm} = \theta_l - \theta_m$. Specified upper and lower limits are denoted by $(\overline{\cdot})$ and $(\underline{\cdot})$, respectively. Buses $i \in \mathcal{N}\backslash\mathcal{G}$ have generation limits set to zero.

Each line $(l,m) \in \mathcal{L}$ is modeled as a Π circuit with mutual admittance $g_{lm} + jb_{lm}$ and shunt admittance $jb_{sh,lm}$. (Our approach is applicable to more general line models, such the MATPOWER [43] model that allows for off-nominal tap ratios and non-zero phase shifts.) Let P_{lm}, Q_{lm}, and $\overline{S}_{lm}$ represent the active and reactive power flows and the maximum apparent power flow limit on the line that connects buses l and m.

Using these definitions, the OPF problem is

$$\min \quad \sum_{i\in\mathcal{G}} c_{2i}\left(P_i^g\right)^2 + c_{1i}\,P_i^g + c_{0i} \tag{1.30a}$$

subject to $\quad (\forall i \in \mathcal{N},\ \forall\,(l,m) \in \mathcal{L})$

$$P_i^g - P_i^d = g_{sh,i}\,V_i^2 + \sum_{\substack{(l,m)\in\mathcal{L}\\ \text{s.t. } l=i}} P_{lm} + \sum_{\substack{(l,m)\in\mathcal{L}\\ \text{s.t. } m=i}} P_{ml}, \tag{1.30b}$$

$$Q_i^g - Q_i^d = -b_{sh,i}\,V_i^2 + \sum_{\substack{(l,m)\in\mathcal{L}\\ \text{s.t. } l=i}} Q_{lm} + \sum_{\substack{(l,m)\in\mathcal{L}\\ \text{s.t. } m=i}} Q_{ml}, \tag{1.30c}$$

$$\theta_{ref} = 0, \tag{1.30d}$$

$$\underline{P}_i^g \leqslant P_i^g \leqslant \overline{P}_i^g, \tag{1.30e}$$

$$\underline{Q}_i^g \leqslant Q_i^g \leqslant \overline{Q}_i^g, \tag{1.30f}$$

$$\underline{V}_i \leqslant V_i \leqslant \overline{V}_i, \tag{1.30g}$$

$$\underline{\theta}_{lm} \leqslant \theta_{lm} \leqslant \overline{\theta}_{lm}, \tag{1.30h}$$

$$P_{lm} = g_{lm}V_l^2 - g_{lm}V_lV_m\cos\left(\theta_{lm}\right) - b_{lm}V_lV_m\sin\left(\theta_{lm}\right), \tag{1.30i}$$

$$Q_{lm} = -\left(b_{lm} + b_{sh,lm}/2\right)V_l^2 + b_{lm}V_lV_m\cos\left(\theta_{lm}\right) - g_{lm}V_lV_m\sin\left(\theta_{lm}\right), \tag{1.30j}$$

$$\left(P_{lm}\right)^2 + \left(Q_{lm}\right)^2 \leqslant \left(\overline{S}_{lm}\right)^2, \tag{1.30k}$$

$$\left(P_{ml}\right)^2 + \left(Q_{ml}\right)^2 \leqslant \left(\overline{S}_{lm}\right)^2. \tag{1.30l}$$

The objective function (1.30a) minimizes the active power generation cost. Power balance at each bus enforces by constraints (1.30b) and (1.30c). Constraint (1.30d) sets the angle reference. Constraints (1.30e)–(1.30h) limit the active and reactive power generation, voltage magnitudes, and angle differences between connected buses. Constraints (1.30i)–(1.30j) relate the voltage phasors and power flows on each line, and (1.30k)–(1.30l) limit the apparent power flows into both terminals of each line.

1.5. QC RELAXATION

The quadratic convex (QC) relaxation [5] is one promising approach that uses convex envelopes around the non-convex terms including trigonometric functions, squared terms, and bilinear products. The tightness of the QC relaxation depends on the size of the variable bounds. QC relaxation is a type of convex optimization that minimizes a linear objective function over the convex area formed by convex envelopes. QC relaxation has been successful in solving or approximating the solutions of many practical problems, including NP-hard optimization problems. Overviews of QC relaxation and practice are available in reference [7].

QC relaxation problems can be solved efficiently (i.e., in polynomial time) for a globally optimal solution with robust primal−dual interior point methods using commercial tools (e.g., CPLEX, Gurobi, and Mosek).

1.6. QC RELAXATION OF THE POWER FLOW EQUATIONS

The QC relaxation is formed by defining new variables w_{ii}, w_{lm}, c_{lm}, and s_{lm} for the products of voltage magnitudes and the trilinear monomials representing the products of voltage magnitudes and trignometric functions for connected buses:

$$w_{ii} = V_i^2, \qquad \forall i \in \mathcal{N}, \tag{1.31a}$$

$$w_{lm} = V_l V_m, \qquad \forall (l,m) \in \mathcal{L}, \tag{1.31b}$$

$$c_{lm} = w_{lm} \cos(\theta_{lm}), \qquad \forall (l,m) \in \mathcal{L}, \tag{1.31c}$$

$$s_{lm} = w_{lm} \sin(\theta_{lm}), \qquad \forall (l,m) \in \mathcal{L}. \tag{1.31d}$$

For each line $(l,m) \in \mathcal{L}$, these definitions imply the following relationships between the variables w_{ll}, c_{lm}, and s_{lm}:

$$c_{lm}^2 + s_{lm}^2 = w_{ll} w_{mm}, \tag{1.32a}$$

$$c_{lm} = c_{ml}, \tag{1.32b}$$

$$s_{lm} = -s_{ml} \tag{1.32c}$$

The QC relaxation is formulated by enclosing the squared and bilinear product terms in convex envelopes, here represented as set-valued functions:

$$\langle x^2 \rangle^T = \left\{ \breve{x} : \begin{cases} \breve{x} \geqslant x^2, \\ \breve{x} \leqslant (\overline{x} + \underline{x})\, x - \overline{x}\underline{x}. \end{cases} \right. \tag{1.33a}$$

$$\langle xy \rangle^M = \left\{ \widetilde{xy} : \begin{cases} \widetilde{xy} \geqslant \underline{x}y + \underline{y}x - \underline{x}\underline{y}, \\ \widetilde{xy} \geqslant \overline{x}y + \overline{y}x - \overline{x}\overline{y}, \\ \widetilde{xy} \leqslant \underline{x}y + \overline{y}x - \underline{x}\overline{y}, \\ \widetilde{xy} \leqslant \overline{x}y + \underline{y}x - \overline{x}\underline{y}. \end{cases} \right. \tag{1.33b}$$

where $\breve{x}$ and $\widetilde{xy}$ are "dummy" variables representing the corresponding set. The envelope $\langle x^2 \rangle^T$ is the convex hull of the square function. The so-called "McCormick envelope" $\langle xy \rangle^M$ is the convex hull of a bilinear product [32].

The QC relaxation also formulates convex envelopes $\langle \sin(x) \rangle^S$ and $\langle \cos(x) \rangle^C$ for the trigonometric functions:

$$\langle \sin(x) \rangle^S = \begin{cases} \breve{S} : \begin{cases} \breve{S} \leqslant \cos\left(\frac{x^m}{2}\right)\left(x - \frac{x^m}{2}\right) + \sin\left(\frac{x^m}{2}\right), \\ \breve{S} \geqslant \cos\left(\frac{x^m}{2}\right)\left(x + \frac{x^m}{2}\right) - \sin\left(\frac{x^m}{2}\right), \\ \breve{S} \geqslant \frac{\sin(\underline{x}) - \sin(\overline{x})}{\underline{x} - \overline{x}}(x - \underline{x}) + \sin(\underline{x}) \text{ if } \underline{x} \geqslant 0, \\ \breve{S} \leqslant \frac{\sin(\underline{x}) - \sin(\overline{x})}{\underline{x} - \overline{x}}(x - \underline{x}) + \sin(\underline{x}) \text{ if } \overline{x} \leqslant 0. \end{cases} \end{cases} \tag{1.34a}$$

$$\langle \cos(x) \rangle^C = \begin{cases} \breve{C} : \begin{cases} \breve{C} \leqslant 1 - \frac{1 - \cos(x^m)}{(x^m)^2} x^2, \\ \breve{C} \geqslant \frac{\cos(\underline{x}) - \cos(\overline{x})}{\underline{x} - \overline{x}}(x - \underline{x}) + \cos(\underline{x}). \end{cases} \end{cases} \tag{1.34b}$$

where $x^m = \max(|\underline{x}|, |\overline{x}|)$. The dummy variables $\breve{S}$ and $\breve{C}$ again represent the corresponding set. For $-90^\circ < \underline{x} < \overline{x} < 90^\circ$, bounds on the sine and cosine functions are

$$\underline{s} = \sin(\underline{x}) \leqslant \sin(x) \leqslant \overline{s} = \sin(\overline{x}), \tag{1.35a}$$

$$\underline{c} = \min(\cos(\underline{x}), \cos(\overline{x})) \leqslant \cos(x) \leqslant \overline{c} = \begin{cases} \max(\cos(\underline{x}), \cos(\overline{x})), & \text{if } \operatorname{sign}(\underline{x}) = \operatorname{sign}(\overline{x}), \\ 1, & \text{otherwise.} \end{cases} \tag{1.35b}$$

Slightly abusing notation, the QC relaxation is formed by replacing the square, product, and trigonometric terms in (1.30) with the variables w_{ii}, w_{lm}, c_{lm}, and s_{lm} in these envelopes:

$$\min \quad \sum_{i\in\mathcal{G}} c_{2i}\left(P_i^g\right)^2 + c_{1i}\,P_i^g + c_{0i} \tag{1.36}$$

subject to $\quad (\forall i \in \mathcal{N},\ \forall\,(l,m) \in \mathcal{L})$

$$P_i^g - P_i^d = g_{sh,i}\,w_{ii} + \sum_{\substack{(l,m)\in\mathcal{L}\\ \text{s.t. } l=i}} P_{lm} + \sum_{\substack{(l,m)\in\mathcal{L}\\ \text{s.t. } m=i}} P_{ml}, \tag{1.37}$$

$$Q_i^g - Q_i^d = -b_{sh,i}\,w_{ii} + \sum_{\substack{(l,m)\in\mathcal{L}\\ \text{s.t. } l=i}} Q_{lm} + \sum_{\substack{(l,m)\in\mathcal{L}\\ \text{s.t. } m=i}} Q_{ml}, \tag{1.38}$$

$$(\underline{V}_i)^2 \leqslant w_{ii} \leqslant (\overline{V}_i)^2, \tag{1.39}$$

$$P_{lm} = g_{lm}w_{ll} - g_{lm}c_{lm} - b_{lm}s_{lm}, \tag{1.40}$$

$$Q_{lm} = -\left(b_{lm} + b_{sh,lm}/2\right)w_{ii} + b_{lm}c_{lm} - g_{lm}s_{lm}, \tag{1.41}$$

$$w_{ii} \in \left\langle V_i^2 \right\rangle^T, \tag{1.42}$$

$$w_{lm} \in \left\langle V_l V_m \right\rangle^M, \tag{1.43}$$

$$c_{lm} \in \left\langle w_{lm}\left\langle \cos\left(\theta_{lm}\right)\right\rangle^C \right\rangle^M, \tag{1.44}$$

$$s_{lm} \in \left\langle w_{lm}\left\langle \sin\left(\theta_{lm}\right)\right\rangle^S \right\rangle^M, \tag{1.45}$$

$$c_{lm}^2 + s_{lm}^2 \leqslant w_{ll}\,w_{mm} \tag{1.46}$$

Equations (1.30d)–(1.30h), (1.30k)–(1.30l), (1.32b), (1.32c). (1.47)

Note that the non-convex constraint (1.32a) is relaxed to (1.46) using a less-stringent rotated second-order cone constraint [21]. Also note that the trilinear terms in (1.30i) and (1.30j) are addressed in (1.43)–(1.45) by recursively applying McCormick envelopes (1.33b) (i.e., first applying (1.33b) to the product of voltage magnitudes to obtain w_{lm} and then to the product of w_{lm} and $\left\langle \cos\left(\theta_{lm}\right)\right\rangle^C$ or $\left\langle \sin\left(\theta_{lm}\right)\right\rangle^S$).

The optimization problem (1.36) is a second-order cone program (SOCP), which is convex and can be solved efficiently using commercial tools (e.g., CPLEX, Gurobi, and Mosek).

1.7. CONTRIBUTIONS

The accuracy of convex relaxation methods strongly depends on the relaxation's tightness. This dissertation proposes multiple improvements to tighten the QC relaxation of the OPF problem. The first improvement is based on the observation that adding redundant constraints to a non-convex optimization problem can tighten a relaxation [49]. One approach for constructing appropriate constraints is to change coordinate systems. We derive constraints based on a coordinate change using voltage magnitude differences in addition to the voltage magnitudes themselves. Bound tightening techniques are often more effective for variables representing voltage magnitude differences, thus resulting in tighter constraints. A bound tightening approach is described in Section 1.6.

The second improvement is related to the trilinear monomials formed by the product of the voltage magnitudes and the trigonometric functions in the polar representation of the power flow equations (i.e., $V_l V_m \cos(\theta_{lm})$ or $V_l V_m \sin(\theta_{lm})$). Previous formulations of the QC relaxation [5, 38] treat these monomials with recursive application of McCormick envelopes [32]. McCormick envelopes are a type of convex relaxation used to convexity bilinear product terms. While McCormick envelopes form the convex hull (the convex hull of set x is the smallest convex set that contains x) of bilinear monomials, recursive application of McCormick envelopes does not necessarily yield the convex hulls of trilinear monomials. We apply the potentially tighter envelopes developed by Meyer and Floudas [39, 40], which form the convex hulls of trilinear monomials.

The third improvement is based on the representation of admittances in polar format in the power flow equations, which can yield tighter envelopes for trigonometric terms compared to those in original QC relaxation. Thus, the new representation of the power flow equations can potentially strengthen the QC relaxations of OPF problems.

The fourth improvement for the QC relaxation of OPF problem exploits the ability to choose a complex base power in the per unit normalization. Selecting a complex base power rotates the power flow equations and put the arguments of trigonometric terms within

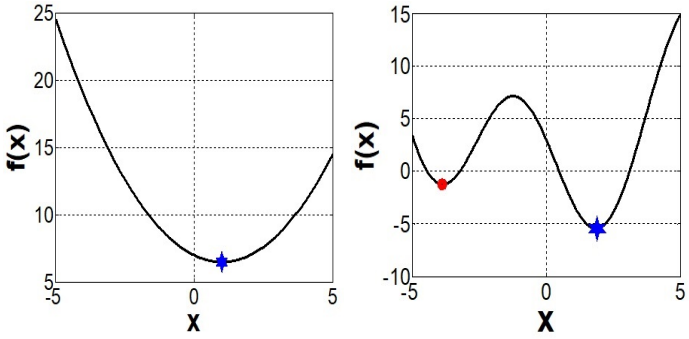

(a) A convex function with corresponding global optimum (blue star).

(b) A nonconvex function with corresponding global (blue star) and local (red circle) optimum.

Figure 1.3. Global and local optimum illustration.

advantageous spans. Appropriately rotating the base power can make the minimum and maximum values taken by trigonometric arguments be sign-definite, which facilitates the application of tighter envelopes for the trigonometric terms. This improvement has the potential to significantly strengthen the QC relaxations of OPF problems.

1.8. TERMINOLOGIES

Different terminologies used throughout the dissertation are defined here before delving into the problem formulation, beginning with global and local solutions. Figure 1.3a shows a function with its minimum (i.e., blue star). The blue star in Figure 1.3a is the global minimum of function since there is no point with a lower objective function value than this point. In Figure 1.3b, the red circle is the minimum point in a close neighboring region but it is not the global minimum for the function because there is another point (the blue star) with lower objective function than this point. Thus, the red circle is a local minimum and the blue star is the global minimum for the function.

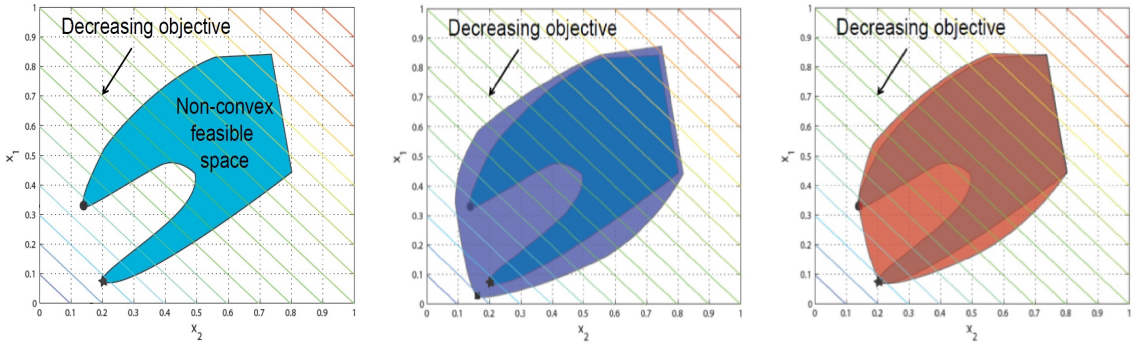

(a) A convex function with corresponding global optimum (blue star).

(b) A nonconvex function with corresponding global (blue star) and local (red circle) optimum.

(c) A nonconvex function with corresponding global (blue star) and local (red circle) optimum.

Figure 1.4. Illustrating of tight and loos relaxations for a nonconvex function.

Another terminology that is used throughout the report is convex relaxation. A space is convex if and only if it contains all points on the line segments connecting every pair of points in that space. A convex relaxation encloses the feasible space of a non-convex problem in a larger convex space. Figure 1.4a illustrates a non-convex feasible space of an example optimization problem where black circle and star indicate the local and global optimum in the feasible space. A convex relaxation of feasible space is illustrated in Figure 1.4b where the global minimum of the original feasible space is not equal to the global minimum of convex relaxation of the problem. The relaxation gap is the difference between the global solution of original problem and the global solution of its convex relaxation. A non-zero relaxation gap implies that the convex relaxation for the problem can be further tightened. Conversely the convex relaxation provided for original function in Figure 1.4c is tight since the global optimum of the original problem and its convex relaxation are equal. The AC OPF problem is defined next.

PAPER

I. EMPIRICAL INVESTIGATION OF NON-CONVEXITIES IN OPTIMAL POWER FLOW PROBLEMS

ABSTRACT

Optimal power flow (OPF) is a central problem in the operation of electric power systems. An OPF problem optimizes a specified objective function subject to constraints imposed by both the non-linear power flow equations and engineering limits. These constraints can yield non-convex feasible spaces that result in significant computational challenges. Despite these non-convexities, local solution algorithms actually find the global optima of some practical OPF problems. This suggests that OPF problems have a range of difficulty: some problems appear to have convex or "nearly convex" feasible spaces in terms of the voltage magnitudes and power injections, while other problems can exhibit significant non-convexities. Understanding this range of problem difficulty is helpful for creating new test cases for algorithmic benchmarking purposes. Leveraging recently developed computational tools for exploring OPF feasible spaces, this paper first describes an empirical study that aims to characterize non-convexities for small OPF problems. This paper then proposes and analyzes several medium-size test cases that challenge a variety of solution algorithms.

1. INTRODUCTION

The optimal power flow (OPF) problem seeks an optimal operating point for an electric power system in terms of a specified objective function (e.g., minimizing generation cost, matching a desired voltage profile, etc.). The feasible space for an OPF problem is dictated by equality constraints corresponding to the network physics (i.e., the power flow equations) and inequality constraints determined by engineering limits on, e.g., voltage magnitudes, line flows, and generator outputs. Non-linear constraints from the power flow equations and the engineering limits can result in non-convex feasible spaces. This paper applies an empirical approach to characterize typical non-convexities that occur in OPF feasible spaces. The geometric structures characterized in this paper are based on projections of the power injections and voltage magnitudes.

OPF problems may have multiple local optima [1] and are generally NP-Hard [2, 3], even for radial networks [4]. Since first being formulated by Carpentier in 1962 [5], a broad range of algorithms have been applied to solve OPF problems, including Newton-Raphson, sequential quadratic programming, interior point methods, etc. [6, 7]. Convergence of many algorithms only ensures local optimality, i.e., no feasible points in the solution's immediate neighborhood have a better objective value. Other locally optimal points may exist outside of this immediate neighborhood, some of which may have substantially better objective values.

In contrast to local solvers, global algorithms seek the lowest-cost point in the entire feasible space. Provably obtaining the global solution is relevant for many analyses, such as multi-stage and robust optimization where providing any theoretical guarantees for the overall problem requires certifying global optimality of solutions to certain subproblems [8, 9]. Moreover, the large scale of power systems means that even small percentage improvements in operational efficiency can have a significant aggregate impact [10], thus motivating the development of global algorithms.

Many recently developed global algorithms employ convex relaxation techniques, which enclose the feasible space of an OPF problem in a larger convex space. Optimizing over the convex space provides a lower bound for the OPF problem's objective value, can certify OPF infeasibility, and, when the relaxation is *exact*, provides the globally optimal decision variables. A variety of convex relaxations are based on semidefinite programming (SDP) [2, 11–13] and second-order cone programming (SOCP) [14, 15]. Recent work is surveyed in [16].

For some practical OPF problems, these convex relaxations certify that the solutions obtained by local solvers are, in fact, globally optimal (or at least very near the global optimum) [2, 11–15, 17]. There also exist challenging test cases for which local solution algorithms may fail to yield globally optimal solutions and convex relaxations have large relaxation gaps [1, 18, 19]. Thus, the challenges inherent to solving OPF problems span a range of difficulties.

An OPF problem's difficulty is closely related to convexity characteristics of the problem's feasible space. The range of difficulties suggests that some OPF feasible spaces are "nearly convex" in terms of the voltage magnitudes and power injections, while others exhibit significant non-convexities. The development of sufficient conditions for exactness of some convex relaxation techniques [20] has implications for the convexity characteristics of a certain limited class of OPF problems [21]. In particular, these conditions imply that portions of the feasible spaces relevant to the minimization of active power generation are convex for OPF problems that satisfy non-trivial technical conditions. Previous work also shows that the feasible spaces of a more general class of OPF problems can have significant non-convexities [1, 22–30].

Although the existing literature makes significant progress, OPF convexity characteristics are not yet fully understood. This paper leverages two recently developed computational tools to better understand non-convexities in OPF feasible spaces. The first tool is an algorithm for reliably computing discretized representations of OPF feasible spaces [28].

The second tool is a continuation algorithm that identifies multiple local optima for OPF problems [31].

Using these tools, this paper describes an empirical analysis to better understand causes of OPF non-convexities. This analysis randomly constructs many small OPF test cases. These test cases are not directly representative of realistic power systems due to their small sizes. However, large problems may have subregions with similar features. Moreover, experience with convex relaxations of large-scale problems suggests that non-convexities are often associated with small subregions of the system [11, 12]. Thus, exploring the characteristics of these small test cases can provide useful lessons for understanding non-convexities in large problems. After construction, the test cases are screened to identify those likely to have non-convexities using a process based on an SDP relaxation. The feasible space computation algorithm in [28] is applied to the screened cases to characterize their non-convexities.

Observations and test cases in [1] suggest the importance of binding lower limits on voltage magnitudes and reactive power generation with regard to OPF non-convexities. All non-convexities characterized in our numerical experiment are also related to the lower limits on voltage magnitudes and reactive power generation. Our numerical experiment thus suggests that non-convexities are more frequently associated with lower limits on voltage magnitudes and reactive power generation than other constraints, at least for problems in the parameter ranges considered in our experiment.

This paper then extends the insights gained from this numerical experiment to develop challenging medium-size OPF problems based on modifications to the IEEE test cases. Modifying the system loading, voltage limits, and reactive power limits yields OPF problems where lower limits on voltage magnitudes and reactive power generation are binding. The resulting OPF problems have multiple local optima and challenge state-of-the-art convex relaxation techniques.

In addition to empirically validating the insights gained from small problems, these medium-size test cases can serve to exercise both local and global OPF solution algorithms. While convex relaxations are exact or close to exact for many previous test cases [19], the medium-size test cases developed in this paper have large optimality gaps between the best-known local solutions and the bounds from the convex relaxations. In order to determine whether the optimality gaps are due to poor local optima or poor bounds, we apply both a random search technique and the continuation algorithm in [31] in order to find additional local optima. This approach yields several additional local solutions and many stationary points, but none with a better objective value than that obtained via the local solver in MATPOWER [32]. This may suggest that the optimality gaps are due to a poor bound from the relaxations, thus motivating the development of improved convex relaxation techniques.

This paper is organized as follows. Section 2 overviews the OPF problem. Section 2.1 reviews computational tools for studying OPF feasible spaces. Section 3 describes the numerical experiment that is the first main contribution of this paper. Using insights from the small test cases, Section 4 presents and studies challenging OPF problems derived by modifying several IEEE test cases, which is the second main contribution of this paper. Section 5 concludes the paper.

2. OVERVIEW OF THE OPF PROBLEM

This section overviews the OPF problem and its SDP relaxation. Further details are provided in [2, 10, 11].

Consider an n-bus system, where $\mathcal{N} = \{1, \ldots, n\}$ is the set of buses, $\mathcal{G}$ is the set of generator buses, and $\mathcal{L}$ is the set of lines. Let Y denote the network admittance matrix. Let $P_{Dk} + jQ_{Dk}$ represent the active and reactive load demand at bus $k \in \mathcal{N}$, where j is the imaginary unit. Let V_k represent the voltage phasor at bus $k \in \mathcal{N}$, with the angle of V_1 equal to zero to set the angle reference. Define the rank-one matrix $W = VV^H \in \mathbb{H}^n$, where $\mathbb{H}^n$ denotes the set of $n \times n$ Hermitian matrices. Superscripts "max" and "min" denote specified

upper and lower limits. Buses without generators have maximum and minimum generation set to zero. Define a convex quadratic cost of active power generation with coefficients $c_{2,k} \geqslant 0$, $c_{1,k}$, and $c_{0,k}$ for $k \in \mathcal{G}$.

Each line $(l,m) \in \mathcal{L}$ is modeled by an ideal transformer with turns ratio $\tau_{lm}e^{j\theta_{lm}} : 1$ in series with a Π circuit with mutual admittance y_{lm} and total shunt susceptance $jb_{sh,lm}$. Define e_k as the k^{th} column of the identity matrix. Let $\overline{(\cdot)}$, $(\cdot)^\intercal$, and $(\cdot)^H$ denote the complex conjugate, transpose, and complex conjugate transpose, respectively. Define the matrices $H_k = \frac{Y^H e_k e_k^\intercal + e_k e_k^\intercal Y}{2}$, $\tilde{H}_k = \frac{Y^H e_k e_k^\intercal - e_k e_k^\intercal Y}{2j}$, $F_{lm} = \frac{1}{\tau_{lm}^2}\left(\overline{y}_{lm} - jb_{sh,lm}/2\right) e_l e_l^\intercal - \overline{y}_{lm}/\left(\tau_{lm}\mathrm{e}^{-j\theta_{lm}}\right) e_m e_l^\intercal$, and $F_{ml} = \left(\overline{y}_{lm} - jb_{sh,lm}/2\right) e_m e_m^\intercal - \overline{y}_{lm}/\left(\tau_{lm}\mathrm{e}^{j\theta_{lm}}\right) e_l e_m^\intercal$.

The OPF problem is

$$\min_{V\in\mathbb{C}^n} \quad \sum_{k\in\mathcal{G}} c_{2,k}\left(\mathrm{tr}\left(H_k W\right) + P_{Dk}\right)^2 + c_{1,k}\left(\mathrm{tr}\left(H_k W\right) + P_{Dk}\right) + c_{0,k} \tag{1a}$$

subject to

$$P_k^{min} \leqslant \mathrm{tr}\left(H_k W\right) + P_{Dk} \leqslant P_k^{max} \qquad \forall k \in \mathcal{N} \tag{1b}$$

$$Q_k^{min} \leqslant \mathrm{tr}(\tilde{H}_k W) + Q_{Dk} \leqslant Q_k^{max} \qquad \forall k \in \mathcal{N} \tag{1c}$$

$$\left(V_k^{min}\right)^2 \leqslant \mathrm{tr}\left(e_k e_k^\intercal W\right) \leqslant \left(V_k^{max}\right)^2 \qquad \forall k \in \mathcal{N} \tag{1d}$$

$$\left\{\mathrm{tr}\left[\left(F_{lm} + F_{lm}^H\right) W\right]\right\}^2 + \left\{\mathrm{tr}\left[j\left(F_{lm}^H - F_{lm}\right) W\right]\right\}^2 \leqslant 4\left(S_{lm}^{max}\right)^2 \qquad \forall\,(l,m) \in \mathcal{L} \tag{1e}$$

$$\left\{\mathrm{tr}\left[\left(F_{ml} + F_{ml}^H\right) W\right]\right\}^2 + \left\{\mathrm{tr}\left[j\left(F_{ml}^H - F_{ml}\right) W\right]\right\}^2 \leqslant 4\left(S_{lm}^{max}\right)^2 \qquad \forall\,(l,m)\,\mathcal{L} \tag{1f}$$

$$W = VV^H \tag{1g}$$

where $\mathrm{tr}\left(\cdot\right)$ is the trace. Constraints (1b)–(1d) are linear in the entries of W. The objective (1a) and line flow constraints (1e)–(1f) are convex in the entries of W. Thus, all the non-convexity in (1) is contained in the rank constraint (1g).

The numerical experiment in Section 3 uses an SDP relaxation of the OPF problem as part of a screening step to identify test cases which may have relevant non-convexities. This SDP relaxation is formed by replacing (1g) with a positive semidefinite constraint $W \succeq 0$ [2]. The solution to the SDP relaxation provides a lower bound on the OPF problem's optimal objective value. If the condition $\text{rank}\,(W) = 1$ is satisfied, the lower bound provided by the SDP relaxation is *exact*. Conversely, if $\text{rank}\,(W) > 1$, the lower bound may be strictly below the OPF problem's global optimum. An *optimality gap* is then computed as the percent difference between the objective values for a local solution to (1) and the lower bound from the SDP relaxation. A non-negligible optimality gap suggests the possible presence of a non-convexity in the OPF problem's feasible space near the global solution.

Note that the OPF problem formulation (1) does not consider some possible sources of non-convexity that are present in more general OPF problem formulations (e.g., contingency constraints, discrete devices such as switched shunts, models of uncertainty, etc.) [8, 33–35]. A variety of approaches address these possible sources of non-convexity (e.g., branch-and-bound and cutting plane methods for discrete variables [36], chance-constrained formulations [33–35], etc.). Many of these approaches solve the OPF formulation (1) as a subproblem within a broader algorithm. Therefore, identifying non-convexities inherent to the OPF formulation (1) is relevant to a wide range of problems. Future work will study the impacts of other types of OPF constraints on the feasible spaces' convexity characteristics.

2.1. TOOLS FOR STUDYING OPF FEASIBLE SPACES

This section first describes an algorithm that computes the feasible space (i.e., the set of points satisfying (1b)–(1g)) for small OPF problems and then discusses approaches for finding multiple local optima. The numerical experiments in the following sections employ both of these algorithms to characterize OPF non-convexities.

2.2. COMPUTING THE FEASIBLE SPACES OF SMALL OPF PROBLEMS

Reference [28] presents an algorithm for computing a discretized representation of the feasible spaces for small OPF problems. The algorithm discretizes an OPF problem's feasible space into a set of points, each of which represents a *power flow problem* (i.e., fixed voltage magnitudes at all generator buses, fixed active power injections at all generator buses except for a single "slack" bus which sets the angle reference, and fixed active and reactive power injections at all load buses). Observe that the expressions for power injections (1b), (1c) and squared voltage magnitudes (1d) can be written as polynomials in V and $\overline{V}$ via substitution of (1g). Expanding these complex polynomials in terms of the real and imaginary components of V and $\overline{V}$ reveals a power flow formulation in terms of quadratic polynomials with real variables. See, e.g., [28, 37] for further details.

Writing the power flow equations in a polynomial representation enables application of the "Numerical Polynomial Homotopy Continuation" (NPHC) algorithm, which is based on theory from algebraic geometry. The theoretical guarantees inherent to the NPHC algorithm ensure that the power flow problems corresponding to each discretization point are solved *reliably*; i.e., the NPHC algorithm either returns all power flow solutions or certifies infeasibility. After solving the power flow equations corresponding to each discretization point, a screening step eliminates the solutions which fail to satisfy all the OPF problem's constraints. The remaining points are all feasible for the OPF problem, thus reliably providing a discretized representation of the entire feasible space.

The feasible space computation algorithm is only applicable to small OPF problems due to both the computational limits of the NPHC algorithm and the "curse of dimensionality" corresponding to the discretization of the feasible space with increasing degrees of freedom. Using convex relaxation techniques to quickly eliminate many infeasible points, the feasible space computation algorithm in [28] is tractable for OPF problems with up to approximately ten buses and three generators. This paper's numerical experiments

work within these limitations to first characterize non-convexities in small OPF problems. Lessons learned from the small problems are then applied to construct and study larger test cases.

2.3. COMPUTING MULTIPLE LOCAL OPTIMA

The presence of multiple local optima indicates the existence of non-convexities in an OPF problem's feasible space. Algorithms for computing multiple local optima therefore provide a means for investigating the associated non-convexities. Convergence of local solution algorithms depends on the selected initialization. Thus, initializing a local algorithm with various power flow solutions corresponding to random operating points is one approach for computing multiple local optima. The numerical experiments in Section 4 search for multiple local optima using at least two hundred initializations for the "MIPS" solver in MATPOWER [32].

A more sophisticated algorithm was recently proposed in [31]. Starting from a single local optimum obtained from a local solver, the algorithm in [31] applies a continuation method to trace between solutions to the first-order necessary conditions for local optimality. To ensure boundedness of the continuation traces, the continuation method is applied to an "elliptical" representation of the first-order optimality conditions. To maintain computational tractability, we use a two-round enumeration approach; see [31] for further details. This approach is capable of finding multiple local optima for problems with several tens to hundreds of buses.

3. INVESTIGATING THE CAUSES OF OPF NON-CONVEXITIES VIA A NUMERICAL EXPERIMENT

The first contribution of this paper is a numerical experiment conducted to better understand the characteristics of OPF problems with non-convex feasible spaces. Specifically, this numerical experiment develops an approach for randomly constructing many

small (three- to five-bus) test cases with realistic ranges for the electrical parameters. Each test case is then screened for possible non-convexities based on the *optimality gap* between the objective value of a local solution and the lower bound from an SDP relaxation. The feasible spaces for the test cases identified via this screening process are then computed using that algorithm in [28], which allows for characterization of the non-convexities via visual inspection. This section discusses this approach in more detail and then presents illustrative examples and various observations about the non-convexities.

3.1. RANDOMLY GENERATING AND SCREENING SMALL TEST CASES

The following procedure was used to randomly construct a large number of small (three- to five-bus) OPF test cases [38–42]. The number of lines were sampled from a uniform distribution, with a topology developed from a random spanning tree [43] augmented with additional lines whose terminal buses were randomly selected. Limits for the voltage magnitudes and angles, active and reactive power generation, load demands, line parameters, etc. were sampled from Gaussian distributions with parameters given in Table 1. Test cases without sufficient generation capacity to serve the loads were discarded as trivially infeasible.

Table 1 provides the parameters used in constructing the random test cases. For each test case, impedance $R + jX$ (yielding admittance $g + jb = 1/(R + jX)$) and shunt susceptance b values for the lines' Π-model equivalent circuits were randomly sampled from Gaussian distributions with mean and standard deviation of μ_R, σ_R; μ_X, σ_X; and μ_b, σ_b, respectively, in per unit using a 100 MVA base, with any negative values sampled for line resistances instead set to zero. Lines had an 8% probability of being transformers with tap ratio τ and phase-shift θ sampled from a Gaussian distribution with mean and standard deviation values of μ_τ, σ_τ per unit and μ_θ, σ_θ, respectively. A bus was specified to be a generator with 30% probability, with the first generator selected as the reference bus. If no buses were selected to be generators, a random bus was assigned a generator and chosen

Table 1. Means and standard deviations for parameter values in the randomly constructed test cases.

	4-bus	**5-bus**	**3-bus (acyclic)**	**3-bus (cyclic)**
μ_R (p.u.)	0.37	0.25	0.40	0.43
σ_R (p.u.)	0.02	0.01	0.05	0.02
μ_X (p.u.)	0.38	0.44	0.44	0.46
σ_X (p.u.)	0.02	0.01	0.01	0.01
μ_b (p.u.)	0.38	0.22	0.45	0.43
σ_b (p.u.)	0.02	0.02	0.01	0.01
μ_τ (p.u.)	0.00	1.00	1.00	1.00
σ_τ (p.u.)	0.00	0.01	0.00	0.00
μ_θ (deg)	0.00	0.00	0.00	0.00
σ_θ (deg.)	0.00	3.00	0.00	0.00
$\mu_{P_{g,max}}$ (MW)	24.00	5000.00	220.00	200.00
$\sigma_{P_{g,max}}$ (MW)	1.00	5.00	2.00	1.00
$\mu_{P_{g,min}}$ (MW)	23.00	100.00	0.00	0.00
$\sigma_{P_{g,min}}$ (MW)	1.00	2.00	0.00	0.00
$\mu_{Q_{g,max}}$ (MVAr)	57.00	1800.00	110.00	100.00
$\sigma_{Q_{g,max}}$ (MVAr)	2.00	5.00	2.00	2.00
$\mu_{Q_{g,min}}$ (MVAr)	-54.00	-30.00	-26.00	-25.00
$\sigma_{Q_{g,min}}$ (MVAr)	1.00	1.00	1.00	1.00
μ_{P_d} (MW)	23.00	95.00	30.00	39.00
σ_{P_d} (MW)	3.00	5.00	5.00	0.00
μ_{Q_d} (MVAr)	16.00	14.00	10.00	20.00
σ_{Q_d} (MVAr)	3.00	1.00	1.00	1.00

to provide the angle reference. The active power injections were sampled from Gaussian distribution with mean and standard deviation values of μ_{P_g} and σ_{P_g}. Loads have a constant active and reactive power component sampled from a Gaussian distribution with mean and standard deviation μ_{P_d}, σ_{P_d} and μ_{Q_d}, σ_{Q_d}, respectively. A variety of numerical experiments not detailed in this paper tested different ranges of parameter values. The parameters in Table 1 were chosen such that the resulting test cases tend to be feasible and provide at least some examples which passed the screening process discussed later in this section. A similar test case construction approach was used to study power flow problems in [44].

Computing and studying the feasible spaces for every test case is unnecessary since many of the test cases have convex or nearly convex feasible spaces that do not further this paper's goal of characterizing non-convexities. Accordingly, the following screening process was used to identify test cases which were likely to have relevant non-convexities. Using multiple random initializations, the local solver in MATPOWER [32] was repeatedly applied to each test case. An optimality gap was then computed by comparing the lowest objective value from any initialization to the lower bound obtained from the SDP relaxation. The screening process selected test cases with large optimality gaps ($\geqslant 1\%$) for further analyses via the feasible space computation algorithm in [28]. Visualizing various projections of the feasible spaces for these test cases revealed the relevant non-convexities. The following section discusses the lessons learned from this experiment and presents instructive examples.

As a caveat for the results in the following section, note that the screening process' reliance on the lower bound from the SDP relaxation could potentially introduce bias into the selection of test cases considered for further analyses. While not observed in any related numerical experiments, it is conceptually possible that there may exist test cases with relevant non-convexities for which the SDP relaxation does not yield large optimality gaps and are therefore excluded from the empirical study. Thus, one direction for future work is to develop alternative screening processes in order to avoid any potential biases induced by the proposed approach.

3.2. ILLUSTRATIVE EXAMPLES OF OPF FEASIBLE SPACES

The empirical experiment constructed more than 10,000 test cases using the procedure in Section 3.1, with fewer than 10 being screened for further analysis. One observation from this empirical experiment is the relatively small fraction of test cases with large optimality gaps. This suggests that relevant non-convexities (i.e., non-convexities that are near the test cases' global optima) appear to be relatively rare, at least for test cases with param-

Table 2. Line shunt values in randomly constructed test cases.

	4-bus	**5-bus**	**3-bus (acyclic)**	**3-bus (cyclic)**
b_{1-2} (p.u.)	0.3804	0.17180	0.4617	0.4068
b_{1-3} (p.u.)	0.4016	0.26470	0.4774	0.4554
b_{2-3} (p.u.)	–	0.20090	–	0.4376
b_{1-4} (p.u.)	–	0.28430	–	–
b_{1-5} (p.u.)	–	0.25632	–	–
b_{2-4} (p.u.)	0.4107	0.02519	–	–
b_{2-5} (p.u.)	–	0.21590	–	–
b_{3-4} (p.u.)	0.3870	0.27260	–	–
b_{3-5} (p.u.)	–	0.20360	–	–
b_{4-5} (p.u.)	–	0.28940	–	–

eters in the ranges described in Table 1. This observation aligns with previous numerical experiments indicating that the lower bound from the SDP relaxation is often close to the global optimum [45].

Visualizing projections of the feasible spaces for various test cases provides further insights regarding OPF non-convexities. Using the algorithm in [28], this section presents several representative projections of OPF feasible spaces generated using the procedure in Section 3.1. Figures. 1–5 show one-line diagrams and projections of the corresponding feasible spaces for selected test cases. Power demands and generation ranges given in MW and MVAr. The feasible space projections are shown in terms of the active and reactive power generations (MW and MVAr) at selected buses, with the colors representing the generation cost. Line parameters are given in per unit (p.u.) on a 100 MVA base, and the shunt susceptances in the Π-circuit line model are given in Table 2. Off-nominal voltage ratios and non-zero phase shifts of transformers are tabulated in Table 3. None of the flow limits are binding in any of the screened test cases. The generation cost functions and voltage magnitude limits are given in Tables 4 and 5, respectively. Local and global optima are labeled with cyan triangles and green stars, respectively.

Table 3. Transformer details for the Five-bus test case.

Line	**Voltage ratio**	**Phase shift (deg.)**
$1-2$	1.0000	0.0000
$1-3$	1.0000	0.0000
$3-2$	0.9925	7.2099
$1-4$	1.0000	0.0000
$1-5$	1.0000	0.0000
$2-4$	1.0000	0.0000
$2-5$	1.0000	0.0000
$4-3$	0.9950	-2.2219
$3-5$	1.0000	0.0000
$5-4$	1.0109	-1.6934

Table 4. Generation cost coefficients.

4-bus	c_2 (\$/(MW-hr)^2)	c_1 (\$/(MW-hr))	c_0 (\$)
Generator at bus 2	0.0663	67.2267	0.00
Generator at bus 3	0.6272	15.0543	0.00
5-bus	c_2 (\$/(MW-hr)^2)	c_1 (\$/(MW-hr))	c_0 (\$)
Generator at bus 3	0.9277	38.7611	0.00
Generator at bus 5	0.2162	54.6499	0.40
3-bus (acyclic)	c_2 (\$/(MW-hr)^2)	c_1 (\$/(MW-hr))	c_0 (\$)
Generator at bus 2	0.5240	19.3591	0.00
Generator at bus 3	0.5480	16.6615	0.00
3-bus (cyclic)	c_2 (\$/(MW-hr)^2)	c_1 (\$/(MW-hr))	c_0 (\$)
Generator at bus 2	0.6408	49.6517	0.00
Generator at bus 3	0.6978	26.7824	0.00

Table 5. Voltage limits.

	V^{max} (p.u.)	V^{min} (p.u.)
4-bus	1.10	0.90
5-bus	1.10	0.90
3-bus (acyclic)	1.21	0.81
3-bus (cyclic)	1.10	0.90

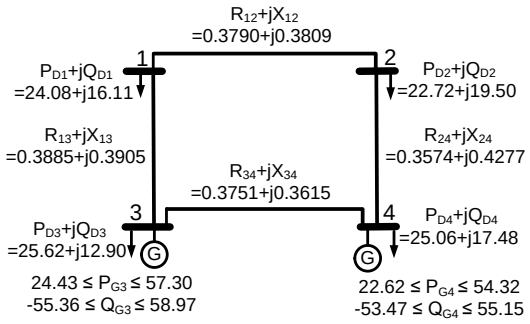

(a) One-line diagram.

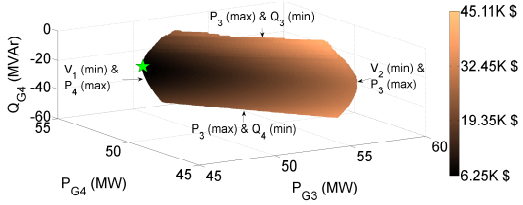

(b) Feasible space projection.

Figure 1. One-line diagram and feasible space projection for a "typical" randomly generated four-bus test case. Observe that this projection shows a convex feasible space.

Figure 1 shows a typical test case that did not pass the screening process (i.e., the optimality gap resulting from the SDP relaxation is small). As expected, the feasible space appears convex in terms of the power injections and voltage magnitudes. Conversely, Figures 2–5 show examples of test cases which the screening process identified as possibly containing relevant non-convexities. The projections of the feasible spaces are indeed non-convex, with Figures. 2b, 3c, and 5b being disconnected. These test cases challenge a variety of optimization algorithms. Some initializations for local solvers result in convergence to suboptimal local solutions in these problems and the SDP relaxation of [2] is not exact.

The labels in Figures. 2b, 3b, 3c, and 5b indicate the binding limits at the boundaries of the feasible spaces. These binding limits are useful for characterizing the causes of the non-convexities. The main observation from extensive numerical experiments on these and other small test cases is that non-convexities in many OPF problems are often associated with lower limits on voltage magnitudes and reactive power generation in combination

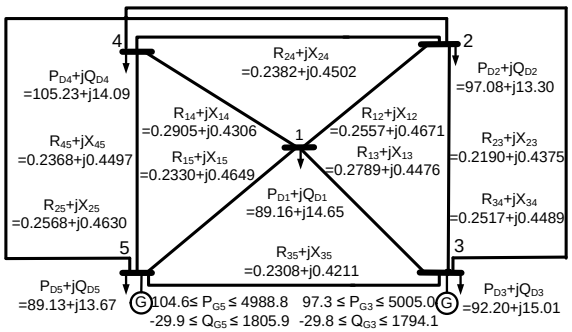

(a) One-line diagram.

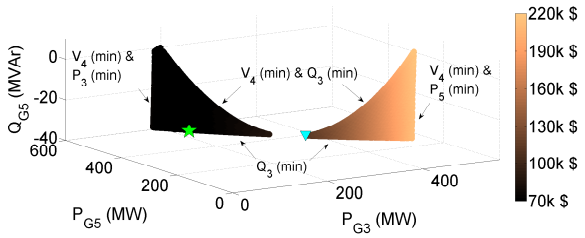

(b) Feasible space projection.

Figure 2. One-line diagram and feasible space projection for a randomly generated five-bus test case. Observe that this projection shows a non-convex and disconnected feasible space.

with large shunt capacitances. The lower voltage limits' relevance to non-convexities is physically intuitive: as shown in Figures. 4, whose axes consist of the real and imaginary parts of the voltage phasors, $\mathrm{Re}\,(V_i)$ and $\mathrm{Im}\,(V_i)$, constraint (1d) restricts the voltage phasors to an annulus. The lower voltage magnitude limits $\left(V_i^{min}\right)^2 \leqslant \mathrm{Re}\,(V_i)^2 + \mathrm{Im}\,(V_i)^2$ are thus non-convex constraints. Since increasing voltage magnitudes tends to reduce line losses, OPF problems typically have binding *upper* voltage magnitude limits. In these examples, the *lower* voltage limits are binding at the global optimum. To explain this, note that the large shunt capacitances in these examples result in an excess of reactive power that cannot be absorbed by the generators due to binding lower reactive power generation limits. Reducing the voltage magnitudes decreases the reactive power generated by the shunt capacitors in

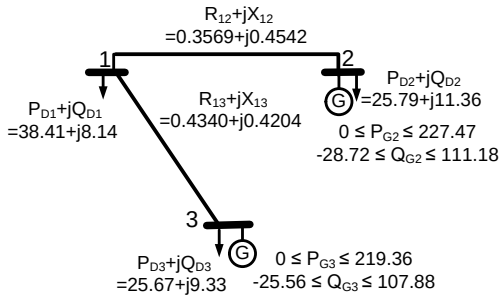

(a) One-line diagram.

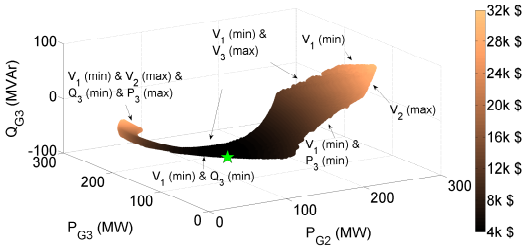

(b) Feasible space projection.

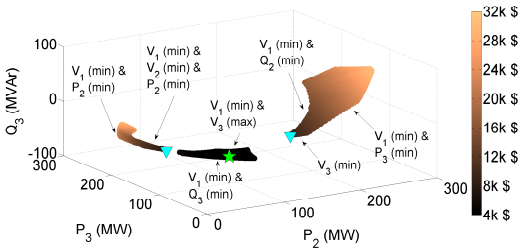

(c) Feasible space projection with tightened constraints.

Figure 3. One-line diagram and feasible space projection for a randomly generated acyclic three-bus test case. Observe that these projections show non-convex feasible spaces. Tightening the constraints yields a disconnected feasible space in Figure. 3c.

the lines' Π-circuit model, thus ameliorating the excess reactive power but resulting in an operating condition near the non-convexitiy associated with the lower voltage magnitude limit.

Non-convexities were previously observed for similar operational conditions in [1]. The test cases considered here thus verify the results in previous literature. Moreover, all the test cases with non-convexities characterized via the numerical experiment were associated with binding lower limits on voltage magnitudes and reactive power generation.

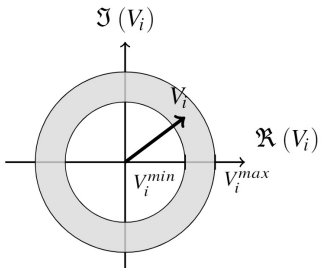

Figure 4. Illustration of the voltage magnitude limits (1d).

This empirically suggests that such an operational condition is a "common" cause of non-convexities, at least among OPF problems with within the range of parameters considered in this experiment.

Note that the characteristics of the non-convexities (particularly disconnectedness) can be sensitive to the OPF problems' parameters. For instance, the feasible space in Figure. 3c results from tightening the limits on lower reactive power generation from $Q_{G2}^{min} = -28.7$ MVAr and $Q_{G3}^{min} = -25.6$ MVAr to $Q_{G2}^{min} = -15.7$ MVAr and $Q_{G3}^{min} = -23.5$ MVAr. These modifications change this projection of the feasible space from non-convex but connected in Figure. 3b to disconnected in Figure 3c.

4. CHALLENGING OPF PROBLEMS DERIVED BY MODIFYING IEEE TEST CASES

This section exploits observations from the small test cases to construct larger OPF test cases with non-convex feasible spaces. Four test cases (named "nmwc14", "nmwc24", "nmwc57", and "nmwc118" after the authors' last names and number of buses) were developed by modifying the IEEE 14-, 24-, 57-, and 118-bus test cases via reducing the loading, slightly tightening the voltage limits, and significantly tightening the lower reactive power generation limits [46–49]. The goal of these modifications is to obtain test cases with operational conditions where lower limits on voltage magnitudes and reactive power generation are binding in a manner similar to the small test cases in Section 3.

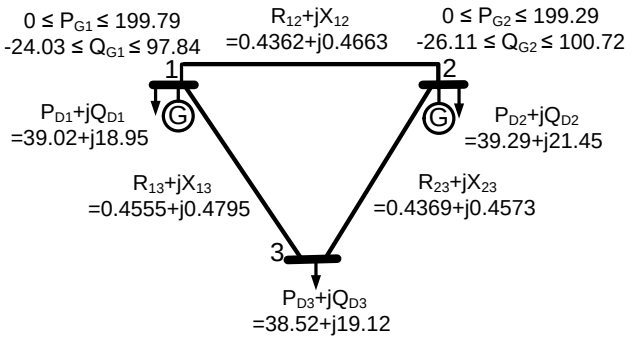

(a) One-line diagram.

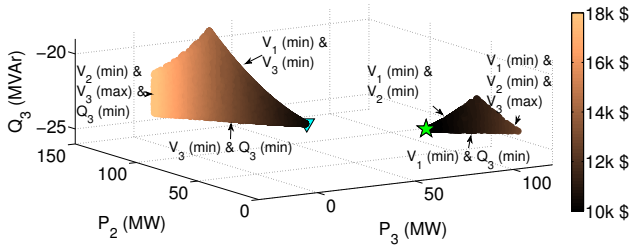

(b) Feasible space projection.

Figure 5. One-line diagram and feasible space projection for a randomly generated cyclic three-bus test case. Observe that this projection shows a non-convex and disconnected feasible space.

Table 6 provides the percentage changes applied to each of the standard IEEE test cases provided by MATPOWER [32]. Modifications to the IEEE test cases consist of decreasing active and reactive loads by δ_{P_d} and δ_{Q_d}, tightening upper and lower bounds on voltage by $\delta_{\overline{V}}$ and $\delta_{\underline{V}}$, and tightening the lower bound on reactive power by δ_{Q_G}.

Applying the algorithms described in Section 2.3 to these test cases yields multiple local optima with a wide range of objective values. Moreover, it is difficult to prove global optimality of the best known local solutions for some of these cases via relaxations with tight lower bounds, even with state-of-the-art techniques. For instance, nmwc118 has 2 local optima, and even the combination of the sparse second-order moment relaxation [12], the QC relaxation [14], bound tightening [50], and a variety of related enhancements [15, 51, 52] yields an optimality gap of 14.0%. This problem therefore appears to be particularly challenging for both traditional solvers (due to the multiple local optima) and convex

Table 6. Descriptions of modifications to the IEEE test systems.

	14-bus	**24-bus**	**57-bus**	**118-bus**
δ_{P_d} (%)	60.00	55.00	72.00	71.00
δ_{Q_d} (%)	60.00	55.00	72.00	71.00
$\delta_{\overline{V}}$ (%)	0.06	0.73	0.06	0.06
$\delta_{\underline{V}}$ (%)	0.06	0.73	0.06	0.06
$\delta_{\overline{Q_G}}$ (%)	95.00	90.00	95.00	95.00

Table 7. Objective values for the modified IEEE test cases.

Case	**Local Optima ($/hr)**		**Lower Bound**	**Optimality**
Name	**Worst**	**Best**	**($/hr)**	**Gap**
nmwc14	3024.46	2529.87	2529.49	0.01%
nmwc24	42667.26	39773.02	39773.02	0.00%
nmwc57	9186.12	9128.72	9030.70	1.09%
nmwc118	40399.17	34663.69	30413.10	14.00%

relaxations. Table 7 summarizes the objective values of the known local optima and lower bounds (using a combination of the relaxations in [12, 14, 15, 50–52]) for these test cases. Note that the objective values for the local optima span wide ranges for these test cases (e.g., from $34664/hr to $40399/hr or equivalently from an optimality gap of 14.0% to 33.0% for nmwc118).

5. CONCLUSION

Despite significant recent progress, there remain problems whose non-convexities challenge state-of-the-art OPF solution algorithms. Better understanding these non-convexities is important for further improving solution algorithms as well as for developing additional challenging test cases. The numerical experiment described in this paper provides a key observation regarding OPF non-convexities: all of the non-convexities identified in the numerical experiment are associated with binding lower bounds on voltage magnitudes and reactive power generation. Exploiting this observation, this paper proposes several new test

cases derived by modifying the loading and tightening certain constraints in the IEEE test cases. With many local optima and large optimality gaps, these cases challenge a variety of state-of-the-art algorithms.

Ongoing work aims to construct larger test cases which exhibit a range of difficulties. Other ongoing work involves studying the feasible spaces for test cases from the NESTA archive [19] with large optimality gaps. Related future work will exploit the observations in this paper to improve convex relaxation algorithms.

BIBLIOGRAPHY

[1] W.A. Bukhsh,A. Grothey, K.I.M. McKinnon, P.A. Trodden, Local Solutions of the Optimal Power Flow Problem, IEEE Transaction on Power Systems, 28 (4) (2013) 4780–4788.

[2] J. Lavaei, S.H. Low, Zero Duality Gap in Optimal Power Flow Problem, IEEE Transaction on Power Systems, 27 (1) (2012) 92–107.

[3] D. Bienstock, A. Verma, Strong NP-hardness of AC Power Flows Feasibility, arXiv:1512.07315 (2015)

[4] K. Lehmann, A. Grastien, P. Van Hentenryck, AC-Feasibility on Tree Networks is NP-Hard, IEEE Transaction on Power Systems 31 (1) (2016) 798-801.

[5] J. Carpentier, Contribution to the Economic Dispatch Problem, Bulletin de la Societe Francoise des Electriciens 8 (3) (1962) 431–447.

[6] J.A. Momoh, R. Adapa, M.E. El-Hawary, A Review of Selected Optimal Power Flow Literature to 1993. Parts I and II, IEEE Transaction on Power Systems 14 (1) (1999) 96–111.

[7] A. Castillo, R.P. O'Neill, Survey of Approaches to Solving the ACOPF (OPF Paper 4) March (2013)

[8] F. Capitanescu, J.L. Martinez Ramos P. Panciatici, D. Kirschen, A. Marano Marcolini, L. Platbrood, L. Wehenkel,State-of-the-Art, Challenges, and Future Trends in Security Constrained Optimal Power Flow, Electric power systems research 81 (8) (2011) 1731–1741.

[9] D.K. Molzahn, L.A. Roald, AC Optimal Power Flow with Robust Feasibility Guarantees, 20th power system computing conference (PSCC) June 2018.

[10] M.B. Cain, R.P. O'Neill, A. Castillo, History of Optimal Power Flow and Formulations, August (2013).

[11] D.K. Molzahn, J.T. Holzer, B.C. Lesieutre, C.L. DeMarco, Implementation of a Large-Scale Optimal Power Flow Solver Based on Semidefinite Programming,IEEE Transaction on Power Systems 28 (4) (2013) 3987–3998.

[12] D.K. Molzahn, I.A. Hiskens, Sparsity-Exploiting Moment-Based Relaxations of the Optimal Power Flow Problem, IEEE Transaction on Power Systems 30 (6) (2015) 3168–3180.

[13] C. Josz, D.K. Molzahn, Multi-Ordered Lasserre Hierarchy for Large Scale Polynomial Optimization in Real and Complex Variables, SIAM Journal on Optimization 28 (2) (2018) 1017–1048.

[14] C. Coffrin, H.L. Hijazi, P. Van Hentenryck, The QC Relaxation: A Theoretical and Computational Study on Optimal Power Flow, IEEE Transaction on Power Systems 31 (4) (2016) 3008–3018.

[15] B. Kocuk, S.S. Dey, A. Sun, Strong SOCP Relaxations of the Optimal Power Flow Problem, Operation Research 64 (6) (2016) 1177–1196.

[16] D. K. Molzahn, I. A. Hiskens, A Survey of Relaxations and Approximations of the Power Flow Equations, Foundations and Trends in Electric Energy Systems February (2019).

[17] D.K. Molzahn, B.C. Lesieutre, C.L. DeMarco, A Sufficient Condition for Global Optimality of Solutions to the Optimal Power Flow Problem, IEEE Transaction on Power Systems, 29 (2) (2014) 978–979.

[18] B.C. Lesieutre, D.K. Molzahn,A.R. Borden, C.L. DeMarco, Examining the Limits of the Application of Semidefinite Programming to Power Flow Problems, 49th Annual Allerton Conference on Communications, Control, and Computing, September (2011).

[19] C. Coffrin, D. Gordon, P. Scott,NESTA, the NICTA Energy System Test Case Archive, arXiv:1411.0359 August (2016).

[20] S.H. Low, Convex Relaxation of Optimal Power Flow–Part II: Exactness, IEEE transactions control network systems 1 (2) (2014) 177–189.

[21] J. Lavaei and D. Tse and B. Zhang, Geometry of Power Flows and Optimization in Distribution Networks, IEEE Transaction on Power Systems 29 (2) (2014) 572–583.

[22] I.A. Hiskens, R.J. Davy, Exploring the Power Flow Solution Space Boundary, IEEE Transaction on Power Systems 16 (3) (2001) 389–395.

[23] B.C. Lesieutre, I.A. Hiskens, Convexity of the Set of Feasible Injections and Revenue Adequacy in FTR Markets, IEEE Transaction on Power Systems 20 (4) (2005) 1790-1798.

[24] Y.V. Makarov, Z.Y. Dong, D.J. Hill, On Convexity of Power Flow Feasibility Boundary, IEEE Transaction on Power Systems 23 (2) (2008) 811–813.

[25] R. Madani, S. Sojoudi, J. Lavaei, Convex Relaxation for Optimal Power Flow Problem: Mesh Networks, asilomar conference signals systems computers, November (2013).

[26] D.K. Molzahn, B.C. Lesieutre, C.L. DeMarco, Investigation of Non-Zero Duality Gap Solutions to a Semidefinite Relaxation of the Power Flow Equations, 47th Hawaii International Conference on System Sciences (HICSS) January (2014).

[27] B. Polyak, and E. Gryazina, Convexity/Nonconvexity Certificates for Power Flow Analysis, Advances in Energy System Optimization (2017) 221–230.

[28] D.K. Molzahn, Computing the Feasible Spaces of Optimal Power Flow Problems, IEEE Transaction on Power Systems, 32 (6) (2017) 4752–4763.

[29] H. D. Chiang, C.Y. Jiang, Feasible Region of Optimal Power Flow: Characterization and Applications, IEEE Transaction on Power Systems 33 (1) (2018) 236–244.

[30] D.K. Molzahn, Identifying and Characterizing Non-Convexities in the Feasible Spaces of Optimal Power Flow Problems, IEEE Transaction on circuits systems 65 (5) (2018) 672–676.

[31] D. Wu, D.K. Molzahn, B.C. Lesieutre, K. Dvijotham, A Deterministic Method to Identify Multiple Local Extrema for the AC Optimal Power Flow Problem, IEEE Transaction on Power Systems 33 (1) (2018) 654–668.

[32] R.D. Zimmerman,C.E. Murillo-Sánchez, R.J. Thomas, MATPOWER: Steady-State Operations, Planning, and Analysis Tools for Power Systems Research and Education, IEEE Transaction on Power Systems, 26 (1) (2011) 1–8.

[33] M. Vrakopoulou, M. Katsampani, K. Margellos,J. Lygeros, G. Andersson, Probabilistic Security-Constrained AC Optimal Power Flow, IEEE PowerTech Grenoble June (2013).

[34] L. Roald, G. Andersson, Chance-Constrained AC Optimal Power Flow: Reformulations and Efficient Algorithms, IEEE Transaction on Power Systems 33 (3) (2018) 2906 –2918.

[35] L.A. Roald, D.K. Molzahn, A.F. Tobler, Power System Optimization with Uncertainty and AC Power Flow: Analysis of an Iterative Algorithm, 10th IREP Symposium Bulk Power System Dynamics Control August (2017).

[36] P. Belotti, C. Kirches, S. Leyffer, J. Linderoth, J. Luedtke, A. Mahajan, Mixed-Integer Nonlinear Optimization, Acta Numerica, (22) (2013) 1–131.

[37] D. Mehta, D.K. Molzahn, K. Turitsyn, Recent Advances in Computational Methods for the Power Flow Equations, American Control Conference (ACC) August (2016).

[38] M.R. Narimani, D.K. Molzahn, D. Wu, M.L. Crow, nmwc3acyclic_connected_feasible_space, Online: http://item.bettergrids.org (2018).

[39] M.R. Narimani, D.K. Molzahn, D. Wu, M.L. Crow, nmwc3acyclic_disconnected_feasible_space, Online: http://item.bettergrids.org (2018).

[40] M.R. Narimani, D.K. Molzahn, D. Wu, M.L. Crow, nmwc3cyclic, Online: http://item.bettergrids.org/handle/1001/408 (2018).

[41] M.R. Narimani, D.K. Molzahn, D. Wu, M.L. Crow, nmwc4, Online: http://item.bettergrids.org/handle/1001/407 (2018)

[42] M.R. Narimani, D.K. Molzahn, D. Wu, M.L. Crow, nmwc5, Online: http://item.bettergrids.org/handle/1001/406 (2018).

[43] A. Broder, Generating Random Spanning Trees, 30th Annual Symposium on Foundations of Computer Science, November (1989) 442–447.

[44] D.K. Molzahn, D. Mehta, M. Niemerg, Toward Topologically Based Upper Bounds on the Number of Power Flow Solutions,American Control Conference (ACC) July (2016).

[45] D.K. Molzahn, C. Josz, I.A. Hiskens, P. Panciatici, A Laplacian-Based Approach for Finding Near Globally Optimal Solutions to OPF Problems, IEEE Transaction on Power Systems 32 (1) (2017) 305-315.

[46] M.R. Narimani, D.K. Molzahn, D. Wu, M.L. Crow, nmwc14, Online:http://item.bettergrids.org/handle/1001/405 (2018).

[47] M.R. Narimani, D.K. Molzahn, D. Wu, M.L. Crow, nmwc24, Online: http://item.bettergrids.org/handle/1001/404n (2018).

[48] M.R. Narimani, D.K. Molzahn, D. Wu, M.L. Crow, nmwc57, Online: http://item.bettergrids.org/handle/1001/403 (2018).

[49] M.R. Narimani, D.K. Molzahn, D. Wu, M.L. Crow, nmwc118, Online: http://item.bettergrids.org/handle/1001/402 (2018).

[50] C. Coffrin, H.L. Hijazi, P. Van Hentenryck, Strengthening Convex Relaxations with Bound Tightening for Power Network Optimization, 21st International Conference Principles and Practice of Constraint Programming (CP) Agust (2015) 39–57.

[51] C. Coffrin, H. L. Hijazi, P. Van Hentenryck, Strengthening the SDP Relaxation of AC Power Flows with Convex Envelopes, Bound Tightening, and Valid Inequalities, IEEE Transaction on Power Systems 32 (5) (2017) 3549–3558.

[52] K. Bestuzheva, H.L. Hijazi, C. Coffrin, Convex Relaxations for Quadratic On/Off Constraints and Applications to Optimal Transmission Switching, http://www.optimization-online.org/DB_FILE/2016/07/5565.pdf (2016).

II. IMPROVING QC RELAXATIONS OF OPF PROBLEMS VIA VOLTAGE MAGNITUDE DIFFERENCE CONSTRAINTS AND ENVELOPES FOR TRILINEAR MONOMIALS

Mohammad Rasoul Narimani, Daniel K. Molzahn, and Mariesa L. Crow

Department of Electrical & and Computer Engineering

Missouri University of Science and Technology

Rolla, Missouri 65409–0050

Email: mn9t5@mst.edu

ABSTRACT

AC optimal power flow (AC OPF) is a challenging non-convex optimization problem that plays a crucial role in power system operation and control. Recently developed convex relaxation techniques provide new insights regarding the global optimality of AC OPF solutions. The quadratic convex (QC) relaxation is one promising approach that constructs convex envelopes around the trigonometric and product terms in the polar representation of the power flow equations. This paper proposes two methods for tightening the QC relaxation. The first method introduces new variables that represent the *voltage magnitude differences* between connected buses. Using "bound tightening" techniques, the bounds on the voltage magnitude difference variables can be significantly smaller than the bounds on the voltage magnitudes themselves, so constraints based on voltage magnitude differences can tighten the relaxation. Second, rather than a potentially weaker "nested McCormick" formulation, this paper applies "Meyer and Floudas" envelopes that yield the convex hull of the trilinear monomials formed by the product of the voltage magnitudes and trignometric terms in the polar form of the power flow equations. Comparison to a state-of-the-art QC implementation demonstrates the advantages of these improvements via smaller optimality gaps.

1. INTRODUCTION

The optimal power flow (OPF) problem seeks an operating point that optimizes a specified objective subject to constraints from the network physics and engineering limits. Using the nonlinear AC power flow model to accurately represent the power flow physics results in the AC OPF problem, which is non-convex, may have multiple local optima [1], and is generally NP-Hard [2, 3]. A wide variety of algorithms have been applied in order to find locally optimal solutions [4, 5].

Many recent research efforts have developed convex relaxations of OPF problems to obtain bounds on the optimal objective values, certify infeasibility, and, in some cases, achieve globally optimal solutions. Solutions from a relaxation are also useful for initializing certain local solution techniques [6]. Convex relaxations are under active development with ongoing efforts aiming to improve the relaxations' computational tractability and tightness. Recent work is surveyed in [7].

The quadratic convex (QC) relaxation [8] is one promising approach that uses convex envelopes around the trigonometric functions, squared terms, and bilinear products in the polar form of the power flow equations. The tightness of the QC relaxation depends on the size of the bounds on the voltage magnitude and angle difference variables. Therefore, bound tightening techniques, which use convex relaxations to infer tighter bounds than those initially specified in the OPF problem data, can improve the QC relaxation's tightness [9–12]. Several enhancements have also been proposed to tighten the QC and other relaxations, including Lifted Nonlinear Cuts [9, 13] that exploit voltage magnitude and angle difference bounds; tighter trigonometric envelopes [9, 14] that leverage sign-definite angle difference bounds, which can sometimes be obtained via bound tightening; and a variety of valid inequalities, convex envelopes, and cutting planes [11, 12].

This paper proposes two additional improvements for tightening the QC relaxation. The first is based on the observation that adding redundant constraints to a non-convex optimization problem can tighten a relaxation [15]. One approach for constructing appropriate

constraints is to change coordinate systems. We derive constraints based on a coordinate change using voltage magnitude *differences* in addition to the voltage magnitudes themselves. Bound tightening techniques are often more effective for variables representing voltage magnitude differences, thus resulting in tighter constraints.

The second improvement is related to the trilinear monomials formed by the product of the voltage magnitudes and the trigonometric functions in the polar representation of the power flow equations. Previous formulations of the QC relaxation [8, 9] treat these monomials with recursive application of McCormick envelopes [16]. While McCormick envelopes form the convex hull of *bilinear* monomials, recursive application of McCormick envelopes does not necessarily yield the convex hulls of *trilinear* monomials. We apply the potentially tighter envelopes developed by Meyer and Floudas [17, 18], which form the convex hulls of trilinear monomials.

This paper is organized as follows. Section 2 overviews the OPF problem. Section 3 reviews the QC relaxation of the OPF problem. Sections 4 and 5 formulate our proposed improvements. Section 6 evaluates the proposed improvements on various test cases. Section 8 concludes the paper.

2. OVERVIEW OF OPTIMAL POWER FLOW PROBLEM

This section overviews the AC OPF problem. Consider an n-bus system, where $\mathcal{N} = \{1, \ldots, n\}$, $\mathcal{G}$, and $\mathcal{L}$ are the sets of buses, generators, and lines. Let $P_i^d + jQ_i^d$ and $P_i^g + jQ_i^g$ represent the active and reactive load demand and generation, respectively, at bus $i \in \mathcal{N}$, where $j = \sqrt{-1}$. Let $g_{sh,i} + jb_{sh,i}$ denote the shunt admittance at bus i. Let V_i and θ_i represent the voltage magnitude and angle at bus $i \in \mathcal{N}$. For each generator $i \in \mathcal{G}$, define a quadratic generation cost function with coefficients $c_{2,i} \geqslant 0$, $c_{1,i}$, and $c_{0,i}$. Denote $\theta_{lm} = \theta_l - \theta_m$. Specified upper and lower limits are denoted by $(\overline{\cdot})$ and $(\underline{\cdot})$, respectively. Buses $i \in \mathcal{N} \backslash \mathcal{G}$ have generation limits set to zero.

Each line $(l,m) \in \mathcal{L}$ is modeled as a Π circuit with mutual admittance $g_{lm} + jb_{lm}$ and shunt admittance $jb_{sh,lm}$. (Our approach is applicable to more general line models, such the MATPOWER [19] model that allows for off-nominal tap ratios and non-zero phase shifts.) Let P_{lm}, Q_{lm}, and $\overline{S}_{lm}$ represent the active and reactive power flows and the maximum apparent power flow limit on the line that connects buses l and m.

Using these definitions, the OPF problem is

$$\min \quad \sum_{i \in \mathcal{G}} c_{2i} \left(P_i^g\right)^2 + c_{1i} P_i^g + c_{0i} \tag{1a}$$

subject to $\quad (\forall i \in \mathcal{N},\ \forall (l,m) \in \mathcal{L})$

$$P_i^g - P_i^d = g_{sh,i} V_i^2 + \sum_{\substack{(l,m)\in\mathcal{L} \\ \text{s.t. } l=i}} P_{lm} + \sum_{\substack{(l,m)\in\mathcal{L} \\ \text{s.t. } m=i}} P_{ml}, \tag{1b}$$

$$Q_i^g - Q_i^d = -b_{sh,i} V_i^2 + \sum_{\substack{(l,m)\in\mathcal{L} \\ \text{s.t. } l=i}} Q_{lm} + \sum_{\substack{(l,m)\in\mathcal{L} \\ \text{s.t. } m=i}} Q_{ml}, \tag{1c}$$

$$\theta_{ref} = 0, \tag{1d}$$

$$\underline{P}_i^g \leqslant P_i^g \leqslant \overline{P}_i^g, \tag{1e}$$

$$\underline{Q}_i^g \leqslant Q_i^g \leqslant \overline{Q}_i^g, \tag{1f}$$

$$\underline{V}_i \leqslant V_i \leqslant \overline{V}_i, \tag{1g}$$

$$\underline{\theta}_{lm} \leqslant \theta_{lm} \leqslant \overline{\theta}_{lm}, \tag{1h}$$

$$P_{lm} = g_{lm} V_l^2 - g_{lm} V_l V_m \cos(\theta_{lm}) - b_{lm} V_l V_m \sin(\theta_{lm}), \tag{1i}$$

$$Q_{lm} = -(b_{lm} + b_{sh,lm}/2) V_l^2 + b_{lm} V_l V_m \cos(\theta_{lm}) - g_{lm} V_l V_m \sin(\theta_{lm}), \tag{1j}$$

$$(P_{lm})^2 + (Q_{lm})^2 \leqslant \left(\overline{S}_{lm}\right)^2, \tag{1k}$$

$$(P_{ml})^2 + (Q_{ml})^2 \leqslant \left(\overline{S}_{lm}\right)^2. \tag{1l}$$

The objective function (1a) minimizes the active power generation cost. Constraints (1b) and (1c) enforce power balance at each bus. Constraint (1d) sets the angle reference. Constraints (1e)–(1f) limit the active and reactive power generation, voltage magnitudes,

and angle differences between connected buses. Constraints (1i)–(1i) relate the voltage phasors and power flows on each line, and (1i)–(1l) limit the apparent power flows into both terminals of each line.

3. REVIEW OF THE QC RELAXATION

3.1. FORMULATION OF THE QC RELAXATION

The QC relaxation is formed by defining new variables w_{ii}, w_{lm}, c_{lm}, and s_{lm} for the products of voltage magnitudes and the trilinear monomials representing the products of voltage magnitudes and trignometric functions for connected buses:

$$w_{ii} = V_i^2, \qquad \forall i \in \mathcal{N}, \tag{2a}$$

$$w_{lm} = V_l V_m, \qquad \forall\, (l,m) \in \mathcal{L}, \tag{2b}$$

$$c_{lm} = w_{lm} \cos\left(\theta_{lm}\right), \qquad \forall\, (l,m) \in \mathcal{L}, \tag{2c}$$

$$s_{lm} = w_{lm} \sin\left(\theta_{lm}\right), \qquad \forall\, (l,m) \in \mathcal{L}. \tag{2d}$$

For each line $(l,m) \in \mathcal{L}$, these definitions imply the following relationships between the variables w_{ll}, c_{lm}, and s_{lm}:

$$c_{lm}^2 + s_{lm}^2 = w_{ll} w_{mm}, \tag{3a}$$

$$c_{lm} = c_{ml}, \tag{3b}$$

$$s_{lm} = -s_{ml} \tag{3c}$$

The QC relaxation is formulated by enclosing the squared and bilinear product terms in convex envelopes, here represented as set-valued functions:

$$\langle x^2 \rangle^T = \left\{ \breve{x} : \begin{cases} \breve{x} \geqslant x^2, \\ \\ \breve{x} \leqslant (\overline{x} + \underline{x})\, x - \overline{x}\underline{x}. \end{cases} \right. \tag{4a}$$

$$\langle xy\rangle^M = \begin{cases} \breve{xy} : \begin{cases} \breve{xy} \geqslant \underline{x}y + \underline{y}x - \underline{x}\underline{y}, \\ \breve{xy} \geqslant \overline{x}y + \overline{y}x - \overline{x}\overline{y}, \\ \breve{xy} \leqslant \underline{x}y + \overline{y}x - \underline{x}\overline{y}, \\ \breve{xy} \leqslant \overline{x}y + \underline{y}x - \overline{x}\underline{y}. \end{cases} \end{cases} \tag{4b}$$

where $\breve{x}$ and $\breve{xy}$ are "dummy" variables representing the corresponding set. The envelope $\langle x^2\rangle^T$ is the convex hull of the square function. The so-called "McCormick envelope" $\langle xy\rangle^M$ is the convex hull of a bilinear product [16]. The QC relaxation also formulates convex envelopes $\langle \sin(x)\rangle^S$ and $\langle \cos(x)\rangle^C$ for the trigonometric functions:

$$\langle \sin(x)\rangle^S = \begin{cases} \breve{S} : \begin{cases} \breve{S} \leqslant \cos\left(\frac{x^m}{2}\right)\left(x - \frac{x^m}{2}\right) + \sin\left(\frac{x^m}{2}\right), \\ \breve{S} \geqslant \cos\left(\frac{x^m}{2}\right)\left(x + \frac{x^m}{2}\right) - \sin\left(\frac{x^m}{2}\right), \\ \breve{S} \geqslant \frac{\sin(\underline{x})-\sin(\overline{x})}{\underline{x}-\overline{x}}(x - \underline{x}) + \sin(\underline{x}) \text{ if } \underline{x} \geqslant 0, \\ \breve{S} \leqslant \frac{\sin(\underline{x})-\sin(\overline{x})}{\underline{x}-\overline{x}}(x - \underline{x}) + \sin(\underline{x}) \text{ if } \overline{x} \leqslant 0. \end{cases} \end{cases}$$

$$\langle \cos(x)\rangle^C = \begin{cases} \breve{C} : \begin{cases} \breve{C} \leqslant 1 - \frac{1-\cos(x^m)}{(x^m)^2}x^2, \\ \breve{C} \geqslant \frac{\cos(\underline{x})-\cos(\overline{x})}{\underline{x}-\overline{x}}(x - \underline{x}) + \cos(\underline{x}). \end{cases} \end{cases}$$

where $x^m = \max(|\underline{x}|, |\overline{x}|)$. The dummy variables $\breve{S}$ and $\breve{C}$ again represent the corresponding set. For $-90^\circ < \underline{x} < \overline{x} < 90^\circ$, bounds on the sine and cosine functions are

$$\underline{s} = \sin(\underline{x}) \leqslant \sin(x) \leqslant \overline{s} = \sin(\overline{x}), \tag{6a}$$

$$\underline{c} = \min(\cos(\underline{x}), \cos(\overline{x})) \leqslant \cos(x) \leqslant \overline{c} = \begin{cases} \max(\cos(\underline{x}), \cos(\overline{x})), & \text{if sign}(\underline{x}) = \text{sign}(\overline{x}), \\ 1, & \text{otherwise.} \end{cases} \tag{6b}$$

Slightly abusing notation, the QC relaxation is formed by replacing the square, product, and trigonometric terms in (1) with the variables w_{ii}, w_{lm}, c_{lm}, and s_{lm} in these envelopes:

$$\min \quad \sum_{i\in\mathcal{G}} c_{2i}\left(P_i^g\right)^2 + c_{1i}\,P_i^g + c_{0i} \tag{7a}$$

$$\text{subject to} \quad (\forall i \in \mathcal{N},\ \forall\,(l,m) \in \mathcal{L})$$

$$P_i^g - P_i^d = g_{sh,i}\,w_{ii} + \sum_{\substack{(l,m)\in\mathcal{L}\\ \text{s.t. } l=i}} P_{lm} + \sum_{\substack{(l,m)\in\mathcal{L}\\ \text{s.t. } m=i}} P_{ml}, \tag{7b}$$

$$Q_i^g - Q_i^d = -b_{sh,i}\,w_{ii} + \sum_{\substack{(l,m)\in\mathcal{L}\\ \text{s.t. } l=i}} Q_{lm} + \sum_{\substack{(l,m)\in\mathcal{L}\\ \text{s.t. } m=i}} Q_{ml}, \tag{7c}$$

$$(\underline{V}_i)^2 \leqslant w_{ii} \leqslant (\overline{V}_i)^2, \tag{7d}$$

$$P_{lm} = g_{lm}w_{ll} - g_{lm}c_{lm} - b_{lm}s_{lm}, \tag{7e}$$

$$Q_{lm} = -\left(b_{lm} + b_{sh,lm}/2\right)w_{ii} + b_{lm}c_{lm} - g_{lm}s_{lm}, \tag{7f}$$

$$w_{ii} \in \left\langle V_i^2 \right\rangle^T, \tag{7g}$$

$$w_{lm} \in \left\langle V_l V_m \right\rangle^M, \tag{7h}$$

$$c_{lm} \in \left\langle w_{lm}\left\langle \cos\left(\theta_{lm}\right)\right\rangle^C \right\rangle^M, \tag{7i}$$

$$s_{lm} \in \left\langle w_{lm}\left\langle \sin\left(\theta_{lm}\right)\right\rangle^S \right\rangle^M, \tag{7j}$$

$$c_{lm}^2 + s_{lm}^2 \leqslant w_{ll}\,w_{mm}, \tag{7k}$$

$$\text{Equations (1d)–(1f), (1i)–(1l), (3b), (3c).} \tag{7l}$$

Note that the non-convex constraint (3a) is relaxed to (7k) using a less-stringent rotated second-order cone constraint [20]. Also note that the trilinear terms in (1i) and (1i) are addressed in (7h)–(7k) by recursively applying McCormick envelopes (5) (i.e., first applying (5) to the product of voltage magnitudes to obtain w_{lm} and then to the product of w_{lm} and $\left\langle \cos\left(\theta_{lm}\right)\right\rangle^C$ or $\left\langle \sin\left(\theta_{lm}\right)\right\rangle^S$). The optimization problem (7) is a second-order cone program (SOCP), which is convex and can be solved efficiently using commercial tools (e.g., CPLEX, Gurobi, and Mosek).

3.2. BOUND TIGHTENING AND OTHER IMPROVEMENTS

The tightness of the QC relaxation strongly depends on the accuracy of the bounds on voltage magnitudes, $\underline{V}_i$, $\overline{V}_i$, and angle differences, $\underline{\theta}_{lm}$, $\overline{\theta}_{lm}$. The values specified in the dataset for these bounds may be significantly larger than the values that are actually achievable due to the restrictions imposed by other constraints. In other words, certain bounds may never be binding. Exploiting this observation, bound tightening algorithms yield tighter bounds that improve the QC relaxation [9–12].

We apply the optimization-based bound tightening algorithm in [9], which iteratively minimizes and maximizes each voltage magnitude and angle difference variable subject to the QC relaxation's constraints. For instance, consider the upper bound on the voltage magnitude at bus 1:

$$w_{11}^* = \max \quad w_{11} \quad \text{subject to} \quad \text{(7b)–(7n)}. \tag{8}$$

The value w_{11}^* upper bounds the maximum achievable value of $(V_1)^2$ within the feasible space. If $w_{11}^* < \left(\overline{V}_1\right)^2$, then (8) provides a smaller value of $\sqrt{w_{11}^*}$ for the upper bound on V_1, which tightens the QC relaxation. Since tightening the bound on any variable may improve the achievable bounds on other variables, the bound tightening algorithm proceeds iteratively until no further bounds can be tightened. Optimization-based bound tightening algorithms, e.g., [9, 11, 12], are typically slower than analytical methods [10] but provide tighter bounds.

Previous literature proposes a variety of other improvements to the QC relaxation. To form a benchmark for comparing our improvements, we augment (7) with quadratic envelopes for the trigonometric terms [14], arctangent envelopes [12], and lifted nonlinear cuts (LNC) [9, 13].

4. VOLTAGE MAGNITUDE DIFFERENCE CONSTRAINTS

As discussed in Section 3.2, the QC relaxation's tightness strongly depends on having accurate bounds on voltage magnitudes and angle differences. While bound tightening techniques are often successful in reducing the range of the phase angle differences, tightening the voltage magnitudes can be more challenging since OPF feasible spaces typically contain points for which the voltage magnitudes are both near the top and near the bottom of their allowed ranges. The bound tightening algorithms are therefore often unable to significantly improve the voltage magnitude bounds.

However, there is usually an exploitable correlation between the voltage magnitudes at neighboring buses. While the voltage magnitudes at a pair of neighboring buses may be near their upper limits or near their lower limits, typical problems with limited reactive power injection capabilities require that these voltage magnitudes must be *close to each other*. This suggests that "box constraints" on the voltage magnitudes (1g) are not a good match to the voltage magnitude variation exhibited in typical OPF feasible spaces.

As an illustrative example, Figure 1 shows a projection of the feasible space, generated using the approach in [21], for the six-bus system "case6_c" [22] in terms of certain voltage magnitudes. The ranges of the voltage magnitude variations after implementing a bound tightening approach are shown by the dashed lines. The best achievable voltage magnitude bounds are only 17.0% tighter than the originally specified bounds for this case. In contrast, as shown in Figure 1, the *difference* in voltage magnitudes between neighboring buses can be significantly tighter (e.g., 80.5% tighter for the example in Figure 1). To exploit this observation, we derive new constraints by representing the decision variables in an alternate coordinate system. Let $A_{inc} \in \mathbb{R}^{|\mathcal{L}|\times|\mathcal{N}|}$ denote the network incidence matrix, which has rows corresponding to the lines $(l,m) \in \mathcal{L}$ with $+1$ in the i^{th} entry and -1 in the k^{th} entry. Define $V^{\Delta} \in \mathbb{R}^{|\mathcal{L}|}$ as the vector of voltage differences between neighboring buses, $V^{\Delta} = A_{inc}V$ (i.e., $V^{\Delta}_{lm} = V_l - V_m$).

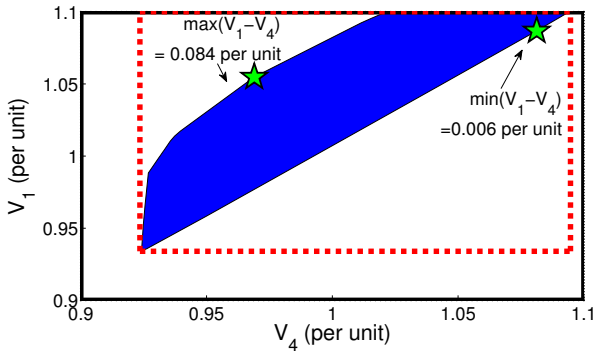

Figure 1. A projection of the feasible space for the "case6_c" [22] test system.

Rewriting the voltage magnitude products $V_l V_m$ using V^{Δ} yields

$$V_l\, V_m = \left(V_l^2 + V_m^2 - \left(V_{lm}^{\Delta}\right)^2\right) / 2. \tag{9}$$

Applying the envelopes in (2) for each term in (9) gives

$$w_{lm} = \left(w_{ll} + w_{mm} - W_{lm}^{\Delta}\right) / 2, \tag{10a}$$

$$W_{lm}^{\Delta} \in \left\langle \left(V_{lm}^{\Delta}\right)^2 \right\rangle^{T}. \tag{10b}$$

A valid inequality is also formed by expanding $(V_l - V_m)^2$:

$$\left(V_{lm}^{\Delta}\right)^2 \leqslant V_l^2 - 2\, V_l\, V_m + V_m^2. \tag{11}$$

Relaxing (11) using (4) yields

$$\left(V_{lm}^{\Delta}\right)^2 \leqslant w_{ll} - 2w_{lm} + w_{mm}. \tag{12}$$

Note that it is not necessary to use a convex envelope on the term V_{lm}^{Δ} since (12) is already an SOCP constraint. Finally, we leverage the relaxation proposed in [23], which is derived by taking linear combinations of the non-linear expressions for the active and reactive line flow expressions. Specifically, the following constraint from [23] couples the

voltage magnitude differences and the power flows:

$$V_l^2 - V_m^2 = \left(\frac{g_{lm}\left(P_{lm} - P_{ml}\right) - b_{lm}\left(Q_{lm} - Q_{ml}\right)}{g_{lm}^2 + b_{lm}^2 + b_{lm}\frac{b_{sh,lm}}{2}} \right). \tag{13}$$

Factoring the left hand side of (13) yields $V_l^2 - V_m^2 = V_{lm}^{\Delta}\left(V_l + V_m\right)$. Relaxing this expression yields

$$\begin{aligned} w_{ll} - w_{mm} &= \hat{W}_{lm,l} + \hat{W}_{lm,m} \\ &= \left(\frac{g_{lm}\left(P_{lm} - P_{ml}\right) - b_{lm}\left(Q_{lm} - Q_{ml}\right)}{g_{lm}^2 + b_{lm}^2 + b_{lm}\frac{b_{sh,lm}}{2}} \right), \end{aligned} \tag{14a}$$

$$\hat{W}_{lm,l} \in \left\langle V_{lm}^{\Delta}\, V_l \right\rangle^M, \tag{14b}$$

$$\hat{W}_{lm,m} \in \left\langle V_{lm}^{\Delta}\, V_m \right\rangle^M. \tag{14c}$$

Observe that (14a) describes two constraints.

Our proposed improvement based on voltage magnitude differences augments the QC relaxation (7) with constraints (10), (12), and (14). The main advantage of these constraints is the quality of the achievable bounds on the voltage magnitude differences V_{lm}^{Δ}. These bounds are computed by extending the bound tightening techniques described in Section 3.2 to directly consider to the variables V_{lm}^{Δ}. This requires initially specified bounds on V_{lm}^{Δ}, which are derived from the bounds on the voltage magnitudes, $\underline{V}_l$, $\overline{V}_l$, $\underline{V}_m$, and $\overline{V}_m$:

$$\underline{V}_l - \overline{V}_m \leqslant V_{lm}^{\Delta} \leqslant \overline{V}_l - \underline{V}_m. \tag{15}$$

After applying bound tightening to the voltage magnitudes, voltage angle differences, and voltage magnitude differences, bounds on the remaining variables (W_{lm}, $\hat{W}_{lm,l}$, and $\hat{W}_{lm,m}$) are derived by straightforward manipulations of the bounds on voltage magnitudes and voltage magnitude differences.

5. TRILINEAR ENVELOPES

Previous formulations of the QC relaxation recursively apply McCormick envelopes (5) to represent the trilinear products formed by the voltage magnitudes and trigonometric terms. However, this approach rarely results in the convex hull of the trilinear products [17]. The Meyer and Floudas envelopes [17, 18] form the convex hulls of trilinear products whose variables range in a box. These envelopes thus provide a mechanism for strengthening the QC relaxation.

Due to the signs of the variables (i.e., positive voltage magnitudes and cosine terms, sign-indefinite sine terms), only certain facets of these envelopes are applicable to the QC relaxation.

Here we show the facets of the Meyer and Floudas envelopes that are applicable to the QC relaxation (7). In the following seven boxes, the upper portion gives conditions for which the constraints in the lower portion apply.

We define $\breve{S} \in \langle \sin(\theta_{lm}) \rangle^{S}$, where this trigonometric envelope is given in (5b), and V_i as the voltage magnitude at bus i as in (7). Let $\langle x\ y\ z \rangle^{MF}$ denote the convex hull defined by the Meyer and Floudas envelopes for the trilinear product of three generic variables, x, y, and z. The variable $\breve{s}_{lm} \in \left\langle V_l\, V_m\, \breve{S} \right\rangle^{MF}$ replaces s_{lm} in (7). Note that multiple cases apply simultaneously (e.g., Case IV implies Case I) such that there are six upper bounds and six lower bounds for each monomial. The same procedure is applied using $\breve{C} \in \langle \cos(\theta_{lm}) \rangle^{C}$, with the variable $\breve{c}_{lm} \in \left\langle V_l\, V_m\, \breve{C} \right\rangle^{MF}$ replacing c_{lm} in (7). Since the cosine function is non-negative in the first and fourth quadrants, only Cases II and III are applicable for this function.

Case I: $\overline{s} \leqslant 0$.

$$
\begin{aligned}
\breve{s}_{lm} &\geqslant \overline{V}_m \underline{s} V_l + \underline{V}_l \underline{s} V_m + \underline{V}_l \underline{V}_m \breve{S} - \underline{V}_l \overline{V}_m \underline{s} - \underline{V}_l \underline{V}_m \underline{s}, \\
\breve{s}_{lm} &\geqslant \overline{V}_m \underline{s} V_l + \underline{V}_l \overline{s} V_m + \underline{V}_l \overline{V}_m \breve{S} - \underline{V}_l \overline{V}_m \underline{s} - \underline{V}_l \overline{V}_m \overline{s}, \\
\breve{s}_{lm} &\geqslant \underline{V}_m \overline{s} V_l + \overline{V}_l \underline{s} V_m + \overline{V}_l \underline{V}_m \breve{S} - \overline{V}_l \underline{V}_m \overline{s} - \overline{V}_l \underline{V}_m \underline{s}, \\
\breve{s}_{lm} &\geqslant \underline{V}_m \overline{s} V_l + \overline{V}_l \overline{s} V_m + \overline{V}_l \overline{V}_m \breve{S} - \overline{V}_l \underline{V}_m \overline{s} - \overline{V}_l \overline{V}_m \overline{s}, \\
\breve{s}_{lm} &\geqslant \underline{V}_m \underline{s} V_l + \overline{V}_l \underline{s} V_m + \underline{V}_l \underline{V}_m \breve{S} - \overline{V}_l \underline{V}_m \underline{s} - \underline{V}_l \underline{V}_m \underline{s}, \\
\breve{s}_{lm} &\geqslant \overline{V}_m \overline{s} V_l + \underline{V}_l \overline{s} V_m + \overline{V}_l \overline{V}_m \breve{S} - \overline{V}_l \overline{V}_m \overline{s} - \underline{V}_l \overline{V}_m \overline{s}.
\end{aligned}
$$

Case II: $\underline{s} \geqslant 0$.

$$
\begin{aligned}
\breve{s}_{lm} &\leqslant \underline{V}_m \underline{s} V_l + \overline{V}_l \underline{s} V_m + \overline{V}_l \overline{V}_m \breve{S} - \overline{V}_l \overline{V}_m \underline{s} - \overline{V}_l \underline{V}_m \underline{s}, \\
\breve{s}_{lm} &\leqslant \overline{V}_m \underline{s} V_l + \underline{V}_l \underline{s} V_m + \overline{V}_l \overline{V}_m \breve{S} - \overline{V}_l \overline{V}_m \underline{s} - \underline{V}_l \overline{V}_m \underline{s}, \\
\breve{s}_{lm} &\leqslant \underline{V}_m \underline{s} V_l + \overline{V}_l \overline{s} V_m + \overline{V}_l \underline{V}_m \breve{S} - \overline{V}_l \underline{V}_m \overline{s} - \overline{V}_l \underline{V}_m \underline{s}, \\
\breve{s}_{lm} &\leqslant \overline{V}_m \overline{s} V_l + \underline{V}_l \underline{s} V_m + \underline{V}_l \overline{V}_m \breve{S} - \underline{V}_l \overline{V}_m \overline{s} - \overline{V}_l \underline{V}_m \underline{s}, \\
\breve{s}_{lm} &\leqslant \underline{V}_m \overline{s} V_l + \overline{V}_l \overline{s} V_m + \underline{V}_l \underline{V}_m \breve{S} - \overline{V}_l \underline{V}_m \overline{s} - \underline{V}_l \underline{V}_m \overline{s}, \\
\breve{s}_{lm} &\leqslant \overline{V}_m \overline{s} V_l + \underline{V}_l \overline{s} V_m + \underline{V}_l \underline{V}_m \breve{S} - \underline{V}_l \overline{V}_m \overline{s} - \underline{V}_l \underline{V}_m \overline{s}.
\end{aligned}
$$

Case III: $\underline{s} \geqslant 0$. Map $\{V_l, V_m, s\}$ to $\{x, y, z\}$ such that
$\overline{x}\underline{y}\underline{z} + \underline{x}\overline{y}\overline{z} \leqslant \underline{x}\overline{y}\underline{z} + \overline{x}\underline{y}\overline{z}$ and $\overline{x}\underline{y}\underline{z} + \underline{x}\overline{y}\overline{z} \leqslant \overline{x}\overline{y}\underline{z} + \underline{x}\underline{y}\overline{z}$.

$$
\begin{aligned}
\breve{s}_{lm} &\geqslant \underline{yz}x + \underline{xz}y + \underline{xy}z - 2\underline{xyz}, \\
\breve{s}_{lm} &\geqslant \overline{yz}x + \overline{xz}y + \overline{xy}z - 2\overline{xyz}, \\
\breve{s}_{lm} &\geqslant \underline{y\overline{z}}x + \underline{x\overline{z}}y + \overline{x}\underline{yz} - \underline{xy}\overline{z} - \overline{x}\underline{y}\overline{z}, \\
\breve{s}_{lm} &\geqslant \overline{y}\underline{z}x + \overline{x}\underline{z}y + \underline{x\overline{y}}z - \overline{x\overline{y}}\underline{z} - \underline{x\overline{y}}\underline{z}, \\
\breve{s}_{lm} &\geqslant \frac{\Lambda_3}{\overline{x} - \underline{x}}x + \overline{x}\underline{z}y + \overline{x}\underline{yz} - \frac{\Lambda_3 \underline{x}}{\overline{x} - \underline{x}} - \overline{x\overline{y}}\underline{z} - \overline{x}\underline{y}\overline{z} + \underline{x\overline{y}}\overline{z}, \\
&\quad \text{where } \Lambda_3 = \overline{xy}\underline{z} - \underline{x\overline{yz}} - \overline{x}\underline{yz} + \overline{x}\underline{y}\overline{z}, \\
\breve{s}_{lm} &\geqslant \frac{\Gamma_3}{\underline{x} - \overline{x}}x + \underline{x\overline{z}}y + \underline{x\overline{y}}z - \frac{\Gamma_3 \overline{x}}{\underline{x} - \overline{x}} - \underline{xy}\overline{z} - \underline{x\overline{y}}\underline{z} + \overline{x}\underline{yz}, \\
&\quad \text{where } \Gamma_3 = \underline{xy}\overline{z} - \overline{x}\underline{yz} - \underline{x\overline{yz}} + \underline{x\overline{y}}\underline{z}.
\end{aligned}
$$

Case IV: $\overline{s} \leqslant 0$,

$$\underline{V}_l\underline{V}_m\underline{s} + \overline{V}_l\overline{V}_m\overline{s} \geqslant \overline{V}_l\underline{V}_m\underline{s} + \underline{V}_l\overline{V}_m\overline{s},$$
$$\underline{V}_l\underline{V}_m\underline{s} + \overline{V}_l\overline{V}_m\overline{s} \geqslant \underline{V}_l\overline{V}_m\underline{s} + \overline{V}_l\underline{V}_m\overline{s}.$$

$$\breve{s}_{lm} \leqslant \underline{V}_m\overline{s}V_l + \underline{V}_l\overline{s}V_m + \underline{V}_l\underline{V}_m\breve{S} - 2\underline{V}_l\underline{V}_m\overline{s},$$
$$\breve{s}_{lm} \leqslant \overline{V}_m\underline{s}V_l + \overline{V}_l\underline{s}V_m + \overline{V}_l\overline{V}_m\breve{S} - 2\overline{V}_l\overline{V}_m\underline{s},$$
$$\breve{s}_{lm} \leqslant \underline{V}_m\underline{s}V_l + \overline{V}_l\overline{s}V_m + \overline{V}_l\underline{V}_m\breve{S} - \overline{V}_l\underline{V}_m\overline{s} - \overline{V}_l\underline{V}_m\underline{s},$$
$$\breve{s}_{lm} \leqslant \overline{V}_m\overline{s}V_l + \underline{V}_l\underline{s}V_m + \underline{V}_l\overline{V}_m\breve{S} - \underline{V}_l\overline{V}_m\overline{s} - \underline{V}_l\overline{V}_m\underline{s},$$
$$\breve{s}_{lm} \leqslant \underline{V}_m\underline{s}V_l + \underline{V}_l\underline{s}V_m + \frac{\Lambda_4}{\underline{s}-\overline{s}}\breve{S} - \frac{\Lambda_4\overline{s}}{\underline{s}-\overline{s}} - \overline{V}_l\underline{V}_m\underline{s}$$
$$- \underline{V}_l\overline{V}_m\underline{s} + \overline{V}_l\overline{V}_m\overline{s},$$
$$\text{where } \Lambda_4 = \overline{V}_l\underline{V}_m\underline{s} - \overline{V}_l\overline{V}_m\overline{s} - \underline{V}_l\underline{V}_m\underline{s} + \underline{V}_l\overline{V}_m\underline{s},$$
$$\breve{s}_{lm} \leqslant \overline{V}_m\overline{s}V_l + \overline{V}_l\overline{s}V_m - \frac{\Gamma_4}{\overline{s}-\underline{s}}\breve{S} - \frac{\Gamma_4\underline{s}}{\overline{s}-\underline{s}} - \overline{V}_l\underline{V}_m\overline{s}$$
$$- \underline{V}_l\overline{V}_m\overline{s} + \underline{V}_l\underline{V}_m\underline{s},$$
$$\text{where } \Gamma_4 = \overline{V}_l\underline{V}_m\overline{s} - \underline{V}_l\underline{V}_m\underline{s} - \overline{V}_l\overline{V}_m\overline{s} + \underline{V}_l\overline{V}_m\overline{s}.$$

Case V: $\overline{s} \leqslant 0$,

$$\overline{V}_l\underline{V}_m\underline{s} + \underline{V}_l\overline{V}_m\overline{s} \geqslant \underline{V}_l\overline{V}_m\underline{s} + \overline{V}_l\underline{V}_m\overline{s},$$
$$\underline{V}_l\underline{V}_m\underline{s} + \overline{V}_l\overline{V}_m\overline{s} < \overline{V}_l\underline{V}_m\underline{s} + \underline{V}_l\overline{V}_m\overline{s},$$
$$\underline{V}_l\underline{V}_m\underline{s} + \overline{V}_l\overline{V}_m\overline{s} < \underline{V}_l\overline{V}_m\underline{s} + \overline{V}_l\underline{V}_m\overline{s}.$$

$$\breve{s}_{lm} \leqslant \underline{V}_m\overline{s}V_l + \underline{V}_l\overline{s}V_m + \underline{V}_l\underline{V}_m\breve{S} - 2\underline{V}_l\underline{V}_m\overline{s},$$
$$\breve{s}_{lm} \leqslant \overline{V}_m\underline{s}V_l + \overline{V}_l\underline{s}V_m + \overline{V}_l\overline{V}_m\breve{S} - 2\overline{V}_l\overline{V}_m\underline{s},$$
$$\breve{s}_{lm} \leqslant \underline{V}_m\underline{s}V_l + \underline{V}_l\underline{s}V_m + \underline{V}_l\overline{V}_m\breve{S} - \underline{V}_l\underline{V}_m\underline{s} - \underline{V}_l\overline{V}_m\underline{s},$$
$$\breve{s}_{lm} \leqslant \overline{V}_m\overline{s}V_l + \overline{V}_l\overline{s}V_m + \overline{V}_l\underline{V}_m\breve{S} - \overline{V}_l\underline{V}_m\overline{s} - \overline{V}_l\overline{V}_m\overline{s},$$
$$\breve{s}_{lm} \leqslant \underline{V}_m\underline{s}V_l + \frac{\Lambda_5}{\underline{V}_m-\overline{V}_m}V_m + \overline{V}_l\underline{V}_m\breve{S} - \frac{\Lambda_5\overline{V}_m}{\underline{V}_m-\overline{V}_m}$$
$$- \underline{V}_l\underline{V}_m\underline{s} - \overline{V}_l\underline{V}_m\overline{s} + \underline{V}_l\overline{V}_m\overline{s},$$
$$\text{where } \Lambda_5 = \underline{V}_l\underline{V}_m\underline{s} - \underline{V}_l\overline{V}_m\overline{s} - \overline{V}_l\underline{V}_m\underline{s} + \overline{V}_l\underline{V}_m\overline{s},$$
$$\breve{s}_{lm} \leqslant \overline{V}_m\overline{s}V_l + \frac{\Gamma_5}{\overline{V}_m-\underline{V}_m}V_m + \underline{V}_l\overline{V}_m\breve{S} - \frac{\Gamma_5\underline{V}_m}{\overline{V}_m-\underline{V}_m}$$
$$- \underline{V}_l\overline{V}_m\underline{s} - \overline{V}_l\overline{V}_m\overline{s} + \overline{V}_l\underline{V}_m\underline{s},$$
$$\text{where } \Gamma_5 = \underline{V}_l\overline{V}_m\underline{s} - \overline{V}_l\underline{V}_m\underline{s} - \underline{V}_l\overline{V}_m\overline{s} + \overline{V}_l\overline{V}_m\overline{s}.$$

Case VI: $\underline{s} \leqslant 0, \overline{s} \geqslant 0$.

$$
\begin{aligned}
&\breve{s}_{lm} \geqslant \overline{V}_m \overline{s} V_l + \overline{V}_l \overline{s} V_m + \overline{V}_l \overline{V}_m \breve{S} - 2\overline{V}_l \overline{V}_m \overline{s}, \\
&\breve{s}_{lm} \geqslant \overline{V}_m \underline{s} V_l + \underline{V}_l \overline{s} V_m + \underline{V}_l \overline{V}_m \breve{S} - \underline{V}_l \overline{V}_m \underline{s} - \underline{V}_l \overline{V}_m \overline{s}, \\
&\breve{s}_{lm} \geqslant \overline{V}_m \underline{s} V_l + \underline{V}_l \underline{s} V_m + \underline{V}_l \underline{V}_m \breve{S} - \underline{V}_l \overline{V}_m \underline{s} - \underline{V}_l \underline{V}_m \underline{s}, \\
&\breve{s}_{lm} \geqslant \underline{V}_m \overline{s} V_l + \overline{V}_l \underline{s} V_m + \overline{V}_l \underline{V}_m \breve{S} - \overline{V}_l \underline{V}_m \overline{s} - \overline{V}_l \underline{V}_m \underline{s}, \\
&\breve{s}_{lm} \geqslant \underline{V}_m \underline{s} V_l + \overline{V}_l \underline{s} V_m + \underline{V}_l \underline{V}_m \breve{S} - \overline{V}_l \underline{V}_m \underline{s} - \underline{V}_l \underline{V}_m \underline{s}, \\
&\breve{s}_{lm} \geqslant \underline{V}_m \overline{s} V_l + \underline{V}_l \overline{s} V_m + \frac{\Lambda_6}{\overline{s} - \underline{s}} \breve{S} - \frac{\Lambda_6 \underline{s}}{\overline{s} - \underline{s}} - \underline{V}_l \overline{V}_m \overline{s} \\
&\qquad - \overline{V}_l \underline{V}_m \overline{s} + \overline{V}_l \overline{V}_m \underline{s}, \\
&\qquad \text{where } \Lambda_6 = \underline{V}_l \overline{V}_m \overline{s} - \overline{V}_l \overline{V}_m \underline{s} - \underline{V}_l \underline{V}_m \overline{s} + \overline{V}_l \underline{V}_m \overline{s}.
\end{aligned}
$$

Case VII: $\underline{s} \leqslant 0, \overline{s} \geqslant 0$.

$$
\begin{aligned}
&\breve{s}_{lm} \leqslant \overline{V}_m \underline{s} V_l + \overline{V}_l \underline{s} V_m + \overline{V}_l \overline{V}_m \breve{S} - 2\overline{V}_l \overline{V}_m \underline{s}, \\
&\breve{s}_{lm} \leqslant \underline{V}_m \underline{s} V_l + \overline{V}_l \overline{s} V_m + \overline{V}_l \underline{V}_m \breve{S} - \overline{V}_l \underline{V}_m \overline{s} - \overline{V}_l \underline{V}_m \underline{s}, \\
&\breve{s}_{lm} \leqslant \overline{V}_m \overline{s} V_l + \underline{V}_l \overline{s} V_m + \underline{V}_l \underline{V}_m \breve{S} - \underline{V}_l \overline{V}_m \overline{s} - \underline{V}_l \underline{V}_m \overline{s}, \\
&\breve{s}_{lm} \leqslant \overline{V}_m \overline{s} V_l + \underline{V}_l \underline{s} V_m + \underline{V}_l \overline{V}_m \breve{S} - \underline{V}_l \overline{V}_m \overline{s} - \underline{V}_l \overline{V}_m \underline{s}, \\
&\breve{s}_{lm} \leqslant \underline{V}_m \overline{s} V_l + \overline{V}_l \overline{s} V_m + \underline{V}_l \underline{V}_m \breve{S} - \overline{V}_l \underline{V}_m \overline{s} - \underline{V}_l \underline{V}_m \overline{s}, \\
&\breve{s}_{lm} \leqslant \underline{V}_m \underline{s} V_l + \underline{V}_l \underline{s} V_m + \frac{\Lambda_7}{\underline{s} - \overline{s}} \breve{S} - \frac{\Lambda_7 \overline{s}}{\underline{s} - \overline{s}} - \overline{V}_l \underline{V}_m \underline{s} \\
&\qquad - \underline{V}_l \overline{V}_m \underline{s} + \overline{V}_l \overline{V}_m \overline{s}, \\
&\qquad \text{where } \Lambda_7 = \overline{V}_l \underline{V}_m \underline{s} - \overline{V}_l \overline{V}_m \overline{s} - \underline{V}_l \underline{V}_m \underline{s} + \underline{V}_l \overline{V}_m \underline{s}.
\end{aligned}
$$

6. NUMERICAL RESULTS

This section demonstrates the proposed improvements using test cases from the NESTA 0.7.0 archive [22] and four cases "nmwc14", "nmwc24," "nmwc57," and "nmwc118" from [24]. With large optimality gaps between the objective values from the best known local optima and the lower bounds from various relaxations, these test cases challenge a variety of solution algorithms and are therefore suitable for our purposes. The implementation uses MATLAB 2013a, YALMIP 2016.09.30 [25], Mosek 8.0.0.42, and a laptop computer with an i5 3.20 GHz processor and 8 GB of RAM. Table 1 details the results for selected test cases. The first column indicates the test case. The second column provides the objective value from MATPOWER [19]. The next group of columns presents the optimality

gaps corresponding to the solution of a QC relaxation variant relative to the local solution from MATPOWER. The optimality gap is

$$\textit{Optimality gap} = \left(\frac{\textit{Local solution} - \textit{QC bound}}{\textit{QC bound}} \right). \tag{25}$$

For many applications, such as branching algorithms that compute global optima [11–13], mixed-integer problems [14, 26], and certain bi-level problems [27], the optimality gap is of primary importance. We therefore use the optimality gap to measure the relaxations' tightness.[1] The final group of columns in Table 1 provides the solution times, listing both the bound tightening time and the QC relaxation's execution time. Note that the bounds were tightened using the corresponding variant of the QC relaxation in the computations. For typographical purposes, Table 1 uses several abbreviations: "All Constraints" (*All Cons.*), "without" (*w/o*), "Meyer and Floudas Envelopes" (*MF*), "Voltage Magnitude Difference constraints" (Δ), and "Bound Tightening" (*BT*).

The results indicate that bound tightening has a substantial impact on the optimality gaps for all variants of the QC relaxation. For instance, comparing the third and seventh columns in Table 1 reveals that applying bound tightening reduces the gaps for "nesta_case30_fsr__api" and "nesta_case118_ieee__api" cases by 77.91% and 58.43%, respectively. The reinforces the fact that the accuracy of the QC relaxation strongly depends on the tightness of the bounds.

Comparing the fourth and seventh columns with the third column demonstrates the impact of the Meyer and Floudas envelopes and voltage difference constraints, both individually and jointly. For instance, the optimality gap for "nesta_case118_ieee__api" without applying these constraints was 22.07% while applying the Meyer and Floudas envelopes and the voltage difference constraints reduces the gap to 19.08% and 21.29%,

[1] Note that the optimality gap depends on both the lower bound from the relaxation and the upper bound from a local solution. Thus, non-zero gaps may be partially due to a suboptimal local solution. However, the same local optima are used to compute the optimality gap for each relaxation, and the gaps can therefore be consistently compared among various relaxations for each test case.

respectively. Applying both at the same time reduces the gap to 18.34%, revealing that the Meyer and Floudas envelopes are the larger contributor to the improvement for this test case. Similar results are obtained for "nesta_case30_fsr__api". Without the Meyer and Floudas envelopes and the voltage difference constraints, the gap is 5.73%. Applying these improvements reduces the gap by 1.0% and 0.25%, respectively. For most of the case studies in Table 1, the Meyer and Floudas envelopes are responsible for more of the improvement than the voltage difference constraints. However, there are cases where the opposite is true, such as "nmwc118", "nmwc57", and "nmwc14". For these cases, the voltage difference constraints outperformed the Meyer and Floudas envelopes in reducing the optimality gap, by up to 5.88% in the case of "nmwc118".

The results suggest that the Meyer and Floudas envelopes and the voltage difference constraints are most effective when applied in combination with a bound tightening algorithm. However, there are cases, such as "nesta_case73_ieee_rts__api" and "nesta_case29_edin__sad" where the proposed improvements have significant impact even without bound tightening (4.7% and 8.27% reductions, respectively). Note that the Meyer and Floudas envelopes play a more important role in both cases. For instance, they reduce the optimality gap for "nesta_case29_edin__sad" by almost 8.25%, whereas the voltage difference constraints only reduce the gap by 0.01%. This matches the intuition that the voltage magnitude difference constraints strongly depend on tight bounds on V_{lm}^{Δ}.

Several comparisons underscore the contributions of different improvements to a basic QC relaxation (with no previous or proposed improvements, i.e., without applying bound tightening, the approaches proposed in this paper, or those in [9, 11–14]). Separately adding different improvements to the basic QC relaxation reveals the individual contributions. The optimality gap of the basic QC relaxation for "nesta_case73_ieee_rts__api" is 16.52%. Separately adding the LNC constraints in [9, 13] and the arctangent envelopes in [12] does not reduce the gap while separately adding the voltage difference constraints and the Meyer and Floudas envelopes reduces the gap by 0.02%, and 4.68%, respectively. Note that using

bound tightening with the basic QC relaxation reduces the gap by 6.43%. Similarly, the optimality gap resulting from applying the basic QC relaxation to "nesta_case29_edin__sad" is 34.53%. Separately enforcing the LNC constraints and the voltage magnitude difference constraints does not reduce the gap while the arctangent envelopes and the Meyer and Floudas envelopes reduce the gap by 6.59% and 14.85%, respectively. For this case, it is interesting to note that the bound tightening approach alone only reduces the gap by 0.62%.

The impact of the voltage magnitude difference constraints strongly depends the quality of the bounds on V_{lm}^{Δ}. Thus, applying these constraints without using bound tightening has a limited effect, as discussed above. In contrast, the voltage magnitude difference constraints contribute to reducing the optimality gap when combined with a bound tightening approach. For instance, these constraints reduce the optimality gap for "nmwc118" by 6.08%, whereas the Meyer and Floudas envelopes only reduce the gap by 0.20%. Thus, the contributions of each improvement to reducing the optimality gap depend on the test case. Our future work includes identifying which system characteristics are most relevant for various types of improvements.

Our proposed improvements substantially reduce the optimality gaps for many challenging test cases. As shown in Table 1, this improved tightness comes at the cost of slower (but still tractable) computational times for some test cases. Comparing the last two columns in Table 1 reveals that enforcing the Meyer and Floudas envelopes and the voltage difference constraints results in less than a 41.9% increase in the time required to solve the QC relaxation (without bound tightening) on average across the test cases. Comparing the execution times in the ninth and twelfth columns of Table 1 shows that adding the Meyer and Floudas envelopes and the voltage difference constraints has a disparate impact on the total execution time (bound tightening plus QC execution). There are cases such as "nesta_case29_edin__sad" where enforcing the Meyer and Floudas envelopes reduces the execution time by 10.8%. For these cases, the bound tightening algorithm converges in fewer iterations, which more than accounts for the additional time required per iteration

Table 1. Results from applying the QC relaxation with various improvements to selected test cases.

		Optimality Gap (%)						All Cons.		w/o MF		w/o Δ		w/o {MF, Δ}		w/o BT	w/o {MF, BT, Δ}
Test Case	**AC ($/hr)**	**All Cons.**	**w/o MF**	**w/o Δ**	**w/o {MF, Δ}**	**w/o BT**	**w/o {BT, MF, Δ}**	**BT time**	**QC time**	**BT time**	**QC time**	**BT time**	**QC time**	**BT time**	**QC time**	**QC time**	**QC time**
nesta_case3_lmbd	5812.64	0.46	0.49	0.46	0.49	1.18	1.26	3.7	0.7	4.3	0.6	4.2	0.7	4.5	0.6	0.3	0.2
nesta_case5_pjm	17551.89	15.22	15.43	15.28	15.54	17.01	17.01	6.7	0.6	6.4	0.5	5.9	0.6	6.3	0.5	0.3	0.2
nesta_case29_edin	29895.49	0.03	0.05	0.03	0.05	0.10	0.10	162.6	0.8	242.1	0.7	91.5	0.8	113.6	0.5	0.4	0.3
nesta_case118_ieee	3718.64	0.37	0.42	0.38	0.43	1.47	1.68	937.7	1.1	789.5	0.9	729.8	1.1	633.3	0.9	0.8	0.6
nesta_case29_edin__api	295291.22	0.08	0.10	0.08	0.10	0.40	0.40	141.6	0.8	114.8	0.6	123.1	0.8	84.9	0.6	0.4	0.3
nesta_case30_fsr__api	366.57	4.57	5.48	4.73	5.73	82.48	82.48	95.2	0.7	79.4	0.6	61.4	0.7	54.7	0.6	0.4	0.3
nesta_case73_ieee_rts__api	19995.00	0.17	0.21	0.18	0.21	11.82	16.52	295.0	1.3	309.3	1.0	190.3	1.3	192.1	1.0	0.6	0.4
nesta_case118_ieee__api	10269.82	18.34	21.29	19.08	22.07	76.77	77.16	1536.2	1.4	1401.9	1.1	701.2	1.2	689.0	0.9	0.8	0.5
nesta_case3_lmbd__sad	5959.33	0.06	0.06	0.16	0.16	1.42	1.45	6.0	0.7	5.8	0.6	6.6	0.7	6.0	0.6	0.3	0.2
nesta_case5_pjm__sad	26115.20	0.10	0.12	0.10	0.12	0.78	1.35	5.7	0.6	5.4	0.5	6.1	0.6	5.2	0.5	0.3	0.2
nesta_case9_wscc__sad	5528.26	0.05	0.06	0.05	0.06	0.48	0.54	5.7	0.7	4.2	0.7	4.8	0.7	3.9	0.6	0.3	0.2
nesta_case24_ieee_rts__sad	76943.25	0.09	0.11	0.10	0.12	2.81	3.20	43.2	1.1	45.1	0.9	33.5	1.1	30.0	0.9	0.4	0.3
nesta_case29_edin__sad	41258.49	1.80	2.74	1.81	2.72	19.68	27.95	174.9	0.8	193.8	0.7	176.2	0.8	102.3	0.6	0.4	0.3
nesta_case30_as__sad	897.49	0.15	0.17	0.15	0.17	2.30	2.38	31.0	0.9	27.5	0.8	23.6	0.9	21.9	0.9	0.4	0.3
nesta_case39_epri__sad	96745.01	0.00	0.01	0.01	0.02	0.05	0.09	84.5	1.1	73.9	1.0	67.7	1.1	47.8	0.9	0.4	0.3
nesta_case118_ieee__sad	4106.72	0.69	0.92	0.70	0.94	4.18	5.03	897.6	1.2	864.4	1.0	951.6	1.1	770.7	1.0	0.9	0.5
nmwc14	2529.87	0.17	0.17	0.19	0.19	0.22	0.22	20.9	0.6	19.0	0.5	14.6	0.5	13.5	0.4	0.4	0.3
nmwc57	9186.12	6.44	6.45	7.22	7.20	9.66	9.66	248.2	1.3	169.2	1.0	269.9	1.4	161.1	1.1	0.5	0.3
nmwc118	34663.69	17.07	17.27	23.15	23.19	24.07	24.07	1660.8	4.1	1438.9	2.9	740.1	3.7	488.6	2.9	2.0	1.7

Abbreviations: “All Constraints” (*All Cons.*), “without” (*w/o*), “Meyer and Floudas Envelopes” (*MF*), “Voltage Magnitude Difference constraints” (Δ), and “Bound Tightening” (*BT*). All times in seconds.

due to the addition of new variables and constraints. Since the bound tightening times dominate the execution time for the QC relaxation, the overall time decreases for some cases. Conversely, other test cases require more time, resulting in an average increase of 5.2% over all the test cases and up to an 31.9% increase for some cases.

7. CONCLUSION

This paper proposes and empirically tests two improvements for the QC relaxation of the OPF problem: a set of constraints based on voltage magnitude differences and the Meyer and Floudas envelopes for trilinear monomials. The former relies on the observation that bound tightening algorithms can effectively tighten the voltage magnitude differences between connected buses. The latter yields the convex hull of the trilinear monomials in contrast to the potentially weaker nested McCormick formulation used in previous work. Comparison to a state-of-the-art QC implementation demonstrates the value of these improvements via reduced optimality gaps on challenging test cases while maintaining computational tractability. Our ongoing work aims to improve computational speed by targeting the application of the bound tightening techniques to the most relevant variables. Other ongoing work is developing further improvements to convex relaxations based on physically intuitive coordinate transformations.

BIBLIOGRAPHY

[1] W.A. Bukhsh,A. Grothey, K.I.M. McKinnon, P.A. Trodden, Local Solutions of the Optimal Power Flow Problem, IEEE Transaction on Power Systems, 28 (4) (2013) 4780–4788.

[2] K. Lehmann, A. Grastien and P. Van Hentenryck, AC-Feasibility on Tree Networks is NP-Hard, IEEE Transaction on Power Systems 31 (1) (2016) 798–801.

[3] D. Bienstock, A. Verma, Strong NP-hardness of AC Power Flows Feasibility, arXiv:1512.07315 (2015).

[4] J.A. Momoh, R. Adapa, M.E. El-Hawary, A Review of Selected Optimal Power Flow Literature to 1993. Parts I and II, IEEE Transaction on Power Systems 14 (1) (1999) 96–111.

[5] A. Castillo, R.P. O'Neill, Survey of Approaches to Solving the ACOPF (OPF Paper 4) March (2013).

[6] J. F. Marley, D. K. Molzahn, I. A. Hiskens, Solving Multiperiod OPF Problems using an AC-QP Algorithm Initialized with an SOCP Relaxation, IEEE Transaction on Power Systems 32 (5) (2017) 3538–3548.

[7] D. K. Molzahn, I. A. Hiskens, A Survey of Relaxations and Approximations of the Power Flow Equations, Foundations and Trends in Electric Energy Systems February (2019).

[8] C. Coffrin, H.L. Hijazi, P. Van Hentenryck, The QC Relaxation: A Theoretical and Computational Study on Optimal Power Flow, IEEE Transaction on Power Systems 31 (4) (2016) 3008–3018.

[9] C. Coffrin, H. L. Hijazi, P. Van Hentenryck, Strengthening the SDP Relaxation of AC Power Flows with Convex Envelopes, Bound Tightening, and Valid Inequalities, IEEE Transaction on Power Systems 32 (5) (2017) 3549–3558.

[10] C. Chen, A. Atamturk, S.S. Oren, Bound Tightening for the Alternating Current Optimal Power Flow Problem, IEEE Transaction on Power Systems 31 (5) (2016) 3729–3736.

[11] B. Kocuk, S.S. Dey, X.A. Sun, Strong SOCP Relaxations for the Optimal Power Flow Problem, Operation Research 64 (4) (2016) 1177–1196.

[12] B. Kocuk, S.S. Dey, X.A. Sun, Matrix Minor Reformulation and SOCP-based Spatial Branch-and-Cut Method for the AC Optimal Power Flow Problem, arXiv:1703.03050 March (2017).

[13] C. Chen, A. Atamturk, S.S Oren, A Spatial Branch-and-Cut Algorithm for Nonconvex QCQP with Bounded Complex Variables, Mathematical Programming 165 (2) (2017) 549–577.

[14] K. Bestuzheva, H.L. Hijazi, C. Coffrin, Convex Relaxations for Quadratic On/Off Constraints and Applications to Optimal Transmission Switching, http://www.optimization-online.org/DB_FILE/2016/07/5565.pdf (2016).

[15] J.P. Ruiz, J.P. Grossmann, Using Redundancy to Strengthen the Relaxation for the Global Optimization of MINLP Problems, Computers & Chemical Engineering 35 (12) (2011) 2729–2740.

[16] G.P. McCormick, Computability of Global Solutions to Factorable Nonconvex Programs: Part I–Convex Underestimating Problems, Mathematical Programming 10 (1) (1976) 147–175.

[17] C.A. Meyer, C.A. Floudas, Trilinear Monomials with Positive or Negative Domains: Facets of the Convex and Concave Envelopes, Frontiers in Global Optimization (2004) 327–352.

[18] C.A. Meyer, C.A. Floudas, Trilinear Monomials with Mixed Sign Domains: Facets of the Convex and Concave Envelopes, Journal of Global Optimization 29 (2) (2004) 125–155.

[19] R.D. Zimmerman, C.E. Murillo-Sanchez, R.J. Thomas, MATPOWER: Steady-State Operations, Planning, and Analysis Tools for Power Systems Research and Education, IEEE Transaction on Power Systems, 26 (1) (2011) 1–8.

[20] R. Jabr, Radial Distribution Load Flow using Conic Programming, IEEE Transaction on Power Systems 21 (3) (2006) 1458–1459.

[21] D.K. Molzahn, Computing the Feasible Spaces of Optimal Power Flow Problems, IEEE Transaction on Power Systems, 32 (6) (2017) 4752–4763.

[22] C. Coffrin, D. Gordon, P. Scott, NESTA, the NICTA Energy System Test Case Archive (v0.7), arXiv:1411.0359 June (2017).

[23] J.A. Taylor, F.S. Hover, Linear Relaxations for Transmission System Planning, IEEE Transaction on Power Systems 26 (4) (2011) 2533-2538. month=Nov.

[24] M.R. Narimani, D. K. Molzahn, D. Wu, M.L. Crow, Empirical Investigation of Non-Convexities in Optimal Power Flow Problems, American Control Conference (ACC) June (2018).

[25] J. Lofberg, YALMIP: A Toolbox for Modeling and Optimization in MATLAB, IEEE International Symposium on Computer-Aided Control System Design, (2004) 284–289.

[26] B. Kocuk, S. S. Dey, X. A. Sun, New Formulation and Strong MISOCP Relaxations for AC Optimal Transmission Switching Problem, IEEE Transaction on Power Systems 32 (6) (2017) 4161–4170.

[27] D.K. Molzahn and L.A. Roald, Towards an AC Optimal Power Flow Algorithm with Robust Feasibility Guarantees, 20th power system computation conference (PSCC) June (2018).

III. COMPARISON OF VARIOUS TRILINEAR MONOMIAL ENVELOPES FOR CONVEX RELAXATIONS OF OPTIMAL POWER FLOW PROBLEMS

Mohammad Rasoul Narimani, Daniel K. Molzahn, Harsha Nagarajan, and Mariesa L. Crow

Department of Electrical and Computer Engineering

Missouri University of Science and Technology

Rolla, Missouri 65409–0050

Email: mn9t5@mst.edu

ABSTRACT

Solutions to optimal power flow (OPF) problems provide operating points for electric power systems that minimize operational costs while satisfying both engineering limits and the power flow equations. OPF problems are non-convex and may have multiple local optima. To search for global optima, recent research has developed a variety of convex relaxations to bound the optimal objective values of OPF problems. Certain relaxations, such as the quadratic convex (QC) relaxation, are derived from OPF representations that contain trilinear monomials. Previous work has considered three techniques for relaxing these trilinear monomials: *recursive McCormick* (RMC) envelopes, *Meyer and Floudas* (MF) envelopes, and *extreme-point* (EP) envelopes. This paper compares the tightness and computational speed of relaxations that employ each of these techniques. Forming the convex hull of a single trilinear monomial, MF and EP envelopes are equivalently tight. Empirical results show that QC formulations using MF and EP envelopes give tighter bounds than those using RMC envelopes. Empirical results also indicate that the EP envelopes have advantages over MF envelopes with respect to computational speed and numerical stability when used with state-of-the-art second-order cone programming solvers.

1. INTRODUCTION

Optimal power flow (OPF) is a fundamental problem in power system operation and control. OPF problems seek operating points that optimize a specified objective function (often generation cost minimization) subject to engineering limits and power flow constraints that model the network physics [1]. OPF problems are non-convex, may have multiple local solutions [2], and are generally NP-hard [3, 4]. Since being introduced by Carpentier in 1962 [5], many solution techniques have been developed for OPF problems [6, 7].

Recently, a plethora of convex relaxation techniques have been applied to OPF problems in order to compute bounds on the objective values and, in some cases, obtain the globally optimal decision variables. Convex relaxations can also certify the infeasibility of OPF problems and provide initializations for local solution algorithms [8]. Convex relaxations have been formulated as semidefinite programs [9–11], second-order cone programs (SOCP) [12–18], and linear programs [19–21]. A detailed survey is provided in [22].

Some relaxations, such as the quadratic convex (QC) relaxation, are derived using polar representations of the complex voltage phasors. Polar representations result in trilinear products consisting of the voltage magnitudes and trigonometric functions of voltage angle differences for each pair of connected buses. The corresponding non-convex trilinear monomials are relaxed using convex envelope enclosures. The tightness of these envelopes and their particular mathematical formulations significantly impact a relaxation's solution quality and computational tractability.

Three formulations for these envelopes have been proposed in previous OPF relaxation literature: recursively applied McCormick (RMC) envelopes [15], Meyer and Floudas (MF) envelopes [23], and extreme-point (EP) envelopes [24]. RMC envelopes first form lifted variables representing voltage magnitude products using the McCormick envelope for bilinear monomials [25], and then use another McCormick envelope to represent the products of these lifted variables with variables corresponding to the trigonometic functions.

Even though the McCormick envelopes yield the convex hulls of bilinear monomials, recursive application of these envelopes does not necessarily yield the convex hulls of trilinear monomials.

Meyer and Floudas derived envelopes constructed via sets of hyperplanes which form the convex hulls of trilinear monomials [26, 27]. The convex hulls of trilinear envelopes can also be formulated via an EP characterization [28–30]. MF and EP envelopes are applied to the QC relaxation in [23] and [24], respectively. Both the MF and the EP envelopes form the convex hulls of the trilinear monomials and therefore result in equivalently tight relaxations. However, their mathematical representations are quite different, which can result in differing numerical performance.

To characterize the performance of various envelopes, this paper compares the solution quality and computational tractability resulting from each of these three approaches for handling trilinear monomials in QC relaxations of OPF problems. Applying each approach to a wide variety of test cases using various solvers indicates that QC relaxations with MF and EP envelopes provide tighter objective value bounds compared to RMC envelopes. Application of multiple solvers indicates that EP and RMC envelopes are numerically stable on all the test cases with comparable computational speeds. MF envelopes yield numerical issues for some solvers.

This paper is organized as follows. Section 2 overviews the OPF problem. Section 3 reviews the QC relaxation of the OPF problem and presents different approaches for handling trilinear monomials. Section 7 empirically compares each approach for various test cases. Section 8 concludes the paper.

2. OPTIMAL POWER FLOW OVERVIEW

This section reviews an OPF formulation using a polar representation of the voltage phasors. The power system network is modeled by a graph $(\mathcal{N}, \mathcal{L})$ with $\mathcal{N}$ and $\mathcal{L}$ representing the sets of buses and branches, respectively. Let "ref" denote the reference

bus. Let $P_i^d + jQ_i^d$ and $P_i^g + jQ_i^g$ represent the complex power demand and generation at bus $i \in \mathcal{N}$, where $j = \sqrt{-1}$. Let $g_{sh,i} + jb_{sh,i}$ denote the shunt admittance at bus $i \in \mathcal{N}$. Let V_i and θ_i represent the voltage magnitude and angle at bus $i \in \mathcal{N}$. For each generator $i \in \mathcal{N}$, define a quadratic generation cost function with coefficients $c_{2,i} \geqslant 0$, $c_{1,i}$, and $c_{0,i}$. Denote $\theta_{lm} = \theta_l - \theta_m$. Specified upper and lower limits are denoted by $(\overline{\cdot})$ and $(\underline{\cdot})$, respectively. Buses without generators have generation limits set to zero.

Each line $(l,m) \in \mathcal{L}$ is modeled as a Π circuit with mutual admittance $g_{lm} + jb_{lm}$ and shunt susceptance $jb_{c,lm}$. Denote the complex power flow on the line $(l,m) \in \mathcal{L}$ as $P_{lm} + jQ_{lm}$. Using these definitions, the OPF problem is

$$\min \quad \sum_{i \in \mathcal{N}} c_{2,i} \left(P_i^g\right)^2 + c_{1,i} P_i^g + c_{0,i} \tag{1a}$$

$$\text{subject to} \quad (\forall i \in \mathcal{N},\ \forall (l,m) \in \mathcal{L})$$

$$P_i^g - P_i^d = g_{sh,i} V_i^2 + \sum_{\substack{(l,m)\in\mathcal{L} \\ \text{s.t. } l=i}} P_{lm} + \sum_{\substack{(l,m)\in\mathcal{L} \\ \text{s.t. } m=i}} P_{ml}, \tag{1b}$$

$$Q_i^g - Q_i^d = -b_{sh,i} V_i^2 + \sum_{\substack{(l,m)\in\mathcal{L} \\ \text{s.t. } l=i}} Q_{lm} + \sum_{\substack{(l,m)\in\mathcal{L} \\ \text{s.t. } m=i}} Q_{ml}, \tag{1c}$$

$$\theta_{ref} = 0, \tag{1d}$$

$$\underline{P}_i^g \leqslant P_i^g \leqslant \overline{P}_i^g, \quad \underline{Q}_i^g \leqslant Q_i^g \leqslant \overline{Q}_i^g, \tag{1e}$$

$$\underline{V}_i \leqslant V_i \leqslant \overline{V}_i, \quad \underline{\theta}_{lm} \leqslant \theta_{lm} \leqslant \overline{\theta}_{lm}, \tag{1f}$$

$$P_{lm} = g_{lm} V_l^2 - g_{lm} V_l V_m \cos(\theta_{lm}) - b_{lm} V_l V_m \sin(\theta_{lm}), \tag{1g}$$

$$Q_{lm} = -(b_{lm} + b_{c,lm}/2) V_l^2 + b_{lm} V_l V_m \cos(\theta_{lm}) - g_{lm} V_l V_m \sin(\theta_{lm}), \tag{1h}$$

$$P_{lm}^2 + Q_{lm}^2 \leqslant \left(\overline{S}_{lm}\right)^2, \quad P_{ml}^2 + Q_{ml}^2 \leqslant \left(\overline{S}_{lm}\right)^2. \tag{1i}$$

The quadratic objective (1a) minimizes the total generation cost. Constraints (1b) and (1c) enforce power balance at each bus. Constraint (1d) sets the angle reference. Constraints (1e)–(1f) limit the active and reactive power generation, voltage magnitudes, and angle differences between connected buses. Constraints (1i)–(1i) model the power

flows on each line, and (1i) limits the apparent power flows into each line terminal. Note that (1) can be extended to more detailed transformer models, such as off-nominal tap ratios and non-zero phase shifts, which are used in computing our numerical results.

3. THE QC RELAXATION

The relevant nonlinear expressions in (1) are $V_i^2,\ \forall i \in \mathcal{N},\ V_l\,V_m\cos(\theta_{lm}),$ and $V_l\,V_m\sin(\theta_{lm}),\ \forall(l,m) \in \mathcal{L}$.[2] The QC relaxation encloses these expressions in convex envelopes.

3.1. SQUARED VOLTAGE MAGNITUDE AND TRIGONOMETRIC ENVELOPES

The envelope $\langle x^2\rangle^T$ is the convex hull of the squared function:

$$\langle x^2\rangle^T = \left\{\breve{x} : \left\{\breve{x} \geqslant x^2, \quad \breve{x} \leqslant (\overline{x}+\underline{x})\,x - \overline{x}\underline{x}. \right\}\right\}, \tag{2}$$

where $\breve{x}$ is a "lifted" variable representing the set. Squared voltage magnitudes are relaxed as $w_{ii} \in \langle V_i^2\rangle^T$.

Envelopes for the sine and cosine functions are

$$\langle \sin(x)\rangle^S = \left\{\breve{S} : \begin{cases} \breve{S} \leqslant \cos\left(\frac{x^m}{2}\right)\left(x - \frac{x^m}{2}\right) + \sin\left(\frac{x^m}{2}\right), \\ \breve{S} \geqslant \cos\left(\frac{x^m}{2}\right)\left(x + \frac{x^m}{2}\right) - \sin\left(\frac{x^m}{2}\right). \end{cases}\right\}, \tag{3a}$$

$$\langle \cos(x)\rangle^C = \left\{\breve{C} : \begin{cases} \breve{C} \leqslant 1 - \frac{1-\cos(x^m)}{(x^m)^2}x^2, \\ \breve{C} \geqslant \frac{\cos(\underline{x})-\cos(\overline{x})}{\underline{x}-\overline{x}}\left(x - \underline{x}\right) + \cos\left(\underline{x}\right). \end{cases}\right\}, \tag{3b}$$

[2]The objective (1d) and constraint (1i) are representable as SOCPs.

where $x^m = \max(|\underline{x}|, |\overline{x}|)$ and the lifted variables $\check{S}$ and $\check{C}$ represent the corresponding set. For each line $(l,m) \in \mathcal{L}$, the QC relaxation is strengthened via constraints proposed in [31] that relate the squared magnitudes of current flows, ℓ_{lm}, the squared voltage magnitudes, and the power flows on the lines:

$$P_{lm} + P_{ml} = \frac{g_{lm}}{g_{lm}^2 + b_{lm}^2} \left(\ell_{lm} + \frac{b_{c,lm}^2}{4} V_l^2 + b_{c,lm}\, Q_{lm} \right), \tag{4a}$$

$$Q_{lm} + Q_{ml} = \frac{-b_{lm}}{g_{lm}^2 + b_{lm}^2} \left(\ell_{lm} + \frac{b_{c,lm}^2}{4} V_l^2 + b_{c,lm}\, Q_{lm} \right) - (b_{c,lm}/2) \left(V_l^2 + V_m^2 \right), \tag{4b}$$

$$P_{lm}^2 + Q_{lm}^2 \leqslant V_l^2\, \ell_{lm}. \tag{4c}$$

Relaxing $\sin(\theta_{lm})$ and $\cos(\theta_{lm})$ via $s_{lm} \in \langle \sin(\theta_{lm}) \rangle^S$ and $c_{lm} \in \langle \cos(\theta_{lm}) \rangle^C$ yields the trilinear monomials $V_l\, V_m\, s_{lm}$ and $V_l\, V_m\, c_{lm}$, $\forall (l,m) \in \mathcal{L}$. This section next presents various relaxations of these monomials.

3.2. RECURSIVE MCCORMICK ENVELOPES FOR TRILINEAR MONOMIALS

The McCormick envelope $\langle x\, y \rangle^M$ forms the convex hull of the bilinear monomial xy. A McCormick envelope is formulated using four linear inequality constraints:

$$\langle x\, y \rangle^M = \left\{ \breve{xy} : \begin{cases} \breve{xy} \geqslant \underline{x}y + \underline{y}x - \underline{x}\,\underline{y}, & \breve{xy} \geqslant \overline{x}y + \overline{y}x - \overline{xy}, \\ \breve{xy} \leqslant \underline{x}y + \overline{y}x - \underline{x}\overline{y}, & \breve{xy} \leqslant \overline{x}y + \underline{y}x - \overline{x}\,\underline{y}. \end{cases} \right\}, \tag{5}$$

where $\breve{xy}$ is a lifted variable. To address trilinear monomials, the QC relaxation in [15] recursively applies McCormick envelopes by first constructing a lifted variable w_{lm} that relaxes the product of the voltage magnitudes, $V_l\, V_m$, i.e., $w_{lm} \in \langle V_l\, V_m \rangle^M$ for all $(l,m) \in \mathcal{L}$. McCormick envelopes are then again applied to represent the trilinear monomials $V_l\, V_m\, s_{lm}$ and $V_l\, V_m\, c_{lm}$ as $w_{s,lm} \in \langle w_{lm}\, s_{lm} \rangle^M$ and $w_{c,lm} \in \langle w_{lm}\, c_{lm} \rangle^M$, respectively, for all $(l,m) \in \mathcal{L}$.

Recursive McCormick envelopes do not generally yield the convex hull of a given trilinear monomial [30, 32]. The following sections describe two alternative envelopes that yield the convex hull of a trilinear monomial.

3.3. MEYER AND FLOUDAS ENVELOPES FOR TRILINEAR MONOMIALS

MF envelopes [26, 27] are hyperplane representations of the convex hull of a trilinear monomial. MF envelopes are formed using linear inequalities that are applied based on the signs of the bounds on the variables that make up the trilinear monomial. We denote the envelopes for $V_l\, V_m\, s_{lm}$ and $V_l\, V_m\, c_{lm}$ as $w_{s,lm} \in \langle V_l\, V_m\, s_{lm} \rangle^{MF}$ and $w_{c,lm} \in \langle V_l\, V_m\, c_{lm} \rangle^{MF}$, respectively, $\forall (l,m) \in \mathcal{L}$.

The cases that are relevant to the monomials $V_l\, V_m\, s_{lm}$, $\forall (l,m) \in \mathcal{L}$, are presented in the boxes denoted "Cases I–VII", where the subscripts on the s_{lm} variable bounds are dropped for notational brevity. The upper portion of each box gives the conditions which must all be satisfied for the constraints in the lower portion to apply. Note that multiple cases apply simultaneously (e.g., Case IV implies Case I).

The same procedure is applied for the monomials $V_l\, V_m\, c_{lm}$, $\forall (l,m) \in \mathcal{L}$, with c_{lm} replacing s_{lm}. Since the cosine function is non-negative in the first and fourth quadrants, only Cases II and III are applicable for these monomials.

3.4. EXTREME POINT ENVELOPES FOR TRILINEAR MONOMIAS

EP envelopes capture the convex hull of a trilinear monomial, or a multilinear monomial in general, in a vertex representation [28]. Given a set X, a point $p \in X$ is *extreme* if it cannot be expressed as a convex combination of two distinct points from X, i.e., there *do not* exist two other distinct points $p_1, p_2 \in X$ and a non-negative multiplier $\lambda \in (0,1)$ such that $p = \lambda p_1 + (1-\lambda) p_2$. Based on this definition of an extreme point, we now describe the convex envelope.

Case I: $\overline{s} \leqslant 0$.

$$
\begin{aligned}
\check{s}_{lm} &\geqslant \overline{V}_m \underline{s} V_l + \underline{V}_l \underline{s} V_m + \underline{V}_l \underline{V}_m \check{S} - \underline{V}_l \overline{V}_m \underline{s} - \underline{V}_l \underline{V}_m \underline{s}, \\
\check{s}_{lm} &\geqslant \overline{V}_m \underline{s} V_l + \underline{V}_l \overline{s} V_m + \underline{V}_l \overline{V}_m \check{S} - \underline{V}_l \overline{V}_m \underline{s} - \underline{V}_l \overline{V}_m \overline{s}, \\
\check{s}_{lm} &\geqslant \underline{V}_m \overline{s} V_l + \overline{V}_l \underline{s} V_m + \overline{V}_l \underline{V}_m \check{S} - \overline{V}_l \underline{V}_m \overline{s} - \overline{V}_l \underline{V}_m \underline{s}, \\
\check{s}_{lm} &\geqslant \underline{V}_m \overline{s} V_l + \overline{V}_l \overline{s} V_m + \overline{V}_l \overline{V}_m \check{S} - \overline{V}_l \underline{V}_m \overline{s} - \overline{V}_l \overline{V}_m \overline{s}, \\
\check{s}_{lm} &\geqslant \underline{V}_m \underline{s} V_l + \overline{V}_l \underline{s} V_m + \underline{V}_l \underline{V}_m \check{S} - \overline{V}_l \underline{V}_m \underline{s} - \underline{V}_l \underline{V}_m \underline{s}, \\
\check{s}_{lm} &\geqslant \overline{V}_m \overline{s} V_l + \underline{V}_l \overline{s} V_m + \overline{V}_l \overline{V}_m \check{S} - \overline{V}_l \overline{V}_m \overline{s} - \underline{V}_l \overline{V}_m \overline{s}.
\end{aligned}
$$

Case II: $\underline{s} \geqslant 0$.

$$
\begin{aligned}
\check{s}_{lm} &\leqslant \underline{V}_m \underline{s} V_l + \overline{V}_l \underline{s} V_m + \overline{V}_l \overline{V}_m \check{S} - \overline{V}_l \overline{V}_m \underline{s} - \overline{V}_l \underline{V}_m \underline{s}, \\
\check{s}_{lm} &\leqslant \overline{V}_m \underline{s} V_l + \underline{V}_l \underline{s} V_m + \overline{V}_l \overline{V}_m \check{S} - \overline{V}_l \overline{V}_m \underline{s} - \underline{V}_l \overline{V}_m \underline{s}, \\
\check{s}_{lm} &\leqslant \underline{V}_m \underline{s} V_l + \overline{V}_l \overline{s} V_m + \overline{V}_l \underline{V}_m \check{S} - \overline{V}_l \underline{V}_m \overline{s} - \overline{V}_l \underline{V}_m \underline{s}, \\
\check{s}_{lm} &\leqslant \overline{V}_m \overline{s} V_l + \underline{V}_l \underline{s} V_m + \underline{V}_l \overline{V}_m \check{S} - \underline{V}_l \overline{V}_m \overline{s} - \underline{V}_l \overline{V}_m \underline{s}, \\
\check{s}_{lm} &\leqslant \underline{V}_m \overline{s} V_l + \overline{V}_l \overline{s} V_m + \underline{V}_l \underline{V}_m \check{S} - \underline{V}_l \underline{V}_m \overline{s} - \underline{V}_l \underline{V}_m \overline{s}, \\
\check{s}_{lm} &\leqslant \overline{V}_m \overline{s} V_l + \underline{V}_l \overline{s} V_m + \underline{V}_l \underline{V}_m \check{S} - \underline{V}_l \overline{V}_m \overline{s} - \underline{V}_l \underline{V}_m \overline{s}.
\end{aligned}
$$

Case III: $\underline{s} \geqslant 0$. Map $\{V_l, V_m, s\}$ to $\{x, y, z\}$ such that
$\overline{x}\underline{y}\underline{z} + \underline{x}\overline{y}\overline{z} \leqslant \underline{x}\overline{y}\underline{z} + \overline{x}\underline{y}\overline{z}$ and $\overline{x}\underline{y}\underline{z} + \underline{x}\overline{y}\overline{z} \leqslant \overline{x}\overline{y}\underline{z} + \underline{x}\underline{y}\overline{z}$.

$$
\begin{aligned}
\check{s}_{lm} &\geqslant \underline{yz}x + \underline{xz}y + \underline{xy}z - 2\underline{xyz}, \\
\check{s}_{lm} &\geqslant \overline{yz}x + \overline{xz}y + \overline{xy}z - 2\overline{xyz}, \\
\check{s}_{lm} &\geqslant \underline{y}\overline{z}x + \underline{x}\overline{z}y + \overline{x}\underline{y}z - \underline{xy}\overline{z} - \overline{x}\underline{y}\overline{z}, \\
\check{s}_{lm} &\geqslant \overline{y}\underline{z}x + \overline{x}\underline{z}y + \underline{x}\overline{y}z - \overline{x}\overline{y}\underline{z} - \underline{x}\overline{y}\underline{z}, \\
\check{s}_{lm} &\geqslant \frac{\Lambda_3}{\overline{x} - \underline{x}}x + \overline{x}\underline{z}y + \overline{x}\underline{y}z - \frac{\Lambda_3 \underline{x}}{\overline{x} - \underline{x}} - \overline{x}\overline{y}\underline{z} - \overline{x}\underline{y}\overline{z} + \underline{x}\overline{y}\overline{z}, \\
&\quad \text{where } \Lambda_3 = \overline{x}\overline{y}\underline{z} - \underline{x}\overline{y}\overline{z} - \overline{x}\underline{y}\underline{z} + \overline{x}\underline{y}\overline{z}, \\
\check{s}_{lm} &\geqslant \frac{\Gamma_3}{\underline{x} - \overline{x}}x + \underline{x}\overline{z}y + \underline{x}\overline{y}z - \frac{\Gamma_3 \overline{x}}{\underline{x} - \overline{x}} - \underline{xy}\overline{z} - \underline{x}\overline{y}\underline{z} + \overline{x}\underline{yz}, \\
&\quad \text{where } \Gamma_3 = \underline{xy}\overline{z} - \overline{x}\underline{yz} - \underline{x}\overline{yz} + \underline{x}\overline{y}\underline{z}.
\end{aligned}
$$

Case IV: $\overline{s} \leqslant 0$,

$$\underline{V}_l \underline{V}_m \underline{s} + \overline{V}_l \overline{V}_m \overline{s} \geqslant \overline{V}_l \underline{V}_m \underline{s} + \underline{V}_l \overline{V}_m \overline{s},$$
$$\underline{V}_l \underline{V}_m \underline{s} + \overline{V}_l \overline{V}_m \overline{s} \geqslant \underline{V}_l \overline{V}_m \underline{s} + \overline{V}_l \underline{V}_m \overline{s}.$$

$$\begin{aligned}
\check{s}_{lm} &\leqslant \underline{V}_m \overline{s} V_l + \underline{V}_l \overline{s} V_m + \underline{V}_l \underline{V}_m \check{S} - 2\underline{V}_l \underline{V}_m \overline{s}, \\
\check{s}_{lm} &\leqslant \overline{V}_m \underline{s} V_l + \overline{V}_l \underline{s} V_m + \overline{V}_l \overline{V}_m \check{S} - 2\overline{V}_l \overline{V}_m \underline{s}, \\
\check{s}_{lm} &\leqslant \underline{V}_m \underline{s} V_l + \overline{V}_l \overline{s} V_m + \overline{V}_l \underline{V}_m \check{S} - \overline{V}_l \underline{V}_m \overline{s} - \overline{V}_l \underline{V}_m \underline{s}, \\
\check{s}_{lm} &\leqslant \overline{V}_m \overline{s} V_l + \underline{V}_l \underline{s} V_m + \underline{V}_l \overline{V}_m \check{S} - \underline{V}_l \overline{V}_m \overline{s} - \underline{V}_l \overline{V}_m \underline{s}, \\
\check{s}_{lm} &\leqslant \underline{V}_m \underline{s} V_l + \underline{V}_l \underline{s} V_m + \frac{\Lambda_4}{\underline{s} - \overline{s}} \check{S} - \frac{\Lambda_4 \overline{s}}{\underline{s} - \overline{s}} - \overline{V}_l \underline{V}_m \underline{s} \\
&\quad - \underline{V}_l \overline{V}_m \underline{s} + \overline{V}_l \overline{V}_m \overline{s}, \\
&\quad \text{where } \Lambda_4 = \overline{V}_l \underline{V}_m \underline{s} - \overline{V}_l \overline{V}_m \overline{s} - \underline{V}_l \underline{V}_m \underline{s} + \underline{V}_l \overline{V}_m \underline{s}, \\
\check{s}_{lm} &\leqslant \overline{V}_m \overline{s} V_l + \overline{V}_l \overline{s} V_m - \frac{\Gamma_4}{\overline{s} - \underline{s}} \check{S} - \frac{\Gamma_4 \underline{s}}{\overline{s} - \underline{s}} - \overline{V}_l \underline{V}_m \overline{s} \\
&\quad - \underline{V}_l \overline{V}_m \overline{s} + \underline{V}_l \underline{V}_m \underline{s}, \\
&\quad \text{where } \Gamma_4 = \overline{V}_l \underline{V}_m \overline{s} - \underline{V}_l \underline{V}_m \underline{s} - \overline{V}_l \overline{V}_m \overline{s} + \underline{V}_l \overline{V}_m \overline{s}.
\end{aligned}$$

Let $\phi(x, y, z) = xyz$ be any trilinear term with respective variable bounds $[\underline{x}, \overline{x}]$, $[\underline{y}, \overline{y}]$, $[\underline{z}, \overline{z}]$. The extreme points of $\phi(\cdot)$ are given by the Cartesian product $(\underline{x}, \overline{x}) \times (\underline{y}, \overline{y}) \times (\underline{z}, \overline{z}) = \langle \xi_1, \xi_2, \ldots, \xi_8 \rangle$ [28, 32]. We use ξ_k^i to denote the coordinate of x_i in ξ_k. The convex hull of the extreme points of $\phi(\cdot)$ is

$$\check{x} = \sum_{k=1,\ldots,8} \lambda_k \, \phi(\xi_k), \quad x_i = \sum_{k=1,\ldots,8} \lambda_k \, \xi_k^i, \tag{6a}$$

$$\sum_{k=1,\ldots,8} \lambda_k = 1, \quad \lambda_k \geqslant 0, \quad k = 1, \ldots, 8. \tag{6b}$$

Given a lifted variable $\check{x}$, the notation $\check{x} \in \langle xyz \rangle^{EP}$ represents the λ-based convex hull envelope of a trilinear term as in (6).

3.5. FORMULATION OF THE QC RELAXATION

Using the envelopes described above, the QC relaxation replaces the relevant non-linearities in the OPF problem (1) to construct an SOCP:

Case V: $\overline{s} \leqslant 0$,

$$\begin{aligned}
\overline{V}_l\underline{V}_m\underline{s} + \underline{V}_l\overline{V}_m\overline{s} &\geqslant \underline{V}_l\overline{V}_m\underline{s} + \overline{V}_l\underline{V}_m\overline{s},\\
\underline{V}_l\underline{V}_m\underline{s} + \overline{V}_l\overline{V}_m\overline{s} &< \overline{V}_l\underline{V}_m\underline{s} + \underline{V}_l\overline{V}_m\overline{s},\\
\underline{V}_l\underline{V}_m\underline{s} + \overline{V}_l\overline{V}_m\overline{s} &< \underline{V}_l\overline{V}_m\underline{s} + \overline{V}_l\underline{V}_m\overline{s}.
\end{aligned}$$

$$\begin{aligned}
\check{s}_{lm} &\leqslant \underline{V}_m\overline{s}V_l + \underline{V}_l\overline{s}V_m + \underline{V}_l\underline{V}_m\check{S} - 2\underline{V}_l\underline{V}_m\overline{s},\\
\check{s}_{lm} &\leqslant \overline{V}_m\underline{s}V_l + \overline{V}_l\underline{s}V_m + \overline{V}_l\overline{V}_m\check{S} - 2\overline{V}_l\overline{V}_m\underline{s},\\
\check{s}_{lm} &\leqslant \underline{V}_m\underline{s}V_l + \underline{V}_l\underline{s}V_m + \underline{V}_l\overline{V}_m\check{S} - \underline{V}_l\underline{V}_m\underline{s} - \underline{V}_l\overline{V}_m\underline{s},\\
\check{s}_{lm} &\leqslant \overline{V}_m\overline{s}V_l + \overline{V}_l\overline{s}V_m + \overline{V}_l\underline{V}_m\check{S} - \overline{V}_l\underline{V}_m\overline{s} - \overline{V}_l\overline{V}_m\overline{s},\\
\check{s}_{lm} &\leqslant \underline{V}_m\underline{s}V_l + \frac{\Lambda_5}{\underline{V}_m - \overline{V}_m}V_m + \overline{V}_l\underline{V}_m\check{S} - \frac{\Lambda_5\overline{V}_m}{\underline{V}_m - \overline{V}_m}\\
&\quad - \underline{V}_l\underline{V}_m\underline{s} - \overline{V}_l\underline{V}_m\overline{s} + \underline{V}_l\overline{V}_m\overline{s},\\
&\quad \text{where } \Lambda_5 = \underline{V}_l\underline{V}_m\underline{s} - \underline{V}_l\overline{V}_m\overline{s} - \overline{V}_l\underline{V}_m\underline{s} + \overline{V}_l\underline{V}_m\overline{s},\\
\check{s}_{lm} &\leqslant \overline{V}_m\overline{s}V_l + \frac{\Gamma_5}{\overline{V}_m - \underline{V}_m}V_m + \underline{V}_l\overline{V}_m\check{S} - \frac{\Gamma_5\underline{V}_m}{\overline{V}_m - \underline{V}_m}\\
&\quad - \underline{V}_l\overline{V}_m\underline{s} - \overline{V}_l\overline{V}_m\overline{s} + \overline{V}_l\underline{V}_m\underline{s},\\
&\quad \text{where } \Gamma_5 = \underline{V}_l\overline{V}_m\underline{s} - \overline{V}_l\underline{V}_m\underline{s} - \underline{V}_l\overline{V}_m\overline{s} + \overline{V}_l\overline{V}_m\overline{s}.
\end{aligned}$$

Case VI: $\underline{s} \leqslant 0, \overline{s} \geqslant 0$.

$$\begin{aligned}
\check{s}_{lm} &\geqslant \overline{V}_m\overline{s}V_l + \overline{V}_l\overline{s}V_m + \overline{V}_l\overline{V}_m\check{S} - 2\overline{V}_l\overline{V}_m\overline{s},\\
\check{s}_{lm} &\geqslant \overline{V}_m\underline{s}V_l + \underline{V}_l\overline{s}V_m + \underline{V}_l\overline{V}_m\check{S} - \underline{V}_l\overline{V}_m\underline{s} - \underline{V}_l\overline{V}_m\overline{s},\\
\check{s}_{lm} &\geqslant \overline{V}_m\underline{s}V_l + \underline{V}_l\underline{s}V_m + \underline{V}_l\underline{V}_m\check{S} - \underline{V}_l\overline{V}_m\underline{s} - \underline{V}_l\underline{V}_m\underline{s},\\
\check{s}_{lm} &\geqslant \underline{V}_m\overline{s}V_l + \overline{V}_l\underline{s}V_m + \overline{V}_l\underline{V}_m\check{S} - \overline{V}_l\underline{V}_m\overline{s} - \overline{V}_l\underline{V}_m\underline{s},\\
\check{s}_{lm} &\geqslant \underline{V}_m\underline{s}V_l + \overline{V}_l\underline{s}V_m + \underline{V}_l\underline{V}_m\check{S} - \overline{V}_l\underline{V}_m\underline{s} - \underline{V}_l\underline{V}_m\underline{s},\\
\check{s}_{lm} &\geqslant \underline{V}_m\overline{s}V_l + \underline{V}_l\overline{s}V_m + \frac{\Lambda_6}{\overline{s} - \underline{s}}\check{S} - \frac{\Lambda_6\underline{s}}{\overline{s} - \underline{s}} - \underline{V}_l\overline{V}_m\overline{s}\\
&\quad - \overline{V}_l\underline{V}_m\overline{s} + \overline{V}_l\overline{V}_m\underline{s},\\
&\quad \text{where } \Lambda_6 = \underline{V}_l\overline{V}_m\overline{s} - \overline{V}_l\overline{V}_m\underline{s} - \underline{V}_l\underline{V}_m\overline{s} + \overline{V}_l\underline{V}_m\overline{s}.
\end{aligned}$$

Case VII: $\underline{s} \leqslant 0, \overline{s} \geqslant 0$.

$$\begin{aligned}
\check{s}_{lm} &\leqslant \overline{V}_m\underline{s}V_l + \overline{V}_l\underline{s}V_m + \overline{V}_l\overline{V}_m\check{S} - 2\overline{V}_l\overline{V}_m\underline{s},\\
\check{s}_{lm} &\leqslant \underline{V}_m\underline{s}V_l + \overline{V}_l\overline{s}V_m + \overline{V}_l\underline{V}_m\check{S} - \overline{V}_l\underline{V}_m\overline{s} - \overline{V}_l\underline{V}_m\underline{s},\\
\check{s}_{lm} &\leqslant \overline{V}_m\overline{s}V_l + \underline{V}_l\overline{s}V_m + \underline{V}_l\underline{V}_m\check{S} - \underline{V}_l\overline{V}_m\overline{s} - \underline{V}_l\underline{V}_m\overline{s},\\
\check{s}_{lm} &\leqslant \overline{V}_m\overline{s}V_l + \underline{V}_l\underline{s}V_m + \underline{V}_l\overline{V}_m\check{S} - \underline{V}_l\overline{V}_m\overline{s} - \underline{V}_l\overline{V}_m\underline{s},\\
\check{s}_{lm} &\leqslant \underline{V}_m\overline{s}V_l + \overline{V}_l\overline{s}V_m + \underline{V}_l\underline{V}_m\check{S} - \overline{V}_l\underline{V}_m\overline{s} - \underline{V}_l\underline{V}_m\overline{s},\\
\check{s}_{lm} &\leqslant \underline{V}_m\underline{s}V_l + \underline{V}_l\underline{s}V_m + \frac{\Lambda_7}{\underline{s} - \overline{s}}\check{S} - \frac{\Lambda_7\overline{s}}{\underline{s} - \overline{s}} - \overline{V}_l\underline{V}_m\underline{s}\\
&\quad - \underline{V}_l\overline{V}_m\underline{s} + \overline{V}_l\overline{V}_m\overline{s},\\
&\quad \text{where } \Lambda_7 = \overline{V}_l\underline{V}_m\underline{s} - \overline{V}_l\overline{V}_m\overline{s} - \underline{V}_l\underline{V}_m\underline{s} + \underline{V}_l\overline{V}_m\underline{s}.
\end{aligned}$$

$$\min \quad \sum_{i \in \mathcal{G}} c_{2i} \left(P_i^g\right)^2 + c_{1i} P_i^g + c_{0i} \tag{7a}$$

$$\text{subject to} \quad (\forall i \in \mathcal{N},\ \forall (l,m) \in \mathcal{L})$$

$$\text{Equations (1b), (1c), (1i), (1i), (4) with substitutions } V_i^2 \rightarrow w_{ii},$$

$$V_l V_m \sin(\theta_{lm}) \rightarrow w_{s,lm}, V_l V_m \cos(\theta_{lm}) \rightarrow w_{c,lm}, \tag{7b}$$

$$\text{Equations (1d)–(1f), (1i)} \tag{7c}$$

$$w_{lm} \in \langle V_l V_m \rangle^M,\ w_{s,lm} \in \langle w_{lm}\, s_{lm} \rangle^M, w_{c,lm} \in \langle w_{lm}\, c_{lm} \rangle^M, \text{or}$$

$$w_{s,lm} \in \langle V_l V_m\, s_{lm} \rangle^{MF \vee EP},\ w_{c,lm} \in \langle V_l V_m\, c_{lm} \rangle^{MF \vee EP}. \tag{7d}$$

4. COMPARISON OF THE TRILINEAR ENVELOPES

There are trade-offs inherent to the choices of trilinear envelopes in the QC relaxation (7d). The MF and EP envelopes both yield the convex hull of an individual trilinear monomial and therefore are equivalently tight. When applied to the summation of trilinears in constraints (1i)–(1i), these envelopes do not explicitly enforce consistency among the shared voltage products $V_l V_m$ in the summation, which is enforced in the recursive McCormick formulation via the common lifted variable w_{lm}. However, for the test cases considered in this paper, we numerically observe that QC formulations using MF and EP envelopes give tighter objective value bounds compared to those using recursive McCormick envelopes.

The number of variables and constraints necessary to describe the trilinear envelopes for a given trilinear monomial is tabulated in Table 1, where $(\cdot)^{\leqslant}$ and $(\cdot)^{=}$ represent the number of inequality and equality constraints, respectively.

Using the algebraic modeling language JuMP [33] in Julia, we formulate each version of the QC relaxation (7) by modifying the relaxation implementations in PowerModels.jl [34]. For each version of the QC relaxation, we apply the solvers *CPLEX* 12.8, *GUROBI* 8.0, and *IPOPT* 3.12.9 (with "ma27" HSL solver [35]) to each OPF problem in the

Table 1. Variables and constraints per trilinear monomial envelope.

Convex envelope	No. of Variables	No. of Constraints
RMC	3 (original) + 2 (lifted)	$8^{\leqslant}$
EP	3 (original) + 9 (lifted)	$5^{=}$
MF	3 (original) + 1 (lifted)	$12^{\leqslant}$

NESTA v0.7 archive [36]. Optimality gaps for the QC relaxation are given by $\frac{UB-LB}{UB} \cdot 100$, where UB is the local feasible solution obtained from solving (1) with *IPOPT* and LB is the lower bound obtained by applying the QC relaxation.

The results in Table 2 for a selected set of instances show that replacing RMC envelopes with MF or EP envelopes tighten the QC relaxation and can reduce the optimality gaps substantially. For instance, the optimality gap for case24_ieee_rts__api is reduced by 3.10%. We expect further gap reductions when the convex hull envelopes are used in combination with bound tightening procedures [16–18, 37].

The box-and-whisker plot shown in Figure 1 compares the run times of various SOCP solvers. The lower and upper ends of the boxes in Figure 1 reflect the first and third quartiles, the lines inside the boxes denote the median, and the plus marks are outliers. "Medium" and "Large" categories correspond to instances including "TYP", "API", and "SAD" with numbers of buses $1354 \leqslant |\mathcal{N}| \leqslant 3375$ and $|\mathcal{N}| \geqslant 6468$, respectively.

For each solver, the RMC envelopes yield the fastest or nearly the fastest results, but have larger optimality gaps than the MF and EP envelopes, particularly for the small problems in Table 2. *GUROBI* and *CPLEX* are faster than *IPOPT* for the RMC and EP envelopes. While slightly faster than the EP envelopes when using *IPOPT*, the MF envelopes are substantially slower than the RMC and EP envelopes when using *GUROBI* and *CPLEX*. Moreover, the solvers *CPLEX* and *GUROBI* encounter numerical issues for approximately 19.5% of the instances when using the MF envelopes and hence do not converge to optimal values. We speculate that the MF envelopes yield dense columns, which is a known issue for the convergence of barrier-based algorithms for solving SOCPs. In summary, *IPOPT*

Table 2. QC relaxation gaps using recursive McCormick (RMC) vs. convex-hull envelopes (MF, EP).

Instances	RMC (%)	MF, EP (%)	Improvement (%)
case3_lmbd	1.21	0.96	0.25
case30_ieee	15.64	15.20	0.44
case2224_edin	6.03	6.01	0.02
case3_lmbd__api	1.79	1.59	0.20
case24_ieee_rts__api	11.88	8.78	3.10
case73_ieee_rts__api	10.97	9.64	1.33
case3_lmbd__sad	1.42	1.37	0.05
case4_gs__sad	1.53	0.96	0.57
case5_pjm__sad	0.99	0.77	0.22
case24_ieee_rts__sad	2.93	2.77	0.16
case73_ieee_rts__sad	2.53	2.38	0.15
case118_ieee__sad	4.61	4.14	0.47

is numerically stable on all the formulations and instances but is slower than *GUROBI* and *CPLEX*. Though equivalently tight, the EP envelopes are significantly faster than the MF envelopes when using *CPLEX* and *GUROBI*.

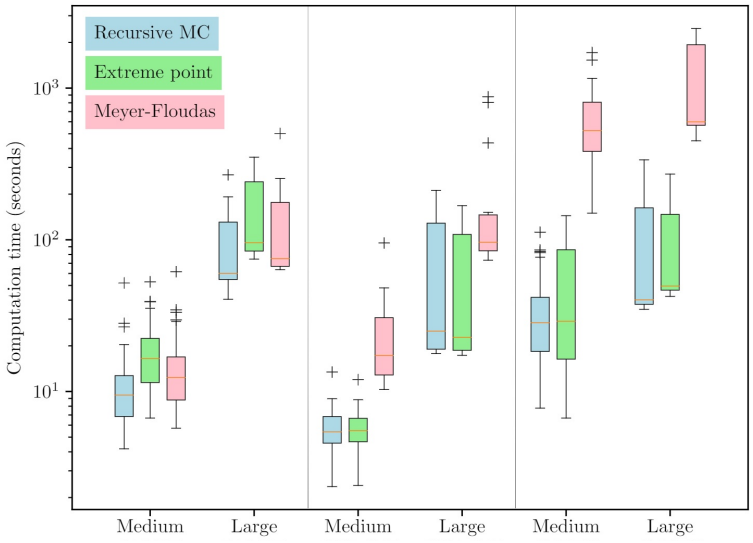

Figure 1. Run time comparisons of various formulations using three solvers.

5. CONCLUSIONS

Convex relaxations of OPF problems derived using polar voltage coordinates give rise to trilinear monomials. Using extensive empirical tests, this paper has compared three previously proposed techniques for addressing the trilinear monomials: recursive McCormick envelopes, Meyer and Floudas envelopes, and extreme point envelopes. The latter two envelopes yield the convex hull of a single trilinear monomial. Empirical results show that MF and EP envelopes improve the QC relaxation gaps, particularly on instances with less than 300 buses. Despite being equivalently tight, the differing mathematical formulations of the MF and EP envelopes yield differing computational performance with various solvers. Given its advantages in ease of implementation and numerical stability with state-of-the-art solvers like CPLEX and GUROBI, we recommend using EP envelopes for OPF relaxations.

BIBLIOGRAPHY

[1] M.B. Cain, R.P. O'Neill, A. Castillo, History of Optimal Power Flow and Formulations, August (2013).

[2] W.A. Bukhsh,A. Grothey, K.I.M. McKinnon, P.A. Trodden, Local Solutions of the Optimal Power Flow Problem, IEEE Transaction on Power Systems, 28 (4) (2013) 4780–4788.

[3] D. Bienstock, A. Verma, Strong NP-hardness of AC Power Flows Feasibility, arXiv:1512.07315 (2015).

[4] K. Lehmann, A. Grastien and P. Van Hentenryck, AC-Feasibility on Tree Networks is NP-Hard, IEEE Transaction on Power Systems 31 (1) (2016) 798–801.

[5] J. Carpentier, Contribution to the Economic Dispatch Problem, Bulletin de la Societe Francoise des Electriciens 8 (3) (1962) 431–447.

[6] J.A. Momoh, R. Adapa, M.E. El-Hawary, A Review of Selected Optimal Power Flow Literature to 1993. Parts I and II, IEEE Transaction on Power Systems 14 (1) (1999) 96–111.

[7] A. Castillo, R.P. O'Neill, Survey of Approaches to Solving the ACOPF (OPF Paper 4) March (2013).

[8] J. F. Marley, D. K. Molzahn, I. A. Hiskens, Solving Multiperiod OPF Problems using an AC-QP Algorithm Initialized with an SOCP Relaxation, IEEE Transaction on Power Systems 32 (5) (2017) 3538–3548.

[9] J. lavaei, S. H. Low, Zero Duality Gap in Optimal Power Flow Problem, IEEE Transaction on Power Systems 27 (2012) 92–107.

[10] C. Josz, D. K. Molzahn, Lasserre Hierarchy for Large Scale Polynomial Optimization in Real and Complex Variables, SIAM Journal on Optimizaion 28 (2) (2018) 1017-1048.

[11] D. K. Molzahn, I. A. Hiskens, Sparsity-Exploiting Moment-Based Relaxations of the Optimal Power Flow Problem, IEEE Transaction on Power Systems 30 (6) (2015) 3168-3180.

[12] R. Jabr, Radial Distribution Load Flow using Conic Programming, IEEE Transaction on Power Systems 21 (3) (2006) 1458–1459.

[13] S. H. Low, Convex Relaxation of Optimal Power Flow–Part I: Formulations and Equivalence, IEEE Transaction on Control Network Systems 1 (1) (2014) 15–27.

[14] S. H. Low, Convex Relaxation of Optimal Power Flow–Part II: Exactness, IEEE Transaction on Control Network Systems 2 (1) (2014) 177–189.

[15] C. Coffrin, H.L. Hijazi, P. Van Hentenryck, The QC Relaxation: A Theoretical and Computational Study on Optimal Power Flow, IEEE Transaction on Power Systems 31 (4) (2016) 3008–3018.

[16] B. Kocuk, S.S. Dey, X.A. Sun, Strong SOCP Relaxations for the Optimal Power Flow Problem, Operation Research 64 (4) (2016) 1177–1196.

[17] C. Coffrin, H. L. Hijazi, P. Van Hentenryck, Strengthening the SDP Relaxation of AC Power Flows with Convex Envelopes, Bound Tightening, and Valid Inequalities, IEEE Transaction on Power Systems 32 (5) (2017) 3549–3558.

[18] B. Kocuk, S.S. Dey, X.A. Sun, Matrix Minor Reformulation and SOCP-based Spatial Branch-and-Cut Method for the AC Optimal Power Flow Problem, arXiv:1703.03050 March (2017).

[19] C. Coffrin, H. L. Hijazi, P. Van Hentenryck, Network Flow and Copper Plate Relaxations for AC Transmission Systems, 19th Power System Computation Conference (PSCC) (2016).

[20] J.A. Taylor, F.S. Hover, Linear Relaxations for Transmission System Planning, IEEE Transaction on Power Systems 26 (4) (2011) 2533-2538.

[21] D. Bienstock, and G. Munoz, On Linear Relaxations of OPF Problems, arXiv:1411.1120 (2014).

[22] D. K. Molzahn, I. A. Hiskens, A Survey of Relaxations and Approximations of the Power Flow Equations, Foundations and Trends in Electric Energy Systems February (2019).

[23] M. R. Narimani, D. K. Molzahn, M. L. Crow, Improving QC Relaxations of OPF Problems via Voltage Magnitude Difference Constraints and Envelopes for Trilinear Monomials, Power System Computation Conference (PSCC) (2018).

[24] M. Lu, H. Nagarajan, R. Bent, S.D. Eksioglu, S. J. Mason, Tight Piecewise Convex Relaxation for Global Optimization of Optimal Power Flow, Power System Computation Conference (PSCC) (2018).

[25] G.P. McCormick, Computability of Global Solutions to Factorable Nonconvex Programs: Part I–Convex Underestimating Problems, Mathematical Programming 10 (1) (1976) 147–175.

[26] C.A. Meyer, C.A. Floudas, Trilinear Monomials with Positive or Negative Domains: Facets of the Convex and Concave Envelopes, Frontiers in Global Optimization (2004) 327–352.

[27] C.A. Meyer, C.A. Floudas, Trilinear Monomials with Mixed Sign Domains: Facets of the Convex and Concave Envelopes, Journal of Global Optimization 29 (2) (2004) 125–155.

[28] A. D. Rikun, A Convex Envelope Formula for Multilinear Functions, Journal of Global Optimization 10 (1997) 425–437.

[29] H. Nagarajan, M. Lu, E. Yamangil, R. Bent, Tightening McCormick Relaxations for Nonlinear Programs via Dynamic Multivariate Partitioning, International Conference on Principles Practice Constraint Programming (2016) 369–387.

[30] H. Nagarajan, M. Lu, S. Wang, R. Bent, K. Sundar, An Adaptive, Multivariate Partitioning Algorithm for Global Optimization of Nonconvex Programs, arXiv:1707.02514 (2017)

[31] M. Farivar, C.R. Clarke, S.H. Low, K.M. Chandy, Inverter VAR Control for Distribution Systems with Renewables, IEEE International Conference on Smart Grid Communication (SmartGridComm) (2011) 457–462.

[32] J. Luedtke, M.Namazifar, J.Linderoth, Some Results on the Strength of Relaxations of Multilinear Functions, Mathematical Programming 136 2) (2012) 325–351.

[33] I. Dunning, J. Huchette, M. Lubin, JuMP: A Modeling Language for Mathematical Optimization, SIAM Review 59 (2) (2017) 295-320.

[34] C. Coffrin, R. Bent, K. Sundar, Y. Ng, and M. Lubin, PowerModels.jl: An Open-Source Framework for Exploring Power Flow Formulations, Power System Computation. Conference (PSCC) (2018).

[35] Research Councils U.K., The HSL Mathematical Software Library, Published online at http://www.hsl.rl.ac.uk

[36] C. Coffrin, D. Gordon, P. Scott, NESTA, the NICTA Energy System Test Case Archive (v0.7), arXiv:1411.0359 June (2017).

[37] C. Chen, A. Atamturk, S.S. Oren, Bound Tightening for the Alternating Current Optimal Power Flow Problem, IEEE Transaction on Power Systems 31 (5) (2016) 3729–3736.

IV. TIGHTENING QC RELAXATIONS OF AC OPTIMAL POWER FLOW PROBLEMS VIA COMPLEX PER UNIT NORMALIZATION

Mohammad Rasoul Narimani, Daniel K. Molzahn, and Mariesa L. Crow

Department of Electrical and Computer Engineering

Missouri University of Science and Technology

Rolla, Missouri 65409–0050

Email: mn9t5@mst.edu

ABSTRACT

Optimal power flow (OPF) is a key problem in power system operations. OPF problems that use the nonlinear AC power flow equations to accurately model the network physics have inherent challenges associated with non-convexity. To address these challenges, recent research has applied various convex relaxation approaches to OPF problems. The QC relaxation is a promising approach that convexifies the trigonometric and product terms in the OPF problem by enclosing these terms in convex envelopes. The accuracy of the QC relaxation strongly depends on the tightness of these envelopes. This paper presents two improvements to these envelopes. The first improvement leverages a polar representation of the branch admittances in addition to the rectangular representation used previously. The second improvement is based on a coordinate transformation via a complex per unit base power normalization that rotates the power flow equations. The trigonometric envelopes resulting from this rotation can be tighter than the corresponding envelopes in previous QC relaxation formulations. Using an empirical analysis with a variety of test cases, this paper suggests an appropriate value for the angle of the complex base power. Comparing the results with a state-of-the-art QC formulation reveals the advantages of the proposed improvements.

1. INTRODUCTION

Power flow (OPF) problems are central to many tasks in power system operations. OPF problems optimize an objective function, such as generation cost, subject to both the network physics and engineering limits. The nonlinear AC power flow equations needed to accurately model the network physics introduce non-convexities in OPF problems. Due to these non-convexities, OPF problems may have multiple local optima [1] and are generally NP-Hard [2].

Many research efforts have focused on algorithms for obtaining locally optimal or approximate OPF solutions [3]. Recent research has also developed convex relaxations of OPF problems [4]. Convex relaxations bound the optimal objective values, can certify infeasibility, and, in some cases, provably provide globally optimal solutions to OPF problems.

The capabilities of convex relaxations are, in many ways, complementary to those of local solution algorithms. For instance, relaxations' objective value bounds can certify how close a local solution is to being globally optimal. Accordingly, local algorithms and relaxations are used together in spatial branch-and-bound methods [5]. Solutions from relaxations are also useful for initializing some local solvers [6]. Relaxations are also needed for certain solution algorithms for robust OPF problems [7]. Moreover, the objective value bounds provided by relaxations are directly useful in other contexts, e.g., [8, 9]. The tractability and accuracy of these and other algorithms are largely determined by the employed relaxation's tightness. Tightening relaxations is thus an active research topic [4].

The quadratic convex (QC) relaxation is a promising approach that encloses the trigonometric and product terms in the polar representation of power flow equations within convex envelopes [10]. These envelopes are formed with linear and second-order cone programming (SOCP) constraints, resulting in a convex formulation. The QC relaxation's tightness strongly depends on the quality of these convex envelopes. This paper focuses on improving these envelopes.

Previous work has proposed a variety of approaches for tightening the QC relaxation. These include valid inequalities, such as "Lifted Nonlinear Cuts" [11, 12] and constraints that exploit bounds on the differences in the voltage magnitudes [13]. Additionally, since the accuracies of the trigonometric and product envelopes in the QC relaxation rely on the voltage magnitude and angle difference bounds, bound tightening approaches can significantly strengthen the QC relaxation [11, 12, 14, 15]. When bound tightening approaches provide sign-definite angle difference bounds (i.e., the upper and lower bounds on the angle differences have the same sign), tighter trigonometric envelopes can be applied [11].

This paper proposes two improvements to further tighten QC relaxations of OPF problems. The first improvement leverages a polar representation of the branch admittances in addition to the rectangular representation used in previous QC formulations. Within certain ranges, portions of the trigonometric envelopes resulting from the polar admittance representation are at least as tight (and generally tighter) than the corresponding portions of the envelopes from the rectangular admittance representation. In other ranges, the trigonometric envelopes from the polar admittance representation neither contain nor are contained within the envelopes from the rectangular admittance representation. Thus, combining these envelopes tightens the QC relaxation, with empirical results showing limited impacts on solution times.

The polar admittance representation also enables our second improvement. We exploit a degree of freedom in the OPF formulation related to the per unit base power normalization. Selecting a *complex base power* ($S_{base} = |S_{base}|\, e^{j\psi}$) results in a coordinate transformation that rotates the power flow equations relative to the typical choice of a real-valued base power. We leverage the associated rotational degree of freedom ψ to obtain tighter envelopes for the trigonometric functions. While previously proposed power flow algorithms [17] and state estimation algorithms [18] use similar formulations, this paper is, to the best of our knowledge, the first to exploit this rotational degree of freedom to improve convex relaxations.

This paper is organized as follows. Sections 2 and 3 review the OPF formulation and the previously proposed QC relaxation, respectively. Section 4 describes the coordinate changes underlying our improved QC relaxation. Section 5 then presents these improvements. Section 7 empirically evaluates our approach. Section 8 concludes the paper.

2. OVERVIEW OF THE OPTIMAL POWER FLOW PROBLEM

This section formulates the OPF problem using a polar voltage phasor representation. The sets of buses, generators, and lines are $\mathcal{N}$, $\mathcal{G}$, and $\mathcal{L}$, respectively. Let $S_i^d = P_i^d + jQ_i^d$ and $S_i^g = P_i^g + jQ_i^g$ represent the complex load demand and generation, respectively, at bus $i \in \mathcal{N}$, where $j = \sqrt{-1}$. Let V_i and θ_i represent the voltage magnitude and angle at bus $i \in \mathcal{N}$. Let $g_{sh,i} + jb_{sh,i}$ denote the shunt admittance at bus $i \in \mathcal{N}$. For each generator, define a quadratic cost function with coefficients $c_{2,i} \geqslant 0$, $c_{1,i}$, and $c_{0,i}$. For simplicity, we consider a single generator at each bus by setting the generation limits at buses without generators to zero. Upper and lower bounds for all variables are indicated by $\overline{(\cdot)}$ and $\underline{(\cdot)}$, respectively.

For ease of exposition, each line $(l,m) \in \mathcal{L}$ is modeled as a Π circuit with mutual admittance $g_{lm} + jb_{lm}$ and shunt admittance $jb_{c,lm}$. Extensions to more general line models that allow for off-nominal tap ratios and non-zero phase shifts are straightforward and available in Section 5.5. Define $\theta_{lm} = \theta_l - \theta_m$ for $(l,m) \in \mathcal{L}$. The complex power flow into each line terminal $(l,m) \in \mathcal{L}$ is denoted by $P_{lm} + jQ_{lm}$, and the apparent power flow limit is $\overline{S}_{lm}$. The OPF problem is

$$\min \quad \sum_{i \in \mathcal{G}} c_{2,i} \left(P_i^g\right)^2 + c_{1,i} P_i^g + c_{0,i} \tag{1a}$$

$$\text{subject to} \quad (\forall i \in \mathcal{N},\ \forall (l,m) \in \mathcal{L})$$

$$P_i^g - P_i^d = g_{sh,i}\, V_i^2 + \sum_{\substack{(l,m)\in\mathcal{L},\\ \text{s.t. } l=i}} P_{lm} + \sum_{\substack{(l,m)\in\mathcal{L},\\ \text{s.t. } m=i}} P_{ml}, \tag{1b}$$

$$Q_i^g - Q_i^d = -b_{sh,i}\, V_i^2 + \sum_{\substack{(l,m)\in\mathcal{L},\\ \text{s.t. } l=i}} Q_{lm} + \sum_{\substack{(l,m)\in\mathcal{L},\\ \text{s.t. } m=i}} Q_{ml}, \tag{1c}$$

$$\theta_{ref} = 0, \tag{1d}$$

$$\underline{P}_i^g \leqslant P_i^g \leqslant \overline{P}_i^g, \quad \underline{Q}_i^g \leqslant Q_i^g \leqslant \overline{Q}_i^g, \tag{1e}$$

$$\underline{V}_i \leqslant V_i \leqslant \overline{V}_i, \tag{1f}$$

$$\underline{\theta}_{lm} \leqslant \theta_{lm} \leqslant \overline{\theta}_{lm}, \tag{1g}$$

$$P_{lm} = g_{lm}V_l^2 - g_{lm}V_lV_m\cos(\theta_{lm}) - b_{lm}V_lV_m\sin(\theta_{lm}), \tag{1h}$$

$$\begin{aligned} Q_{lm} = &-(b_{lm} + b_{c,lm}/2)\, V_l^2 + b_{lm}V_lV_m\cos(\theta_{lm}) \\ &- g_{lm}V_lV_m\sin(\theta_{lm}), \end{aligned} \tag{1i}$$

$$P_{ml} = g_{lm}V_m^2 - g_{lm}V_lV_m\cos(\theta_{lm}) + b_{lm}V_lV_m\sin(\theta_{lm}), \tag{1j}$$

$$\begin{aligned} Q_{ml} = &-(b_{lm} + b_{c,lm}/2)\, V_m^2 + b_{lm}V_lV_m\cos(\theta_{lm}) \\ &+ g_{lm}V_lV_m\sin(\theta_{lm}), \end{aligned} \tag{1k}$$

$$(P_{lm})^2 + (Q_{lm})^2 \leqslant \left(\overline{S}_{lm}\right)^2, \quad (P_{ml})^2 + (Q_{ml})^2 \leqslant \left(\overline{S}_{lm}\right)^2. \tag{1l}$$

The objective (1a) minimizes the generation cost. Constraints (1b) and (1c) enforce power balance at each bus. Constraint (1d) sets the reference bus angle, θ_{ref}. The constraints in (1e) bound the active and reactive power generation at each bus. Constraints (1g)–(1h), respectively, bound the voltage magnitudes and voltage angle differences. Constraints (1i)–(1i) relate the active and reactive power flows with the voltage phasors at the terminal buses. The constraints in (1k) limit the apparent power flows into both terminals of each line.

3. THE QC RELAXATION OF THE OPF PROBLEM

The QC relaxation convexifies the OPF problem (1) by enclosing the nonconvex terms in convex envelopes [10]. The relevant nonconvex terms are the square V_i^2, $\forall i \in \mathcal{N}$, and the products $V_lV_m\cos(\theta_{lm})$ and $V_lV_m\sin(\theta_{lm})$, $\forall (l,m) \in \mathcal{L}$. The envelope for the generic

squared function x^2 is $\langle x^2 \rangle^T$:

$$\langle x^2 \rangle^T = \begin{cases} \breve{x} : \begin{cases} \breve{x} \geqslant x^2, \\ \breve{x} \leqslant (\overline{x} + \underline{x})\, x - \overline{x}\underline{x}. \end{cases} \end{cases} \tag{2}$$

where $\breve{x}$ is a lifted variable representing the envelope. Envelopes for the generic trigonometric functions $\sin(x)$ and $\cos(x)$ are $\langle \sin(x) \rangle^S$ and $\langle \cos(x) \rangle^C$:

$$\langle \sin(x) \rangle^S = \begin{cases} \breve{S} : \begin{cases} \breve{S} \leqslant \cos\left(\frac{x^m}{2}\right)\left(x - \frac{x^m}{2}\right) + \sin\left(\frac{x^m}{2}\right) \text{ if } \underline{x} \leqslant 0 \leqslant \overline{x}, \\ \breve{S} \geqslant \cos\left(\frac{x^m}{2}\right)\left(x + \frac{x^m}{2}\right) - \sin\left(\frac{x^m}{2}\right) \text{ if } \underline{x} \leqslant 0 \leqslant \overline{x}, \\ \breve{S} \geqslant \frac{\sin(\underline{x}) - \sin(\overline{x})}{\underline{x} - \overline{x}} (x - \underline{x}) + \sin(\underline{x}) \text{ if } \underline{x} \geqslant 0, \\ \breve{S} \leqslant \frac{\sin(\underline{x}) - \sin(\overline{x})}{\underline{x} - \overline{x}} (x - \underline{x}) + \sin(\underline{x}) \text{ if } \overline{x} \leqslant 0, \end{cases} \end{cases} \tag{3}$$

$$\langle \cos(x) \rangle^C = \begin{cases} \breve{C} : \begin{cases} \breve{C} \leqslant 1 - \frac{1 - \cos(x^m)}{(x^m)^2} x^2, \\ \breve{C} \geqslant \frac{\cos(\underline{x}) - \cos(\overline{x})}{\underline{x} - \overline{x}} (x - \underline{x}) + \cos(\underline{x}), \end{cases} \end{cases} \tag{4}$$

where $x^m = \max(|\underline{x}|, |\overline{x}|)$. The variables $\breve{S}$ and $\breve{C}$ are associated with the envelopes for the functions $\sin(\theta_{lm})$ and $\cos(\theta_{lm})$. The QC relaxation of the OPF problem in (1) is:

$$\min \quad \sum_{i \in \mathcal{N}} c_{2,i} \left(P_i^g\right)^2 + c_{1,i}\, P_i^g + c_{0,i} \tag{5a}$$

$$\text{subject to} \quad (\forall i \in \mathcal{N},\ \forall\, (l,m) \in \mathcal{L})$$

$$P_i^g - P_i^d = g_{sh,i}\, w_{ii} + \sum_{\substack{(l,m) \in \mathcal{L}, \\ \text{s.t. } l = i}} P_{lm} + \sum_{\substack{(l,m) \in \mathcal{L}, \\ \text{s.t. } m = i}} P_{ml}, \tag{5b}$$

$$Q_i^g - Q_i^d = -b_{sh,i}\, w_{ii} + \sum_{\substack{(l,m) \in \mathcal{L}, \\ \text{s.t. } l = i}} Q_{lm} + \sum_{\substack{(l,m) \in \mathcal{L}, \\ \text{s.t. } m = i}} Q_{ml}, \tag{5c}$$

$$(\underline{V}_i)^2 \leqslant w_{ii} \leqslant (\overline{V}_i)^2, \qquad w_{ii} \in \left\langle V_i^2 \right\rangle^T, \tag{5d}$$

$$P_{lm} = g_{lm} w_{ll} - g_{lm} c_{lm} - b_{lm} s_{lm}, \tag{5e}$$

$$Q_{lm} = -\left(b_{lm} + b_{c,lm}/2\right) w_{ll} + b_{lm} c_{lm} - g_{lm} s_{lm}, \tag{5f}$$

$$P_{ml} = g_{lm} w_{mm} - g_{lm} c_{lm} + b_{lm} s_{lm}, \tag{5g}$$

$$Q_{ml} = -\left(b_{lm} + b_{c,lm}/2\right) w_{mm} + b_{lm} c_{lm} + g_{lm} s_{lm}, \tag{5h}$$

$$c_{lm} = \sum_{k=1,\ldots,8} \lambda_k \, \rho_1^{(k)} \rho_2^{(k)} \rho_3^{(k)}, \quad \breve{C}_{lm} \in \langle \cos(\theta_{lm}) \rangle^C,$$

$$V_l = \sum_{k=1,\ldots,8} \lambda_k \rho_1^{(k)}, \; V_m = \sum_{k=1,\ldots,8} \lambda_k \rho_2^{(k)}, \; \breve{C}_{lm} = \sum_{k=1,\ldots,8} \lambda_k \rho_3^{(k)},$$

$$\sum_{k=1,\ldots,8} \lambda_k = 1, \quad \lambda_k \geqslant 0, \quad k = 1, \ldots, 8. \tag{5i}$$

$$s_{lm} = \sum_{k=1,\ldots,8} \gamma_k \, \zeta_1^{(k)} \zeta_2^{(k)} \zeta_3^{(k)}, \quad \breve{S}_{lm} \in \langle \sin(\theta_{lm}) \rangle^S,$$

$$V_l = \sum_{k=1,\ldots,8} \gamma_k \zeta_1^{(k)}, \; V_m = \sum_{k=1,\ldots,8} \gamma_k \zeta_2^{(k)}, \; \breve{S}_{lm} = \sum_{k=1,\ldots,8} \gamma_k \zeta_3^{(k)},$$

$$\sum_{k=1,\ldots,8} \gamma_k = 1, \quad \gamma_k \geqslant 0, \quad k = 1, \ldots, 8. \tag{5j}$$

$$P_{lm}^2 + Q_{lm}^2 \leqslant V_l^2 \, \ell_{lm}, \tag{5k}$$

$$\ell_{lm} = \left(Y_{lm}^2 - \frac{b_{c,lm}^2}{4} \right) V_l^2 + Y_{lm}^2 V_m^2 - 2 Y_{lm}^2 c_{lm} - b_{c,lm} Q_{lm}, \tag{5l}$$

$$\text{Equations (1d)–(1h), (1k), [19, Eq. (9)]}, \tag{5m}$$

where the lifted variable ℓ_{lm} represents the squared magnitude of the current flow into terminal l of line $(l, m) \in \mathcal{L}$. The relationship between ℓ_{lm} and the power flows P_{lm} and Q_{lm} in (7l) tightens the QC relaxation [10, 20]. Section 5.5 gives an expression for ℓ_{lm} that considers lines with off-nominal tap ratios and non-zero phase shifts. Also, as shown in (7d), w_{ii} is associated with the squared voltage magnitude at bus i.

The lifted variables c_{lm} and s_{lm} represent relaxations of the trilinear terms $V_l V_m \cos(\theta_{lm})$ and $V_l V_m \sin(\theta_{lm})$, respectively, with (7j) and (7k) formulating an "extreme point" representation of the convex hulls for the trilinear terms $V_l V_m \breve{C}_{lm}$ and $V_l V_m \breve{S}_{lm}$ [5]. The auxiliary variables $\lambda_k, \; \gamma_k \in [0, 1]$, $k = 1, \ldots, 8$, are used in the formulations of these convex hulls.

The extreme points of $V_l V_m \breve{C}_{lm}$ are $\rho^{(k)} \in [\underline{V_l}, \overline{V_l}] \times [\underline{V_m}, \overline{V_m}] \times [\underline{\breve{C}}_{lm}, \overline{\breve{C}}_{lm}]$, $k = 1, \ldots, 8$ and the extreme points of $V_l V_m \breve{S}_{lm}$ are $\zeta^{(k)} \in [\underline{V_l}, \overline{V_l}] \times [\underline{V_m}, \overline{V_m}] \times [\underline{\breve{S}}_{lm}, \overline{\breve{S}}_{lm}]$, $k = 1, \ldots, 8$. Since sine and cosine are odd and even functions, respectively, $c_{lm} = c_{ml}$ and $s_{lm} = -s_{ml}$.

A "linking constraint" from [19, Eq. (9)] is also enforced. This linking constraint is associated with the bilinear terms $V_l V_m$ that are shared in $V_l V_m \cos(\theta_{lm})$ and $V_l V_m \sin(\theta_{lm})$.

4. COORDINATE TRANSFORMATIONS

The improvements to the QC relaxation's envelopes that are our main contributions are based on certain coordinate transformations. This section describes these transformations. We first form the power flow equations using polar representations of the lines' mutual admittances. We then introduce a complex base power in the per unit normalization that provides a rotational degree of freedom in the power flow equations.

While this section uses a Π circuit line model for the sake of simplicity, extensions to more general line models are straightforward. These extensions are presented in Section 5.5.

4.1. POWER FLOW EQUATIONS WITH ADMITTANCE IN POLAR FORM

Equations (1i) and (1i) model the power flows through a line $(l, m) \in \mathcal{L}$ via a rectangular representation of the line's mutual admittance, $g_{lm} + j b_{lm}$. In (7f)–(7g), the QC relaxation from [10] uses this rectangular admittance representation.

The line flows can be equivalently modeled using a polar representation of the mutual admittance, $Y_{lm} e^{j\delta_{lm}}$, where $Y_{lm} = \sqrt{g_{lm}^2 + b_{lm}^2}$ and $\delta_{lm} = \arctan(b_{lm}/g_{lm})$ are the magnitude and angle of the mutual admittance for line $(l, m) \in \mathcal{L}$, respectively. Using polar admittance coordinates, the complex power flows S_{lm} and S_{ml} into each line terminal are:

$$S_{lm} = V_l e^{j\theta_l} \left(\left(Y_{lm} e^{j\delta_{lm}} + j\frac{b_{c,lm}}{2} \right) V_l e^{j\theta_l} - Y_{lm} e^{j\delta_{lm}} V_m e^{j\theta_m} \right)^*, \tag{6a}$$

$$S_{ml} = V_m e^{j\theta_m} \left(-Y_{lm} e^{j\delta_{lm}} V_l e^{j\theta_l} + \left(Y_{lm} e^{j\delta_{lm}} + j\frac{b_{c,lm}}{2} \right) V_m e^{j\theta_m} \right)^*, \tag{6b}$$

where $(\cdot)^*$ is the complex conjugate. Taking the real and imaginary parts of (8) yields the active and reactive line flows:

$$P_{lm} = \mathrm{Re}(S_{lm}) = Y_{lm}\cos(\delta_{lm})V_l^2 - Y_{lm}V_lV_m\cos(\theta_{lm} - \delta_{lm}), \tag{7a}$$

$$Q_{lm} = \mathrm{Im}(S_{lm}) = -\left(Y_{lm}\sin(\delta_{lm}) + b_{c,lm}/2\right)V_l^2 - Y_{lm}V_lV_m\sin(\theta_{lm} - \delta_{lm}), \tag{7b}$$

$$P_{ml} = \mathrm{Re}(S_{ml}) = Y_{lm}\cos(\delta_{lm})V_m^2 - Y_{lm}V_lV_m\cos(\theta_{lm} + \delta_{lm}), \tag{7c}$$

$$Q_{ml} = \mathrm{Im}(S_{ml}) = -\left(Y_{lm}\sin(\delta_{lm}) + b_{c,lm}/2\right)V_m^2 + Y_{lm}V_lV_m\sin(\theta_{lm} + \delta_{lm}). \tag{7d}$$

With the rectangular admittance representation, the active and reactive power flow equations (1i)–(1i) each have two trigonometric terms (i.e., $\cos(\theta_{lm})$ and $\sin(\theta_{lm})$). Conversely, there is only one trigonometric term in each of the power flow equations that use the polar admittance representation (9) (e.g., $\cos(\theta_{lm} - \delta_{lm})$ for P_{lm} and $\sin(\theta_{lm} - \delta_{lm})$ for Q_{lm}). While these formulations are equivalent, the differing representations of the trigonometric terms suggest the possibility of using different trigonometric envelopes. The QC formulation we will propose in Section 5.3 exploits these differences.

4.2. ROTATED POWER FLOW FORMULATION

The base power used in the per unit normalization is traditionally chosen to be a real-valued quantity. More generally, complex-valued choices for the base power are also acceptable and can provide benefits for some algorithms. For instance, certain power flow [17] and state estimation algorithms [18, 21] leverage formulations with a complex-valued base power. To improve the QC relaxation's trigonometric envelopes, this section reformulates the OPF problem with a complex base power. Let S_{base}^{orig} and $S_{base}^{new}e^{j\psi}$ denote

the original and the new base power, respectively, where S_{base}^{orig}, S_{base}^{new}, and ψ are real-valued. Thus, the original base S_{base}^{orig} is real-valued, while the new base $S_{base}^{new}e^{j\psi}$ is complex-valued with magnitude S_{base}^{new} and angle ψ. Quantities associated with the new base power will be accented with a tilde, $(\tilde{\cdot})$. Complex power flows in the original base and the new base are related as:

$$\tilde{S}_{lm} = S_{lm} \cdot \frac{S_{base}^{orig}}{S_{base}^{new}e^{j\psi}}, \qquad \tilde{S}_{ml} = S_{ml} \cdot \frac{S_{base}^{orig}}{S_{base}^{new}e^{j\psi}}.$$

Since changing the magnitude of the base power does not affect the arguments of the trigonometric functions in the power flow equations, we choose $S_{base}^{new} = S_{base}^{old}$. With this choice,

$$\tilde{S}_{lm} = S_{lm}/e^{j\psi}, \qquad \tilde{S}_{ml} = S_{ml}/e^{j\psi}.$$

The angle of the base power, ψ, affects the arguments of the trigonometric functions, as shown in the following derivation:

$$\tilde{S}_{lm} = S_{lm}/e^{j\psi} = \left(Y_{lm}e^{-j(\delta_{lm}+\psi)} + (b_{c,lm}/2)e^{-j(\frac{\pi}{2}+\psi)}\right)V_l^2 - Y_{lm}V_lV_me^{j(-\delta_{lm}+\theta_{lm}-\psi)}, \tag{8a}$$

$$\tilde{S}_{ml} = S_{ml}/e^{j\psi} = \left(Y_{lm}e^{-j(\delta_{lm}+\psi)} + (b_{c,lm}/2)e^{-j(\frac{\pi}{2}+\psi)}\right)V_m^2 - Y_{lm}V_mV_le^{-j(\delta_{lm}+\theta_{lm}+\psi)}. \tag{8b}$$

Taking the real and imaginary parts of (8) yields:

$$\tilde{P}_{lm} = \mathrm{Re}(\tilde{S}_{lm}) = (Y_{lm}\cos(\delta_{lm}+\psi) - (b_{c,lm}/2)\sin(\psi))V_l^2 - Y_{lm}V_lV_m\cos(\theta_{lm}-\delta_{lm}-\psi), \tag{9a}$$

$$\tilde{Q}_{lm} = \mathrm{Im}(\tilde{S}_{lm}) = -(Y_{lm}\sin(\delta_{lm}+\psi) + (b_{c,lm}/2)\cos(\psi))V_l^2 - Y_{lm}V_lV_m\sin(\theta_{lm}-\delta_{lm}-\psi), \tag{9b}$$

$$\tilde{P}_{ml} = \mathrm{Re}(\tilde{S}_{ml}) = (Y_{lm}\cos(\delta_{lm}+\psi) - (b_{c,lm}/2)\sin(\psi))V_m^2 - Y_{lm}V_mV_l\cos(\theta_{lm}+\delta_{lm}+\psi), \tag{9c}$$

$$\tilde{Q}_{ml} = \mathrm{Im}(\tilde{S}_{ml}) = -(Y_{lm}\sin(\delta_{lm}+\psi) + (b_{c,lm}/2)\cos(\psi))V_m^2 + Y_{lm}V_mV_l\sin(\theta_{lm}+\delta_{lm}+\psi). \tag{9d}$$

The arguments of the trigonometric functions $\cos(\theta_{lm}-\delta_{lm}-\psi)$, $\sin(\theta_{lm}-\delta_{lm}-\psi)$, $\cos(\theta_{lm}+\delta_{lm}+\psi)$, and $\sin(\theta_{lm}+\delta_{lm}+\psi)$ in (9) are linear in ψ. For a given ψ, all other trigonometric terms in (9) are constants that do not require special handling.

4.3. ROTATED OPF PROBLEM

We next represent the complex power generation and load demands using the new base power:

$$\tilde{S}_i^g = S_i^g \cdot \frac{S_{base}^{orig}}{S_{base}^{new} e^{j\psi}} = \frac{S_i^g}{e^{j\psi}} = \frac{P_i^g + jQ_i^g}{e^{j\psi}}.$$

Define $\tilde{S}_i^g = \tilde{P}_i^g + j\tilde{Q}_i^g$, $\forall i \in \mathcal{N}$. Taking the real and imaginary parts of $\tilde{S}_i^g$ yields the following relationship between the power generation in the new and original bases:

$$\begin{bmatrix} \tilde{P}_i^g \\ \tilde{Q}_i^g \end{bmatrix} = \begin{bmatrix} \cos(\psi) & \sin(\psi) \\ -\sin(\psi) & \cos(\psi) \end{bmatrix} \begin{bmatrix} P_i^g \\ Q_i^g \end{bmatrix}. \tag{10}$$

The inverse relationship is well defined for any choice of ψ since the matrix in (10) is invertible.

The analogous relationship for the power demands is:

$$\begin{bmatrix} \tilde{P}_i^d \\ \tilde{Q}_i^d \end{bmatrix} = \begin{bmatrix} \cos(\psi) & \sin(\psi) \\ -\sin(\psi) & \cos(\psi) \end{bmatrix} \begin{bmatrix} P_i^d \\ Q_i^d \end{bmatrix}. \tag{11}$$

Applying (9)–(11) to (1) yields a "rotated" OPF problem:

$$\min \quad \sum_{i\in\mathcal{G}} c_{2,i}\left(\tilde{P}_i^g\cos(\psi)-\tilde{Q}_i^g\sin(\psi)\right)^2+c_{1,i}\left(\tilde{P}_i^g\cos(\psi)-\tilde{Q}_i^g\sin(\psi)\right)+c_{0,i} \tag{12a}$$

$$\text{subject to} \quad (\forall i\in\mathcal{N},\ \forall\,(l,m)\in\mathcal{L})$$

$$\tilde{P}_i^g-\tilde{P}_i^d=\left(g_{sh,i}\cos(\psi)-b_{sh,i}\sin(\psi)\right)V_i^2+\sum_{\substack{(l,m)\in\mathcal{L},\\ \text{s.t. } l=i}}P_{lm}+\sum_{\substack{(l,m)\in\mathcal{L},\\ \text{s.t. } m=i}}P_{ml}, \tag{12b}$$

$$\tilde{Q}_i^g-\tilde{Q}_i^d=-\left(g_{sh,i}\sin(\psi)+b_{sh,i}\cos(\psi)\right)V_i^2+\sum_{\substack{(l,m)\in\mathcal{L},\\ \text{s.t. } l=i}}Q_{lm}+\sum_{\substack{(l,m)\in\mathcal{L},\\ \text{s.t. } m=i}}Q_{ml}, \tag{12c}$$

$$\theta_{ref}=0, \tag{12d}$$

$$\underline{P}_i^g\leqslant\tilde{P}_i^g\cos(\psi)-\tilde{Q}_i^g\sin(\psi)\leqslant\overline{P}_i^g, \tag{12e}$$

$$\underline{Q}_i^g\leqslant\tilde{Q}_i^g\cos(\psi)+\tilde{P}_i^g\sin(\psi)\leqslant\overline{Q}_i^g, \tag{12f}$$

$$\underline{V}_i\leqslant V_i\leqslant\overline{V}_i,\qquad \underline{\theta}_{lm}\leqslant\theta_{lm}\leqslant\overline{\theta}_{lm}, \tag{12g}$$

$$(\tilde{P}_{lm})^2+(\tilde{Q}_{lm})^2\leqslant(\overline{S}_{lm})^2,\quad (\tilde{P}_{ml})^2+(\tilde{Q}_{ml})^2\leqslant(\overline{S}_{lm})^2, \tag{12h}$$

$$\text{Eq. (9).} \tag{12i}$$

The rotated OPF problem (15) is equivalent to (1) in that any solution to (15) (i.e. $\{V^*,\theta^*,\tilde{P}^{g\star},\tilde{Q}^{g\star}\}$) can be mapped to a solution $\{V^*,\theta^*,P^{g\star},Q^{g\star}\}$ to (1) using (10). Solutions to both formulations have the same voltage magnitudes and angles, V^* and θ^*. Thus, (15) can be interpreted as revealing a degree of freedom associated with choosing the base power's phase angle ψ. The next section exploits this degree of freedom to tighten the QC relaxation's trigonometric envelopes.

5. ROTATED QC RELAXATION

This section leverages the coordinate transformations presented in Section 4 to tighten the QC relaxation. We first propose and analyze new envelopes for the trigonometric functions and trilinear terms. We then describe an empirical analysis that informs the choice of the base power angle ψ in order to tighten the relaxation for typical OPF problems.

5.1. CONVEX ENVELOPES FOR THE TRIGONOMETRIC TERMS

A key determinant of the QC relaxation's tightness is the quality of the convex envelopes for the trigonometric terms in the power flow equations. The rotated OPF formulation (15) has four relevant trigonometric terms for each line: $\cos(\theta_{lm} - \delta_{lm} - \psi)$, $\sin(\theta_{lm} - \delta_{lm} - \psi)$, $\cos(\theta_{lm} + \delta_{lm} + \psi)$, and $\sin(\theta_{lm} + \delta_{lm} + \psi)$, $\forall (l,m) \in \mathcal{L}$. This contrasts with the two unique trigonometric terms ($\cos(\theta_{lm})$ and $\sin(\theta_{lm})$) per pair of connected buses in the OPF formulation (1).

While this would seem to suggest that at least twice as many convex envelopes would be required for the rotated OPF formulation (15), the arguments of the trigonometric terms in this formulation are not independent. For notational convenience, define $\hat{\delta}_{lm} = \delta_{lm} + \psi$. The angle sum and difference identities imply the following relationships:

$$\begin{bmatrix} \sin(\hat{\delta}_{lm} + \theta_{lm}) \\ \cos(\hat{\delta}_{lm} + \theta_{lm}) \\ \sin(\hat{\delta}_{lm} - \theta_{lm}) \\ \cos(\hat{\delta}_{lm} - \theta_{lm}) \end{bmatrix} = \begin{bmatrix} \sin(\hat{\delta}_{lm}) & \cos(\hat{\delta}_{lm}) \\ \cos(\hat{\delta}_{lm}) & -\sin(\hat{\delta}_{lm}) \\ \sin(\hat{\delta}_{lm}) & -\cos(\hat{\delta}_{lm}) \\ \cos(\hat{\delta}_{lm}) & \sin(\hat{\delta}_{lm}) \end{bmatrix} \begin{bmatrix} \cos(\theta_{lm}) \\ \sin(\theta_{lm}) \end{bmatrix}. \tag{13}$$

Rearranging these relationships yields:

$$\begin{bmatrix} \sin(\theta_{lm} + \hat{\delta}_{lm}) \\ \cos(\theta_{lm} + \hat{\delta}_{lm}) \end{bmatrix} = \begin{bmatrix} \alpha_{lm} & \beta_{lm} \\ -\beta_{lm} & \alpha_{lm} \end{bmatrix} \begin{bmatrix} \sin(\theta_{lm} - \hat{\delta}_{lm}) \\ \cos(\theta_{lm} - \hat{\delta}_{lm}) \end{bmatrix}. \tag{14}$$

where, for notational convenience, α_{lm} and β_{lm} are defined as $(\cos(\hat{\delta}_{lm}))^2 - (\sin(\hat{\delta}_{lm}))^2$ and $\beta_{lm} = 2\cos(\hat{\delta}_{lm})\sin(\hat{\delta}_{lm})$, respectively. The key implication of the linear relationship (17) is that only two (rather than four) convex envelopes need to be defined per line (one for each of the trigonometric terms $\sin(\theta_{lm} - \hat{\delta}_{lm})$ and $\cos(\theta_{lm} - \hat{\delta}_{lm})$). The remaining trigonometric functions, $\sin(\theta_{lm} + \hat{\delta}_{lm})$ and $\cos(\theta_{lm} + \hat{\delta}_{lm})$, are representable in terms of $\sin(\theta_{lm} - \hat{\delta}_{lm})$ and $\cos(\theta_{lm} - \hat{\delta}_{lm})$ via the linear relationship (17). Since the matrix in (17) is invertible for all $\hat{\delta}_{lm}$, the transformation in (17) is always well-defined.

Related special consideration is needed for parallel lines. In the original QC relaxation (7), the power flow equations for parallel lines between buses l and m shared the same envelopes, $\langle\cos(\theta_{lm})\rangle^C$ and $\langle\sin(\theta_{lm})\rangle^S$. In the RQC relaxation (21), the arguments of the trigonometric terms for parallel lines can differ due to the inclusion of the δ_{lm} terms. Rather than defining separate envelopes, we derive a linear relationship between the trigonometric terms for parallel lines. Let δ_{lm_1}, δ_{lm_2} and $\theta_{lm_1}^{shift}$, $\theta_{lm_2}^{shift}$ be the admittance angles and phase shifts, respectively, for two parallel lines between buses l and m. Applying the angle sum identity yields

$$\begin{bmatrix} \sin(\sigma_{lm_1} - \theta_{lm}) \\ \cos(\sigma_{lm_1} - \theta_{lm}) \\ \sin(\sigma_{lm_2} - \theta_{lm}) \\ \cos(\sigma_{lm_2} - \theta_{lm}) \end{bmatrix} = \begin{bmatrix} \sin(\sigma_{lm_1}) & -\cos(\sigma_{lm_1}) \\ \cos(\sigma_{lm_1}) & \sin(\sigma_{lm_1}) \\ \sin(\sigma_{lm_2}) & -\cos(\sigma_{lm_2}) \\ \cos(\sigma_{lm_2}) & \sin(\sigma_{lm_2}) \end{bmatrix} \begin{bmatrix} \cos(\theta_{lm}) \\ \sin(\theta_{lm}) \end{bmatrix}, \tag{15}$$

where, for notational convenience, $\sigma_{lm_1} = \delta_{lm_1} + \theta_{lm_1}^{shift} + \psi$ and $\sigma_{lm_2} = \delta_{lm_2} + \theta_{lm_2}^{shift} + \psi$. Rearranging (18) to eliminate $\cos(\theta_{lm})$ and $\sin(\theta_{lm})$ yields the desired linear relationship:

$$\begin{bmatrix} \sin(\theta_{lm} - \sigma_{lm_2}) \\ \cos(\theta_{lm} - \sigma_{lm_2}) \end{bmatrix} = \\ \begin{bmatrix} \cos(\sigma_{lm_1} - \sigma_{lm_2}) & \sin(\sigma_{lm_1} - \sigma_{lm_2}) \\ -\sin(\sigma_{lm_1} - \sigma_{lm_2}) & \cos(\sigma_{lm_1} - \sigma_{lm_2}) \end{bmatrix} \begin{bmatrix} \sin(\theta_{lm} - \sigma_{lm_1}) \\ \cos(\theta_{lm} - \sigma_{lm_1}) \end{bmatrix}. \tag{16}$$

Since the matrix in (19) is invertible, this relationship is always well defined.

The rest of this section considers systems without parallel lines for simplicity. Using the linear relationships in (17) (and in (19) for systems with parallel lines), all relevant trigonometric terms in (15) can be represented as linear combinations of $\sin(\theta_{lm} - \delta_{lm} - \psi)$ and $\cos(\theta_{lm} - \delta_{lm} - \psi)$ for each unique pair of connected buses $(l, m) \in \mathcal{L}$. The corresponding envelopes are $\langle\sin(\theta_{lm} - \delta_{lm} - \psi)\rangle^S$ and $\langle\cos(\theta_{lm} - \delta_{lm} - \psi)\rangle^C$. The QC relaxations of (1) and (15) hence have the same number of envelopes.

There are two characteristics that distinguish the relaxations of the trigonometric expressions in (1) and (15): First, the relaxations of the power flow equations (1i)–(1k) each use the weighted sums of two trigonometric envelopes, while the relaxations of (9a)–(9d) each use a single trigonometric envelope. Second, the base power angle ψ used to formulate (15) provides a degree of freedom that shifts the arguments of the trigonometric envelopes. We next discuss how both of these characteristics can be exploited to tighten the QC relaxation.

Regarding the first distinguishing characteristic, factoring out $-V_l V_m$ to focus on the trigonometric functions shows that the relaxation of (1i) depends on the quality of a weighted sum of trigonometric envelopes: $g_{lm}\left\langle \cos\left(\theta_{lm}\right)\right\rangle^{C} + b_{lm}\left\langle \sin\left(\theta_{lm}\right)\right\rangle^{S}$. The relaxation of (9a) depends on the quality of the envelope $Y_{lm}\left\langle \cos\left(\theta_{lm} - \delta_{lm} - \psi\right)\right\rangle^{C}$. (The relaxations of (1i)–(1k) and (9a)–(9d) are analogous.) To focus on the first characteristic, consider the latter envelope with $\psi = 0$.

Figure. 1 illustrates examples of these envelopes for a line with the same mutual admittance ($g_{lm} + jb_{lm} = 0.6 - j0.8$) for different intervals of angle differences ($\underline{\theta}_{lm} \leqslant \theta_{lm} \leqslant \overline{\theta}_{lm}$).

To compare these envelopes, we consider their lower and upper boundaries. The lower boundary of the envelope for $Y_{lm}\left\langle \cos\left(\theta_{lm} - \delta_{lm}\right)\right\rangle^{C}$ is at least as tight as the lower boundary of the envelope for $g_{lm}\left\langle \cos\left(\theta_{lm}\right)\right\rangle^{C} + b_{lm}\left\langle \sin\left(\theta_{lm}\right)\right\rangle^{S}$ when $Max(-90^{\circ}, -90^{\circ} + \delta_{lm}) \leqslant \underline{\theta}_{lm} \leqslant \overline{\theta}_{lm} \leqslant Min(90^{\circ}, 90^{\circ} + \delta_{lm})$ and is tighter for some line admittances and phase angle difference limits. For other intervals, the lower boundary of the envelope for $Y_{lm}\left\langle \cos\left(\theta_{lm} - \delta_{lm}\right)\right\rangle^{C}$ neither dominates nor is dominated by the lower boundary of the envelope for $g_{lm}\left\langle \cos\left(\theta_{lm}\right)\right\rangle^{C} + b_{lm}\left\langle \sin\left(\theta_{lm}\right)\right\rangle^{S}$. Following is the proof for the above statement.

To assist the derivations here, we define a function $F(\theta_{lm})$ which represents the difference between the trigonometric function $\cos(\theta_{lm} - \delta_{lm})$ itself and the line which connects the endpoints of $\cos(\theta_{lm} - \delta_{lm})$ at θ_{lm}^{min} and θ_{lm}^{max}:

$$\begin{aligned} F(\theta_{lm}) = &\cos(\theta_{lm} - \delta_{lm}) - \cos(\theta_{lm}^{max} - \delta_{lm}) \\ &- \frac{\cos(\theta_{lm}^{max} - \delta_{lm}) - \cos(\theta_{lm}^{min} - \delta_{lm})}{\theta_{lm}^{max} - \theta_{lm}^{min}} \left(\theta_{lm} - \theta_{lm}^{max}\right) \end{aligned} \tag{17}$$

Figure. 1 shows illustrative examples of the function $Y_{lm}\cos(\theta_{lm} - \delta_{lm})$ (black curve) and the line connecting the endpoints of this function at θ_{lm}^{min} and θ_{lm}^{max} (dashed red line) on the left, with corresponding visualizations of the function $F(\theta_{lm})$ itself on the right.

The derivative of $F(\theta_{lm})$ is

$$\begin{aligned} \frac{dF(\theta_{lm})}{d\theta_{lm}} = &-\sin(\theta_{lm} - \delta_{lm}) \\ &- \frac{\cos(\theta_{lm}^{max} - \delta_{lm}) - \cos(\theta_{lm}^{min} - \delta_{lm})}{\theta_{lm}^{max} - \theta_{lm}^{min}}. \end{aligned} \tag{18}$$

A key quantity in the following proposition is the set of zeros of the derivative of $F(\theta_{lm})$, i.e., the set of solutions to $\frac{dF(\theta_{lm})}{d\theta_{lm}} = 0$. This set, which we denote by $\mathcal{Z}_{\theta_{lm}^{min},\theta_{lm}^{max},\delta_{lm}}$ where the subscripts indicate that the set is parameterized by θ_{lm}^{min}, θ_{lm}^{max}, and δ_{lm}, is

$$\begin{aligned} &\mathcal{Z}_{\theta_{lm}^{min},\theta_{lm}^{max},\delta_{lm}} = \\ &\Bigg\{(-1)^{\kappa}\arcsin\left(\frac{\cos(\theta_{lm}^{min} - \delta_{lm}) - \cos(\theta_{lm}^{max} - \delta_{lm})}{\left(\theta_{lm}^{max} - \theta_{lm}^{min}\right)}\right) + \pi\kappa, \\ &\qquad \kappa = \ldots, -3, -2, -1, 0, 1, 2, 3, \ldots \Bigg\}. \end{aligned}$$

Finally, we let $|\cdot|$ denote the cardinality of a set.

Using these definitions, we next state and prove the following proposition. The lower boundary of the envelope $Y_{lm}\langle\cos(\theta_{lm} - \delta_{lm})\rangle^{C}$ is at least as tight as the lower boundary of the envelope $g_{lm}\langle\cos(\theta_{lm})\rangle^{C} + b_{lm}\langle\sin(\theta_{lm})\rangle^{S}$ if θ_{lm}^{min}, θ_{lm}^{max}, and δ_{lm} satisfy

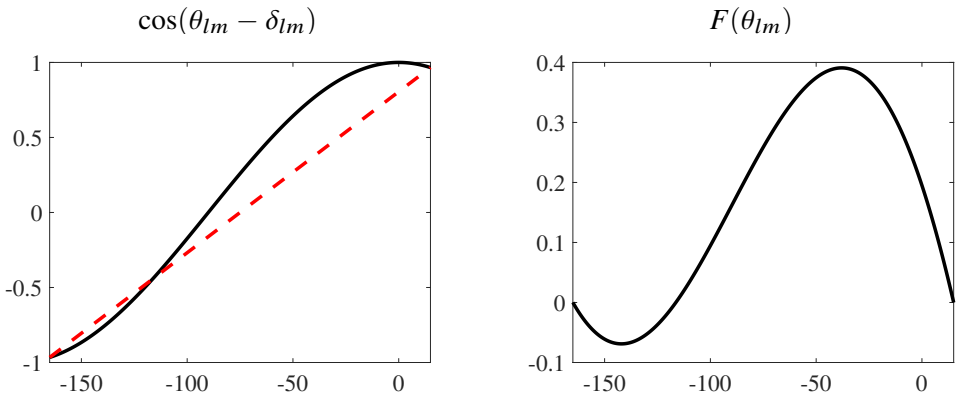

(a) $165^\circ \leqslant \theta_{lm} - \delta_{lm} \leqslant 15^\circ$

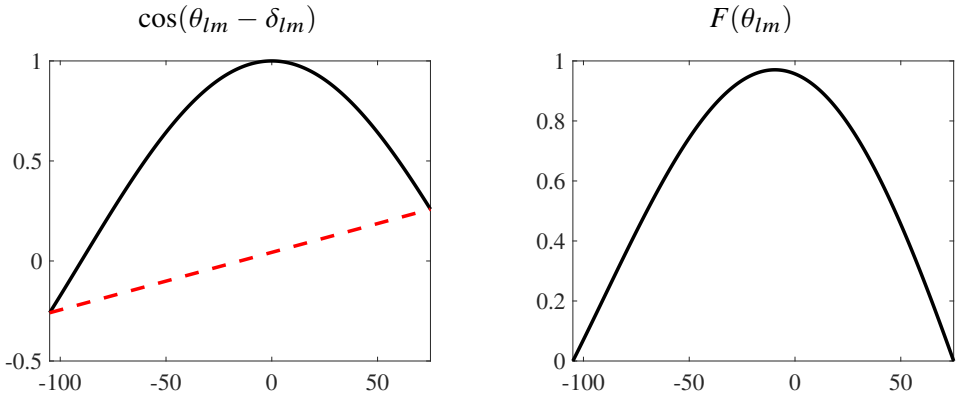

(b) $165^\circ \leqslant \theta_{lm} - \delta_{lm} \leqslant 15^\circ$

Figure 1. The left figures show visualizations of the function $\cos(\theta_{lm} - \delta_{lm})$ (black curve) and the line connecting the endpoints of this function at θ_{lm}^{min} and θ_{lm}^{max} (dashed red line) for different values of δ_{lm}, θ_{lm}^{min}, and θ_{lm}^{max}. The right figures show the corresponding function $F(\theta_{lm})$.

both of the following conditions:

$$\left| \mathcal{Z}_{\theta_{lm}^{min}, \theta_{lm}^{max}, \delta_{lm}} \bigcap \left\{ \theta_{lm}^{min} < \theta_{lm} < \theta_{lm}^{max} \right\} \right| = 1, \tag{19a}$$

$$F\left(\left(\theta_{lm}^{max} + \theta_{lm}^{min} \right) / 2 \right) > 0. \tag{19b}$$

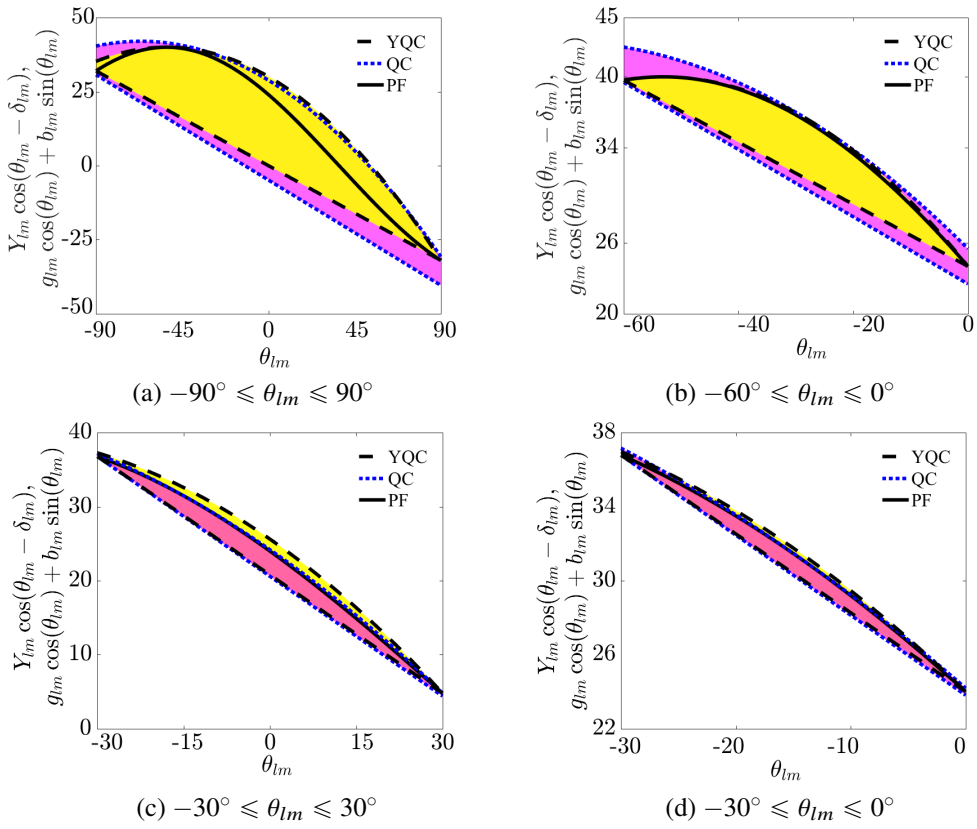

(a) $-90^\circ \leqslant \theta_{lm} \leqslant 90^\circ$ (b) $-60^\circ \leqslant \theta_{lm} \leqslant 0^\circ$

(c) $-30^\circ \leqslant \theta_{lm} \leqslant 30^\circ$ (d) $-30^\circ \leqslant \theta_{lm} \leqslant 0^\circ$

Figure 2. Comparison of envelopes for the trigonometric terms in (1) and (15). The yellow and magenta regions (with dotted and dashed borders, respectively) in (a)–(d) show the envelopes $g_{lm}\langle\cos(\theta_{lm})\rangle^C + b_{lm}\langle\sin(\theta_{lm})\rangle^S$ and $Y_{lm}\langle\cos(\theta_{lm}-\delta_{lm})\rangle^C$, respectively. The black solid lines correspond to the function $g_{lm}\cos(\theta_{lm}) + b_{lm}\sin(\theta_{lm}) = Y_{lm}\cos(\theta_{lm}-\delta_{lm})$.

Moreover, the upper boundary of the envelope $Y_{lm}\langle\cos(\theta_{lm}-\delta_{lm})\rangle^C$ is at least as tight as the upper boundary of the envelope $g_{lm}\langle\cos(\theta_{lm})\rangle^C + b_{lm}\langle\sin(\theta_{lm})\rangle^S$ if θ_{lm}^{min}, θ_{lm}^{max}, and δ_{lm} satisfy both (19a) and the condition

$$F\left(\left(\theta_{lm}^{max}+\theta_{lm}^{min}\right)/2\right) < 0. \tag{20}$$

The proof is based on the following observation: if the line connecting the points $(\theta_{lm}^{min}, \cos(\theta_{lm}^{min}-\delta_{lm}))$ and $(\theta_{lm}^{max}, \cos(\theta_{lm}^{max}-\delta_{lm}))$ (i.e., the dashed red line in Figure. 1) does not intersect the function $\cos(\theta_{lm}-\delta_{lm})$ itself within the range $\theta_{lm}^{min} < \theta_{lm} < \theta_{lm}^{max}$,

then this line is either the lower boundary or upper boundary of the tighest convex envelope for the function $\cos(\theta_{lm} - \delta_{lm})$ within this range. (For instance, the dashed red line in Figure. 1b is the lower boundary of the tighest envelope for $\cos(\theta_{lm} - \delta_{lm})$ within the range $-165^\circ \leqslant \theta_{lm} \leqslant 15^\circ$.) In this case, the line is the tightest lower (upper) boundary if the function $\cos(\theta_{lm} - \delta_{lm})$ is above (below) the line for any point between θ_{lm}^{min} and θ_{lm}^{max} (e.g., the midpoint $(\theta_{lm}^{min} + \theta_{lm}^{max})/2$, which is used in (19b) and (20)).

Observe that the line connecting the points $(\theta_{lm}^{min}, \cos(\theta_{lm}^{min} - \delta_{lm}))$ and $(\theta_{lm}^{max}, \cos(\theta_{lm}^{max} - \delta_{lm}))$ does not intersect the function $\cos(\theta_{lm} - \delta_{lm})$ between θ_{lm}^{min} and θ_{lm}^{max} if and only if $F(\theta_{lm})$ is non-zero for all $\theta_{lm}^{min} < \theta_{lm} < \theta_{lm}^{max}$. We next argue that this is implied by (19a).

The condition (19a) is equivalent to the existence of one critical point θ_{lm}^{*} of the function $F(\theta_{lm})$. (i.e., the derivative of $F(\theta)$ has a single zero, θ_{lm}^{*}, in the range $\theta_{lm}^{min} < \theta_{lm} < \theta_{lm}^{max}$. Since $F(\theta_{lm})$ is continuous and $F(\theta_{lm}^{min}) = F(\theta_{lm}^{max}) = 0$, the critical point θ_{lm}^{*} must either correspond to a minimum or maximum of $F(\theta_{lm})$. Since the function $F(\theta_{lm})$ is zero at the endpoints θ_{lm}^{min} and θ_{lm}^{max}, having a single minimum or maximum in the range $\theta_{lm}^{min} < \theta_{lm} < \theta_{lm}^{max}$ implies that $F(\theta_{lm}) \neq 0$ within this range.

To complete the conditions in the proposition, (19b) and (20) determine whether the line connecting the points $(\theta_{lm}^{min}, \cos(\theta_{lm}^{min} - \delta_{lm}))$ and $(\theta_{lm}^{max}, \cos(\theta_{lm}^{max} - \delta_{lm}))$ is above or below the function $\cos(\theta_{lm} - \delta_{lm})$ by evaluating the function $F(\theta_{lm})$ at an arbitrary point between θ_{lm}^{min} and θ_{lm}^{max}, here selected to be the midpoint $\left(\theta_{lm}^{min} + \theta_{lm}^{max}\right)/2$.

Since multiplication by Y_{lm} only rescales (but does not otherwise change) the envelope $\langle \cos(\theta_{lm} - \delta_{lm}) \rangle^{C}$, the arguments above trivially extend to $Y_{lm} \langle \cos(\theta_{lm} - \delta_{lm}) \rangle^{C}$. Moreover, since $Y_{lm} \cos(\theta_{lm} - \delta_{lm}) = g_{lm} \cos(\theta_{lm}) + b_{lm} \sin(\theta_{lm})$, the envelope $g_{lm} \langle \cos(\theta_{lm}) \rangle^{C} + b_{lm} \langle \sin(\theta_{lm}) \rangle^{S}$ cannot be tighter than the tightest possible envelope for $Y_{lm} \cos(\theta_{lm} - \delta_{lm})$. Since the boundaries of $Y_{lm} \langle \cos(\theta_{lm} - \delta_{lm}) \rangle^{C}$ considered in the proof form portions of the tightest possible convex envelope for $Y_{lm} \cos(\theta_{lm} - \delta_{lm})$, they are at least as tight as the corresponding boundaries of the envelope $g_{lm} \langle \cos(\theta_{lm}) \rangle^{C} + b_{lm} \langle \sin(\theta_{lm}) \rangle^{S}$. Fur-

thermore, the example envelopes in Figure. 2 show that the corresponding boundaries of $Y_{lm}\langle\cos(\theta_{lm}-\delta_{lm})\rangle^{C}$ are strictly tighter than those of $g_{lm}\langle\cos(\theta_{lm})\rangle^{C}+b_{lm}\langle\sin(\theta_{lm})\rangle^{S}$ for some values of δ_{lm}, θ_{lm}^{min}, and θ_{lm}^{max}.

We finally note that values of θ_{lm}^{min}, θ_{lm}^{max}, and δ_{lm} such that $\max(-90^{\circ},-90^{\circ}+\delta_{lm}) \leqslant \theta_{lm}^{min} < \theta_{lm}^{max} \leqslant \min(90^{\circ},90^{\circ}+\delta_{lm})$ satisfy (19). Thus, the trigonometric envelopes corresponding to the polar admittance representation have lower boundaries that are at least as tight as those in the original QC relaxation for many typical values of θ_{lm}^{min}, θ_{lm}^{max}, and δ_{lm}.

In general, the upper boundary of $Y_{lm}\langle\cos(\theta_{lm}-\delta_{lm})\rangle^{C}$ neither dominates nor is dominated by the upper boundary of $g_{lm}\langle\cos(\theta_{lm})\rangle^{C}+b_{lm}\langle\sin(\theta_{lm})\rangle^{S}$. Thus, a QC relaxation that enforces the intersection of these envelopes is generally tighter than relaxations constructed using either of these envelopes individually. Section 5.4 further discusses this topic.

The second characteristic distinguishing between the envelopes for (1) and (15) is the ability to choose ψ in the latter envelopes. As shown in Figure. 2, changing ψ rotates the arguments of these envelopes. Analytically comparing the impacts of different values for ψ is not straightforward. Accordingly, this section will later describe an empirical study that suggests a good choice for ψ for typical OPF problems.

5.2. ENVELOPES FOR TRILINEAR TERMS

The rotated OPF formulation (15) has four trilinear terms for each line: $V_l V_m \cos(\theta_{lm}-\delta_{lm}-\psi)$, $V_l V_m \sin(\theta_{lm}-\delta_{lm}-\psi)$, $V_l V_m \cos(\theta_{lm}+\delta_{lm}+\psi)$, and $V_l V_m \sin(\theta_{lm}+\delta_{lm}+\psi)$, $\forall(l,m) \in \mathcal{L}$. This contrasts with the two unique trilinear terms ($V_l V_m \cos(\theta_{lm})$ and $V_l V_m \sin(\theta_{lm})$) per pair of connected buses in the OPF formulation (1). This would seem to suggest that at least twice as many envelopes would be required to relax the trilinear terms in the rotated OPF formulation (15). However, the four trilinear terms in (15) are related. We next describe how to exploit these relationships to only enforce two envelopes for the trilinear terms associated with each line.

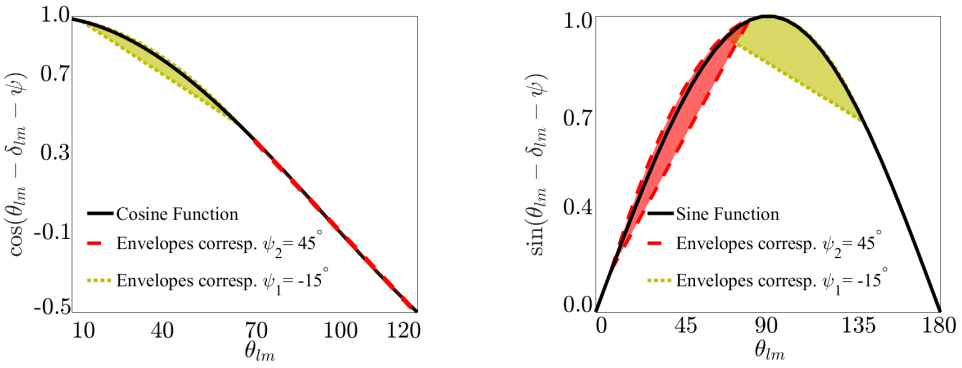

(a) $\langle \cos(\theta_{lm} - \delta_{lm} - \psi) \rangle^C$ (b) $\langle \sin(\theta_{lm} - \delta_{lm} - \psi) \rangle^S$

Figure 3. Comparison of envelopes for the sine and cosine functions for different values of ψ. The yellow and red regions (with dashed and dotted borders, respectively) in (a) and (b) show the envelopes $\langle \cos(\theta_{lm} - \delta_{lm} - \psi) \rangle^C$ and $\langle \sin(\theta_{lm} - \delta_{lm} - \psi) \rangle^S$, for $\psi_1 = -15^\circ$ and $\psi_2 = 45^\circ$, respectively. The angle difference θ_{lm} varies within $0^\circ \leqslant \theta_{lm} \leqslant 72^\circ$, and $\delta_{lm} = -53^\circ$.

Similar to (7k)–(7j), we relax the trilinear products by constructing linear envelopes using the upper and lower bounds on V_l, V_m, $\cos(\theta_{lm} - \delta_{lm} - \psi)$, $\sin(\theta_{lm} - \delta_{lm} - \psi)$, $\cos(\theta_{lm} + \delta_{lm} + \psi)$, and $\sin(\theta_{lm} + \delta_{lm} + \psi)$. We use the linear relationship (17) to represent the upper and lower bounds on the receiving end quantities $\cos(\theta_{lm} + \delta_{lm} + \psi)$ (denoted $\underline{\tilde{C}}_{lm}^{(r)}$, $\overline{\tilde{C}}_{lm}^{(r)}$) and $\sin(\theta_{lm} + \delta_{lm} + \psi)$ (denoted $\underline{\tilde{S}}_{lm}^{(r)}$, $\overline{\tilde{S}}_{lm}^{(r)}$) in terms of the bounds on the sending end quantities $\cos(\theta_{lm} - \delta_{lm} - \psi)$ (denoted $\underline{\tilde{C}}_{lm}^{(s)}$, $\overline{\tilde{C}}_{lm}^{(s)}$) and $\sin(\theta_{lm} - \delta_{lm} - \psi)$ (denoted $\underline{\tilde{S}}_{lm}^{(s)}$, $\overline{\tilde{S}}_{lm}^{(s)}$). We then enforce constraints on the sending end quantities derived from the intersection of the transformed bounds associated with the receiving end quantities along with the bounds on the sending end quantities. Intersecting these bounds forms a polytope in terms of the sending end quantities $\tilde{C}_{lm}^{(s)} \in \langle \cos(\theta_{lm} - \delta_{lm} - \psi) \rangle^C$ and $\tilde{S}_{lm}^{(s)} \in \langle \sin(\theta_{lm} - \delta_{lm} - \psi) \rangle^S$, expressible as a convex combination of its extreme points.

Figure. 3 shows the bounds on both the sending and receiving end quantities in terms of the sending end quantities. The yellow region shows the polytope formed by the bounds on $\cos(\theta_{lm} - \delta_{lm} - \psi)$ and $\sin(\theta_{lm} - \delta_{lm} - \psi)$. The red region represents the polytope formed by using (17) to represent the bounds on the receiving end quantities $\cos(\theta_{lm} + \delta_{lm} + \psi)$ and $\sin(\theta_{lm} + \delta_{lm} + \psi)$ in terms of the sending end quantities $\cos(\theta_{lm} - \delta_{lm} - \psi)$ and

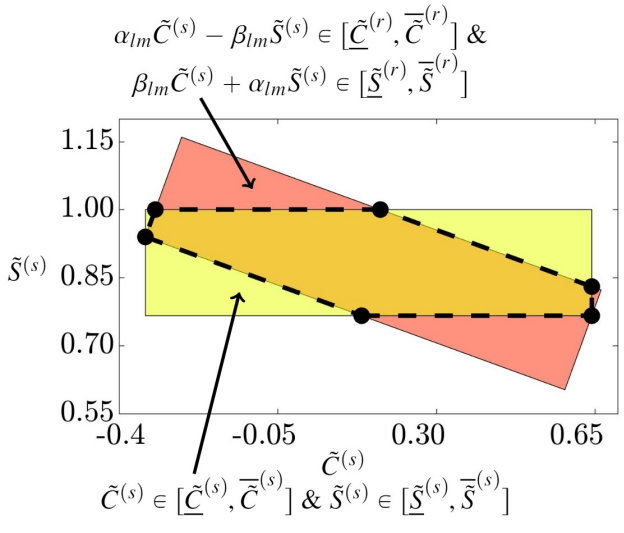

;

Figure 4. A projection of the four-dimensional polytope associated with the trilinear products between voltage magnitudes and trigonometric functions, in terms of the sending end variables $\tilde{S}_{lm}^{(s)}$ and $\tilde{C}_{lm}^{(s)}$ representing $\cos(\theta_{lm} - \delta_{lm} - \psi)$ and $\sin(\theta_{lm} - \delta_{lm} - \psi)$. The polytope formed by intersecting the sending end polytope (yellow) and receiving end polytope (red) is outlined with the dashed black lines and has vertices shown by the black dots.

$\sin(\theta_{lm} - \delta_{lm} - \psi)$. The black dots are the vertices of the polytope shown by the dashed black lines formed from the intersection of the yellow and red polytopes. Here we present expressions for the vertices of the polytope consisting of the black dashed lines in Figure. 3. To compute the coordinates of these vertices (black dots in Figure. 5), we intersect the edges of the receiving end polytope, which is formed by the upper and lower bounds on the receiving end quantities, $\overline{\tilde{S}}_{lm}^{(r)}$, $\overline{\tilde{C}}_{lm}^{(r)}$ and $\underline{\tilde{S}}_{lm}^{(r)}$, $\underline{\tilde{C}}_{lm}^{(r)}$, respectively, with the edges of the sending end polytope, which is formed by the upper and lower bounds on the sending end quantities $\overline{\tilde{S}}_{lm}^{(s)}$, $\overline{\tilde{C}}_{lm}^{(s)}$ and $\underline{\tilde{S}}_{lm}^{(s)}$, $\underline{\tilde{C}}_{lm}^{(s)}$, respectively.

When written in terms of the sending end quantities $\tilde{S}_{lm}^{(s)}$ and $\tilde{C}_{lm}^{(s)}$, the coordinates for the upper and lower bounds on the receiving end quantities are functions of ψ. To write the coordinates of the vertices as functions of ψ, consider the line segments labeled in Figure. 5. The yellow and purple polytopes in this figure represent the bounds on the sending and receiving end quantities, respectively. Table 1 describes the relevant intersections of

Table 1. Line segment intersections corresponding to Figure 5

ψ (degrees)	$A'B'$	$B'C'$	$C'D'$	$A'D'$
$-45 \leqslant \psi \leqslant 0$	AB & BC	BC & CD	CD & AD	AB & AD
$-90 \leqslant \psi \leqslant -45$	BC & CD	CD & AD	AB & AD	AB & BC
$-135 \leqslant \psi \leqslant -90$	CD & AD	AB & AD	AB & BC	BC & CD
$-180 \leqslant \psi \leqslant -135$	AB & AD	AB & BC	BC & CD	CD & AD
$0 \leqslant \psi \leqslant 45$	AD & AB	AB & BC	BC & CD	CD & AD
$45 \leqslant \psi \leqslant 90$	CD & AD	AD & AB	AB & BC	BC & CD
$90 \leqslant \psi \leqslant 135$	BC & CD	CD & AD	AD & AB	AB & BC
$135 \leqslant \psi \leqslant 180$	AB & BC	BC & CD	CD & AD	AD & AB

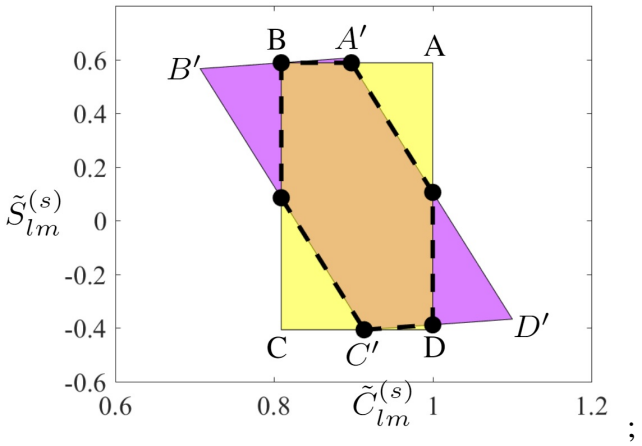

Figure 5. A projection of the four-dimensional polytope associated with the trilinear products between the voltage magnitudes and the trigonometric functions, expressed in terms of the sending end variables $\tilde{S}_{lm}^{(s)}$ and $\tilde{C}_{lm}^{(s)}$ representing $\cos(\theta_{lm} - \delta_{lm} - \psi)$ and $\sin(\theta_{lm} - \delta_{lm} - \psi)$. The polytope formed by intersecting the sending end polytope (ABCD) and receiving end polytope ($A'B'C'D'$) is outlined with the dashed black lines and has vertices shown by the black dots.

the line segments that form these polytopes. For the ranges of ψ in the first column of Table 1, the remaining columns indicate the line segments whose intersections form the corresponding vertices. The coordinates of these intersections are given in Table 2. As an example for $-45^\circ \leqslant \psi \leqslant 0^\circ$, the $A'D'$ line segment in Figure. 5 should intersect line segments AB and AD. The coordinates of these intersections are given in rows 13 and 16 of Table 2.

Table 2. Coordinates of the line segment intersections in Table 1.

Line Segments	Coordinates of the Intersection Point
$A'B'$ & AB	$\left(\frac{\alpha_{lm}}{\beta_{lm}}\overline{\tilde{S}}_{lm}^{(s)} - \beta_{lm}\overline{\tilde{S}}_{lm}^{(r)}) - \frac{\alpha_{lm}^2\overline{\tilde{S}}_{lm}^{(r)})}{\beta_{lm}},\ \overline{\tilde{S}}_{lm}^{(s)}\right)$
$A'B'$ & BC	$\left(\underline{\tilde{C}}_{lm}^{(s)},\ \frac{\beta_{lm}\underline{\tilde{C}}_{lm}^{(s)})}{\alpha_{lm}} + \frac{\beta_{lm}^2\overline{\tilde{S}}_{lm}^{(r)})}{\alpha_{lm}} + \alpha_{lm}\overline{\tilde{S}}_{lm}^{(r)}\right)$
$A'B'$ & CD	$\left(\frac{\alpha_{lm}}{\beta_{lm}}\underline{\tilde{S}}_{lm}^{(s)} - \beta_{lm}\overline{\tilde{S}}_{lm}^{(r)}) - \frac{\alpha_{lm}^2\overline{\tilde{S}}_{lm}^{(r)})}{\beta_{lm}},\ \underline{\tilde{S}}_{lm}^{(s)}\right)$
$A'B'$ & AD	$\left(\overline{\tilde{C}}_{lm}^{(s)},\ \frac{\beta_{lm}\overline{\tilde{C}}_{lm}^{(s)})}{\alpha_{lm}} + \frac{\beta_{lm}^2\overline{\tilde{S}}_{lm}^{(r)})}{\alpha_{lm}} + \alpha_{lm}\overline{\tilde{S}}_{lm}^{(r)}\right)$
$B'C'$ & BC	$\left(\underline{\tilde{C}}_{lm}^{(s)},\ -\frac{\alpha_{lm}\underline{\tilde{C}}_{lm}^{(s)})}{\beta_{lm}} + \frac{\alpha_{lm}^2\underline{\tilde{C}}_{lm}^{(r)})}{\beta_{lm}} + \beta_{lm}\underline{\tilde{C}}_{lm}^{(r)}\right)$
$B'C'$ & CD	$\left(-\frac{\beta_{lm}}{\alpha_{lm}}\underline{\tilde{S}}_{lm}^{(s)} + \alpha_{lm}\underline{\tilde{C}}_{lm}^{(r)}) + \frac{\beta_{lm}^2\underline{\tilde{C}}_{lm}^{(r)})}{\alpha_{lm}},\ \underline{\tilde{S}}_{lm}^{(s)}\right)$
$B'C'$ & AB	$\left(-\frac{\beta_{lm}}{\alpha_{lm}}\overline{\tilde{S}}_{lm}^{(s)} + \alpha_{lm}\underline{\tilde{C}}_{lm}^{(r)}) + \frac{\beta_{lm}^2\underline{\tilde{C}}_{lm}^{(r)})}{\alpha_{lm}},\ \overline{\tilde{S}}_{lm}^{(s)}\right)$
$B'C'$ & AD	$\left(\overline{\tilde{C}}_{lm}^{(s)},\ -\frac{\alpha_{lm}\overline{\tilde{C}}_{lm}^{(s)})}{\beta_{lm}} + \frac{\alpha_{lm}^2\underline{\tilde{C}}_{lm}^{(r)})}{\beta_{lm}} + \beta_{lm}\underline{\tilde{C}}_{lm}^{(r)}\right)$
$C'D'$ & AB	$\left(\frac{\alpha_{lm}}{\beta_{lm}}\overline{\tilde{S}}_{lm}^{(s)} - \beta_{lm}\underline{\tilde{S}}_{lm}^{(r)}) - \frac{\alpha_{lm}^2\underline{\tilde{S}}_{lm}^{(r)})}{\beta_{lm}},\ \overline{\tilde{S}}_{lm}^{(s)}\right)$
$C'D'$ & BC	$\left(\underline{\tilde{C}}_{lm}^{(s)},\ \frac{\beta_{lm}\underline{\tilde{C}}_{lm}^{(s)})}{\alpha_{lm}} + \frac{\beta_{lm}^2\underline{\tilde{S}}_{lm}^{(r)})}{\alpha_{lm}} + \alpha_{lm}\underline{\tilde{S}}_{lm}^{(r)}\right)$
$C'D'$ & CD	$\left(\frac{\alpha_{lm}}{\beta_{lm}}\underline{\tilde{S}}_{lm}^{(s)} - \beta_{lm}\underline{\tilde{S}}_{lm}^{(r)}) - \frac{\alpha_{lm}^2\underline{\tilde{S}}_{lm}^{(r)})}{\beta_{lm}},\ \underline{\tilde{S}}_{lm}^{(s)}\right)$
$C'D'$ & AD	$\left(\overline{\tilde{C}}_{lm}^{(s)},\ \frac{\beta_{lm}\overline{\tilde{C}}_{lm}^{(s)})}{\alpha_{lm}} + \frac{\beta_{lm}^2\underline{\tilde{S}}_{lm}^{(r)})}{\alpha_{lm}} + \alpha_{lm}\underline{\tilde{S}}_{lm}^{(r)}\right)$
$A'D'$ & AB	$\left(-\frac{\beta_{lm}}{\alpha_{lm}}\overline{\tilde{S}}_{lm}^{(s)} + \alpha_{lm}\overline{\tilde{C}}_{lm}^{(r)}) + \frac{\beta_{lm}^2\overline{\tilde{C}}_{lm}^{(r)})}{\alpha_{lm}},\ \overline{\tilde{S}}_{lm}^{(s)}\right)$
$A'D'$ & BC	$\left(\underline{\tilde{C}}_{lm}^{(s)},\ -\frac{\alpha_{lm}\underline{\tilde{C}}_{lm}^{(s)})}{\beta_{lm}} + \frac{\alpha_{lm}^2\overline{\tilde{C}}_{lm}^{(r)})}{\beta_{lm}} + \beta_{lm}\overline{\tilde{C}}_{lm}^{(r)}\right)$
$A'D'$ & CD	$\left(-\frac{\beta_{lm}}{\alpha_{lm}}\underline{\tilde{S}}_{lm}^{(s)} + \alpha_{lm}\overline{\tilde{C}}_{lm}^{(r)}) + \frac{\beta_{lm}^2\overline{\tilde{C}}_{lm}^{(r)})}{\alpha_{lm}},\ \underline{\tilde{S}}_{lm}^{(s)}\right)$
$A'D'$ & AD	$\left(\overline{\tilde{C}}_{lm}^{(s)},\ -\frac{\alpha_{lm}\overline{\tilde{C}}_{lm}^{(s)})}{\beta_{lm}} + \frac{\alpha_{lm}^2\overline{\tilde{C}}_{lm}^{(r)})}{\beta_{lm}} + \beta_{lm}\overline{\tilde{C}}_{lm}^{(r)}\right)$

Enforcing the constraints associated with both the yellow and red polytopes adds an unnecessary computational burden. We instead restrict the sending end quantities $\cos(\theta_{lm} - \delta_{lm} - \psi)$ and $\sin(\theta_{lm} - \delta_{lm} - \psi)$ to lie within the polytope shown by the black dashed line in Figure. 3. This implicitly ensures satisfaction of the bounds on the receiving end quantities.

To relax the product terms $V_l V_m \cos(\theta_{lm} - \delta_{lm} - \psi)$ and $V_l V_m \sin(\theta_{lm} - \delta_{lm} - \psi)$, we first represent the quantities $\cos(\theta_{lm} - \delta_{lm} - \psi)$ and $\sin(\theta_{lm} - \delta_{lm} - \psi)$ using lifted variables $\tilde{C}_{lm}^{(s)}$ and $\tilde{S}_{lm}^{(s)}$, respectively. We then extend the polytope shown by the black dashed lines in Figure. 3 using the upper and lower bounds on V_l and V_m. The resulting four-dimensional polytope is the convex hull of the quadrilinear polynomial $V_l V_m \tilde{C}_{lm}^{(s)} \tilde{S}_{lm}^{(s)}$, which we represent using an extreme point formulation similar to (7k)–(7j). Let $\mathcal{T}_{lm} = \{(\tilde{C}_{lm}^{int,1}, \tilde{S}_{lm}^{int,1}), (\tilde{C}_{lm}^{int,2}, \tilde{S}_{lm}^{int,2}), \ldots, (\tilde{C}_{lm}^{int,\tilde{N}}, \tilde{S}_{lm}^{int,\tilde{N}})\}$ denote the coordinates of the intersection points (black dots) in Figure. 3, where $\tilde{N}$ is the number of intersection points which ranges from 4 to 8 depending on the value of ψ. The extreme points of $V_l V_m \tilde{C}_{lm}^{(s)} \tilde{S}_{lm}^{(s)}$ are then denoted as $\eta^{(k)} \in [\underline{V_l}, \overline{V_l}] \times [\underline{V_m}, \overline{V_m}] \times \mathcal{T}_{lm}$, $k = 1, \ldots, 4\tilde{N}$. The auxiliary variables $\lambda_k \in [0, 1]$, $k = 1, \ldots, 4\tilde{N}$, are used to form the convex hull of the quadrilinear term $V_l V_m \tilde{C}_{lm}^{(s)} \tilde{S}_{lm}^{(s)}$.

The envelopes for the trilinear terms are:

$$
\begin{aligned}
&\tilde{c}_{lm} = \sum_{k=1,\ldots,4\tilde{N}} \lambda_k \, \eta_1^{(k)} \eta_2^{(k)} \eta_3^{(k)}, \quad \tilde{s}_{lm} = \sum_{k=1,\ldots,4\tilde{N}} \lambda_k \, \eta_1^{(k)} \eta_2^{(k)} \eta_4^{(k)}, \\
&V_l = \sum_{k=1,\ldots,4\tilde{N}} \lambda_k \eta_1^{(k)}, \;\; V_m = \sum_{k=1,\ldots,4\tilde{N}} \lambda_k \eta_2^{(k)}, \;\; \tilde{S}_{lm}^{(s)} = \sum_{k=1,\ldots,4\tilde{N}} \lambda_k \eta_4^{(k)}, \\
&\tilde{C}_{lm}^{(s)} = \sum_{k=1,\ldots,4\tilde{N}} \lambda_k \eta_3^{(k)}, \; \sum_{k=1,\ldots,4\tilde{N}} \lambda_k = 1, \quad \lambda_k \geqslant 0, \;\; k = 1, \ldots, 4\tilde{N}, \\
&\tilde{C}_{lm}^{(s)} \in \left\langle \cos(\theta_{lm} - \delta_{lm} - \psi) \right\rangle^C, \; \tilde{S}_{lm}^{(s)} \in \left\langle \sin(\theta_{lm} - \delta_{lm} - \psi) \right\rangle^S .
\end{aligned} \tag{21}
$$

Note that (20) precludes the need for the linking constraint in [19, Eq. (9)] that relates the common term $V_l V_m$ in the products $V_l V_m \sin(\theta_{lm})$ and $V_l V_m \cos(\theta_{lm})$.

5.3. QC RELAXATION OF THE ROTATED OPF PROBLEM

Replacing the squared and trilinear terms with the corresponding lifted variables in the rotated OPF formulation (15) results in the "Rotated QC" (RQC) relaxation:

$$\text{min} \quad \text{(15a)} \tag{22a}$$

$$\text{subject to} \quad (\forall i \in \mathcal{N}, \forall\, (l,m) \in \mathcal{L})$$

$$\tilde{P}_i^g - \tilde{P}_i^d = \left(g_{sh,i}\cos(\psi) - b_{sh,i}\sin(\psi)\right) w_{ii} + \sum_{\substack{(l,m)\in\mathcal{L},\\ \text{s.t. } l=i}} \tilde{P}_{lm} + \sum_{\substack{(l,m)\in\mathcal{L},\\ \text{s.t. } m=i}} \tilde{P}_{ml}, \tag{22b}$$

$$\tilde{Q}_i^g - \tilde{Q}_i^d = -\left(g_{sh,i}\sin(\psi) + b_{sh,i}\cos(\psi)\right) w_{ii} + \sum_{\substack{(l,m)\in\mathcal{L},\\ \text{s.t. } l=i}} \tilde{Q}_{lm} + \sum_{\substack{(l,m)\in\mathcal{L},\\ \text{s.t. } m=i}} \tilde{Q}_{ml}, \tag{22c}$$

$$\tilde{P}_{lm} = \left(Y_{lm}\cos(\delta_{lm}+\psi) - b_{c,lm}/2\sin(\psi)\right) w_{ll} - Y_{lm}\tilde{c}_{lm}, \tag{22d}$$

$$\tilde{Q}_{lm} = -\left(Y_{lm}\sin(\delta_{lm}+\psi) + b_{c,lm}/2\cos(\psi)\right) w_{ll} - Y_{lm}\tilde{s}_{lm}, \tag{22e}$$

$$\tilde{P}_{ml} = -Y_{lm}\tilde{c}_{lm} + \left(Y_{lm}\cos(\delta_{lm}+\psi) - b_{c,lm}/2\sin(\psi)\right) w_{mm}, \tag{22f}$$

$$\tilde{Q}_{ml} = Y_{lm}\tilde{s}_{lm} - \left(Y_{lm}\sin(\delta_{lm}+\psi) + b_{c,lm}/2\cos(\psi)\right) w_{mm}, \tag{22g}$$

$$\tilde{P}_{lm}^2 + \tilde{Q}_{lm}^2 \leqslant w_{ll}\,\tilde{\ell}_{lm}, \tag{22h}$$

$$\begin{aligned}\tilde{\ell}_{lm} = {} & \left(\frac{b_{c,lm}^2}{4} + Y_{lm}^2 - Y_{lm}b_{c,lm}\cos(\delta_{lm}+\psi)\sin(\psi)\right. \\ & \left. + Y_{lm}b_{c,lm}\sin(\delta_{lm}+\psi)\cos(\psi)\right) V_l^2 + Y_{lm}^2 V_m^2 \\ & + \left(-2Y_{lm}^2\cos(\delta_{lm}+\psi) + Y_{lm}b_{c,lm}\sin(\psi)\right)\tilde{c}_{lm} \\ & + \left(2Y_{lm}^2\sin(\delta_{lm}+\psi) + Y_{lm}b_{c,lm}\cos(\psi)\right)\tilde{s}_{lm},\end{aligned} \tag{22i}$$

$$\text{Equations (7d), (15l)–(15q), (20).} \tag{22j}$$

Note that trilinear terms in (21) are relaxed via the extreme point approach in (20) that yields the convex hulls for these terms. The lifted variables $\tilde{c}_{lm}$ and $\tilde{s}_{lm}$ represent relaxations of the trilinear terms $V_l V_m \cos(\theta_{lm} - \delta_{lm} - \psi)$ and $V_l V_m \sin(\theta_{lm} - \delta_{lm} - \psi)$, respectively. Section 5.5 gives an expression for $\tilde{\ell}_{lm}$ that considers off-nominal tap ratios and non-zero phase shifts.

5.4. TIGHTENED QC RELAXATION OF THE ROTATED OPF PROBLEM

Applying the angle sum and difference identities in combination with (17) reveals a linear relationship between the trigonometric functions used in the original QC relaxation (7), $\cos(\theta_{lm})$ and $\sin(\theta_{lm})$, and those in the RQC relaxation (21), $\cos(\theta_{lm} - \delta_{lm} - \psi)$ and $\sin(\theta_{lm} - \delta_{lm} - \psi)$:

$$\begin{bmatrix} \cos(\theta_{lm}) \\ \sin(\theta_{lm}) \end{bmatrix} = M_{lm} \begin{bmatrix} \sin(\theta_{lm} - \delta_{lm} - \psi) \\ \cos(\theta_{lm} - \delta_{lm} - \psi) \end{bmatrix}, \tag{23}$$

where the constant matrix M_{lm} is defined as

$$\begin{aligned} M_{lm} = \frac{1}{2} \Bigg(& \begin{bmatrix} \sin(\delta_{lm} + \psi) & \cos(\delta_{lm} + \psi) \\ \cos(\delta_{lm} + \psi) & -\sin(\delta_{lm} + \psi) \end{bmatrix} \begin{bmatrix} \alpha_{lm} & \beta_{lm} \\ -\beta_{lm} & \alpha_{lm} \end{bmatrix} \\ & + \begin{bmatrix} -\sin(\delta_{lm} + \psi) & \cos(\delta_{lm} + \psi) \\ \cos(\delta_{lm} + \psi) & \sin(\delta_{lm} + \psi) \end{bmatrix} \Bigg) \end{aligned}$$

with α_{lm} and β_{lm} defined as in (17). As mentioned in Section 5.1, the RQC relaxation (21) can be further tightened by additionally enforcing the envelopes $\langle \cos(\theta_{lm}) \rangle^C$ and $\langle \sin(\theta_{lm}) \rangle^S$ used in the original QC relaxation (7). This results in the "Tightened Rotated QC" (TRQC) relaxation:

$$\min \quad \text{(15a)} \tag{24a}$$

$$\text{subject to} \quad (\forall i \in \mathcal{N}, \forall (l,m) \in \mathcal{L})$$

$$M_{lm} \begin{bmatrix} \tilde{C}_{lm}^{(s)} \\ \tilde{S}_{lm}^{(s)} \end{bmatrix} \in \begin{bmatrix} \langle \cos(\theta_{lm}) \rangle^C \\ \langle \sin(\theta_{lm}) \rangle^S \end{bmatrix} \tag{24b}$$

$$\text{Equations (7d), (15l)–(15q), (20), (21b)–(21m).} \tag{24c}$$

5.5. AN EMPIRICAL ANALYSIS FOR DETERMINING THE ROTATION ψ

The key parameter in our proposed QC formulation is the rotation ψ. We next describe an empirical analysis for choosing a value for ψ that works well for a range of test cases.

Figure. 6 shows the optimality gaps for the PGLib-OPF test cases as a function of ψ, each normalized by the maximum gap for that case over all values for ψ. The results in the figure were generated by sweeping ψ from -90° to 90° in steps of 0.5°. (The figure is exactly symmetric for values of ψ from 90° to -90°.) The shaded bands around the median line (in black) show every fifth percentile of the results. The best value of ψ for each case is denoted as ψ^*.

The results in Figure. 6 indicate that good values of ψ are consistent across the test systems. Thus, we suggest using $\psi = 80^\circ$, which is where the median of the optimality gaps over all the test cases was smallest. Moreover, the symmetry in Figure. 6 implies that selecting ψ within the intervals $[-90^\circ, -80^\circ]$, $[-15^\circ, -5^\circ]$, and $[80^\circ, 90^\circ]$ results in nearly the smallest optimality gaps for almost all of the test cases compared to the optimality gaps from the RQC relaxation using ψ^*.

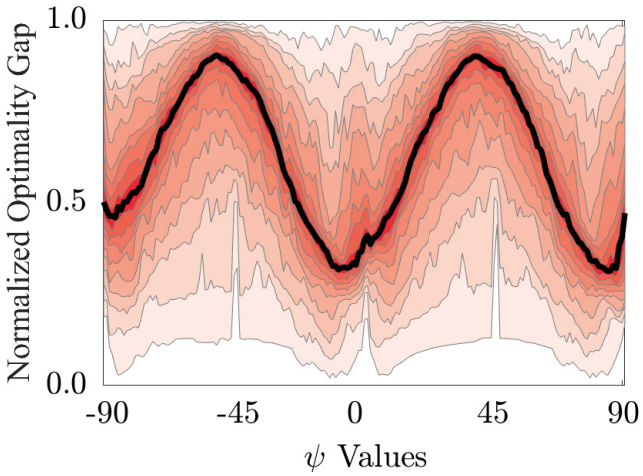

Figure 6. Normalized optimality gap as a function of ψ for PGLib-OPF cases.

6. MORE GENERAL LINE MODELS

This section extends the paper's results to a line model that considers transformers with a non-zero phase shift θ_{lm}^{shift} and/or an off-nominal voltage ratio τ_{lm}. With this model, the complex power flows into both terminals of line $(l,m) \in \mathcal{L}$ are:

$$S_{lm} = V_l e^{j\theta_l}\left[\left(Y_{lm}e^{j\delta_{lm}} + j\frac{b_{c,lm}}{2}\right)\frac{V_l e^{j\theta_l}}{\tau_{lm}^2} - \frac{Y_{lm}e^{j\delta_{lm}}V_m e^{j\theta_m}}{\tau_{lm}e^{-j\theta_{lm}^{shift}}}\right]^* \tag{25a}$$

$$S_{ml} = V_m e^{j\theta_m}\left[\left(Y_{lm}e^{j\delta_{lm}} + j\frac{b_{c,lm}}{2}\right)V_m e^{j\theta_m} - \frac{Y_{lm}e^{j\delta_{lm}}V_l e^{j\theta_l}}{\tau_{lm}e^{j\theta_{lm}^{shift}}}\right]^* \tag{25b}$$

We follow the procedure in Section 4.2 by applying a complex base power normalization:

$$\tilde{S}_{lm} = \frac{S_{lm}}{e^{j\psi}} = \left(\frac{Y_{lm}}{\tau_{lm}^2}e^{-j(\delta_{lm}+\psi)} + \frac{b_{c,lm}}{2}\frac{e^{-j(\frac{\pi}{2}+\psi)}}{\tau_{lm}^2}\right)V_l^2 - \frac{Y_{lm}}{\tau_{lm}}V_l V_m e^{j(\theta_{lm}-\delta_{lm}-\theta_{lm}^{shift}-\psi)}, \tag{26a}$$

$$\tilde{S}_{ml} = \frac{S_{ml}}{e^{j\psi}} = \left(Y_{lm}e^{-j(\delta_{lm}+\psi)} + \frac{b_{c,lm}}{2}e^{-j(\frac{\pi}{2}+\psi)}\right)V_m^2 - \frac{Y_{lm}}{\tau_{lm}}V_l V_m e^{j(-\theta_{lm}-\delta_{lm}+\theta_{lm}^{shift}-\psi)}. \tag{26b}$$

Taking the real and imaginary parts of (25) yields:

$$\tilde{P}_{lm} = \mathrm{Re}(\tilde{S}_{lm}) = \left(\frac{Y_{lm}}{\tau_{lm}^2}\cos(\delta_{lm}+\psi) - \frac{b_{c,lm}}{2\tau_{lm}^2}\sin(\psi)\right)V_l^2 - \frac{Y_{lm}}{\tau_{lm}}V_l V_m\cos(\theta_{lm}-\delta_{lm}-\theta_{lm}^{shift}-\psi), \tag{27a}$$

$$\tilde{Q}_{lm} = \mathrm{Im}(\tilde{S}_{lm}) = \left(-\frac{Y_{lm}}{\tau_{lm}^2}\sin(\delta_{lm}+\psi) - \frac{b_{c,lm}}{2\tau_{lm}^2}\cos(\psi)\right)V_l^2 - \frac{Y_{lm}}{\tau_{lm}}V_l V_m\sin(\theta_{lm}-\delta_{lm}-\theta_{lm}^{shift}-\psi), \tag{27b}$$

$$\tilde{P}_{ml} = \mathrm{Re}(\tilde{S}_{ml}) = \left(Y_{lm}\cos(\delta_{lm}+\psi) - \frac{b_{c,lm}}{2}\sin(\psi)\right)V_m^2 - \frac{Y_{lm}}{\tau_{lm}}V_m V_l\cos(\theta_{lm}+\delta_{lm}-\theta_{lm}^{shift}+\psi), \tag{27c}$$

$$\tilde{Q}_{ml} = \mathrm{Im}(\tilde{S}_{ml}) = \left(-Y_{lm}\sin(\delta_{lm}+\psi) - \frac{b_{c,lm}}{2}\cos(\psi)\right)V_m^2 + \frac{Y_{lm}}{\tau_{lm}}V_m V_l\sin(\theta_{lm}+\delta_{lm}-\theta_{lm}^{shift}+\psi). \tag{27d}$$

The arguments of the trigonometric terms in (26) are not independent since $\cos(\theta_{lm} + \delta_{lm} - \theta_{lm}^{shift} + \psi)$ and $\sin(\theta_{lm} + \delta_{lm} - \theta_{lm}^{shift} + \psi)$ are linearly related with $\cos(\theta_{lm} - \delta_{lm} - \theta_{lm}^{shift} - \psi)$ and $\sin(\theta_{lm} - \delta_{lm} - \theta_{lm}^{shift} - \psi)$ via the general form of (17). Extending (17) to consider off-nominal voltage ratios and non-zero phase shifts in accomplished by replacing θ_{lm} in (17) with $\theta_{lm} - \theta_{lm}^{shift}$.

Extensions of the expressions for the squared magnitudes of the current flows in the original QC relaxation (7) and the RQC relaxation (21), ℓ_{lm} and $\tilde{\ell}_{lm}$, respectively, are derived by dividing $(P_{lm}^2 + Q_{lm}^2)$ and $(\tilde{P}_{lm}^2 + \tilde{Q}_{lm}^2)$ by V_l^2:

$$\begin{aligned}
\ell_{lm} = & \left(\frac{Y_{lm}^2}{\tau_{lm}^4} - \frac{b_{c,lm}^2}{4\tau_{lm}^4} \right) V_l^2 + \frac{Y_{lm}^2}{\tau_{lm}^2} V_m^2 - \frac{b_{c,lm}}{\tau_{lm}^2} Q_{lm} \\
& - 2\frac{Y_{lm}^2}{\tau_{lm}^3} \left(\cos(\delta_{lm}) c_{lm} + \sin(\delta_{lm}) s_{lm} \right), \qquad (28) \\
\tilde{\ell}_{lm} = & \left(\frac{Y_{lm}^2}{\tau_{lm}^4} + \frac{b_{c,lm}^2}{4\tau_{lm}^4} - \frac{Y_{lm}}{\tau_{lm}^4} b_{c,lm} \cos(\delta_{lm} + \psi) \sin(\psi) \right. \\
& \left. + \frac{Y_{lm}}{\tau_{lm}^4} b_{c,lm} \sin(\delta_{lm} + \psi) \cos(\psi) \right) V_l^2 + \frac{Y_{lm}^2}{\tau_{lm}^2} V_m^2 \\
& + \left(\frac{Y_{lm}}{\tau_{lm}^3} b_{c,lm} (\sin(\psi) - \frac{2Y_{lm}^2}{\tau_{lm}^3} \cos(\delta_{lm} + \psi) \right) \tilde{c}_{lm} \\
& + \left(\frac{Y_{lm}}{\tau_{lm}^3} b_{c,lm} \cos(\psi) + \frac{2Y_{lm}^2}{\tau_{lm}^3} \sin(\delta_{lm} + \psi) \right) \tilde{s}_{lm} \qquad (29)
\end{aligned}$$

Extending the TRQC relaxation (23) to the more general line model is derived by changing the matrix M_{lm} in (22).

$$\begin{bmatrix} \cos(\theta_{lm}) \\ \sin(\theta_{lm}) \end{bmatrix} = M'_{lm} \begin{bmatrix} \sin(\theta_{lm} - \delta_{lm} - \psi - \theta_{lm}^{shift}) \\ \cos(\theta_{lm} - \delta_{lm} - \psi - \theta_{lm}^{shift}) \end{bmatrix}. \qquad (30)$$

where the constant matrix M'_{lm} is defined as

$$M'_{lm} = \frac{1}{2}\left(\begin{bmatrix} -\sin(\hat{\delta}_{lm} + \theta_{lm}^{shift}) & \cos(\hat{\delta}_{lm} + \theta_{lm}^{shift}) \\ \cos(\hat{\delta}_{lm} + \theta_{lm}^{shift}) & \sin(\hat{\delta}_{lm} + \theta_{lm}^{shift}) \end{bmatrix} + \begin{bmatrix} \sin(\hat{\delta}_{lm} - \theta_{lm}^{shift}) & \cos(\hat{\delta}_{lm} - \theta_{lm}^{shift}) \\ \cos(\hat{\delta}_{lm} - \theta_{lm}^{shift}) & -\sin(\hat{\delta}_{lm} - \theta_{lm}^{shift}) \end{bmatrix} \begin{bmatrix} \alpha_{lm} & \beta_{lm} \\ -\beta_{lm} & \alpha_{lm} \end{bmatrix}\right)$$

where for notational convenience, define $\hat{\delta}_{lm} = \delta_{lm} + \psi$.

7. NUMERICAL RESULTS

This section demonstrates the effectiveness of the proposed approach using selected test cases from the PGLib-OPF v18.08 benchmark library [22]. These test cases were selected since existing relaxations fail to provide tight bounds on the best known objective values. Our implementations use Julia 0.6.4, JuMP v0.18 [23], PowerModels.jl [25], and Gurobi 8.0 as modeling tools and the solver. The results are computed using a laptop with an i7 1.80 GHz processor and 16 GB of RAM.

Table 3 summarizes the results from applying the QC (7), RQC (21), and TRQC (23) relaxations to selected test cases. The first column lists the test cases. The next group of columns represents optimality gaps, defined as

$$\textit{Optimality Gap} = \left(\frac{\textit{Local Solution} - \textit{QC Bound}}{\textit{Local Solution}}\right). \tag{31}$$

The optimality gaps are defined using the local solutions to the non-convex problem (1) from PowerModels.jl. The final group of columns show the solver times.

Comparing the second and third columns in Table 3 reveals that using admittances in polar form without rotation (i.e., the RQC relaxation (21) with $\psi = 0$) can improve the optimality gaps of some test cases (e.g., improvements of 3.76% and 3.19% for "case30_ieee"

Table 3. Results from applying the QC and RQC relaxations with various options to selected PGLib test cases.

Test Cases	QC Gap (%)	RQC ($\psi = 0$) Gap (%)	RQC ($\psi = 80^\circ$) Gap (%)	RQC ($\psi*$)		TRQC ($\psi = 80^\circ$) Gap (%)	TRQC ($\psi*$)		QC Time (sec)	RQC Time (sec)	TRQC Time (sec)
				Gap (%)	$\psi*$		Gap (%)	$\psi*$			
case3_lmbd	0.97	0.97	0.89	0.79	-81°	0.84	0.63	11°	0.34	0.01	0.01
case30_ieee	18.67	14.91	13.14	12.11	65°	13.14	11.82	-25°	0.33	0.03	0.03
case118_ieee	0.77	0.90	0.65	0.64	70°	0.64	0.62	70°	0.55	0.19	0.23
case300_ieee	2.56	2.58	2.43	2.26	-13°	2.32	2.24	-13°	1.54	1.50	3.15
case9241_pegase	1.71	1.70	1.70	1.69	-10°	1.70	1.69	-10°	265.39	190.80	297.56
case3_lmbd__api	4.57	4.31	4.42	4.28	2°	4.17	3.93	-71°	0.51	0.01	0.01
case24_ieee_rts__api	11.02	7.83	7.51	7.24	79°	7.31	6.98	-11°	0.71	0.03	0.04
case39_epri__api	1.71	1.38	1.33	1.33	-11°	1.32	1.32	79°	0.39	0.05	0.05
case73_ieee_rts__api	9.54	8.12	7.36	7.36	-10°	7.24	7.24	-10°	1.00	0.29	0.37
case118_ieee__api	28.67	28.03	26.82	26.52	-8°	27.11	26.38	-8°	0.53	0.20	0.97
case179_goc__api	5.86	6.01	5.57	4.90	-81°	4.90	4.06	-78°	0.82	0.61	0.64
case14_ieee__sad	19.16	21.45	17.89	16.30	77°	15.82	15.39	-12°	0.35	0.03	0.03
case24_ieee_rts__sad	2.74	2.55	2.31	2.19	78°	2.26	2.12	-12°	0.40	0.05	0.06
case30_ieee__sad	5.66	5.95	4.81	4.59	-13°	4.56	4.45	66°	0.32	0.05	0.06
case73_ieee_rts__sad	2.37	2.24	1.98	1.90	79°	1.84	1.82	78°	0.41	0.28	0.41
case118_ieee__sad	6.67	8.10	5.45	5.39	81°	5.45	5.07	69°	0.58	0.25	0.39
case162_ieee_dtc__sad	6.22	6.30	5.65	5.59	-14°	5.65	5.54	76°	0.86	0.55	0.84
case300_ieee__sad	2.34	2.59	1.80	1.61	83°	1.78	1.59	83°	1.94	1.29	2.06

AC: AC local solution from (1), *QC Gap*: Optimality gap for the QC relaxation from (7), *RQC Gap*: Optimality gap for the Rotated QC relaxation from (21), *TRQC Gap*: Optimality gap for the Tightened Rotated QC Relaxation from (23), $\psi*$: Use of the best ψ for this case.

and "case24_ieee_rts__api", respectively, relative to the original QC relaxation (7)) . However, the RQC relaxation with $\psi = 0$ has worse performance in other cases, such as "case300_ieee" and "case14_ieee__sad", which have 0.02% and 2.29% larger optimality gaps, respectively.

Using a non-zero value for ψ can improve the optimality gaps. Solving the RQC relaxation (21) with the suggested $\psi = 80^\circ$ obtained from the empirical analysis in Section 5.5 results in 1.08% better optimality gaps, on average, compared to the original QC relaxation. The RQC relaxation (21) with ψ^* (the best value of ψ for each case) provides optimality gaps that are not worse than those obtained by the original QC relaxation (7) for all test cases, yielding an improvement of 1.36% on average compared to the original QC relaxation. As one specific example, the gap from the original QC relaxation for "case162_ieee_dtc__sad" is 6.22% compared to 6.30% for the RQC relaxation (21) with $\psi = 0$ relaxation (21). Use of the suggested $\psi = 80^\circ$ reduces the gap to 5.65%, which is superior to the gap obtained from the QC relaxation (7). Using ψ^* further reduces the optimality gap to 5.59%.

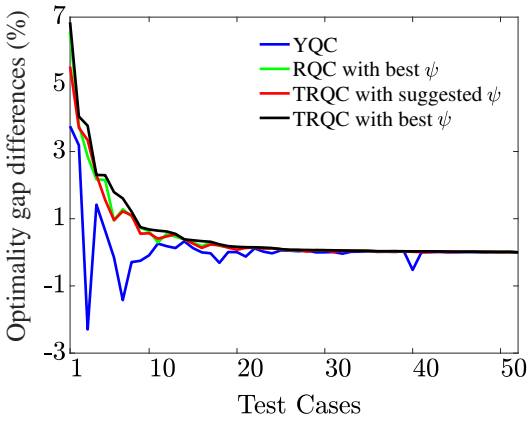

Figure 7. Comparison of optimality gap differences with respect to the original QC relaxation (7) for different QC relaxation variants.

Enforcing the envelopes from both the original QC relaxation and the RQC relaxation, i.e., the TRQC relaxation (23), further improves the optimality gaps. Solving the TRQC relaxation (23) with the suggested $\psi = 80^\circ$ results in 1.29% better gaps, on average, compared to the original QC relaxation. The TRQC relaxation with ψ^* yields optimality gaps that are 1.57% and 0.21% better, on average, compared to the original QC relaxation and the RQC relaxation with ψ^*. The additional envelopes $\langle \sin(\theta_{lm}) \rangle^S$ and $\langle \cos(\theta_{lm}) \rangle^C$ in the TRQC relaxation increase the average solver time by 22%.

Figure. 7 visualizes the optimality gaps for variants of the QC relaxation over a range of test cases. Positive values indicate an improvement in the optimality gap of the associated variant relative to the original QC relaxation (7). The test cases are sorted in order of increasing optimality gaps obtained from the original QC relaxation. The TRQC relaxation with ψ^* achieves the smallest optimality gaps. While the RQC relaxation with $\psi = 0$ obtains a worse optimality gap for some test cases compared to the original QC relaxation, both the RQC and the TRQC relaxations with ψ^* outperform the QC relaxation for all test cases. As expected from the analysis in Section 5.5, applying the suggested $\psi = 80^\circ$ results in good performance across a variety of test cases.

8. CONCLUSION

This paper proposes and empirically tests two improvements for strengthening QC relaxations of OPF problems by tightening the envelopes used for the trigonometric terms. The first improvement represents the line admittances in polar form. The second improvement applies a complex base power normalization with angle ψ in order to rotate the arguments of the trigonometric terms. An empirical analysis is used to suggest a good value for ψ. Comparison to the state-of-the-art QC relaxation reveals the effectiveness of the proposed improvements. Our ongoing work is extending the RQC relaxation to allow for distinct values of ψ for each line.

BIBLIOGRAPHY

[1] W.A. Bukhsh,A. Grothey, K.I.M. McKinnon, P.A. Trodden, Local Solutions of the Optimal Power Flow Problem, IEEE Transaction on Power Systems, 28 (4) (2013) 4780–4788.

[2] D. Bienstock, A. Verma, Strong NP-hardness of AC Power Flows Feasibility, arXiv:1512.07315 (2015).

[3] A. Castillo, R.P. O'Neill, Survey of Approaches to Solving the ACOPF (OPF Paper 4) March (2013)

[4] D. K. Molzahn, I. A. Hiskens, A Survey of Relaxations and Approximations of the Power Flow Equations, Foundations and Trends in Electric Energy Systems February (2019).

[5] M. Lu, H. Nagarajan, R. Bent, S.D Eksioglu, S.J. Mason, Tight Piecewise Convex Relaxations for Global Optimization of Optimal Power Flow, 20th Power Systems Computation Conference (PSCC), June (2018).

[6] J. F. Marley, D. K. Molzahn, I. A. Hiskens, Solving Multiperiod OPF Problems using an AC-QP Algorithm Initialized with an SOCP Relaxation, IEEE Transaction on Power Systems 32 (5) (2017) 3538–3548.

[7] D.K. Molzahn, L.A. Roald, AC Optimal Power Flow with Robust Feasibility Guarantees, 20th Power System Computation Conference (PSCC) June 2018.

[8] D.K. Molzahn, B.C. Lesieutre, C.L. DeMarco, A Sufficient Condition for Power Flow Insolvability With Applications to Voltage Stability Margins, IEEE Transaction on Power Systems 28 (3) (2013) 2592–2601.

[9] D.K. Molzahn, Computing the Feasible Spaces of Optimal Power Flow Problems, IEEE Transaction on Power Systems, 32 (6) (2017) 4752–4763.

[10] C. Coffrin, H.L. Hijazi, P. Van Hentenryck, The QC Relaxation: A Theoretical and Computational Study on Optimal Power Flow, IEEE Transaction on Power Systems 31 (4) (2016) 3008–3018.

[11] C. Coffrin, H.L. Hijazi, P. Van Hentenryck, Strengthening the SDP Relaxation of AC Power Flows with Convex Envelopes, Bound Tightening, and Valid Inequalities, IEEE Transactions on Power Systems 32 (5) (2017) 3549-3558.

[12] C. Chen, A. Atamturk, S.S. Oren, Bound Tightening for the Alternating Current Optimal Power Flow Problem, IEEE Transaction on Power Systems 31 (5) (2016) 3729–3736.

[13] M.R. Narimani, D.K. Molzahn, M.L. Crow, Improving QC Relaxations of OPF Problems via Voltage MagnitudeDifference Constraints and Envelopes for Trilinear Monomials, 20th Power Systems Computation Conference (PSCC), June (2018).

[14] B. Kocuk, S.S. Dey, X.A. Sun, Strong SOCP Relaxations for the Optimal Power Flow Problem, Operation Research 64 (4) (2016) 1177–1196.

[15] B. Kocuk, S.S. Dey, X.A. Sun, Matrix Minor Reformulation and SOCP-based Spatial Branch-and-Cut Method for the AC Optimal Power Flow Problem, arXiv:1703.03050 March (2017).

[16] K. Bestuzheva, H.L. Hijazi, C. Coffrin, Convex Relaxations for Quadratic On/Off Constraints and Applications to Optimal Transmission Switching, Optimization Online.pdf (2016).

[17] O.L. Tortelli, E.M. Lourenço, A.V. Garcia, B.C. Pal, Fast Decoupled Power Flow to Emerging Distribution Systems via Complex pu Normalization, IEEE Transactions on Power Systems 30 (3) (2015) 1351–1358.

[18] Y. Ju, W. Wu, F. Ge, K. Ma, Y. Lin, L. Ye, Fast Decoupled State Estimation for Distribution Networks Considering Branch Ampere Measurements, IEEE Transactions on Smart Grid 9 (6) (2018) 6338-6347.

[19] K. Sundar, H. Nagarajan, S. Misra, M. Lu , C. Coffrin, R. Bent, Optimization-Based Bound Tightening using a Strengthened QC-Relaxation of the Optimal Power Flow Problem, arXiv:1809.04565v2 (2018).

[20] M. Farivar, C.R. Clarke, S.H. Low, K.M. Chandy, Inverter VAR Control for Distribution Systems with Renewables, 2011 IEEE International Conference on Smart Grid Communications (SmartGridComm) October (2011) (457–462).

[21] Z. Wei, X. Chen, G. Sun, H. Zang, Distribution System Fast Decoupled State Estimation based on Complex PU Normalization, 5th International Conference on Electric Utility Deregulation and Restructuring and Power Technologies (DRPT) (November) (2015) (840–845).

[22] IEEE PES Task Force on Benchmarks for Validation of Emerging Power System Algorithms, The Power Grid Library for Benchmarking AC Optimal Power Flow Algorithms, arXiv:1908.02788 (2019).

[23] I. Dunning, J. Huchette, M. Lubin, JuMP: A modeling language for mathematical optimization, SIAM Review 59 (2) (2017) 259–320.

[24] Gurobi Optimization, Gurobi Optimizer Reference Manual, (2019) url:http://www.gurobi.com.

[25] C. Coffrin, R. Bent, K. Sundar, Y. Ng, and M. Lubin, PowerModels.jl: An Open-Source Framework for Exploring Power Flow Formulations, 2018 Power Systems Computation Conference (PSCC), (2018) 1–8.

V. TIGHTENING QC RELAXATIONS OF OPF PROBLEMS BY INDEPENDENTLY ROTATING THE TRIGONOMETRIC TERMS

Mohammad Rasoul Narimani, Daniel K. Molzahn, and Mariesa L. Crow

Department of Electrical and Computer Engineering

Missouri University of Science and Technology

Rolla, Missouri 65409–0050

Email: mn9t5@mst.edu

ABSTRACT

Optimal power flow (OPF) is a fundamental problem in power system operations. Recently developed convex relaxation techniques have provided new insights regarding the global optimality of AC OPF solutions. The QC relaxation is a promising approach that convexifies the trigonometric and product terms in the OPF problem by enclosing these terms in convex envelopes. The accuracy of the QC relaxation strongly depends on the tightness of these envelopes. This paper strengthens the QC relaxation of OPF problem by proposing a modified formulation of the power flow equations. The proposed modified formulation facilitates tightening the envelopes on the trigonometric functions in the power flow equations by controlling the parameterized variables that appear in the trigonometric functions' arguments and shift them independently. This paper describes an empirical analysis used to determine the proper variables for shifting the sine and cosine functions in each branch. Comparing the results of the proposed approach with a state-of-the-art QC implementation illustrates the obtained improvements.

Keywords: Optimal power flow, QC relaxation, Coordinate transformation

1. INTRODUCTION

The optimal power flow (OPF) problem seeks a minimum cost operating point for an electric power system, subject to both the power flow equations modeling the network physics and engineering limits [1]. The nonlinear power flow equations which form the basis of the AC OPF problem, along with a variety of engineering limits, make the OPF problem a nonconvex optimization problem that, in general, is NP-hard [2] and might have multiple local optima [3].

A wide variety of algorithms have been applied to finding locally optimal solutions [4]. Recent research has developed convex relaxations of OPF problems to obtain bounds on the optimal objective values, certify infeasibility, and in some cases, achieve globally optimal solutions. Solutions from a relaxation are also useful for initializing certain local solution techniques [5]. Improving convex relaxation methods, from tightness and tractability perspectives, is an ongoing avenue of research [6].

The quadratic convex (QC) relaxation [7] is one promising approach that uses convex envelopes around the trigonometric functions, squared terms, and bilinear products in the polar form of the power flow equations. The tightness of the QC relaxation strongly depends on the quality of these convex envelopes. The proposed approach in this paper aims at strengthening the QC relaxation by improving these envelopes.

Several improvements have been proposed to strengthen the QC relaxation of the OPF problem. The quality of these convex envelopes strongly depends on the size of the bounds on voltage magnitude and angle difference. Therefore, analytical and optimization based bound tightening techniques can improve the QC relaxation's tightness [8–12]. The tightness of the convex envelopes plays a crucial role in improving QC relaxation accuracy. Tighter envelopes for trigonometric functions that leverage sign-definite angle difference bounds have been presented to tighten the QC relaxation of the OPF problem [8, 13]. Multiple proposed enhancements to tighten the QC relaxation of the OPF problem include Lifted Nonlinear Cuts (LNC) that exploit voltage magnitude and angle difference bounds [8,

14]; a variety of valid inequalities, cutting planes, and convex envelopes [10, 11]; redundant constraints based on voltage magnitude differences [15], and tighter envelopes for trilinear terms in the polar form of the OPF problem [15–17].

A polar representation of the branch admittances, in addition to the rectangular representation used previously in the QC relaxation, is proposed in [18] to tighten the QC relaxation of the OPF problem. A coordinate transformation via a complex per-unit base power normalization that rotates the power flow equations is proposed in [18] to apply tighter envelopes on trigonometric functions that can be tighter than the corresponding envelopes in previous QC relaxation formulations.

This paper proposes an additional improvement to [18] for tightening the QC relaxation of the OPF problem. Leveraging the polar representation of the branch admittance, this paper presents an approach that exploits multiple degrees of freedom in the OPF formulation. By reformulating the power flow equations such that linearly shifted variables appear in the trigonometric functions' argument in each branch (i.e., $\psi_{lm}^{(1)}$ and $\psi_{lm}^{(2)}$) results in shifting the arguments of the trigonometric terms in the power flow equations. The associated degrees of freedom for shifting the arguments of the trigonometric terms in each branch, $\psi_{lm}^{(1)}$ and $\psi_{lm}^{(2)}$, facilitate the application of tighter envelopes on trigonometric functions in each branch, which can strengthen the QC relaxation of OPF problems. The shifting variables for shifting the arguments of trigonometric functions in the proposed power flow equations play an important role in applying tighter envelopes on trigonometric functions. An empirical analysis based on the smaller area between upper and lower portion envelopes is proposed to determine the proper values for $\psi_{lm}^{(1)}$ and $\psi_{lm}^{(2)}$.

This paper is organized as follows: Sections 2 and 3 review the OPF formulation and the previously proposed QC relaxation, respectively. Section 4 describes the new definition of the power flow equations underlying the proposed improved QC relaxation. Section 5 then presents these improvements.

2. OVERVIEW OF OPTIMAL POWER FLOW PROBLEM

This section overviews the AC OPF problem using a polar representation of voltage phasors. The power system is modeled by a graph $(\mathcal{N}, \mathcal{L})$ with $\mathcal{N}$ and $\mathcal{L}$ representing the sets of buses and branches, respectively. Let $\mathcal{G}$ denote the set of generators. Let $P_i^d + jQ_i^d$ and $P_i^g + jQ_i^g$ represent the active and reactive load demand and generation, respectively, at bus $i \in \mathcal{N}$, where $j = \sqrt{-1}$. Let V_i and θ_i represent the voltage magnitude and angle at bus $i \in \mathcal{N}$. Let $g_{sh,i} + jb_{sh,i}$ denote the shunt admittance at bus i. For each generator $i \in \mathcal{G}$, define a quadratic generation cost function with coefficients $c_{2,i} \geqslant 0$, $c_{1,i}$, and $c_{0,i}$. Define $\theta_{lm} = \theta_l - \theta_m$ for $(l,m) \in \mathcal{L}$. Specified upper and lower limits are denoted by $(\overline{\cdot})$ and $(\underline{\cdot})$, respectively. Buses $i \in \mathcal{N} \backslash \mathcal{G}$ have generation limits set to zero.

For ease of exposition, each line $(l,m) \in \mathcal{L}$ is modeled as a Π circuit with mutual admittance $g_{lm} + jb_{lm}$ and shunt admittance $jb_{c,lm}$. Extensions to more general line models that allow for off-nominal tap ratios and non-zero phase shifts are straightforward and available in Appendix 5.5. Let P_{lm}, Q_{lm}, and $\overline{S}_{lm}$ represent the active and reactive power flows and the maximum apparent power flow limit on the line that connects buses l and m.

Using these definitions, the OPF problem is

$$\min \quad \sum_{i \in \mathcal{G}} c_{2,i} \left(P_i^g\right)^2 + c_{1,i} P_i^g + c_{0,i} \tag{1a}$$

$$\text{subject to} \quad (\forall i \in \mathcal{N},\ \forall (l,m) \in \mathcal{L})$$

$$P_i^g - P_i^d = g_{sh,i} V_i^2 + \sum_{\substack{(l,m) \in \mathcal{L}, \\ \text{s.t. } l=i}} P_{lm} + \sum_{\substack{(l,m) \in \mathcal{L}, \\ \text{s.t. } m=i}} P_{ml}, \tag{1b}$$

$$Q_i^g - Q_i^d = -b_{sh,i} V_i^2 + \sum_{\substack{(l,m) \in \mathcal{L}, \\ \text{s.t. } l=i}} Q_{lm} + \sum_{\substack{(l,m) \in \mathcal{L}, \\ \text{s.t. } m=i}} Q_{ml}, \tag{1c}$$

$$\theta_{ref} = 0, \tag{1d}$$

$$\underline{P}_i^g \leqslant P_i^g \leqslant \overline{P}_i^g, \tag{1e}$$

$$\underline{Q}_i^g \leqslant Q_i^g \leqslant \overline{Q}_i^g, \tag{1f}$$

$$\underline{V}_i \leqslant V_i \leqslant \overline{V}_i, \tag{1g}$$

$$\underline{\theta}_{lm} \leqslant \theta_{lm} \leqslant \overline{\theta}_{lm}, \tag{1h}$$

$$P_{lm} = g_{lm}V_l^2 - g_{lm}V_lV_m\cos(\theta_{lm}) - b_{lm}V_lV_m\sin(\theta_{lm}), \tag{1i}$$

$$Q_{lm} = -(b_{lm} + b_{c,lm}/2)\,V_l^2 + b_{lm}V_lV_m\cos(\theta_{lm}) - g_{lm}V_lV_m\sin(\theta_{lm}),$$

$$P_{ml} = g_{lm}V_m^2 - g_{lm}V_lV_m\cos(\theta_{lm}) + b_{lm}V_lV_m\sin(\theta_{lm}), \tag{1j}$$

$$Q_{ml} = -(b_{lm} + b_{c,lm}/2)\,V_m^2 + b_{lm}V_lV_m\cos(\theta_{lm}) + g_{lm}V_lV_m\sin(\theta_{lm}),$$

$$(P_{lm})^2 + (Q_{lm})^2 \leqslant \left(\overline{S}_{lm}\right)^2, \tag{1k}$$

$$(P_{ml})^2 + (Q_{ml})^2 \leqslant \left(\overline{S}_{lm}\right)^2. \tag{1l}$$

The objective (1a) minimizes the generation cost. Constraints (1b) and (1c) enforce the power balance at each bus. Constraint (1d) sets the reference bus angle, θ_{ref}. The constraints in (1e) bound the active and reactive power generation at each bus. Constraints (1g)–(1h), respectively, bound the voltage magnitudes and voltage angle differences. Constraints (1i)–(1i) relate the active and reactive power flows with the voltage phasors at the terminal buses. The constraints in (1k) limit the apparent power flows into both terminals of each line.

3. OVERVIEW OF QC RELAXATION

The QC relaxation convexifies the OPF problem (1) by enclosing nonconvex terms in convex envelopes. To formulate the QC relaxation of the OPF problem, multiple lifted variables including w_{ii}, w_{lm}, c_{lm}, and s_{lm} are defined for the product of voltage magnitude and trilinear terms.

$$w_{ii} = V_i^2, \qquad \forall i \in \mathcal{N}, \tag{2a}$$

$$w_{lm} = V_lV_m, \qquad \forall\,(l,m) \in \mathcal{L}, \tag{2b}$$

$$c_{lm} = w_{lm} \cos(\theta_{lm}), \qquad \forall (l,m) \in \mathcal{L}, \tag{2c}$$

$$s_{lm} = w_{lm} \sin(\theta_{lm}), \qquad \forall (l,m) \in \mathcal{L}. \tag{2d}$$

These definitions inherently imply the following relationship between the variables w_{ll}, c_{lm}, and s_{lm} for $(l,m) \in \mathcal{L}$:

$$c_{lm}^2 + s_{lm}^2 = w_{ll} w_{mm}, \tag{3a}$$

$$c_{lm} = c_{ml}, \tag{3b}$$

$$s_{lm} = -s_{ml} \tag{3c}$$

The core concept of QC relaxation is enclosing the squared and bilinear terms in convex enclosures which are represented as set-valued functions in (4).

$$\langle x^2 \rangle^T = \left\{ \breve{x} : \begin{cases} \breve{x} \geqslant x^2, \\ \breve{x} \leqslant (\overline{x} + \underline{x})\, x - \overline{x}\underline{x}. \end{cases} \right. \tag{4}$$

where $\breve{x}$ is a "lifted" variable representing the set of square term and the envelope $\langle x^2 \rangle^T$ is the convex hull of square function.

The convex hull for the trigonometric terms $\langle \sin(x) \rangle^S$ and $\langle \cos(x) \rangle^C$ in the QC relaxation of the OPF problem can be represented by (5)–(5a).

$$\langle \cos(x) \rangle^C = \left\{ \breve{C} : \begin{cases} \breve{C} \leqslant 1 - \frac{1-\cos(x^m)}{(x^m)^2} x^2, \\ \breve{C} \geqslant \frac{\cos(\underline{x}) - \cos(\overline{x})}{\underline{x} - \overline{x}} (x - \underline{x}) + \cos(\underline{x}), \\ \breve{C} \leqslant \alpha_{ik}^{cp} (\frac{\pi}{2} - x)^2 + \beta_{ik}^{cp} (\frac{\pi}{2} - x) + \gamma_{ik}^{cp}, \text{if } \underline{x} \geqslant 0 \\ \breve{C} \leqslant \alpha_{ik}^{cn} (\frac{\pi}{2} + x)^2 + \beta_{ik}^{cn} (\frac{\pi}{2} + x) + \gamma_{ik}^{cn}, \text{if } \overline{x} \leqslant 0. \end{cases} \right. \tag{5a}$$

$$\langle \sin(x) \rangle^S = \begin{cases} \check{S} : \begin{cases} \check{S} \leqslant \cos\left(\frac{x^m}{2}\right)\left(x - \frac{x^m}{2}\right) + \sin\left(\frac{x^m}{2}\right) \text{ if } \underline{x} \leqslant 0 \leqslant \overline{x}, \\ \check{S} \geqslant \cos\left(\frac{x^m}{2}\right)\left(x + \frac{x^m}{2}\right) - \sin\left(\frac{x^m}{2}\right) \text{ if } \underline{x} \leqslant 0 \leqslant \overline{x}, \\ \check{S} \geqslant \frac{\sin(\underline{x}) - \sin(\overline{x})}{\underline{x} - \overline{x}}(x - \underline{x}) + \sin(\underline{x}) \quad \text{if } \underline{x} \geqslant 0, \\ \check{S} \leqslant \frac{\sin(\underline{x}) - \sin(\overline{x})}{\underline{x} - \overline{x}}(x - \underline{x}) + \sin(\underline{x}) \quad \text{if } \overline{x} \leqslant 0, \\ \check{S} \leqslant \alpha_{ik}^{sp} x^2 + \beta_{ik}^{sp} x + \gamma_{ik}^{sp}, \qquad \text{if } \underline{x} \geqslant 0, \\ \check{S} \geqslant \alpha_{ik}^{sn} x^2 + \beta_{ik}^{sn} x + \gamma_{ik}^{sn}, \qquad \text{if } \overline{x} \leqslant 0. \end{cases} \end{cases} \tag{5b}$$

where $\check{S}$ and $\check{C}$ represent lifted variables for corresponding sets. $x^m = \max(|\underline{x}|, |\overline{x}|)$.

Tighter envelopes for trigonometric terms that leverage sign-definite variable bounds [8] ($0^\circ \leqslant \underline{x} \leqslant \overline{x} \leqslant 90^\circ$ or $-90^\circ \leqslant \underline{x} \leqslant \overline{x} \leqslant 0^\circ$) can be represented by the last two equations in (5b)-(5a). For each line $(l, m) \in \mathcal{L}$ that has a sign-definite angle difference, define scalars α_{lm}, β_{lm}, and γ_{lm} that are function of three parameters denoted as a, b, and c:

$$\alpha_{lm}(a, b, c) = \frac{(sin(a + c) - sin(a))(a - b) - c(sin(a) - sin(b))}{c(a - b)(a - b + c)} \tag{6a}$$

$$\beta_{lm}(a, b, c) = \frac{sin(a) - sin(b)}{a - b} - \alpha_{lm}(a, b, c)(a + b) \tag{6b}$$

$$\gamma_{lm}(a, b, c) = \alpha_{lm}(a, b, c)ab + sin(a) - \frac{a(sin(a) - sin(b))}{a - b} \tag{6c}$$

Let $0 < \epsilon < 90^\circ - \overline{x}$ be a small positive constant. Using (6), define: $\alpha_{lm}^{(sp)}$, $\beta_{lm}^{(sp)}$, and $\gamma_{lm}^{(sp)}$ as α_{lm}, β_{lm}, and γ_{lm} evaluated as $(a, b, c) = (\overline{x}, \underline{x}, \epsilon)$; $\alpha_{lm}^{(sn)}$, $\beta_{lm}^{(sn)}$, and $\gamma_{lm}^{(sn)}$ as α_{lm}, β_{lm}, and γ_{lm} evaluated as $(a, b, c) = (\underline{x}, \overline{x}, -\epsilon)$; $\alpha_{lm}^{(cp)}$, $\beta_{lm}^{(cp)}$, and $\gamma_{lm}^{(cp)}$ as α_{lm}, β_{lm}, and γ_{lm} evaluated as $(a, b, c) = (\frac{pi}{2} - \underline{x}, \frac{pi}{2} - \overline{x}, \epsilon)$; $\alpha_{lm}^{(cn)}$, $\beta_{lm}^{(cn)}$, and $\gamma_{lm}^{(cn)}$ as α_{lm}, β_{lm}, and γ_{lm} evaluated as $(a, b, c) = (\frac{pi}{2} + \overline{x}, \frac{pi}{2} + \underline{x}, \epsilon)$. Note that the convex quadratic expressions for the last two equations in (5b)-(5a) can be formulated as second-order conic programming (SOCP) constraints. The QC relaxation of the OPF problem in (1) can be formulated by

substituting square, product, and trigonometric terms with the variables w_{ii}, w_{lm}, c_{lm}:

$$\min \quad \sum_{i\in\mathcal{N}} c_{2,i}\left(P_i^g\right)^2 + c_{1,i}\,P_i^g + c_{0,i} \tag{7a}$$

$$\text{subject to} \quad (\forall i \in \mathcal{N},\ \forall\,(l,m) \in \mathcal{L})$$

$$P_i^g - P_i^d = g_{sh,i}\,w_{ii} + \sum_{\substack{(l,m)\in\mathcal{L},\\ \text{s.t. } l=i}} P_{lm} + \sum_{\substack{(l,m)\in\mathcal{L},\\ \text{s.t. } m=i}} P_{ml}, \tag{7b}$$

$$Q_i^g - Q_i^d = -b_{sh,i}\,w_{ii} + \sum_{\substack{(l,m)\in\mathcal{L},\\ \text{s.t. } l=i}} Q_{lm} + \sum_{\substack{(l,m)\in\mathcal{L},\\ \text{s.t. } m=i}} Q_{ml}, \tag{7c}$$

$$(\underline{V}_i)^2 \leqslant w_{ii} \leqslant (\overline{V}_i)^2, \tag{7d}$$

$$w_{ii} \in \left\langle V_i^2 \right\rangle^T, \tag{7e}$$

$$P_{lm} = g_{lm}w_{ll} - g_{lm}c_{lm} - b_{lm}s_{lm}, \tag{7f}$$

$$Q_{lm} = -\left(b_{lm} + b_{c,lm}/2\right)w_{ll} + b_{lm}c_{lm} - g_{lm}s_{lm}, \tag{7g}$$

$$P_{ml} = g_{lm}w_{mm} - g_{lm}c_{lm} + b_{lm}s_{lm}, \tag{7h}$$

$$Q_{ml} = -\left(b_{lm} + b_{c,lm}/2\right)w_{mm} + b_{lm}c_{lm} + g_{lm}s_{lm}, \tag{7i}$$

$$c_{lm} = \sum_{k=1,\ldots,8} \lambda_k\,\rho_1^{(k)}\rho_2^{(k)}\rho_3^{(k)}, \quad \breve{C}_{lm} \in \left\langle \cos(\theta_{lm}) \right\rangle^C,$$

$$V_l = \sum_{k=1,\ldots,8} \lambda_k \rho_1^{(k)},\ V_m = \sum_{k=1,\ldots,8} \lambda_k \rho_2^{(k)},\ \breve{C}_{lm} = \sum_{k=1,\ldots,8} \lambda_k \rho_3^{(k)},$$

$$\sum_{k=1,\ldots,8} \lambda_k = 1, \quad \lambda_k \geqslant 0, \quad k = 1,\ldots,8. \tag{7j}$$

$$s_{lm} = \sum_{k=1,\ldots,8} \gamma_k\,\zeta_1^{(k)}\zeta_2^{(k)}\zeta_3^{(k)}, \quad \breve{S}_{lm} \in \left\langle \sin(\theta_{lm}) \right\rangle^S,$$

$$V_l = \sum_{k=1,\ldots,8} \gamma_k \zeta_1^{(k)},\ V_m = \sum_{k=1,\ldots,8} \gamma_k \zeta_2^{(k)},\ \breve{S}_{lm} = \sum_{k=1,\ldots,8} \gamma_k \zeta_3^{(k)},$$

$$\sum_{k=1,\ldots,8} \gamma_k = 1, \quad \gamma_k \geqslant 0, \quad k = 1,\ldots,8. \tag{7k}$$

$$P_{lm}^2 + Q_{lm}^2 \leqslant V_l^2\,\ell_{lm}, \tag{7l}$$

$$\ell_{lm} = Y_{lm}^2(V_l^2 + V_m^2) - 2Y_{lm}^2 c_{lm} - \frac{b_{c,lm}^2}{4}V_l^2 - b_{c,lm}Q_{lm}, \tag{7m}$$

$$\text{Equations (1d)–(1h), (1k), [17, Eq. (9)],} \tag{7n}$$

where the lifted variable ℓ_{lm} represents the squared magnitude of the current flow into terminal l of line $(l, m) \in \mathcal{L}$. The relationship between ℓ_{lm} and the power flows P_{lm} and Q_{lm} in (7l) tightens the QC relaxation [7, 19]. An expression for ℓ_{lm} that considers more general line models that allow for off-nominal tap ratios and non-zero phase shifts is available in Appendix 5.5. Also, as shown in (7d), w_{ii} is associated with the squared voltage magnitude at bus i.

The lifted variables c_{lm} and s_{lm} represent relaxations of the trilinear terms $V_l V_m \cos(\theta_{lm})$ and $V_l V_m \sin(\theta_{lm})$, respectively, with (7j) and (7k) formulating an "extreme point" representation of the convex hulls for the trilinear products $V_l V_m \breve{C}_{lm}$ and $V_l V_m \breve{S}_{lm}$ [20]. The λ and γ are non-negative auxiliary variables $\in [0, 1]$ that are used to form the convex hull of the $V_l V_m \cos(\theta_{lm})$ and $V_l V_m \sin(\theta_{lm})$ trilinear terms, respectively. The extreme points of $V_l V_m \breve{C}_{lm}$ are $\rho^{(k)} \in [\underline{V_l}, \overline{V_l}] \times [\underline{V_m}, \overline{V_m}] \times [\underline{\breve{C}}_{lm}, \overline{\breve{C}}_{lm}]$, $k = 1, \ldots, 8$ and the extreme points of $V_l V_m \breve{S}_{lm}$ are $\zeta^{(k)} \in [\underline{V_l}, \overline{V_l}] \times [\underline{V_m}, \overline{V_m}] \times [\underline{\breve{S}}_{lm}, \overline{\breve{S}}_{lm}]$, $k = 1, \ldots, 8$. Since sine and cosine are odd and even functions, respectively, $c_{lm} = c_{ml}$ and $s_{lm} = -s_{ml}$.

A "linking constraint" from [17, Eq. (9)] is also enforced. This linking constraint is associated with the bilinear terms $V_l V_m$ that are shared in $V_l V_m \cos(\theta_{lm})$ and $V_l V_m \sin(\theta_{lm})$.

4. MODIFIED POWER FLOW EQUATIONS

The improvements to the QC relaxation's envelopes that are the main contributions of this work are based on the modified representation of the power flow equations. The modified representation of the power flow equations is based on shifting the arguments of the trigonometric terms in the power flow equations in each branch. This section describes this argument shifting in the power flow equations. We first form the power flow equations using a polar representations of the lines' mutual admittances. We then introduce two complex base powers in the per-unit normalization for each branch that provide independent shifting

degrees of freedom for the trigonometric terms in the power flow equations in each branch. While this section uses a Π circuit line model for the sake of simplicity, extensions to more general line models are straightforward.

4.1. POWER FLOW EQUATIONS WITH ADMITTANCE IN POLAR FORM

Equations (1i) and (1i) model the power flows through a line $(l,m) \in \mathcal{L}$ via a rectangular representation of the line's mutual admittance, $g_{lm} + jb_{lm}$. In (7f)–(7g), the QC relaxation from [7] uses this rectangular admittance representation.

The line flows can be equivalently modeled using a polar representation of the mutual admittance, $Y_{lm}e^{j\delta_{lm}}$, where $Y_{lm} = \sqrt{g_{lm}^2 + b_{lm}^2}$ and $\delta_{lm} = \arctan\left(b_{lm}/g_{lm}\right)$ are the magnitude and angle of the mutual admittance for line $(l,m) \in \mathcal{L}$, respectively. Using polar admittance coordinates, the complex power flows S_{lm} and S_{ml} into each line terminal are:

$$S_{lm} = V_l e^{j\theta_l}\left(\left(Y_{lm}e^{j\delta_{lm}} + j\frac{b_{c,lm}}{2}\right)V_l e^{j\theta_l} - Y_{lm}e^{j\delta_{lm}}V_m e^{j\theta_m}\right)^*, \tag{8a}$$

$$S_{ml} = V_m e^{j\theta_m}\left(-Y_{lm}e^{j\delta_{lm}}V_l e^{j\theta_l} + \left(Y_{lm}e^{j\delta_{lm}} + j\frac{b_{c,lm}}{2}\right)V_m e^{j\theta_m}\right)^*, \tag{8b}$$

where $(\cdot)^*$ denotes the complex conjugate. Taking the real and imaginary parts of (8) yields the active and reactive power flows into each line terminal:

$$P_{lm} = \mathrm{Re}(S_{lm}) = Y_{lm}\cos(\delta_{lm})V_l^2 - Y_{lm}V_lV_m\cos(\theta_{lm} - \delta_{lm}), \tag{9a}$$

$$Q_{lm} = \mathrm{Im}(S_{lm}) = -\left(Y_{lm}\sin(\delta_{lm}) + b_{c,lm}/2\right)V_l^2 - Y_{lm}V_lV_m\sin(\theta_{lm} - \delta_{lm}), \tag{9b}$$

$$P_{ml} = \mathrm{Re}(S_{ml}) = Y_{lm}\cos(\delta_{lm})V_m^2 - Y_{lm}V_lV_m\cos(\theta_{lm} + \delta_{lm}), \tag{9c}$$

$$Q_{ml} = \mathrm{Im}(S_{ml}) = -\left(Y_{lm}\sin(\delta_{lm}) + b_{c,lm}/2\right)V_m^2 + Y_{lm}V_lV_m\sin(\theta_{lm} + \delta_{lm}). \tag{9d}$$

With the rectangular admittance representation, the active and reactive power flow equations (1i)–(1i) each have two trigonometric terms (i.e., $\cos(\theta_{lm})$ and $\sin(\theta_{lm})$). Conversely, there is only one trigonometric term in each of the power flow equations that use the polar admittance representation (9) (e.g., $\cos(\theta_{lm} - \delta_{lm})$ for P_{lm} and $\sin(\theta_{lm} - \delta_{lm})$ for

Q_{lm}). While these formulations are equivalent, the differing representations of the trigonometric terms suggest the possibility of using different trigonometric envelopes. The QC formulation we propose in Section 5.3 exploits these differences.

4.2. DIFFERENT REPRESENTATION OF POWER FLOW EQUATIONS

To improve the QC relaxation's trigonometric envelopes, this section reformulates the power flow equations with an independent shifting variable that linearly enters the trigonometric arguments' terms in the power flow equation in each line. Multiplying the power flow equations in $e^{-j\psi_{lm}^{(1)}}$ and $e^{-j\psi_{lm}^{(2)}}$ as shifting angles, two per line, can reshape the power flow in the lines as follows:

$$S_{lm}e^{-j\psi_{lm}^{(1)}} = (P_{lm} + jQ_{lm})(\cos(\psi_{lm}^{(1)}) - j\sin(\psi_{lm}^{(1)})), \tag{10a}$$

$$S_{lm}e^{-j\psi_{lm}^{(2)}} = (P_{lm} + jQ_{lm})(\cos(\psi_{lm}^{(2)}) - j\sin(\psi_{lm}^{(2)})). \tag{10b}$$

Define $\tilde{P}_{lm} = \mathrm{Re}(S_{lm}e^{j\psi_{lm}^{(1)}})$ and $\tilde{Q}_{lm} = \mathrm{Im}(S_{lm}e^{j\psi_{lm}^{(2)}})$. Taking real and imaginary parts of (10) yields:

$$\begin{bmatrix} \tilde{P}_{lm} \\ \tilde{Q}_{lm} \end{bmatrix} = \begin{bmatrix} \cos(\psi_{lm}^{(1)}) & \sin(\psi_{lm}^{(1)}) \\ -\sin(\psi_{lm}^{(2)}) & \cos(\psi_{lm}^{(2)}) \end{bmatrix} \begin{bmatrix} P_{lm} \\ Q_{lm} \end{bmatrix}. \tag{11}$$

Choosing $\psi_{lm}^{(1)}$ and $\psi_{lm}^{(2)}$ such that $\cos(\psi_{lm}^{(1)} - \psi_{lm}^{(2)}) \neq 0$, then we can invert (11) to obtain:

$$\begin{bmatrix} P_{lm} \\ Q_{lm} \end{bmatrix} = \frac{1}{\cos(\psi_{lm}^{(1)} - \psi_{lm}^{(2)})} \begin{bmatrix} \cos(\psi_{lm}^{(2)}) & -\sin(\psi_{lm}^{(1)}) \\ \sin(\psi_{lm}^{(2)}) & \cos(\psi_{lm}^{(1)}) \end{bmatrix} \begin{bmatrix} \tilde{P}_{lm} \\ \tilde{Q}_{lm} \end{bmatrix}. \tag{12}$$

Now consider $\tilde{P}_{lm}$ and $\tilde{Q}_{lm}$ in terms of the voltage magnitudes and angles (for a Π-model circuit). The angle of the base power, $\psi_{lm}^{(1)}$, and $\psi_{lm}^{(2)}$, affect the arguments of the trigonometric functions, as shown in the following derivation:

$$\tilde{P}_{lm} = V_l^2 \left(Y_{lm} \cos(\psi_{lm}^{(1)} + \delta_{lm}) - \frac{b_{lm,c}}{2} \sin(\psi_{lm}^{(1)}) \right) - V_l V_m Y_{lm} \cos(\theta_{lm} - \psi_{lm}^{(1)} - \delta_{lm}), \tag{13a}$$

$$\tilde{Q}_{lm} = V_l^2 \left(-Y_{lm} \sin(\psi_{lm}^{(2)} + \delta_{lm}) + \frac{b_{lm,c}}{2} \cos(\psi_{lm}^{(2)}) \right) - V_l V_m Y_{lm} \sin(\theta_{lm} - \psi_{lm}^{(2)} - \delta_{lm}). \tag{13b}$$

The P_{ml} and Q_{ml} can be obtained similarly as follows:

$$\tilde{P}_{ml} = -Y_{lm} V_m V_l \cos(\theta_{lm} + \delta_{lm} + \psi_{lm}^{(1)}) + \left(Y_{lm} \cos(\delta_{lm} + \psi_{lm}^{(1)}) - (b_{c,lm}/2) \sin(\psi_{lm}^{(1)}) \right) V_m^2, \tag{14a}$$

$$\tilde{Q}_{ml} = Y_{lm} V_m V_l \sin(\theta_{lm} + \delta_{lm} + \psi_{lm}^{(2)}) - \left(Y_{lm} \sin(\delta_{lm} + \psi_{lm}^{(2)}) + (b_{c,lm}/2) \cos(\psi_{lm}^{(2)}) \right) V_m^2. \tag{14b}$$

The arguments of the trigonometric functions $\cos(\theta_{lm} - \delta_{lm} - \psi_{lm}^{(1)})$, $\sin(\theta_{lm} - \delta_{lm} - \psi_{lm}^{(2)})$, $\cos(\theta_{lm} + \delta_{lm} + \psi_{lm}^{(1)})$, and $\sin(\theta_{lm} + \delta_{lm} + \psi_{lm}^{(2)})$ in (13) and (14) are linear in $\psi_{lm}^{(1)}$ and $\psi_{lm}^{(2)}$. For given $\psi_{lm}^{(1)}$ and $\psi_{lm}^{(2)}$, all other trigonometric terms in (13) and (14) are constants that do not require special handling.

4.3. THE OPF PROBLEM WITH MODIFIED POWER FLOW EQUATIONS

Applying (13) and (14) to (1) yields an OPF problem with a modified representation of power flow equations:

$$\min \quad \textstyle\sum_{i \in \mathcal{G}} c_{2,i} P_i^{g\,2} + c_{1,i} P_i^g + c_{0,i} \tag{15a}$$

$$\text{subject to} \quad (\forall i \in \mathcal{N},\ \forall (l,m) \in \mathcal{L})$$

$$P_i^g - P_i^d = g_{sh,i} V_i^2 + \sum_{\substack{(l,m) \in \mathcal{L}, \\ \text{s.t. } l=i}} P_{lm} + \sum_{\substack{(l,m) \in \mathcal{L}, \\ \text{s.t. } m=i}} P_{ml}, \tag{15b}$$

$$Q_i^g - Q_i^d = -b_{sh,i} V_i^2 + \sum_{\substack{(l,m)\in\mathcal{L},\\ \text{s.t. } l=i}} Q_{lm} + \sum_{\substack{(l,m)\in\mathcal{L},\\ \text{s.t. } m=i}} Q_{ml}, \tag{15c}$$

$$\tilde{P}_{lm} = V_l^2 \left(Y_{lm} \cos(\psi_{lm}^{(1)} + \delta_{lm}) - \frac{b_{lm,c}}{2} \sin(\psi_{lm}^{(1)}) \right) - V_l V_m Y_{lm} \cos(\theta_{lm} - \psi_{lm}^{(1)} - \delta_{lm}), \tag{15d}$$

$$\tilde{Q}_{lm} = V_l^2 \left(-Y_{lm} \sin(\psi_{lm}^{(2)} + \delta_{lm}) + \frac{b_{lm,c}}{2} \cos(\psi_{lm}^{(2)}) \right) - V_l V_m Y_{lm} \sin(\theta_{lm} - \psi_{lm}^{(2)} - \delta_{lm}), \tag{15e}$$

$$\tilde{P}_{ml} = -Y_{lm} V_m V_l \cos(\theta_{lm} + \delta_{lm} + \psi_{lm,1}) + \left(Y_{lm} \cos(\delta_{lm} + \psi_{lm,1}) - (b_{c,lm}/2) \sin(\psi_{lm,1}) \right) V_m^2, \tag{15f}$$

$$\tilde{Q}_{ml} = Y_{lm} V_m V_l \sin(\theta_{lm} + \delta_{lm} + \psi_{lm,2}) - \left(Y_{lm} \sin(\delta_{lm} + \psi_{lm,2}) + (b_{c,lm}/2) \cos(\psi_{lm,2}) \right) V_m^2, \tag{15g}$$

$$P_{lm} = \frac{\cos(\psi_{lm}^{(2)}) \tilde{P}_{lm}}{\cos(\psi_{lm}^{(1)} - \psi_{lm}^{(2)})} - \frac{\sin(\psi_{lm}^{(1)}) \tilde{Q}_{lm}}{\cos(\psi_{lm}^{(1)} - \psi_{lm}^{(2)})} \tag{15h}$$

$$Q_{lm} = \frac{\sin(\psi_{lm}^{(2)}) \tilde{P}_{lm}}{\cos(\psi_{lm}^{(1)} - \psi_{lm}^{(2)})} + \frac{\cos(\psi_{lm}^{(1)}) \tilde{Q}_{lm}}{\cos(\psi_{lm}^{(1)} - \psi_{lm}^{(2)})} \tag{15i}$$

$$P_{lm} = \frac{\cos(\psi_{lm}^{(2)}) \tilde{P}_{ml}}{\cos(\psi_{lm}^{(1)} - \psi_{lm}^{(2)})} - \frac{\sin(\psi_{lm}^{(1)}) \tilde{Q}_{ml}}{\cos(\psi_{lm}^{(1)} - \psi_{lm}^{(2)})} \tag{15j}$$

$$Q_{lm} = \frac{\sin(\psi_{lm}^{(2)}) \tilde{P}_{ml}}{\cos(\psi_{lm}^{(1)} - \psi_{lm}^{(2)})} + \frac{\cos(\psi_{lm}^{(1)}) \tilde{Q}_{ml}}{\cos(\psi_{lm}^{(1)} - \psi_{lm}^{(2)})} \tag{15k}$$

$$\theta_{ref} = 0, \tag{15l}$$

$$\underline{P}_i^g \leqslant P_i^g \leqslant \overline{P}_i^g, \tag{15m}$$

$$\underline{Q}_i^g \leqslant Q_i^g \leqslant \overline{Q}_i^g, \tag{15n}$$

$$\underline{V}_i \leqslant V_i \leqslant \overline{V}_i, \tag{15o}$$

$$\underline{\theta}_{lm} \leqslant \theta_{lm} \leqslant \overline{\theta}_{lm}, \tag{15p}$$

$$(\tilde{P}_{lm})^2 + (\tilde{Q}_{lm})^2 \leqslant (\overline{S}_{lm})^2, \tag{15q}$$

$$(\tilde{P}_{ml})^2 + (\tilde{Q}_{ml})^2 \leqslant (\overline{S}_{lm})^2. \tag{15r}$$

The rotated OPF problem (15) is equivalent to (1) in that any solution $\{V^*, \theta^*, P^{g*}, Q^{g*}\}$ to (15) is equal to a solution $\{V^*, \theta^*, P^{g*}, Q^{g*}\}$ to (1). Solutions to both formulations have the same voltage magnitudes, voltage angles, V^* and θ^* as well as active and reactive power

generation, P^{g*} and Q^{g*}. Therefore, (15) can be interpreted as revealing a degree of freedom associated with choosing shifting variables phase angle $\psi_{lm}^{(1)}$ and $\psi_{lm}^{(2)}$. The next section exploits these degrees of freedom to tighten the QC relaxation's trigonometric envelopes.

5. QC RELAXATION OF THE PROPOSED OPF PROBLEM

This section leverages the modified representation of the power flow equations presented in Section 4 to tighten the QC relaxation of the OPF problem. We first propose and analyze new envelopes for the trigonometric functions and trilinear terms. We then describe an empirical analysis that informs the choice of the base power angles $\psi_{lm}^{(1)}$ and $\psi_{lm}^{(2)}$ for each branch in order to tighten the relaxation for typical OPF problems.

5.1. CONVEX ENVELOPES FOR THE TRIGONOMETRIC TERMS

Tightened convex envelopes for trigonometric terms in the power flow equations play a crucial role in strengthening the QC relaxation of the OPF problem. The differing OPF formulation (15) has four relevant trigonometric terms for each line: $\cos(\theta_{lm} - \delta_{lm} - \psi^{(1)})$, $\sin(\theta_{lm} - \delta_{lm} - \psi^{(2)})$, $\cos(\theta_{lm} + \delta_{lm} + \psi^{(1)})$, and $\sin(\theta_{lm} + \delta_{lm} + \psi^{(2)})$, $\forall (l,m) \in \mathcal{L}$. This contrasts with the two unique trigonometric terms ($\cos(\theta_{lm})$ and $\sin(\theta_{lm})$) per pair of connected buses in the OPF formulation (1).

While this would seem to suggest that at least twice as many convex envelopes would be required for the rotated OPF formulation (15), the arguments of the trigonometric terms in this formulation are not independent. For notational convenience, define $\hat{\delta}_{lm}^{(1)} = \delta_{lm} + \psi_{lm}^{(1)}$ and $\hat{\delta}_{lm}^{(2)} = \delta_{lm} + \psi_{lm}^{(2)}$. The angle sum and difference identities imply the following relationships:

$$\begin{bmatrix} \sin(\hat{\theta}_{lm} + \hat{\delta}_{lm}^{(2)}) \\ \cos(\hat{\theta}_{lm} + \hat{\delta}_{lm}^{(1)}) \\ \sin(\hat{\theta}_{lm} - \hat{\delta}_{lm}^{(2)}) \\ \cos(\hat{\theta}_{lm} - \hat{\delta}_{lm}^{(1)}) \end{bmatrix} = \begin{bmatrix} \sin(\hat{\delta}_{lm}^{(2)}) & \cos(\hat{\delta}_{lm}^{(2)}) \\ \cos(\hat{\delta}_{lm}^{(1)}) & -\sin(\hat{\delta}_{lm}^{(1)}) \\ -\sin(\hat{\delta}_{lm}^{(2)}) & \cos(\hat{\delta}_{lm}^{(2)}) \\ \cos(\hat{\delta}_{lm}^{(1)}) & \sin(\hat{\delta}_{lm}^{(1)}) \end{bmatrix} \begin{bmatrix} \cos(\hat{\theta}_{lm}) \\ \sin(\hat{\theta}_{lm}) \end{bmatrix}. \tag{16}$$

Rearranging these relationships yields:

$$\begin{bmatrix} \cos(\theta_{lm} + \hat{\delta}_{lm}^{(1)}) \\ \sin(\theta_{lm} + \hat{\delta}_{lm}^{(2)}) \end{bmatrix} = \frac{1}{\alpha_{lm}} \begin{bmatrix} \beta_{lm} & \sigma_{lm} \\ \mu_{lm} & \beta_{lm} \end{bmatrix} \begin{bmatrix} \cos(\theta_{lm} - \hat{\delta}_{lm}^{(1)}) \\ \sin(\theta_{lm} - \hat{\delta}_{lm}^{(2)}) \end{bmatrix}. \tag{17}$$

where, for notational convenience, $\alpha_{lm} = (\cos(\hat{\delta}_{lm}^{(1)}) - \sin(\hat{\delta}_{lm}^{(2)}))$, $\beta_{lm} = (\cos(\hat{\delta}_{lm}^{(1)}) + \sin(\hat{\delta}_{lm}^{(2)}))$, $\sigma_{lm} = -2\cos(\hat{\delta}_{lm}^{(1)})\sin(\hat{\delta}_{lm}^{(1)})$, and $\mu_{lm} = 2\cos(\hat{\delta}_{lm}^{(2)})\sin(\hat{\delta}_{lm}^{(2)})$. The linear relationship (17) prevents defining the convex envelopes for redundant trigonometric terms. In other words, the relation (17) indicates that two (rather than four) convex envelopes need to be defined per line (one for each of the trigonometric terms $\sin(\theta_{lm} - \hat{\delta}_{lm}^{(2)})$ and $\cos(\theta_{lm} - \hat{\delta}_{lm}^{(1)})$). The remaining trigonometric functions, $\sin(\theta_{lm} + \hat{\delta}_{lm,}^{(2)})$ and $\cos(\theta_{lm} + \hat{\delta}_{lm}^{(2)})$, are representable in terms of $\sin(\theta_{lm} - \hat{\delta}_{lm}^{(2)})$ and $\cos(\theta_{lm} - \hat{\delta}_{lm}^{(1)})$ via the linear relationship (17). The matrix in (17) can be factored into $\begin{bmatrix} \cos(\hat{\delta}_{lm_1}) & -\sin(\hat{\delta}_{lm_1}) \\ \sin(\hat{\delta}_{lm_2}) & \cos(\hat{\delta}_{lm_2}) \end{bmatrix}$ and $\begin{bmatrix} \cos(\hat{\delta}_{lm_2}) & -\sin(\hat{\delta}_{lm_1}) \\ \sin(\hat{\delta}_{lm_2}) & \cos(\hat{\delta}_{lm_1}) \end{bmatrix}$ which their determinant are equal to $\cos(\hat{\delta}_{lm_1} - \hat{\delta}_{lm_2})$. The matrix in (17) is invertable for all values of $\hat{\delta}_{lm_1}$ and $\hat{\delta}_{lm_2}$ except $\hat{\delta}_{lm_1}$-$\hat{\delta}_{lm_2} = K\frac{\pi}{2}$, where $K \in \mathbb{R}$. Thus, the relationship in (17) is well-defined for $\hat{\delta}_{lm_1}$-$\hat{\delta}_{lm_2} \neq K\frac{\pi}{2}$.

A related special consideration is needed for parallel lines. While the rest of this section considers systems without parallel lines for simplicity, following **??** discusses this issue in detail.

In the original QC relaxation (7), the power flow equations for parallel lines between buses l and m shared the same envelopes, $\langle\cos(\theta_{lm})\rangle^C$ and $\langle\sin(\theta_{lm})\rangle^S$. In the proposed QC relaxation (21), the arguments of the trigonometric terms for parallel lines can differ due to the inclusion of the δ_{lm} terms. Rather than defining separate envelopes, we derive a linear

relationship between the trigonometric terms for parallel lines. Let δ_{lm_1}, δ_{lm_2} and $\theta_{lm_1}^{shift}$, $\theta_{lm_2}^{shift}$ be the admittance angles and phase shifts, respectively, for two parallel lines between buses l and m. Applying the angle sum identity yields

$$\begin{bmatrix} \sin(\theta_{lm} - \sigma_{lm_{2,2}}) \\ \cos(\theta_{lm} - \sigma_{lm_{1,1}}) \\ \sin(\theta_{lm} - \sigma_{lm_{2,1}}) \\ \cos(\theta_{lm} - \sigma_{lm_{1,1}}) \end{bmatrix} = \begin{bmatrix} -\sin(\sigma_{lm_{2,2}}) & \cos(\sigma_{lm_{2,2}}) \\ \cos(\sigma_{lm_{1,2}}) & \sin(\sigma_{lm_{1,2}}) \\ -\sin(\sigma_{lm_{2,1}}) & \cos(\sigma_{lm_{2,1}}) \\ \cos(\sigma_{lm_{1,1}}) & \sin(\sigma_{lm_{1,1}}) \end{bmatrix} \begin{bmatrix} \cos(\theta_{lm}) \\ \sin(\theta_{lm}) \end{bmatrix}, \tag{18}$$

where, for notational convenience, $\sigma_{lm_{1,1}} = \delta_{lm_1} + \theta_{lm_1}^{shift} + \psi_{lm}^{(1)}$, $\sigma_{lm_{1,2}} = \delta_{lm_2} + \theta_{lm_2}^{shift} + \psi_{lm}^{(1)}$, $\sigma_{lm_{2,1}} = \delta_{lm_1} + \theta_{lm_1}^{shift} + \psi_{lm}^{(2)}$, $\sigma_{lm_{2,2}} = \delta_{lm_2} + \theta_{lm_2}^{shift} + \psi_{lm}^{(2)}$. Rearranging (18) to eliminate $\cos(\theta_{lm})$ and $\sin(\theta_{lm})$ yields the desired linear relationship:

$$\begin{bmatrix} \sin(\theta_{lm} - \sigma_{lm_2}) \\ \cos(\theta_{lm} - \sigma_{lm_2}) \end{bmatrix} = \begin{bmatrix} \cos(\sigma_{lm_1} - \sigma_{lm_2}) & \sin(\sigma_{lm_1} - \sigma_{lm_2}) \\ -\sin(\sigma_{lm_1} - \sigma_{lm_2}) & \cos(\sigma_{lm_1} - \sigma_{lm_2}) \end{bmatrix} \begin{bmatrix} \sin(\theta_{lm} - \sigma_{lm_1}) \\ \cos(\theta_{lm} - \sigma_{lm_1}) \end{bmatrix}. \tag{19}$$

Since the matrix in (19) is invertible, this relationship is always well defined.

Using the linear relationships in (17) and in (19) **??** for systems with parallel lines, all relevant trigonometric terms in (15) can be represented as linear combinations of $\sin(\theta_{lm} - \hat{\delta}_{lm}^{(2)})$ and $\cos(\theta_{lm} - \hat{\delta}_{lm}^{(1)})$ for each unique pair of connected buses $(l, m) \in \mathcal{L}$. The corresponding envelopes are $\left\langle \sin\left(\theta_{lm} - \delta_{lm} - \psi_{lm}^{(2)}\right)\right\rangle^S$ and $\left\langle \cos\left(\theta_{lm} - \delta_{lm} - \psi_{lm}^{(1)}\right)\right\rangle^C$. The QC relaxations of (1) and (15) therefore have the same number of envelopes.

Two contributions of this paper distinguish the relaxations of the trigonometric expressions in (1) and (15). First, the relaxations of the power flow equations (1i)–(1k) each use the weighted sums of two trigonometric envelopes, while the relaxations of (15d)–(15g) each use a single trigonometric envelope. Second, the shifting angle variables $\psi_{lm}^{(1)}$

and $\psi_{lm}^{(2)}$ used to formulate (15) provide degree of freedom that shift the arguments of the trigonometric envelopes. We next discuss how both of these characteristics can be exploited to strengthen of the QC relaxation of the OPF problem.

Focusing on the first distinguishing characteristic, factoring out $-V_l V_m$ shows that the relaxation of (1i) depends on the quality of a weighted sum of trigonometric envelopes: $g_{lm}\langle\cos(\theta_{lm})\rangle^c + b_{lm}\langle\sin(\theta_{lm})\rangle^S$. The relaxation of (15d) depends on the quality of the envelope $Y_{lm}\left\langle\cos\left(\theta_{lm}-\delta_{lm}-\psi_{lm}^{(1)}\right)\right\rangle^C$. (The relaxations of (1i)–(1k) and (15d)–(15g) are analogous.) To focus on the first characteristic, consider the latter envelope with $\psi_{lm}^{(1)}=0$.

As an illustration, Fig. 1 shows examples of these envelopes for a line with the same mutual admittance ($g_{lm}+jb_{lm}=0.6-j0.8$) for different intervals of angle differences ($\underline{\theta}_{lm}\leqslant\theta_{lm}\leqslant\overline{\theta}_{lm}$).

For comparing the tightness of these envelopes, we compare their lower and upper boundaries. As proven in [18], the lower boundary of the envelope for $Y_{lm}\langle\cos(\theta_{lm}-\delta_{lm})\rangle^C$ is at least as tight as the lower boundary of the envelope for $g_{lm}\langle\cos(\theta_{lm})\rangle^C+b_{lm}\langle\sin(\theta_{lm})\rangle^S$ when $-90^\circ\leqslant\underline{\theta}_{lm}\leqslant\overline{\theta}_{lm}\leqslant 90^\circ$ and is tighter for some line admittances and phase angle difference limits. For other intervals, the lower boundary of the envelope for $Y_{lm}\langle\cos(\theta_{lm}-\delta_{lm})\rangle^C$ neither dominates, nor is dominated by, the lower boundary of the envelope for $g_{lm}\langle\cos(\theta_{lm})\rangle^C + b_{lm}\langle\sin(\theta_{lm})\rangle^S$.

The upper portion envelope of $Y_{lm}\langle\cos(\theta_{lm}-\delta_{lm})\rangle^C$ neither dominates, nor is dominated by, the upper bound of $g_{lm}\langle\cos(\theta_{lm})\rangle^C + b_{lm}\langle\sin(\theta_{lm})\rangle^S$. Therefore, in general a QC relaxation that enforces the intersection of these envelopes is tighter than the relaxations constructed using either of these envelopes individually. Section 5.5 presents linear relationships obtained from angle sum and difference identities which facilitate the joint enforcement of the envelopes $\left\langle\cos\left(\theta_{lm}-\delta_{lm}-\psi_{lm}^{(1)}\right)\right\rangle^C$ and $\left\langle\sin\left(\theta_{lm}-\delta_{lm}-\psi_{lm}^{(2)}\right)\right\rangle^S$ along with $\langle\cos(\theta_{lm})\rangle^C$ and $\langle\sin(\theta_{lm})\rangle^S$ using a single set of lifted variables. While en-

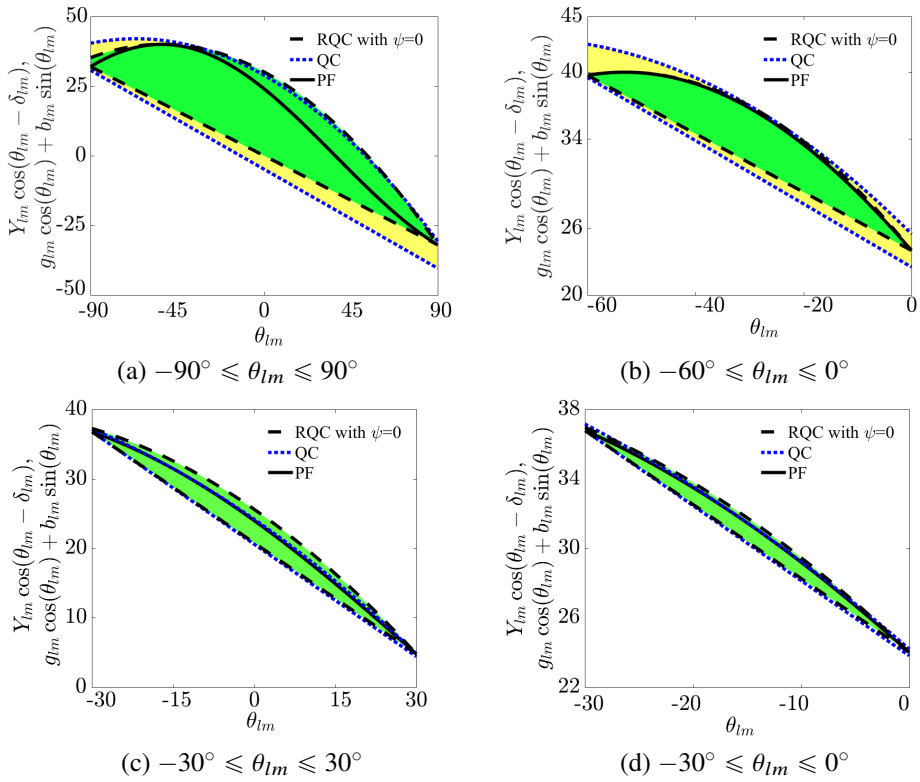

(a) $-90^\circ \leqslant \theta_{lm} \leqslant 90^\circ$ (b) $-60^\circ \leqslant \theta_{lm} \leqslant 0^\circ$

(c) $-30^\circ \leqslant \theta_{lm} \leqslant 30^\circ$ (d) $-30^\circ \leqslant \theta_{lm} \leqslant 0^\circ$

Figure 1. Comparison of envelopes for the trigonometric terms in (1) and (15). The yellow and magenta regions (with dotted and dashed borders, respectively) in (a)–(d) show the envelopes $g_{lm}\langle\cos(\theta_{lm})\rangle^C + b_{lm}\langle\sin(\theta_{lm})\rangle^S$ and $Y_{lm}\langle\cos(\theta_{lm}-\delta_{lm})\rangle^C$, respectively. The black solid lines correspond to the function $g_{lm}\cos(\theta_{lm}) + b_{lm}\sin(\theta_{lm}) = Y_{lm}\cos(\theta_{lm}-\delta_{lm})$.

forcing the intersection of these envelopes introduces additional constraints into the QC relaxation of (15), numerical experiments suggest that typical impacts on solution times are minimal.

The second contribution distinguishing between the envelopes for (1) and (15) is the ability to use two degrees of freedom, $\psi_{lm}^{(1)}$ and $\psi_{lm}^{(2)}$, in the latter envelopes. As shown in Fig. 2, changing $\psi_{lm}^{(1)}$ and $\psi_{lm}^{(2)}$ shift the arguments of these envelopes. One degree of freedom, ψ, has been defined in [18] to rotate the argument of the trigonometric terms in the power flow equations in all branches. Using one degree of freedom for shifting the arguments in both sine and cosine function compromises choosing the best shifting value for these functions. Fig. 2 clearly shows that a shifting variable that can provide tighter

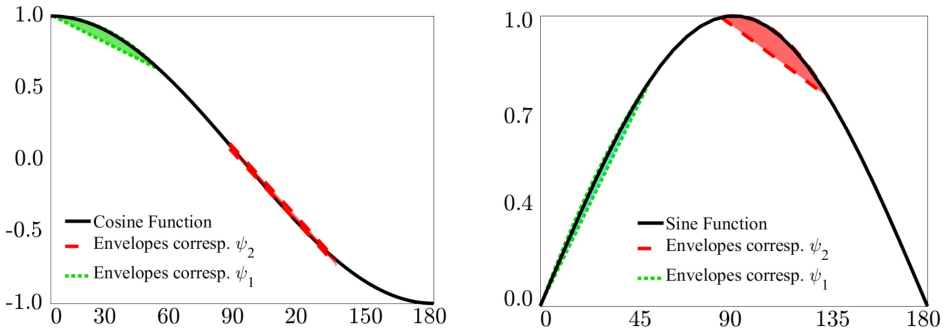

(a) (b)

Figure 2. Comparison of envelopes for the sine and cosine functions for different values of $\psi_{lm}^{(1)}$ and $\psi_{lm}^{(2)}$. The green and red regions (with dotted and dashed borders, respectively) in (a) show the envelopes $\left\langle \cos\left(\theta_{lm} - \delta_{lm} - \psi_{lm}^{(1)}\right)\right\rangle^{C}$ and $\left\langle \cos\left(\theta_{lm} - \delta_{lm} - \psi_{lm}^{(2)}\right)\right\rangle^{C}$, for $\psi_1 = 27^\circ$ and $\psi_2 = -56^\circ$, respectively. The green and red regions (with dotted and dashed borders, respectively) in (b) show the envelopes $\left\langle \sin\left(\theta_{lm} - \delta_{lm} - \psi_{lm}^{(1)}\right)\right\rangle^{S}$ and $\left\langle \sin\left(\theta_{lm} - \delta_{lm} - \psi_{lm}^{(2)}\right)\right\rangle^{S}$, for $\psi_1 = 27^\circ$ and $\psi_2 = -56^\circ$, respectively. The angle difference θ_{lm} varies within $-25^\circ \leqslant \theta_{lm} \leqslant 25^\circ$, and $\delta_{lm} = -53^\circ$.

envelopes for the sine function cannot necessarily provide a tighter envelope for the cosine function. This issue is resolved in this paper by defining independent shifting variables for the sine and cosine terms in the power flow equations.

Each line in a power system has its own voltage angle difference limits, (θ_{lm}^{min} and θ_{lm}^{max}), and mutual admittance angle, δ_{lm}, in which one shifting variable, ψ, cannot effectively shift the arguments of the trigonometric terms for all branches. This paper resolves this issue by defining separate shifting variables for each line. Analytically comparing the impacts of different values for $\psi_{lm}^{(1)}$ and $\psi_{lm}^{(2)}$ is not straightforward. Accordingly, this section will later describe a empirical study that suggests good choices for $\psi_{lm}^{(1)}$ and $\psi_{lm}^{(2)}$ for typical OPF problems.

5.2. ENVELOPES FOR TRILINEAR TERMS

The OPF problem with the modified definition of the power flow equations in (15) has four trilinear terms for each line: $V_l V_m \cos(\theta_{lm} - \delta_{lm} - \psi_{lm}^{(1)})$, $V_l V_m \sin(\theta_{lm} - \delta_{lm} - \psi_{lm}^{(2)})$, $V_l V_m \cos(\theta_{lm} + \delta_{lm} + \psi_{lm}^{(1)})$, and $V_l V_m \sin(\theta_{lm} + \delta_{lm} + \psi_{lm}^{(2)})$, $\forall (l,m) \in \mathcal{L}$. This contrasts with the two unique trilinear terms ($V_l V_m \cos(\theta_{lm})$ and $V_l V_m \sin(\theta_{lm})$) per pair of connected buses in the OPF formulation (1). This would seem to suggest that at least twice as many envelopes would be required to relax the trilinear terms in the OPF formulation (15). However, the four trilinear terms in (15) are related. We next describe how to exploit these relationships to only enforce two envelopes for the trilinear terms associated with each line.

Similar to (7k)–(7j), we relax the trilinear products by constructing linear envelopes using the upper and lower bounds on V_l, V_m, $\cos(\theta_{lm} - \delta_{lm} - \psi_{lm}^{(1)})$, $\sin(\theta_{lm} - \delta_{lm} - \psi_{lm}^{(2)})$, $\cos(\theta_{lm} + \delta_{lm} + \psi_{lm}^{(1)})$, and $\sin(\theta_{lm} + \delta_{lm} + \psi_{lm}^{(2)})$. We use the linear relationship (17) to represent the upper and lower bounds on the receiving end quantities $\cos(\theta_{lm} + \delta_{lm} + \psi_{lm}^{(1)})$ (denoted $\underline{\tilde{C}}_{lm}^{(r)}$, $\overline{\tilde{C}}_{lm}^{(r)}$) and $\sin(\theta_{lm} + \delta_{lm} + \psi_{lm}^{(2)})$ (denoted $\underline{\tilde{S}}_{lm}^{(r)}$, $\overline{\tilde{S}}_{lm}^{(r)}$) in terms of the bounds on the sending end quantities $\cos(\theta_{lm} - \delta_{lm} - \psi_{lm}^{(1)})$ (denoted $\underline{\tilde{C}}_{lm}^{(s)}$, $\overline{\tilde{C}}_{lm}^{(s)}$) and $\sin(\theta_{lm} - \delta_{lm} - \psi_{lm}^{(2)})$ (denoted $\underline{\tilde{S}}_{lm}^{(s)}$, $\overline{\tilde{S}}_{lm}^{(s)}$). We then enforce the constraints on the sending end quantities derived from the intersection of the transformed bounds associated with the receiving end quantities along with the bounds on the sending end quantities. Intersecting these bounds forms a polytope in terms of the sending end quantities $\tilde{C}_{lm}^{(s)} \in \left\langle \cos(\theta_{lm} - \delta_{lm} - \psi_{lm}^{(1)}) \right\rangle^{C}$ and $\tilde{S}_{lm}^{(s)} \in \left\langle \sin(\theta_{lm} - \delta_{lm} - \psi_{lm}^{(2)}) \right\rangle^{S}$, expressible as a convex combination of its extreme points.

Fig. 3 shows the bounds on both the sending and receiving end quantities in terms of the sending end quantities. The yellow region shows the polytope formed by the bounds on $\cos(\theta_{lm} - \delta_{lm} - \psi_{lm}^{(1)})$ and $\sin(\theta_{lm} - \delta_{lm} - \psi_{lm}^{(2)})$. The red region represents the polytope formed by using (17) to represent the bounds on the receiving end quantities $\cos(\theta_{lm} + \delta_{lm} + \psi_{lm}^{(1)})$ and $\sin(\theta_{lm} + \delta_{lm} + \psi_{lm}^{(2)})$ in terms of the sending end quantities $\cos(\theta_{lm} - \delta_{lm} - \psi_{lm}^{(1)})$ and $\sin(\theta_{lm} - \delta_{lm} - \psi_{lm}^{(2)})$. The black dots are the vertices of polytope shown by the dashed black lines that is formed from the intersection of the yellow and red polytopes.

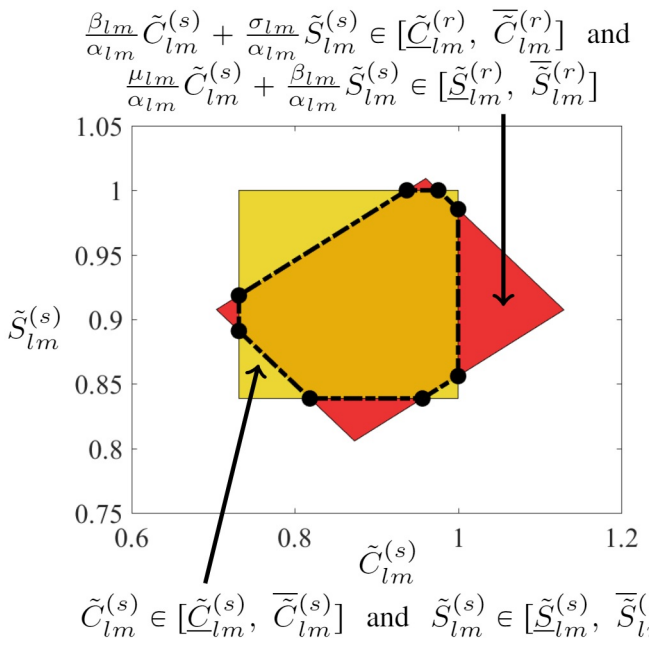

Figure 3. A projection of the four-dimensional polytope associated with the trilinear products between voltage magnitudes and trigonometric functions, in terms of the sending end variables $\tilde{S}^{(s)}_{lm}$ and $\tilde{C}^{(s)}_{lm}$ representing $\cos(\theta_{lm} - \delta_{lm} - \psi^{(1)}_{lm})$ and $\sin(\theta_{lm} - \delta_{lm} - \psi^{(2)}_{lm})$. The polytope formed by intersecting the sending end polytope (yellow) and receiving end polytope (red) is outlined with the dashed black lines and has vertices shown by the black dots.

Enforcing the constraints associated with both the yellow and red polytopes adds an unnecessary computational burden. We instead restrict the sending end quantities $\cos(\theta_{lm} - \delta_{lm} - \psi^{(1)}_{lm})$ and $\sin(\theta_{lm} - \delta_{lm} - \psi^{(2)}_{lm})$ to lie within the polytope shown by the black dashed line in Fig. 3. This implicitly ensures satisfaction of the bounds on the receiving end quantities. To relax the product terms $V_l V_m \cos(\theta_{lm} - \delta_{lm} - \psi^{(1)}_{lm})$ and $V_l V_m \sin(\theta_{lm} - \delta_{lm} - \psi^{(2)}_{lm})$, we first represent the quantities $\cos(\theta_{lm} - \delta_{lm} - \psi^{(1)}_{lm})$ and $\sin(\theta_{lm} - \delta_{lm} - \psi^{(2)}_{lm})$ using lifted variables $\tilde{C}^{(s)}_{lm}$ and $\tilde{S}^{(s)}_{lm}$, respectively. We then extend the polytope shown by the black dashed lines in Fig. 3 using the upper and lower bounds on V_l and V_m. The resulting four-dimensional polytope is the convex hull of the quadrilinear polynomial $V_l V_m \tilde{C}^{(s)}_{lm} \tilde{S}^{(s)}_{lm}$, which we represent using an extreme point formulation similar to (7k)–(7j). Let $\mathcal{T}_{lm} = \{(\tilde{C}^{int,1}_{lm}, \tilde{S}^{int,1}_{lm}), (\tilde{C}^{int,2}_{lm}, \tilde{S}^{int,2}_{lm}), \ldots, (\tilde{C}^{int,\tilde{N}}_{lm}, \tilde{S}^{int,\tilde{N}}_{lm})\}$ denote the coordinates of the intersection points (black dots) in Fig. 3, where $\tilde{N}$ is the number of intersection points

which ranges from 4 to 8 depending on the value of ψ. The extreme points of $V_l V_m \tilde{C}_{lm}^{(s)} \tilde{S}_{lm}^{(s)}$ are then denoted as $\eta^{(k)} \in [\underline{V_l}, \overline{V_l}] \times [\underline{V_m}, \overline{V_m}] \times \mathcal{T}_{lm}$, $k = 1, \ldots, 4\tilde{N}$. The λ is non-negative auxiliary variable $\in [0, 1]$ that is used to form the convex hull of the $V_l V_m \cos(\theta_{lm}) \sin(\theta_{lm})$ quadrilinear term. The envelopes for the trilinear terms are:

$$
\begin{aligned}
&\tilde{c}_{lm} = \sum_{k=1,\ldots,4\tilde{N}} \lambda_k \, \eta_1^{(k)} \eta_2^{(k)} \eta_3^{(k)}, \quad \tilde{s}_{lm} = \sum_{k=1,\ldots,4\tilde{N}} \lambda_k \, \eta_1^{(k)} \eta_2^{(k)} \eta_4^{(k)}, \\
&V_l = \sum_{k=1,\ldots,4\tilde{N}} \lambda_k \eta_1^{(k)}, \;\; V_m = \sum_{k=1,\ldots,4\tilde{N}} \lambda_k \eta_2^{(k)}, \;\; \tilde{S}_{lm}^{(s)} = \sum_{k=1,\ldots,4\tilde{N}} \lambda_k \eta_4^{(k)}, \\
&\tilde{C}_{lm}^{(s)} = \sum_{k=1,\ldots,4\tilde{N}} \lambda_k \eta_3^{(k)}, \;\; \sum_{k=1,\ldots,4\tilde{N}} \lambda_k = 1, \; \lambda_k \geqslant 0, \; k = 1, \ldots, 4\tilde{N}.
\end{aligned} \tag{20}
$$

Note that (20) precludes the need for the linking constraint in [17, Eq. (9)] that relates the common term $V_l V_m$ in the products $V_l V_m \sin(\theta_{lm})$ and $V_l V_m \cos(\theta_{lm})$.

5.3. QC RELAXATION OF THE OPF PROBLEM WIHT MODIFIED DEFINITION OF THE POWER FLOW EQUATIONS

Replacing the squared and trilinear terms with the corresponding lifted variables in the OPF formulation (15) results in the proposed QC "PQC" relaxation of the OPF problem:

$$\text{min} \quad \text{(15a)} \tag{21a}$$

$$\text{subject to} \quad (\forall i \in \mathcal{N}, \forall (l,m) \in \mathcal{L})$$

$$P_i^g - P_i^d = g_{sh,i} w_{ii} + \sum_{\substack{(l,m)\in\mathcal{L}, \\ \text{s.t. } l=i}} P_{lm} + \sum_{\substack{(l,m)\in\mathcal{L}, \\ \text{s.t. } m=i}} P_{ml}, \tag{21b}$$

$$Q_i^g - Q_i^d = -b_{sh,i} w_{ii} + \sum_{\substack{(l,m)\in\mathcal{L}, \\ \text{s.t. } l=i}} Q_{lm} + \sum_{\substack{(l,m)\in\mathcal{L}, \\ \text{s.t. } m=i}} Q_{ml}, \tag{21c}$$

$$\tilde{P}_{lm} = \left(Y_{lm} \cos(\delta_{lm} + \psi_{lm,1}) - \frac{b_{c,lm}}{2} \sin(\psi_{lm,1}) \right) w_{ll} - Y_{lm} \tilde{c}_{lm}, \tag{21d}$$

$$\tilde{Q}_{lm} = -\left(Y_{lm} \sin(\delta_{lm} + \psi_{lm,2}) + \frac{b_{c,lm}}{2} \cos(\psi_{lm,2}) \right) w_{ll} - Y_{lm} \tilde{s}_{lm}, \tag{21e}$$

$$\tilde{P}_{ml} = -Y_{lm}\tilde{c}_{lm} + \left(Y_{lm}\cos(\delta_{lm}+\psi_{lm,1}) - \frac{b_{c,lm}}{2}\sin(\psi_{lm,1})\right)w_{mm}, \tag{21f}$$

$$\tilde{Q}_{ml} = Y_{lm}\tilde{s}_{lm} - \left(Y_{lm}\sin(\delta_{lm}+\psi_{lm,2}) + \frac{b_{c,lm}}{2}\cos(\psi_{lm,2})\right)w_{mm}, \tag{21g}$$

$$P_{lm} = \frac{\cos(\psi^{(2)}_{lm})\tilde{P}_{lm}}{\cos(\psi^{(1)}_{lm}-\psi^{(2)}_{lm})} - \frac{\sin(\psi^{(1)}_{lm})\tilde{Q}_{lm}}{\cos(\psi^{(1)}_{lm}-\psi^{(2)}_{lm})} \tag{21h}$$

$$Q_{lm} = \frac{\sin(\psi^{(2)}_{lm})\tilde{P}_{lm}}{\cos(\psi^{(1)}_{lm}-\psi^{(2)}_{lm})} + \frac{\cos(\psi^{(1)}_{lm})\tilde{Q}_{lm}}{\cos(\psi^{(1)}_{lm}-\psi^{(2)}_{lm})} \tag{21i}$$

$$P_{lm} = \frac{\cos(\psi^{(2)}_{lm})\tilde{P}_{ml}}{\cos(\psi^{(1)}_{lm}-\psi^{(2)}_{lm})} - \frac{\sin(\psi^{(1)}_{lm})\tilde{Q}_{ml}}{\cos(\psi^{(1)}_{lm}-\psi^{(2)}_{lm})} \tag{21j}$$

$$Q_{lm} = \frac{\sin(\psi^{(2)}_{lm})\tilde{P}_{ml}}{\cos(\psi^{(1)}_{lm}-\psi^{(2)}_{lm})} + \frac{\cos(\psi^{(1)}_{lm})\tilde{Q}_{ml}}{\cos(\psi^{(1)}_{lm}-\psi^{(2)}_{lm})} \tag{21k}$$

$$\tilde{P}^2_{lm} + \tilde{Q}^2_{lm} \leqslant w_{ll}\,\tilde{\ell}_{lm}, \tag{21l}$$

$$\tilde{\ell}_{lm} = Y^2_{lm}V^2_l + Y_{lm}V^2_l b_{c,lm}\sin(\delta_{lm}) + Y^2_{lm}V^2_m + \frac{b^2_{c,lm}V^2_l}{4} - 2Y^2_{lm}V_lV_m\cos(\theta_{lm}-\theta^{shift}_{lm}) + \frac{Y_{lm}V_lV_m}{\tau_{lm}}\sin(\theta_{lm}-\delta_{lm}), \tag{21m}$$

Equations (15l)–(15q), (20). (21n)

Note that trilinear terms in (21) are relaxed via the extreme point approach in (20) that yields the convex hulls for these terms. The lifted variables $\tilde{c}_{lm}$ and $\tilde{s}_{lm}$ represent relaxations of the trilinear terms $V_lV_m\cos(\theta_{lm}-\delta_{lm}-\psi^{(1)}_{lm})$ and $V_lV_m\sin(\theta_{lm}-\delta_{lm}-\psi^{(2)})$, respectively. Section 5.5 gives an expression for $\tilde{\ell}_{lm}$ that considers off-nominal tap ratios and non-zero phase shifts.

5.4. TIGHTENED QC RELAXATION OF THE ROTATED OPF PROBLEM

Applying the angle sum and difference identities in combination with (17) reveals a linear relationship between the trigonometric functions used in the original QC relaxation (7), $\cos(\theta_{lm})$ and $\sin(\theta_{lm})$, and those in the proposed QC relaxation (21),

$\cos(\theta_{lm} - \delta_{lm} - \psi_{lm}^{(1)})$ and $\sin(\theta_{lm} - \delta_{lm} - \psi_{lm}^{(2)})$:

$$\begin{bmatrix} \cos(\theta_{lm}) \\ \sin(\theta_{lm}) \end{bmatrix} = M_{lm} \begin{bmatrix} \sin(\theta_{lm} - \delta_{lm} - \psi_{lm}^{(2)}) \\ \cos(\theta_{lm} - \delta_{lm} - \psi_{lm}^{(1)}) \end{bmatrix}, \tag{22}$$

where

$$\begin{aligned} M_{lm} = & \frac{1}{\Delta_{lm}} \left(\begin{bmatrix} \sin(\delta_{lm} + \psi_{lm}^{(2)}) & \cos(\delta_{lm} + \psi_{lm}^{(1)}) \\ \cos(\delta_{lm} + \psi_{lm}^{(1)}) & \sin(\delta_{lm} + \psi_{lm}^{(2)}) \end{bmatrix} \right. \\ & \left. + \begin{bmatrix} \cos(\delta_{lm} + \psi_{lm}^{(2)}) & \sin(\delta_{lm} + \psi_{lm}^{(1)}) \\ \sin(\delta_{lm} + \psi_{lm}^{(2)}) & -\cos(\delta_{lm} + \psi_{lm}^{(1)}) \end{bmatrix} \frac{1}{\alpha_{lm}} \begin{bmatrix} \beta_{lm} & \alpha_{lm} \\ \mu_{lm} & \beta_{lm} \end{bmatrix} \right) \end{aligned}$$

with α_{lm}, β_{lm}, and μ_{lm} defined as in (17) and Δ_{lm} equals to $\sin(2(\delta_{lm} + \psi_{lm}^{(2)})) + \sin(2(\delta_{lm} + \psi_{lm}^{(1)}))$. As discussed in Section 5.1, the proposed QC relaxation (21) can be further tightened by additionally enforcing the envelopes $\langle \cos(\theta_{lm}) \rangle^C$ and $\langle \sin(\theta_{lm}) \rangle^S$ used in the original QC relaxation (7). This results in the "Tightened Proposed QC" (TPQC) relaxation:

$$\min \quad \text{(15a)} \tag{23a}$$

$$\text{subject to} \quad (\forall i \in \mathcal{N}, \forall (l,m) \in \mathcal{L})$$

$$M_{lm} \begin{bmatrix} \tilde{C}_{lm}^{(s)} \\ \tilde{S}_{lm}^{(s)} \end{bmatrix} \in \begin{bmatrix} \langle \cos(\theta_{lm}) \rangle^C \\ \langle \sin(\theta_{lm}) \rangle^S \end{bmatrix} \tag{23b}$$

$$\text{Equations (15l)–(15q), (20), (21b)–(21m).} \tag{23c}$$

5.5. AN APPROACH FOR DETERMINING THE SHIFTING VARIABLES $\psi_{lm}^{(1)}$ AND $\psi_{lm}^{(2)}$

The key parameters in our proposed QC formulation are the shifting variables $\psi_{lm}^{(1)}$ and $\psi_{lm}^{(2)}$. We next describe an approach for choosing values of $\psi_{lm}^{(1)}$ and $\psi_{lm}^{(2)}$ that works well for a range of test cases. A key determinant of the QC relaxation's tightness is the quality of the convex envelopes for the trigonometric terms in the power flow equations. One effective

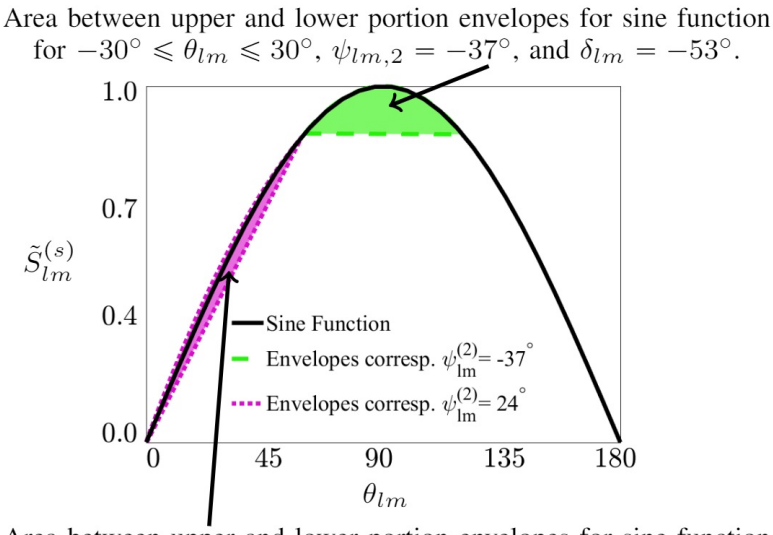

;

Figure 4. Thea area between upper and lower portion envelopes of the sine function for $-30^\circ \leqslant \theta_{lm} \leqslant 30^\circ$, $\delta_{lm} = -53^\circ$ and $\psi_{lm,2} = 24^\circ$ (purple) and $\psi_{lm,2} = -37^\circ$ (green).

approach for determining the proper shifting variables ($\psi_{lm}^{(1)}$ and $\psi_{lm}^{(2)}$) is minimization of the area encompassed by the upper and lower portion envelope corresponding to a shifting variable. Typically a smaller area implies tighter upper and lower portion envelopes for the trigonometric functions.

Fig. 4 illustrates the upper and lower portion envelope of the sine function for the voltage angle difference limits, $\theta_{lm}^{min} = -30^\circ$ and $\theta_{lm}^{max} = 30^\circ$, and mutual admittance angle, $\delta_{lm} = -53^\circ$ and different values of the shifting variable,$\psi_{lm}^{(2)} = 24^\circ$ (purple region) and $\psi_{lm}^{(2)} = -37^\circ$ (green region). Fig. 4 illustrates that the smaller area (purple region) encompassed by the upper and lower portion envelopes of the sine function compared to the larger area (green region), provides a tighter envelope for the sine function.

More General Line Models This appendix extends the paper's results to a line model that considers transformers with a non-zero phase shift θ_{lm}^{shift} and/or an off-nominal voltage ratio τ_{lm}. With this model, the complex power flow into both terminals of line $(l,m) \in \mathcal{L}$

are:

$$S_{lm} = V_l e^{j\theta_l}\left[\left(Y_{lm}e^{j\delta_{lm}} + j\frac{b_{c,lm}}{2}\right)\frac{V_l e^{j\theta_l}}{\tau_{lm}^2} - \frac{Y_{lm}e^{j\delta_{lm}}V_m e^{j\theta_m}}{\tau_{lm}e^{-j\theta_{lm}^{shift}}}\right]^* \tag{24a}$$

$$S_{ml} = V_m e^{j\theta_m}\left[\left(Y_{lm}e^{j\delta_{lm}} + j\frac{b_{c,lm}}{2}\right)V_m e^{j\theta_m} - \frac{Y_{lm}e^{j\delta_{lm}}V_l e^{j\theta_l}}{\tau_{lm}e^{j\theta_{lm}^{shift}}}\right]^* \tag{24b}$$

We follow the procedure in Section 4 by applying different shifting variables to independently shift the arguments of the trigonometric functions:

$$\begin{aligned}\tilde{S}_{lm} = \frac{S_{lm}}{e^{j\psi_{lm}^{(1)}}} &= \left(\frac{Y_{lm}}{\tau_{lm}^2}e^{-j(\delta_{lm}+\psi_{lm}^{(1)})} + \frac{b_{c,lm}}{2}\frac{e^{-j(\frac{\pi}{2}+\psi_{lm}^{(1)})}}{\tau_{lm}^2}\right)V_l^2 \\ &\quad - \frac{Y_{lm}}{\tau_{lm}}V_l V_m e^{j(\theta_{lm}-\delta_{lm}-\theta_{lm}^{shift}-\psi_{lm}^{(1)})},\end{aligned} \tag{25a}$$

$$\begin{aligned}\tilde{S}_{ml} = \frac{S_{ml}}{e^{j\psi_{lm}^{(1)}}} &= \left(Y_{lm}e^{-j(\delta_{lm}+\psi_{lm}^{(1)})} + \frac{b_{c,lm}}{2}e^{-j(\frac{\pi}{2}+\psi_{lm}^{(1)})}\right)V_m^2 \\ &\quad - \frac{Y_{lm}}{\tau_{lm}}V_l V_m e^{j(-\theta_{lm}-\delta_{lm}+\theta_{lm}^{shift}-\psi_{lm}^{(1)})},\end{aligned} \tag{25b}$$

$$\begin{aligned}\tilde{S}_{lm} = \frac{S_{lm}}{e^{j\psi_{lm}^{(2)}}} &= \left(\frac{Y_{lm}}{\tau_{lm}^2}e^{-j(\delta_{lm}+\psi_{lm}^{(2)})} + \frac{b_{c,lm}}{2}\frac{e^{-j(\frac{\pi}{2}+\psi_{lm}^{(2)})}}{\tau_{lm}^2}\right)V_l^2 \\ &\quad - \frac{Y_{lm}}{\tau_{lm}}V_l V_m e^{j(\theta_{lm}-\delta_{lm}-\theta_{lm}^{shift}-\psi_{lm}^{(2)})},\end{aligned} \tag{25c}$$

$$\begin{aligned}\tilde{S}_{ml} = \frac{S_{ml}}{e^{j\psi_{lm}^{(2)}}} &= \left(Y_{lm}e^{-j(\delta_{lm}+\psi_{lm}^{(2)})} + \frac{b_{c,lm}}{2}e^{-j(\frac{\pi}{2}+\psi_{lm}^{(2)})}\right)V_m^2 \\ &\quad - \frac{Y_{lm}}{\tau_{lm}}V_l V_m e^{j(-\theta_{lm}-\delta_{lm}+\theta_{lm}^{shift}-\psi_{lm}^{(2)})}.\end{aligned} \tag{25d}$$

Taking the real and imaginary parts of (25) yields:

$$\begin{aligned}\tilde{P}_{lm} = \mathrm{Re}(\tilde{S}_{lm}) &= \left(\frac{Y_{lm}}{\tau_{lm}^2}\cos(\delta_{lm}+\psi_{lm}^{(1)}) - \frac{b_{c,lm}}{2\tau_{lm}^2}\sin(\psi_{lm}^{(1)})\right)V_l^2 \\ &\quad - \frac{Y_{lm}}{\tau_{lm}}V_l V_m\cos(\theta_{lm}-\delta_{lm}-\theta_{lm}^{shift}-\psi_{lm}^{(1)}),\end{aligned} \tag{26a}$$

$$\tilde{Q}_{lm} = \mathrm{Im}(\tilde{S}_{lm}) = \left(-\frac{Y_{lm}}{\tau_{lm}^2} \sin(\delta_{lm} + \psi_{lm}^{(2)}) - \frac{b_{c,lm}}{2\tau_{lm}^2} \cos(\psi_{lm}^{(2)}) \right) V_l^2 - \frac{Y_{lm}}{\tau_{lm}} V_l V_m \sin(\theta_{lm} - \delta_{lm} - \theta_{lm}^{shift} - \psi_{lm}^{(2)}), \tag{26b}$$

$$\tilde{P}_{ml} = \mathrm{Re}(\tilde{S}_{ml}) = \left(Y_{lm} \cos(\delta_{lm} + \psi_{lm}^{(1)}) - \frac{b_{c,lm}}{2} \sin(\psi_{lm}^{(1)}) \right) V_m^2 - \frac{Y_{lm}}{\tau_{lm}} V_m V_l \cos(\theta_{lm} + \delta_{lm} - \theta_{lm}^{shift} + \psi_{lm}^{(1)}), \tag{26c}$$

$$\tilde{Q}_{ml} = \mathrm{Im}(\tilde{S}_{ml}) = \left(-Y_{lm} \sin(\delta_{lm} + \psi_{lm}^{(2)}) - \frac{b_{c,lm}}{2} \cos(\psi_{lm}^{(2)}) \right) V_m^2 + \frac{Y_{lm}}{\tau_{lm}} V_m V_l \sin(\theta_{lm} + \delta_{lm} - \theta_{lm}^{shift} + \psi_{lm}^{(2)}). \tag{26d}$$

The arguments of the trigonometric terms in (26) are not independent since $\cos(\theta_{lm} + \delta_{lm} - \theta_{lm}^{shift} + \psi_{lm}^{(1)})$ and $\sin(\theta_{lm} + \delta_{lm} - \theta_{lm}^{shift} + \psi_{lm}^{(2)})$ are linearly related with $\cos(\theta_{lm} - \delta_{lm} - \theta_{lm}^{shift} - \psi_{lm}^{(1)})$ and $\sin(\theta_{lm} - \delta_{lm} - \theta_{lm}^{shift} - \psi_{lm}^{(2)})$ via the general form of equation (17). Generalizing (17) to consider off-nominal voltage ratios and non-zero phase shifts in accomplished by replacing θ_{lm} in (17) with $\theta_{lm} - \theta_{lm}^{shift}$.

Extensions of the expressions for the squared magnitudes of the current flows in the original QC relaxation (7) and the proposed QC relaxation (21), ℓ_{lm} and $\tilde{\ell}_{lm}$, are as follows:

$$\ell_{lm} = \left(\frac{Y_{lm}^2}{\tau_{lm}^4} - \frac{b_{c,lm}^2}{4\tau_{lm}^4} \right) V_l^2 + \frac{Y_{lm}^2}{\tau_{lm}^2} V_m^2 - \frac{b_{c,lm}}{\tau_{lm}^2} Q_{lm} - 2\frac{Y_{lm}^2}{\tau_{lm}^3} \left(\cos(\delta_{lm}) c_{lm} + \sin(\delta_{lm}) s_{lm} \right), \tag{27}$$

$$\tilde{\ell}_{lm} = \frac{Y_{lm}^2 V_l^2}{\tau_{lm}^2} + \frac{Y_{lm} V_l^2 b_{c,lm}}{\tau_{lm}^2} \sin(\delta_{lm}) - \frac{2Y_{lm}^2 V_l V_m}{\tau_{lm}} \cos(\theta_{lm} - \theta_{lm}^{shift}) + \frac{b_{c,lm}^2 V_l^2}{4\tau_{lm}^2} + \frac{Y_{lm} V_l V_m}{\tau_{lm}} \sin(\theta_{lm} - \delta_{lm} - \theta_{lm}^{shift}) + Y_{lm}^2 V_m^2. \tag{28}$$

Note that the argument of the trigonometric functions in equation (28) are different than those in equation (21). However, there are linear relations that relate arguments in equation (28) to those in equation (21). Those relations, i.e., equations (30) and (29), are utilized to prevent defining new envelopes and strengthen the RQC relaxation of OPF problem.

$$\sin(\theta_{lm} - \delta_{lm} - \theta_{lm}^{shift}) = \frac{1}{\cos(\psi_{lm}^{(1)} - \psi_{lm}^{(2)})} \begin{bmatrix} \cos(\psi_{lm}^{(1)}) & \sin(\psi_{lm}^{(2)}) \end{bmatrix} \begin{bmatrix} \sin(\theta_{lm} - \hat{\delta}_{lm,2} - \theta_{lm}^{shift}) \\ \cos(\theta_{lm} - \hat{\delta}_{lm,1} - \theta_{lm}^{shift}) \end{bmatrix} \tag{29}$$

$$\cos(\theta_{lm} - \theta_{lm}^{shift}) = \frac{1}{2\cos(\delta_{lm} + \psi_{lm}^{(1)})} \begin{bmatrix} 1 & 1 \end{bmatrix} \begin{bmatrix} \cos(\theta_{lm} + \hat{\delta}_{lm,1} - \theta_{lm}^{shift}) \\ \cos(\theta_{lm} - \hat{\delta}_{lm,1} - \theta_{lm}^{shift}) \end{bmatrix}. \tag{30}$$

changing the matrix M_{lm} in (22).

Extending the IRQC relaxation (23) to the more general line model is derived by

$$\begin{bmatrix} \cos(\theta_{lm}) \\ \sin(\theta_{lm}) \end{bmatrix} = M'_{lm} \begin{bmatrix} \sin(\theta_{lm} - \delta_{lm} - \psi_{lm}^{(2)} - \theta_{lm}^{shift}) \\ \cos(\theta_{lm} - \delta_{lm} - \psi_{lm}^{(1)} - \theta_{lm}^{shift}) \end{bmatrix}. \tag{31}$$

where the constant matrix M'_{lm} is defined as

$$\begin{aligned} M'_{lm} = & \frac{1}{\Delta_{lm}} \left(\begin{bmatrix} \sin(\delta_{lm} + \psi_{lm}^{(2)} - \theta_{lm}^{shift})) & \cos(\delta_{lm} + \psi_{lm}^{(1)} - \theta_{lm}^{shift})) \\ \cos(\delta_{lm} + \psi_{lm}^{(1)} - \theta_{lm}^{shift})) & \sin(\delta_{lm} + \psi_{lm}^{(2)} - \theta_{lm}^{shift})) \end{bmatrix} \right. \\ & \left. + \begin{bmatrix} \cos(\hat{\delta}_{lm} + \psi_{lm}^{(2)}) & \sin(\hat{\delta}_{lm} + \psi_{lm}^{(1)}) \\ \sin(\hat{\delta}_{lm} + \psi_{lm}^{(2)}) & -\cos(\hat{\delta}_{lm} + \psi_{lm}^{(1)}) \end{bmatrix} \frac{1}{\alpha_{lm}} \begin{bmatrix} \beta_{lm} & \alpha_{lm} \\ \mu_{lm} & \beta_{lm} \end{bmatrix} \right) \end{aligned}$$

where for notational convenience, define $\hat{\delta}_{lm} = \delta_{lm} + \theta_{lm}^{shift}$. with α_{lm}, β_{lm}, and μ_{lm} as in (17) and Δ_{lm} equals to $\sin(2(\delta_{lm} + \psi_{lm}^{(2)})) + \sin(2(\delta_{lm} + \psi_{lm}^{(1)}))$. defined

BIBLIOGRAPHY

[1] J. Carpentier, Contribution to the Economic Dispatch Problem, Bulletin de la Societe Francoise des Electriciens 8 (3) (1962) 431–447.

[2] D. Bienstock, A. Verma, Strong NP-hardness of AC Power Flows Feasibility, arXiv:1512.07315 (2015).

[3] W.A. Bukhsh,A. Grothey, K.I.M. McKinnon, P.A. Trodden, Local Solutions of the Optimal Power Flow Problem, IEEE Transaction on Power Systems, 28 (4) (2013) 4780–4788.

[4] A. Castillo, R.P. O'Neill, Survey of Approaches to Solving the ACOPF (OPF Paper 4) March (2013)

[5] J. F. Marley, D. K. Molzahn, I. A. Hiskens, Solving Multiperiod OPF Problems using an AC-QP Algorithm Initialized with an SOCP Relaxation, IEEE Transaction on Power Systems 32 (5) (2017) 3538–3548.

[6] D. K. Molzahn, I. A. Hiskens, A Survey of Relaxations and Approximations of the Power Flow Equations, Foundations and Trends in Electric Energy Systems February (2019).

[7] C. Coffrin, H.L. Hijazi, P. Van Hentenryck, The QC Relaxation: A Theoretical and Computational Study on Optimal Power Flow, IEEE Transaction on Power Systems 31 (4) (2016) 3008–3018.

[8] C. Coffrin, H.L. Hijazi, P. Van Hentenryck, Strengthening the SDP Relaxation of AC Power Flows with Convex Envelopes, Bound Tightening, and Valid Inequalities, IEEE Transactions on Power Systems 32 (5) (2017) 3549-3558.

[9] C. Chen, A. Atamturk, S.S. Oren, Bound Tightening for the Alternating Current Optimal Power Flow Problem, IEEE Transaction on Power Systems 31 (5) (2016) 3729–3736.

[10] B. Kocuk, S.S. Dey, X.A. Sun, Strong SOCP Relaxations for the Optimal Power Flow Problem, Operation Research 64 (4) (2016) 1177–1196.

[11] B. Kocuk, S.S. Dey, X.A. Sun, Matrix Minor Reformulation and SOCP-based Spatial Branch-and-Cut Method for the AC Optimal Power Flow Problem, arXiv:1703.03050 March (2017).

[12] D. Shchetinin, Optimization of Power System Operation: Approxima-tions, Relaxations, and Decomposition, ETH Zurich (2018).

[13] K. Bestuzheva, H.L. Hijazi, C. Coffrin, Convex Relaxations for Quadratic On/Off Constraints and Applications to Optimal Transmission Switching, http://www.optimization-online.org/DB_FILE/2016/07/5565.pdf (2016).

[14] C. Chen, A. Atamturk, S.S. Oren, Bound Tightening for the Alternating Current Optimal Power Flow Problem, IEEE Transaction on Power Systems 31 (5) (2016) 3729–3736.

[15] M.R. Narimani, D.K. Molzahn, M.L. Crow, Improving QC Relaxations of OPF Problems via Voltage MagnitudeDifference Constraints and Envelopes for Trilinear Monomials, 20th Power Systems Computation Conference (PSCC), June (2018).

[16] M. Lu, H. Nagarajan, R. Bent, S.D. Eksioglu, S. J. Mason, Tight Piecewise Convex Relaxation for Global Optimization of Optimal Power Flow, Power System Computation Conference (PSCC) (2018).

[17] K. Sundar, H. Nagarajan, S. Misra, M. Lu , C. Coffrin, R. Bent, Optimization-Based Bound Tightening using a Strengthened QC-Relaxation of the Optimal Power Flow Problem, arXiv:1809.04565v2 (2018).

[18] M. R. Narimani, D. K. Molzahn, M. L. Crow, Tightening QC Relaxations of AC Optimal Power Flow Problems Via Complex Per Unit Normalization, arxive, 2019.

[19] M. Farivar, C.R. Clarke, S.H. Low, K.M. Chandy, Inverter VAR Control for Distribution Systems with Renewables, 2011 IEEE International Conference on Smart Grid Communications (SmartGridComm) October (2011) (457–462).

[20] M. Lu, H. Nagarajan, R. Bent, S.D Eksioglu, S.J. Mason, Tight Piecewise Convex Relaxations for Global Optimization of Optimal Power Flow, 20th Power Systems Computation Conference (PSCC), June (2018).

SECTION

2. CONCLUSION

The first goal of this dissertation is to understand various causes of non-convexities in OPF problems to further improve solution algorithms and develop challenging test cases. The numerical experiment described in this dissertation provides a key observation regarding OPF non-convexities: all of the nonconvexities identified in the numerical experiment are associated with binding lower bounds on voltage magnitudes and reactive power generation. Leveraging the learned lessons from investigating the feasible spaces of small test cases, different improvements are proposed to strengthen the QC relaxations of OPF problems. A set of constraints based on voltage magnitude differences and the Meyer and Floudas envelopes for trilinear monomials are proposed. Comparison to a state-ofthe-art QC implementation demonstrates the value of these improvements via reduced optimality gaps on challenging test cases while maintaining computational tractability. This dissertation also proposes and empirically tests two improvements for strengthening QC relaxations of OPF problems by tightening the envelopes used for the trigonometric terms. The first improvement represents the line admittances in polar form. The second improvement applies a complex base power normalization with angle ψ in order to rotate the arguments of the trigonometric terms. An empirical analysis is used to suggest a good value for ψ. Comparison to the state-of-the-art QC relaxation reveals the effectiveness of the proposed improvements. Building on the ideas in this dissertation, our future work includes extending the RQC relaxation to allow for distinct values of ψ for the power flow equations associated with each line in the system.

BIBLIOGRAPHY

[1] M.B. Cain, R.P. O'Neill, A. Castillo, History of Optimal Power Flow and Formulations, August (2013).

[2] Energy Information Agency, Summary Electricity Statistics 1999-2010, Online. Available: http://www.eia.gov/electricity/annual/pdf/tablees1.pdf.

[3] D. Bienstock, A. Verma, Strong NP-hardness of AC Power Flows Feasibility, arXiv:1512.07315 (2015)

[4] K. Lehmann, A. Grastien and P. Van Hentenryck, AC-Feasibility on Tree Networks is NP-Hard, IEEE Transaction on Power Systems 31 (1) (2016) 798–801.

[5] C. Coffrin, H.L. Hijazi, P. Van Hentenryck, The QC Relaxation: A Theoretical and Computational Study on Optimal Power Flow, IEEE Transaction on Power Systems 31 (4) (2016) 3008–3018.

[6] H. Saadat, Power System Analysis. McGraw-Hill, 2005.

[7] D. K. Molzahn, I. A. Hiskens, A Survey of Relaxations and Approximations of the Power Flow Equations, Foundations and Trends in Electric Energy Systems February (2019).

[8] J. D. Glover, M. S. Sarma, T. J. Overbye, Power System Analysis and Design, Cengage Learning (2008).

[9] W. Zangwill and C. Garcia, Pathways to Solutions, Fixed Points, and Equilibria. PrenticeHall, 1981.

[10] J. Baillieul and C. Byrnes, Geometric Critical Point Analysis of Lossless Power System Models, IEEE Transactions on Circuits and Systems 29 (11) (1982) 724–737.

[11] T. Overbye and C. DeMarco, Improved Techniques for Power System Voltage Stability Assessment Using Energy Methods, IEEE Transactions on Power Systems 6 (4) (1991) 1446–1452.

[12] Y. Tamura, H. Mori, and S. Iwamoto, Relationship Between Voltage Instability and Multiple Load Flow Solutions in Electric Power Systems, IEEE Transactions on Power Apparatus and Systems 102 (5) (1983) 1115–1125.

[13] M. Ribbens-Pavella and F. Evans, Direct Methods for Studying Dynamics of Large-Scale Electric Power Systems-A Survey, Automatica 21 (1) (1985) 1–21.

[14] H.-D. Chiang, F. Wu, and P. Varaiya, Foundations of Direct Methods for Power System Transient Stability Analysis, IEEE Transactions on Circuits and Systems 34 (2) (1987) 160–173.

[15] V. Venikov, V. Stroev, V. Idelchick, and V. Tarasov, Estimation of Electrical Power System Steady-State Stability in Load Flow Calculations, IEEE Transactions on Power Apparatus and Systems 94 (3) (1975) 1034–1041.

[16] N. Z. Shor, Quadratic Optimization Problems, Soviet Journal of Computer and System Sciences 25 (1987) 1–11.

[17] X. Bai, H. Wei, K. Fujisawa, and Y. Wang, Semidefinite Programming for Optimal Power Flow Problems, International Journal of Electrical Power Energy Systems 30 (2008) 383–392.

[18] J. lavaei, S. H. Low, Zero Duality Gap in Optimal Power Flow Problem, IEEE Transaction on Power Systems 27 (2012) 92–107.

[19] J. B. Lasserre, Global Optimization with Polynomials and the Problem of Moments, SIAM Journal on Optimization 11 (2001) 796–817.

[20] J. B. Lasserre, Moments, Positive Polynomials and Their Applications, Imperial College Press 1 (2010).

[21] R. Jabr, Radial Distribution Load Flow using Conic Programming, IEEE Transaction on Power Systems 21 (3) (2006) 1458–1459.

[22] B. Kocuk, S.S. Dey, X.A. Sun, Strong SOCP Relaxations for the Optimal Power Flow Problem, Operation Research 64 (4) (2016) 1177–1196.

[23] A. Gomez Exposito, and E. Romero Ramos, Reliable Load Flow Technique for Radial Distribution Networks, IEEE Transaction on Power Systems 14 (3) (1999) 1063–1069.

[24] H. Hijazi, C. Coffrin, and P. Van Hentenryck, Convex Quadratic Relaxation for Mixed-Integer Nonlinear Programs in Power Systems, Mathematical Programming Computation 9 (3) (2017) 321–367.

[25] D. Bienstock, and G. Munoz, On Linear Relaxations of OPF Problems, arXiv:1411.1120 (2014).

[26] D. Bienstock, and G. Munoz, Approximation Method for AC Transmission Switching Based on a Simple Relaxation for ACOPF Problems, IEEE Power and Energy Society General Meeting (2015) 1–5.

[27] M. E. Baran, and F. F Wu, Optimal Capacitor Placement on Radial Distribution Systems, IEEE Transaction on Power Delivery 4 (1) (1989) 725–734.

[28] M. E. Baran, and F. F Wu, Optimal Sizing of Capacitors Placed on a Radial Distribution System, IEEE Transaction on Power Delivery 4 (1) (1989) 735–743.

[29] C. Coffrin, H. L. Hijazi, and P. Van Hentenryck, Network Flow and Copper Plate Relaxations for AC Transmission Systems, 19th Power System Computation Conference (2016) 1–8.

[30] C. Coffrin, H. L. Hijazi, and P. Van Hentenryck, Network Flow and Copper Plate Relaxations for AC Transmission Systems, arXiv: 1506.05202 (2015).

[31] J.A. Taylor, and F.S. Hover, Linear Relaxations for Transmission System Planning, IEEE Transaction on Power Systems 26 (4) (2011) 2533–2538.

[32] G.P. McCormick, Computability of Global Solutions to Factorable Nonconvex Programs: Part I–Convex Underestimating Problems, Mathematical Programming 10 (1) (1976) 147–175.

[33] D. Bienstock, and G. Munoz, LP Formulations for Polynomial Optimization Problems, SIAM Journal on Optimization 28 (2) (2018) 1121–1150.

[34] F. Glover, Improved Linear Integer Programming Formulations of Nonlinear Integer Problems, Management Science 22 (4) (1975) 455–460.

[35] K. Dvijotham, M. Chertkov, P. Van Hentenryck, M. Vuffary, and S. Misra, Graphical Models for Optimal Power Flow, Constraints 22 (1) (2017) 24–49.

[36] J. D. Foster, Mixed-Integer Quadratically-Constrained Programming, Piecewise-Linear Approximation and Error Analysis with Applications in Power Flow, dissertation, The University of Newcastle, Australia, School of Mathematical and Physical Sciences (2013). Constraints 22 (1) (2017) 24–49.

[37] W.A. Bukhsh,A. Grothey, K.I.M. McKinnon, P.A. Trodden, Local Solutions of the Optimal Power Flow Problem, IEEE Transaction on Power Systems, 28 (4) (2013) 4780–4788.

[38] C. Coffrin, H. L. Hijazi, P. Van Hentenryck, Strengthening the SDP Relaxation of AC Power Flows with Convex Envelopes, Bound Tightening, and Valid Inequalities, IEEE Transaction on Power Systems 32 (5) (2017) 3549–3558.

[39] C.A. Meyer, C.A. Floudas, Trilinear Monomials with Positive or Negative Domains: Facets of the Convex and Concave Envelopes, Frontiers in Global Optimization (2004) 327–352.

[40] C.A. Meyer, C.A. Floudas, Trilinear Monomials with Mixed Sign Domains: Facets of the Convex and Concave Envelopes, Journal of Global Optimization 29 (2) (2004) 125–155.

[41] J.A. Momoh, R. Adapa, M.E. El-Hawary, A Review of Selected Optimal Power Flow Literature to 1993. Parts I and II, IEEE Transaction on Power Systems 14 (1) (1999) 96–111.

[42] A. Castillo, R.P. O'Neill, Survey of Approaches to Solving the ACOPF (OPF Paper 4) March (2013)

[43] R.D. Zimmerman,C.E. Murillo-Sánchez, R.J. Thomas, MATPOWER: Steady-State Operations, Planning, and Analysis Tools for Power Systems Research and Education, IEEE Transaction on Power Systems, 26 (1) (2011) 1–8.

[44] J. Lofberg, YALMIP: A Toolbox for Modeling and Optimization in MATLAB, IEEE International Symposium on Computer-Aided Control System Design, (2004) 284–289.

[45] D.K. Molzahn, Computing the Feasible Spaces of Optimal Power Flow Problems, IEEE Transaction on Power Systems, 32 (6) (2017) 4752–4763.

[46] K. Bestuzheva, H.L. Hijazi, C. Coffrin, Convex Relaxations for Quadratic On/Off Constraints and Applications to Optimal Transmission Switching, http://www.optimization-online.org/DB_FILE/2016/07/5565.pdf (2016).

[47] C. Chen, A. Atamturk, S.S. Oren, Bound Tightening for the Alternating Current Optimal Power Flow Problem, IEEE Transaction on Power Systems 31 (5) (2016) 3729–3736.

[48] J.A. Taylor, F.S. Hover, Linear Relaxations for Transmission System Planning, IEEE Transaction on Power Systems 26 (4) (2011) 2533-2538. month=Nov.

[49] J.P. Ruiz, J.P. Grossmann, Using Redundancy to Strengthen the Relaxation for the Global Optimization of MINLP Problems, Computers & Chemical Engineering 35 (12) (2011) 2729–2740.

[50] C. Coffrin, D. Gordon, P. Scott, NESTA, the NICTA Energy System Test Case Archive (v0.7), arXiv:1411.0359 June (2017).

[51] B. Kocuk, S.S. Dey, X.A. Sun, Matrix Minor Reformulation and SOCP-based Spatial Branch-and-Cut Method for the AC Optimal Power Flow Problem, arXiv:1703.03050 March (2017).

[52] M.R. Narimani, D. K. Molzahn, D. Wu, M.L. Crow, Empirical Investigation of Non-Convexities in Optimal Power Flow Problems, American Control Conference (ACC) June (2018).

[53] D.K. Molzahn and L.A. Roald, Towards an AC Optimal Power Flow Algorithm with Robust Feasibility Guarantees, 20th power system computation conference (PSCC) June (2018).

[54] B. Kocuk, S. S. Dey, X. A. Sun, New Formulation and Strong MISOCP Relaxations for AC Optimal Transmission Switching Problem, IEEE Transaction on Power Systems 32 (6) (2017) 4161–4170.

[55] J. F. Marley, D. K. Molzahn, I. A. Hiskens, Solving Multiperiod OPF Problems using an AC-QP Algorithm Initialized with an SOCP Relaxation, IEEE Transaction on Power Systems 32 (5) (2017) 3538–3548.

[56] C. Chen, A. Atamturk, S.S Oren, A Spatial Branch-and-Cut Algorithm for Nonconvex QCQP with Bounded Complex Variables, Mathematical Programming 165 (2) (2017) 549–577.

[57] J. Thorp and S. Naqavi, Load Flow Fractals, in Proceedings of the 28th IEEE Conference on Decision and Control 2 (1989) 1822–1827.

VITA

Mohammad Rasoul Narimani received his bachelor of science (B.S.) in Electrical Engineering from Razi University, Kermanshah, Iran in May 2008. He received his master of science (M.Sc.) in Electrical Engineering from Shiraz University of Technology, Shiraz, Iran in September 2011. He received PhD in Electrical Engineering from Missouri University of Science and Technology, Rolla, Missouri in May 2020. His research interests included power system operation and Control, Mathematical Programming, and convex optimization.